Haptic steering support

Effects and acceptance of haptic shared control design choices for car steering

Kelsey Huijsing

Technische Universiteit Delft

TU Delft

Haptic steering support

Effects and acceptance of haptic shared control design choices for car steering

by

Kelsey Huijsing

to obtain the degree of Master of Science in Aerospace Engineering

at the Delft University of Technology,

to be defended publicly on Tuesday July 12, 2022 at 09:00 AM.

Student number:	4155394	
Thesis committee:	Prof. dr. ir. M. (Max) Mulder,	Control & Simulation Chair
	Dr. ir. D.M. Pool	Daily Supervisor
	Dr. ir. M.M. van Paassen	Supervisor
	Dr. Barys Shyrokau	Examiner

An electronic version of this thesis is available at `http://repository.tudelft.nl/`.

TU Delft

Preface

This work marks the end of my time as an aerospace engineering student at Delft University of Technology. I am grateful for the lovely people at this university and could not have finished this degree without the support of my friends and family. Studying the design of a haptic shared control system for car steering has been insightful and very enjoyable.

Starting this thesis right around the start of the COVID-19 pandemic was not always easy but considering the circumstances we made the best of it. The support of the people at Control & Simulation has been invaluable and the constructive feedback of Daan, René and Max has improved my work tremendously.

I may have hit some road bumps along the way which slowed me down but they did not prevent me from completing my goals. I hope this research proves to be valuable in the pursuit of building even better haptic shared control systems in the future.

Kelsey Huijsing
Delft, July 2022

Contents

List of Abbreviations

ADAS	advanced driver-assistance systems
ANOVA	analysis of variance
CARS	controller acceptance rating scale
CC	curve cutting
CNS	central nervous system
EVP	extended Van Paassen driver model
FB	feedback
FDCA	four design choices architecture
FF	feedforward
HCR	human-compatible reference
HDR	human-defined reference
HMI	human-machine interaction
HSC	haptic shared control
LoHA	level of haptic authority
LoHS	level of haptic support
MLP	mean lateral position
NASA-TLX	NASA task load index
NGP	nearest global point
NMS	neuromuscular system
RMSE	root-mean-square error
RT	relax task
SD	standard deviation
SDLP	standard deviation of lateral position
SoHF	strength of haptic feedback
SW	steering wheel
SWRR	steering wheel reversal rate
TLC	time-to-line crossing
UAV	unmanned aerial vehicle
VP	standard Van Paassen driver model
V2X	vehicle-to-everything communication

List of Symbols

B_{NMS}	human neuromuscular damping coefficient [Nms/rad]
B_{SW}	steering wheel damping coefficient [Nms/rad]
H_{nm}	transfer function for neuromuscular dynamics [-]
I_Z	vehicle yaw moment of inertia [kg m^2]
J_{cost}	cost function value [-]
J_{NMS}	human neuromuscular inertia [kg m^2]
J_{SW}	steering wheel inertia [kg m^2]
K_δ	identified driver curve negotiation gain [rad/Nm]
K_{Driver}	driver collaboration gain [-]
K_{eff}	effective steering ratio [-]
K_{FB}	driver feedback gain [-]
K_{FDCA}	FDCA collaboration gain [-]
K_{FF}	driver feedforward gain [-]
K_{LoHS}	level of haptic support setting in simulations [-]
K_{NMS}	human neuromuscular stiffness [Nm/rad]
K_s	lateral position feedback gain [N]
K_{SoHF}	strength of haptic feedback setting in simulations [-]
K_{SW}	steering wheel stiffness [Nm/rad]
K_{SW_0}	default steering wheel stiffness before LoHA scaling [Nm/rad]
K_w	steering wheel stiffness in Van Paassen model [Nm/rad]
K_ψ	heading feedback gain [Nm/deg] or [Nm/rad]
L_{wb}	wheelbase length [m]
M	total vehicle mass [kg]
$M_{conflict}$	conflict magnitude [Nms]
M_{rms}	root mean square of torque conflict [Nm]
M_{sgn}	torque conflict as a fraction of time [-]
N	total number of data points in time series
$O_{conflict}$	conflict occurrence [-]
$O_{reversal}$	steering wheel reversal occurrence [-]
R	randomly generated number between zero and one [-]
R_s	steering gear ratio [-]
SEf	steering effort [(Nm)^2 s]
T	torque [Nm]
T_{conf}	conflict torque [Nm]
T_{Driver}	driver torque [Nm]
T_{FB}	feedback torque [Nm]
T_{FF}	feedforward torque [Nm]
T_{FDCA}	FDCA controller torque [Nm]
T_{Haptic}	haptic torque [Nm]
T_h	median human torque contribution in simulations [-]
T_{hs}	road curvature filter break frequency [s]
T_N	neuromuscular time delay [s]
T_{SW}	steering wheel torque [Nm]
T_{total}	total torque [Nm]
V	longitudinal vehicle velocity [m/s]
W_h	human work done on steering wheel in simulations [Nm]

c_f	front cornering stiffness [N/rad]
c_r	rear cornering stiffness [N/rad]
e_{lat}	lateral error with respect to a trajectory [m]
l_f	distance from center of gravity to front axle [m]
l_r	distance from center of gravity to rear axle [m]
l_s	linear bicycle model lookahead distance [m]
r	yaw rate [rad/s]
s_{lat}	lateral position with respect to road centerline [m]
t_{run}	time duration for one run of the experiment [s]
x_{car}	vehicle longitudinal position in global reference frame [m]
y_b	straight section lateral position bias [m]
y_{car}	vehicle lateral position in global reference frame [m]
y_{cc}	curve cutting distance [m]
y_e	curve entry position [m]
y_{fr}	future position reference [m]
y_{max}	maximum prepositioning distance [m]
y_{prep}	prepositioning lateral position [m]

Greek Symbols	
β	side slip angle [rad]
δ_r	reference feedforward steering angle [rad]
δ_s	commanded steering angle [rad]
Δi	discrete time step shift [-]
Δs	lateral position error [m]
Δy_e	curve entry position relative to straight section bias [m]
Δy_{max}	maximum prepositioning distance relative to straight section bias [m]
$\Delta\psi$	heading error [rad]
θ	steering wheel angle [rad]
κ	road curvature [1/m]
κ_n	noisy road curvature [1/m]
κ_{prep}	prepositioning curvature [1/m]
μ	mean [-]
μ_e	mean of lateral error [m]
σ	standard deviation [-]
σ_e	standard deviation of lateral error [m]
τ_{in}	turn in time [s]
τ_{LH}	lookahead time [s]
τ_p	prediction time [s]
τ_{pre}	prepositioning time [s]
ψ_L	heading angle

I

Scientific Article

Effects and acceptance of Haptic Shared Control design choices for car steering

Author: K.N. Huijsing
Dep. Control and Simulation, Aerospace Engineering
Delft University of Technology, Delft, The Netherlands
Email: k.n.huijsing@student.tudelft.nl

***Abstract* — A haptic shared control implementation for car steering is developed using the four design choices architecture guidelines. Nowadays, haptic shared control systems are often tuned heuristically and there is little knowledge on how to set the design parameters. In this research a novel driver model was used to generate human-compatible references for the haptic controller with a moderate amount of curve-cutting. In a driving simulator study with different levels of haptic support (LoHS) it is found that driver acceptance increases with higher LoHS values up to 1. In this implementation a higher LoHS equates to stronger steering angle feedforward. Objective driver acceptance is measured by analyzing the torque conflict data and the total conflict is found to decrease by 70% for the highest LoHS condition compared to the lowest setting. This result is verified with higher subjective ratings of the haptic support as the LoHS is increased. The required driver steering effort decreases significantly for higher LoHS values with a reduction of 81% for the highest LoHS condition compared to manual driving. Likewise a small decrease in the steering wheel reversal rate is found as the haptic support is increased. Under high LoHS values the remaining torque conflict is found in the curve entry and exit phases. The addition of individualised prepositioning into the reference has the potential to reduce the remaining conflict. The findings suggest that choosing the right LoHS is of great importance in achieving high acceptance and should thus be the first parameter to be tuned for a haptic controller of the four design choices architecture type.**

***Index Terms* — Haptic Shared Control, Human-Machine Interaction, Acceptance, Conflict, Feedforward, Design Choices, Car Steering**

I. INTRODUCTION

Haptic shared control (HSC) for car steering is a novel control architecture that enables the human to steer a car together with an automated agent [1]. A benefit of such a control system is that the human remains directly involved in the control loop at all times [2]. Additionally, the driver can directly sense the intention of the steering support at the steering wheel. Haptic shared control systems could potentially be part of the solution to ease the future transition from manual driving to fully autonomous vehicles [3]. HSC systems can offer improved path following performance and reductions in the driver's visual demand and control effort [4] [5]. However, torque conflict is commonly found to occur between the driver and the haptic support [6]. Torque conflict occurs when the driver and the support agent's torque contributions are opposed to each other. The severity of such conflict will affect the human acceptance of the overall HSC system. A knowledge gap in HSC research exists with regards to how human acceptance varies across different settings for haptic steering support systems.

The four design choices architecture (FDCA) summarizes design considerations for the adjustable components of HSC systems [7]. A block diagram is given in Figure 1 that shows the FDCA structure. The FDCA stipulates

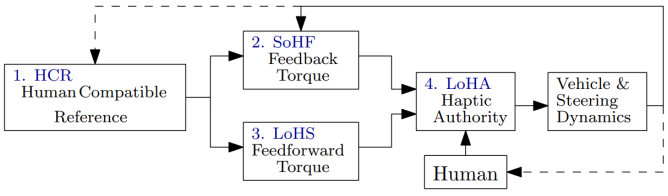

Figure 1: FDCA structure and its design parameters

that the basis for the trajectory of the haptic support should be compatible with the reference of the human. This is known as the human-compatible reference (HCR). Additionally, the haptic guidance consists of a feedforward and a feedback component which are generated based on the selected HCR. The feedforward component is scaled by the level of haptic support (LoHS) and the feedback component is scaled by the strength of haptic feedback (SoHF). Finally, the level of haptic authority (LoHA) sets the control authority of the haptic automation by adjusting the steering wheel stiffness. Together, these four design choices shape the feel of the haptic feedback on the steering wheel as perceived by the human. The acceptance of the supplied steering support will therefore depend to

a large degree on these settings since they determine all characteristics of the haptic steering response. Moreover, the degree to which the driver is engaged with the steering task is also known to change for different settings of the haptic support [8]. Previous research has indicated that the HCR can be adjusted to match the individual driver in order to reduce conflict [9].

There is a gap in haptic shared control research when it comes to identifying the exact relationship between the haptic design settings and the driver's acceptance. It is known that reference trajectories can be individualized to match the driver's path through the curve [9]. Then, given the appropriate reference how strong should the haptic support be and how do the feedback and feedforward components affect the acceptance level? The layout of a FDCA type controller enables the designer to separately tune the feedback and feedforward parts of the haptic steering loop. Due to the novelty of this approach there are currently no comprehensive methods to selecting the feedback and feedforward settings. Haptic shared control systems are mainly tuned heuristically in an iterative process [10]. The goal of this research is to identify the relationship between the Level of Haptic Support and driver's acceptance. It is decided to focus on this design parameter as it has a large and immediate impact on the amount of steering support received by the human. The complete range of values from manual driving to fully automated driving will be investigated in order to obtain a complete view of the human response along the whole spectrum of settings. Simulations will be done with a driver model after which a compatible reference is generated. This HCR will be used in a driving simulator experiment which varies the LoHS between six different settings. By computing the torque conflict the objective acceptance of each LoHS setting can be measured. Furthermore, subjective acceptance is assessed using a questionnaire which is completed by the subjects after each condition. Finally, driver engagement is evaluated by analyzing the steering response in order to determine if human control activity changes across the conditions.

This paper starts by discussing the preliminary simulations in Section II that were run in an effort to gain a first understanding of the cooperation and conflict between human and automation. Subsequently, the driving simulator experiment will be explained in detail in Section III. Hereafter, the data analysis procedure is treated in detail and the results are summarized in Section IV. Finally, the results are discussed in Section V and conclusions are drawn in Section VI.

II. SIMULATIONS

Preliminary simulations were performed in order to assess how the driver and haptic support might interact. Firstly, the parameters of a driver model are varied for a single curve with the intent of establishing their sensitivity on the resulting lateral trajectory and steering output. The results are used to define a good HCR for the FDCA controller. In the second set of simulations the output from this driver model is used as a reference for the haptic controller in the complete HSC simulation. This simulation will be used to study the effects of changing the FDCA design parameters.

A. Human Driver Model

A large number of driving styles exist and individuals are known to have their own preferences. Curve cutting is found in a large number of drivers and the driven trajectory changes depending on the individual and the type of curve [11]. The human steering response to a given road can be simulated with a driver model. The obtained road position and steering angle at each point in the trajectory can then be used as a human-compatible reference in the FDCA implementation for the haptic steering support.

The human driver is modelled according to the Van Paassen model [7] which was found to be the most suitable for generating personalised reference trajectories in a driver model comparison study [12]. This model predicts a steering angle based on the curvature of the road in the feedforward path and an error from the curve cutting reference in the feedback loop, see Figure 2. The curvature input is taken at the lookahead time τ_{LH} and the signal is filtered with a second-order low pass filter with filter constant T_{hs} to ensure smooth transitions between straight roads and curve driving. A driver feedforward gain K_{FF} is then applied together with some static terms for the vehicle steering system (steering wheel stiffness K_w, wheel base L_{wb}, vehicle speed V and effective steering ratio K_{eff}). The filtered curvature is also used to construct the curve cutting reference position at the lookahead point. Subsequently, the lateral error with respective to the curve cutting reference is computed at the prediction time τ_p and scaled by the driver feedback gain K_{FB}. Finally, the combined feedback and feedforward is sent through a first-order human neuromuscular dynamics transfer function which produces a steering angle. This steering angle together with the road curvature become the inputs to the vehicle dynamics to complete the closed-loop control model.

The vehicle dynamics are described by a simplified linear bicycle model [14] with the road curvature κ at the vehicle location and commanded steering angle δ_s as inputs. Furthermore, the state vector includes the side slip angle β, yaw rate r, heading angle ψ_L and lateral distance from centerline s_{lat}. The coefficients in Equation (1) are defined according to Equations (2) - (7), V is the longitudinal speed and l_s is the lookahead distance of the linear bicycle model.

$$\begin{bmatrix} \dot{\beta} \\ \dot{r} \\ \dot{\psi}_L \\ \dot{s}_{lat} \end{bmatrix} = \begin{bmatrix} a_{11} & a_{21} & 0 & 0 \\ a_{12} & a_{22} & 0 & 0 \\ 0 & 1 & 0 & 0 \\ V & l_s & v & 0 \end{bmatrix} \begin{bmatrix} \beta \\ r \\ \psi_L \\ s_{lat} \end{bmatrix} + \begin{bmatrix} 0 & a_{15} \\ 0 & a_{25} \\ -V & 0 \\ -l_s V & 0 \end{bmatrix} \begin{bmatrix} \kappa \\ \delta_s \end{bmatrix} \tag{1}$$

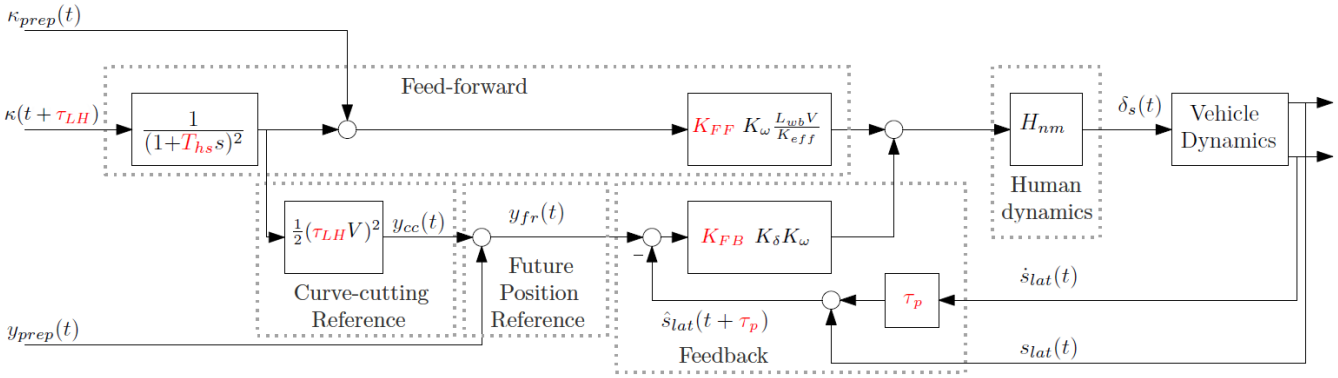

Figure 2: Block diagram of the extended Van Paassen driver model [13].

$$a_{11} = -\frac{2(c_f + c_r)}{MV} \quad (2) \qquad a_{12} = \frac{2(c_r l_r + c_f l_f)}{MV^2} - 1 \quad (3)$$

$$a_{15} = \frac{2c_f}{MVR_s} \quad (4) \qquad a_{21} = \frac{2(c_r l_r - c_f l_f)}{I_Z} \quad (5)$$

$$a_{22} = -\frac{2(c_r l_r^2 + c_f l_f^2)}{I_Z V} \quad (6) \qquad a_{25} = \frac{2c_f l_f}{I_Z R_s} \quad (7)$$

Table I provides an overview of the parameter settings for the driver model [7] and vehicle dynamics [14]. In summary, the standard Van Paassen driver model (VP) contains five parameters which tune the steering response: driver feedforward and feedback gains (K_{FF}, K_{FB}), curvature filter constant (T_{hs}), lookahead time (τ_{LH}) and prediction time (τ_p). These are indicated in red in Figure 2.

Table I: Parameter settings for the driver model and vehicle dynamics.

c_f	front cornering stiffness	65000 [N/rad]
c_r	rear cornering stiffness	5700 [N/rad]
I_Z	yaw moment of inertia	1810 [kg·m^2]
K_δ	human curve negotiation parameter	1.25/K_w [rad/Nm]
K_{eff}	effective steering ratio	1/15 [-]
K_w	steering wheel stiffness VP model	1 [Nm/rad]
l_f	front axle distance	1.127 [m]
l_r	rear axle distance	1.485 [m]
l_s	lookahead distance	5 [m]
L_{wb}	wheelbase length	2.8 [m]
M	vehicle mass	1476 [kg]
R_s	steering gear ratio	16 [-]
V	longitudinal vehicle velocity	22.22 [m/s]

B. *Extending the Van Paassen Model with Prepositioning*

It is possible to extend the Van Paassen model such that it includes prepositioning. This is important to achieve realistic individualized reference trajectories since prepositioning before a curve is very common amongst human drivers [12]. A prepositioning-path extension to the Van Paassen model was derived geometrically by Barendswaard et al. [13]. The degrees of freedom in the prepositioning model are the driver class (outer, middle or inner types) and the straight section bias which together determine the complete prepositioning trajectory. In order to extend the Van Paassen model the prepositioning position y_{prep} is added to the curve cutting reference in the feedback loop to generate the so-called future position reference y_{fr}, see Figure 2. Additionally, a corresponding prepositioning curvature κ_{prep} is added as an independent component to the feedforward loop. These two prepositioning inputs are computed with parameters for the identified driver classes and the straight section bias, see Barendswaard for a more detailed description [13]. Thanks to the addition of prepositioning the extended Van Paassen driver model (EVP) now contains seven model parameters that can be tuned to fit a reference trajectory to the individual.

Due to the fact that this driver model assumes a certain amount of curve cutting in the feedback path it is simple to generate references that exhibit some degree of curve cutting. However, it is also possible yet naturally more difficult to come up with a reference that includes the opposite of curve cutting (i.e., a widely driven corner). Figure 3 includes the lateral position over time for four trajectory types that can be obtained just by varying the two driver gain parameters. A light amount of prepositioning without straight section bias is included before the curvature section. The resulting trajectories include: strong curve cutting, moderate curve cutting, centerline driving and wide curve driving. Different types of steering behavior can be built by tuning the other parameters. A middle driver class type of prepositioning is included in these trajectories without any straight section bias.

Table II lists the baseline values that were used in these

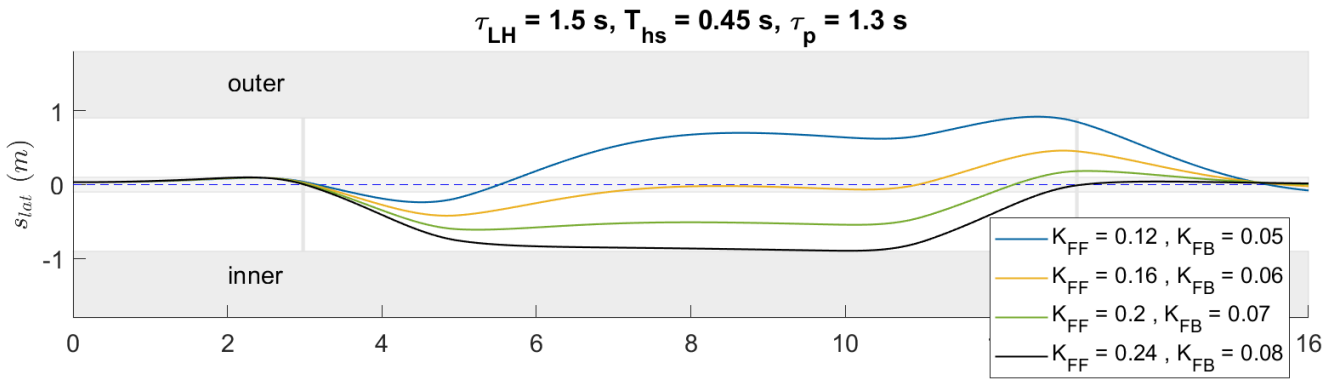

Figure 3: Different types of steering behavior as obtained with the extended Van Paassen model.

simulations for the Van Paassen model parameters. Additionally, the driver class is kept fixed to an outer driver class type with zero straight section bias. This produces a small amount of prepositioning towards the outside of the curve. This parameter set was found to produce a moderate amount of curve cutting for a single curve road section with a road radius of 205m at a speed of 80kph.

Table II: Van Paassen model baseline parameter set for preliminary simulations.

K_{FF}	K_{FB}	T_{hs}	τ_{LH}	τ_p
0.21 [-]	0.07 [-]	0.45 [s]	1.5 [s]	1.3 [s]

C. *Shared Control Simulation*

After establishing a baseline trajectory for the human driver it can be used as the HCR in the complete shared control simulation. This next simulation consists of a human controller based on the Van Paassen driver model and a haptic controller based on the FDCA which generates a steering torque from the human-compatible reference that was generated in the first step. This setup makes it possible to select different references for the human and haptic controllers enabling an analysis of dissimilar references. The references are known as the human defined reference (HDR) and the human-compatible reference (HCR), respectively. The human controller functions in the same way as detailed before and uses the standard Van Paassen model. Figure 4 provides a block diagram overview of the complete HSC simulation and its components.

The haptic controller includes a feedforward component that scales the steering angle from the reference by the Level of Haptic Support (LoHS). Additionally, a feedback component is part of the haptic controller which combines heading and lateral errors and ends up scaling the sum of these by the Strength of Haptic Feedback (SoHF). The lateral and heading error components themselves are scaled by the gains K_s and K_ψ, respectively, which were set to 0.1 N and 2 Nm/rad in this simulation after tuning them such that the controller feedback response is satisfactory.

Before the feedforward steering angle δ_R can be combined with the feedback torque it needs to be converted back into a torque. The conversion method is based on an approximation of the inverse steering wheel dynamics. While the steering wheel angle θ is known its derivatives are needed as well as can be seen from Equation (8). A robust method for computing these derivatives is by approximating their values in the Laplace domain with the transfer function from Equation (9) as was proven to be effective by Ghys [9]. The second derivative can be obtained using the same approximation by substituting the found value for the first derivative.

$$T_{SW} = J_{SW}\ddot{\theta} + B_{SW}\dot{\theta} + K_{SW}\theta \tag{8}$$

$$\frac{\dot{\theta}(s)}{\theta(s)} = \frac{s}{\frac{s}{20}+1} \tag{9}$$

As a result of this approximation there is a time lag in the feedforward torque computation after converting the feedforward steering angle to a feedforward torque. In order to compensate for this effect the feedforward steering angle signal was shifted forward in time by one time step after comparing several settings for this time shift.

If the human and haptic controller output torques were added together without any adjustment there would be too much steering torque in total. This problem is fixed by assigning collaboration gains to the driver and haptic controllers. The scaling of these torque contributions is then given by Equation (10) with the sum of these gains adding up to 1.

$$T_{total} = K_{FDCA} \cdot T_{FDCA} + K_{Driver} \cdot T_{Driver} \tag{10}$$

The haptic (FDCA) controller collaboration gain was set to 0.63 while the human gain was set to 0.37 in line with previous research on this topic [9].

Due to the direct link between the human limbs and the steering wheel it is possible to lump the neuromuscular (NMS) and steering wheel (SW) mechanical properties into one. A transfer function of the combined system is given by Equation (11). As a first approximation the mechanical properties are added together to determine the total values. In order to compensate for the increased inertia, damping and stiffness the torque conversion method must be updated. The steering wheel mechanical properties will now have to include the neuromuscular contributions as well which leads to the updated steering wheel

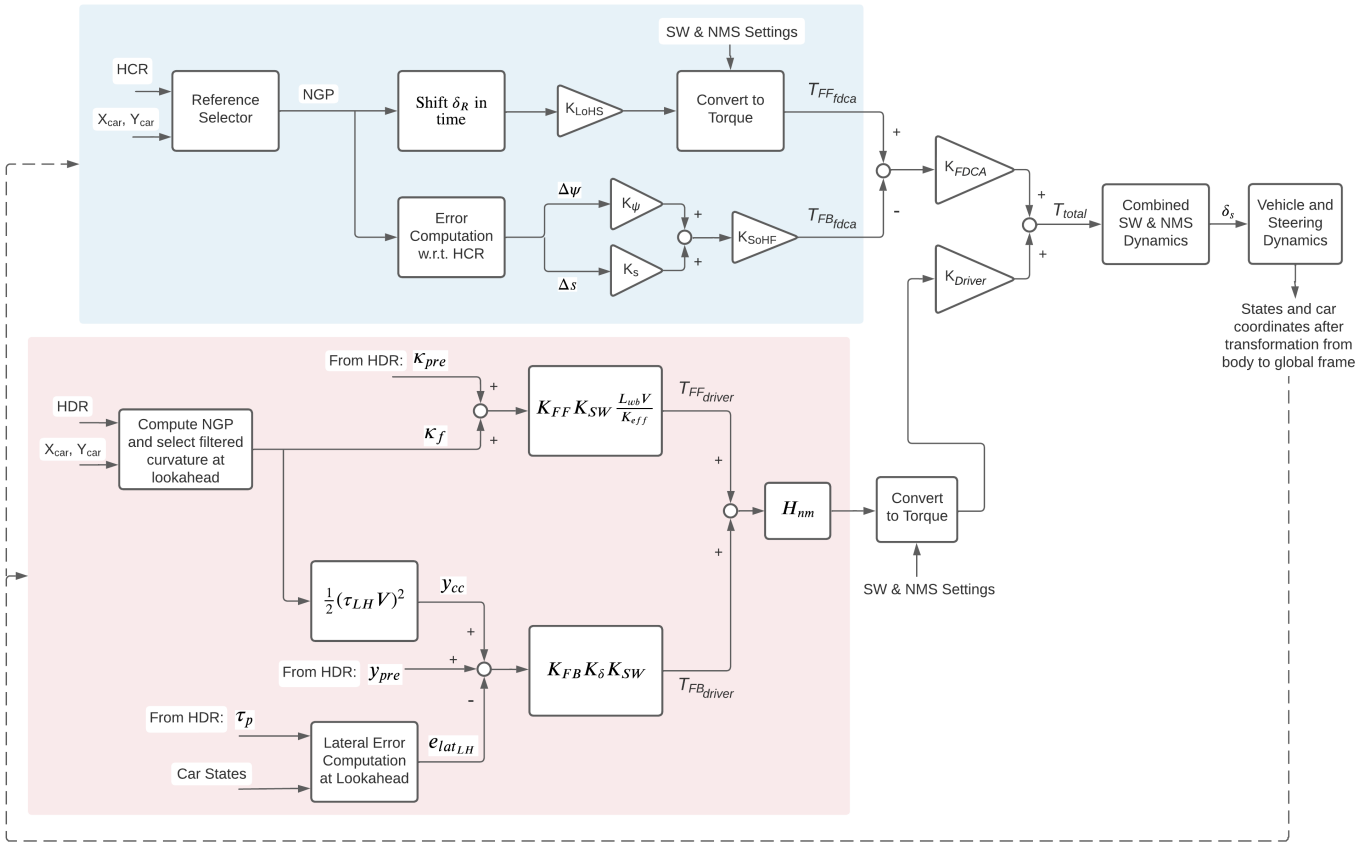

Figure 4: Block diagram of the HSC simulation. Top blue is the haptic FDCA controller and bottom red is the human controller based on the Van Paassen driver model.

dynamics, see Equation (11).

$$\frac{\theta(s)}{T_{SW}(s)} = \frac{1}{J_{total}s^2 + B_{total}s + K_{total}} \tag{11}$$

The baseline values for the steering wheel, neuromuscular and total mechanical properties in this simulation are given in Table III.

Table III: Baseline values for steering wheel and neuromuscular mechanical properties.

	J	B	K
SW	0.005 [kg·m^2]	0.03 [Nms/rad]	1 [Nm/rad]
NMS	0.064 [kg·m^2]	0.1 [Nms/rad]	1 [Nm/rad]
Total	0.069 [kg·m^2]	0.13 [Nms/rad]	2 [Nm/rad]

In addition to the above changes required to combine the torques it is now possible to include the Level of Haptic Authority (LoHA) into the haptic shared control simulation. The chosen LoHA implementation effectively sets the authority level of the haptic support by scaling the stiffness of the steering wheel based on its default stiffness value K_{SW_0}, see Equation (12). A LoHA setting of 1 thus corresponds to the default steering wheel stiffness, while a LoHA value of 2 for example doubles the stiffness.

$$K_{SW} = LoHA * K_{SW_0} \tag{12}$$

Finally, changing the steering wheel stiffness through the LoHA will shift the control authority balance between the human and the haptic support. The human parameters will not be adjusted to account for this change in steering wheel stiffness. With the torque combination process complete the steering dynamics can be computed for every steering input.

D. FDCA Parameter Sensitivity

In the shared control simulation the sensitivity of each FDCA parameter can be tested by varying them one by one. All other parameters such as the Van Paassen driver model parameters are kept constant. For each scenario in the simulation the torque conflict, mean human torque contribution, human steering effort and the lateral performance are calculated. The torque conflict has been computed by checking if the driver and haptic support torques are of opposite sign for every point in time. No minimum threshold is used for which conflict will be registered and as a result even the smallest opposing torques will be counted. If there is a conflict the absolute of the difference between the two torques then gives the conflict torque at that instant, see Equation (13).

$$T_{conf} = \begin{cases} |T_{Driver} - T_{FDCA}| \text{ if } T_{Driver} \cdot T_{FDCA} < 0 \\ 0, \quad \text{otherwise} \end{cases} \tag{13}$$

The average of all the torque conflicts is then obtained and reported as the torque conflict T_{conf} in these results as well as the time percentage for which there is conflict. The human torque contribution T_h is computed as the median of the human torque fraction of the total torque for the complete time series. Furthermore, the HSC performance is determined by the average of the lateral position error (e_{lat}) with respect to both the HCR and HDR, see Equation (14), and the standard deviation of e_{lat} which is computed similarly.

$$e_{lat}(\mu) = \frac{\mu(|e_{lat_{HCR}}|) + \mu(|e_{lat_{HDR}}|)}{2} \tag{14}$$

Finally, the human work done W_h is computed using the human torque on the steering wheel over a change in steering angle for each time step, see Equation (15).

$$W_h = \sum_{i=1}^{N} |T_{Driver}(i) \cdot \Delta\theta(i)| \tag{15}$$

1. LoHS Sensitivity

Firstly, the Level of Haptic Support is varied in steps of 0.2 from 0.4 (low haptic support) to 1.0 (full haptic support). The resulting lateral trajectories can be seen in Figure 5. As expected a full feedforward of the steering angle ($K_{LoHS} = 1$) in the haptic part of the simulation causes the shared control system to exactly follow the haptic reference (HCR). As the level of haptic support is reduced the degree to which the model exhibits curve cutting reduces. The vehicle trajectory in the curve goes from curve cutting at high LoHS values (> 0.75) to more sloppy curve negotiation where the curve is driven closer to the outer edge at intermediate LoHS values ($0.4 - 0.6$). For low LoHS values the vehicle may exceed the road boundaries, especially towards the end of the curve. Increasing the LoHS reduces the amount of torque conflict while increasing lateral steering performance, see Table IV. Furthermore, the necessary human steering torque decreases significantly for higher LoHS settings as indicated by the human torque contributions and total work done on the steering wheel.

Table IV: Resulting metrics for LoHS simulations.

LoHS	T_{conf}	T_h	e_{lat} (μ/σ)	W_h
0.4	0.0616 Nm 1.374%	0.521	0.548 m 0.464 m	0.920 Nm
0.6	0.0556 Nm 1.124%	0.471	0.364 m 0.308 m	0.801 Nm
0.8	0.0332 Nm 0.874%	0.422	0.181 m 0.153 m	0.690 Nm
1	0.0128 Nm 0.937%	0.370	0.00503 m 0.00706 m	0.590 Nm

2. SoHF Sensitivity

Secondly, the Strength of Haptic Feedback is varied from 0.5 (low feedback) to 1.5 (strong feedback) at a LoHS fixed at 0.7 such that differences between SoHF levels can be better observed. The resulting lateral trajectories are shown in Figure 6. It is clear that even if the SoHF is increased it cannot make up for an incomplete LoHS. This is due to a relatively weak feedback response which is generated using the lateral and heading gains K_s and K_ψ. A more optimal setting for these two gains would produce a stronger feedback response and close the distance towards the HCR to an extent. Increasing the SoHF from a low to intermediate value does provide a slight increase in performance whereas an increase in SoHF from intermediate to high only adds a further small increase in performance. According to these simulations there is thus no need for increasing the SoHF past intermediate values of around 1.2.

From the metrics in Table V it appears that the conflict will decrease as SoHF is increased. However, from literature and previous experiments it is known that jerky steering feedback can be perceived as obtrusive and more conflict can be expected. This HSC model is thus not suitable for making realistic predictions on the amount of torque conflict across SoHF settings. The human torque contribution and steering work appear to decrease for higher SoHF as the haptic controller is better able to follow the HCR. This is also seen in the lateral performance results. From additional simulations it is concluded that SoHF values above 2 should not be used as excessive feedback gains can cause lateral instability of the steering system.

Table V: Resulting metrics for SoHF simulations.

SoHF	T_{conf}	T_h	e_{lat} (μ/σ)	W_h
0.5	0.0910 Nm 1.999%	0.527	0.464 m 0.403 m	0.848 Nm
0.8	0.0773 Nm 1.624%	0.498	0.384 m 0.330 m	0.806 Nm
1.2	0.0631 Nm 1.187%	0.471	0.311 m 0.265 m	0.765 Nm
1.5	0.0447 Nm 1.062%	0.462	0.273 m 0.231 m	0.744 Nm

3. LoHA Sensitivity

The Level of Haptic Authority is varied between 0.5 (SW stiffness halved), 1 (default SW stiffness), 2 (SW stiffness doubled) and 3. The resulting lateral trajectories are shown in Figure 7. The LoHA setting in these simulations directly impacts the amount of curve cutting that occurs in the shared control case. This effect originates from the human loop of the shared control system since the computation for the amount of human steering torque includes two steering wheel stiffness terms K_{SW} (one in the human feedforward and one in the human feedback, see Figure 4). A LoHA value of 0.5 only reduced the amount of curve cutting by a very small margin. A higher LoHA value of 2 increased the amount of curve cutting significantly at the cost of requiring the human to exert just over 50% more torque compared to the default set-

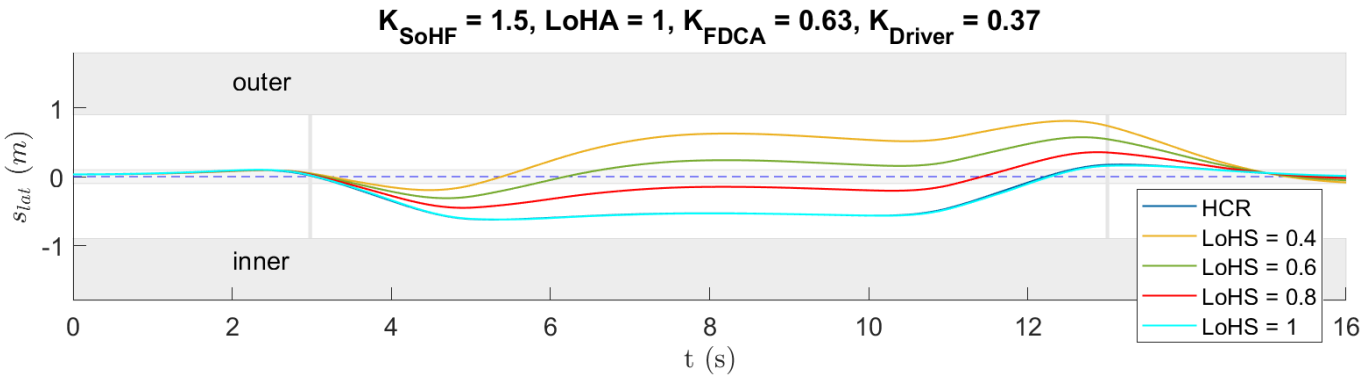

Figure 5: Level of Haptic Support lateral position sensitivity, HCR = HDR.

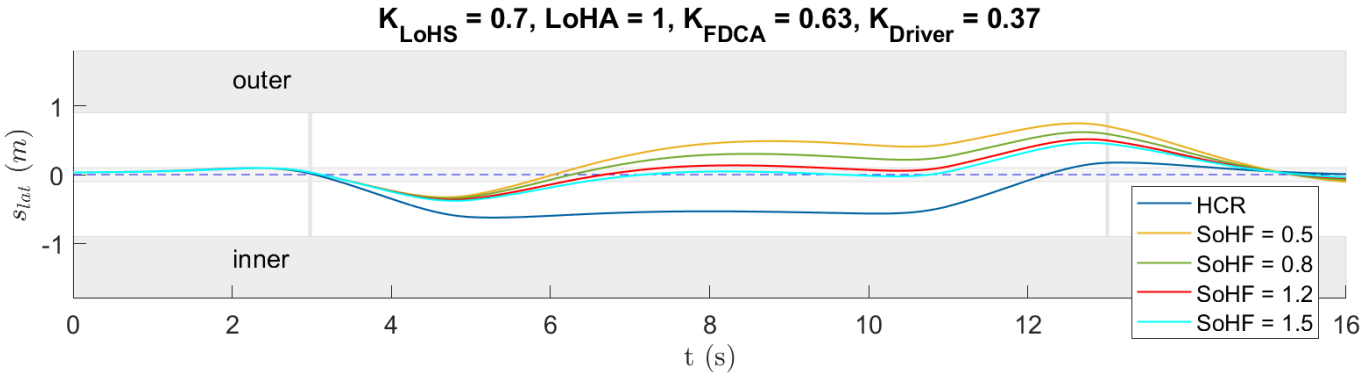

Figure 6: Strength of Haptic Feedback lateral position sensitivity, HCR = HDR.

ting. Exceedingly high LoHA values such as 3 ended up steering the car too strongly in the middle section of the curve which results in the vehicle driving off the road temporarily. The chosen simulation setup does not account for changes in the human neuromuscular system which are to be expected when the steering feel changes as a result of a LoHA setting unequal to 1. This makes it difficult to predict how acceptance and individual LoHA settings are related. From the simulations results, however, it is clear that the amount of torque conflict increases drastically when the LoHA setting increases, see Table VI.

Table VI: Resulting metrics for LoHA simulations.

LoHA	T_{conf}	T_h	e_{lat} (μ/σ)	W_h
0.5	0.0160 Nm 0.687%	0.347	0.0407 m 0.0350 m	0.426 Nm
1	0.0128 Nm 0.937%	0.370	0.00503 m 0.00706 m	0.590 Nm
2	0.0433 Nm 7.495%	0.405	0.135 m 0.116 m	0.929 Nm
3	0.0910 Nm 1.874%	0.429	0.306 m 0.266 m	1.309 Nm

4. Dissimilar References Sensitivity

By investigating what happens when the human and haptic references are different it is immediately clear that any mismatch between the human and haptic reference will result in torque conflict and a reduction in steering performance, see Table VII. From the simulations it appears that a mismatch from the human side increases the conflict slightly more compared to the same mismatch from the haptic support side of the system. Although conflict rises rapidly when reference dissimilarity increases it can be concluded that a HSC model using the EVP driver model is comparably less sensitive in terms of lateral performance as the overall curve cutting steering response prevails. When the misalignment between references increases the severity of torque conflict increases non-linearly.

In this analysis two types of extreme reference misalignment were studied: a strong curve cutting (strong CC) reference combined with normal curve cutting (default) and a normal curve cutting reference with anti curve cutting (anti CC). By comparing these two it is interesting to note that an overly strong curve cutting reference is nearly as bad as a lackluster one which is too weak and would individually end up steering the vehicle near the outer side of the curve. As a result, it may be important to ensure that a reference is implemented which includes a conservative amount of curve cutting (i.e., no excessive amount of curve cutting).

E. Simulation Results

From these simulations it can be concluded that the LoHS setting has a large effect on the trajectory that is driven. As the LoHS reduces the steering feedforward becomes increasingly incomplete. As a result, the vehicle trajec-

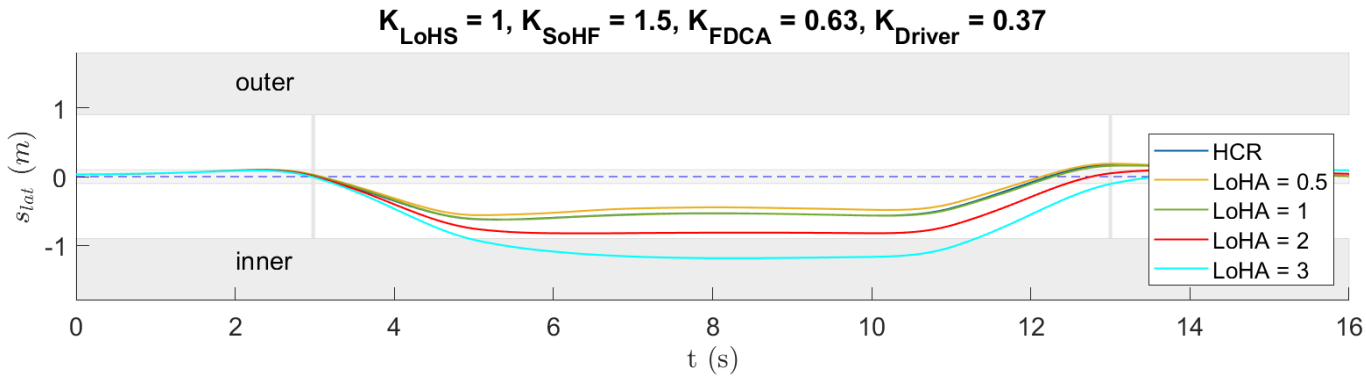

Figure 7: Level of Haptic Authority lateral position sensitivity, HCR = HDR.

Table VII: Resulting metrics for simulations with different combinations of human and haptic references compared to the baseline values when references are equal.

HSC Settings	T_{conf}	e_{lat} (μ/σ)	W_h
HCR = HDR LoHS = 0.92	0.012 Nm 0.625%	0.0708 m 0.0594 m	0.628 Nm
HCR default HDR weak CC	0.019 Nm 0.81%	0.0637 m 0.0542 m	0.609 Nm
HCR weak CC HDR default	0.0088 Nm 0.44%	0.0784 m 0.0657 m	0.656 Nm
HCR default HDR strong CC	0.076 Nm 5.68%	0.0944 m 0.0804 m	0.667 Nm
HCR strong CC HDR default	0.072 Nm 7.99%	0.0777 m 0.0684 m	0.583 Nm
HCR strong CC HDR anti CC	0.083 Nm 9.56%	0.290 m 0.232 m	0.490 Nm
HCR anti CC HDR strong CC	0.090 Nm 5.93%	0.290 m 0.232 m	0.814 Nm

tory in the curve goes from curve cutting at high LoHS values (> 0.75) to more sloppy curve negotiation where the curve is driven closer to the outer edge at intermediate LoHS values (0.4 - 0.6). As long as the human and haptic references match, increasing the LoHS reduces the amount of torque conflict while improving lateral steering performance. Furthermore, the necessary human steering torque decreases significantly as the LoHS is increased. Due to the strong effects of the selected LoHS on the vehicle trajectory, the corresponding conflict and the required human steering effort it should be considered as the first and most prominent parameter to tune once a HCR has been established that matches the human reference.

Increasing the SoHF from a low to intermediate value provides a significant increase to performance, whereas an increase in SoHF from intermediate to high only adds a further small increase in performance. This HSC model is unsuited for making realistic predictions on the amount of torque conflict across SoHF settings. However, it remains important to prevent jerky steering feedback which can be perceived as obtrusive. Therefore, instead of focusing on the SoHF setting it is probably more beneficial to find a good setting for the LoHS of a suitable HCR which only requires the addition of a little feedback (i.e. small SoHF).

The LoHA setting in these simulations directly impacts the amount of curve cutting that occurs in the shared control case. This effect originates from the human loop of the shared control system. A LoHA value of 0.5 which sets the steering wheel stiffness to half its original value only reduced the amount of curve cutting by a very small margin. A higher LoHA value increases the amount of curve cutting significantly at the cost of requiring the human to exert more torque compared to the default setting.

The chosen simulation setup does not account for changes in the human neuromuscular system, which are to be expected when the steering feel changes as a result of a LoHA setting unequal to 1. This makes it difficult to predict how acceptance and individual LoHA settings are related. From the simulations results, however, it is clear that the amount of torque conflict increases drastically when the LoHA setting increases.

It is evident that any mismatch between the human and haptic reference will inherently result in torque conflict and a reduction in steering performance. Conflict rises rapidly and increases non-linearly when reference dissimilarity between human and haptic support increases. From the simulations it appears that a mismatch from the human side increases the conflict slightly more compared to the same mismatch from the haptic support side of the system. In this analysis two types of extreme reference misalignment are studied: a strong curve cutting reference combined with normal curve cutting and a normal curve cutting reference with anti curve cutting. By comparing these two it is interesting to note that an overly strong curve cutting reference is nearly as bad as a lackluster one which is too weak. As a result, a reference with a conservative amount of curve cutting should be implemented.

III. EXPERIMENT

Based on the results from the simulations it was decided to use the LoHS as the independent variable. This parameter has a large influence on the driven trajectory and there is currently not much information in the literature on this specific aspect of the FDCA controller. A previous

study used values of 0.5 and 0.92 for the LoHS [9]. An experiment with six levels for the LoHS has been suggested in an assessment of individualized trajectories for HSC in car steering [15]. To get more insight with regards to the influence of this parameter on conflict torque occurrence and driver acceptance it is decided to vary the LoHS between 0, 0.25, 0.50, 0.75, 0.92 and 1.0. Additionally, this is in line with the study done by Mars et al. [16] which provides a good candidate for comparing findings even though their HSC system is not based on the FDCA. The SoHF is fixed at 1.5 and the LoHA setting is set to 1 (no change in the steering wheel intrinsic stiffness), which is in line with previous research [9] [17]. Keeping the SoHF fixed at a satisfactory level should make interpretation of the results more straightforward as compared to when both the LoHS and SoHF are varied simultaneously. The HCR is generated with the VP model using the model parameters from Table II and exhibits a moderate amount of curve-cutting without prepositioning. This represents a middle-of-the-road type of solution between centreline driving and a reference which cuts the corners agressively. The moderate curve cutting is distributed smoothly along the road curvature sections and contains no unexpected transients, which is representative of experienced drivers. This kind of reference is suitable within the context of this research as full HCR personalisation did not lead to significant improvements in subjective acceptance in previous studies [15].

A. *Apparatus*

The HMI Laboratory at the Aerospace Engineering faculty of Delft University of Technology consists of a fixed-base platform that can be used for aircraft or car simulation. The car controls include a control-loaded steering wheel, a control-loaded gas pedal and a passive spring loaded brake pedal. For this experiment, the gas pedal and brake pedal are unused as the vehicle speed is kept fixed at 80 kph. The image is projected in front of the car seat onto a three-sided projection screen at a resolution of 1920 x 1080 pixels which enables a horizontal field of view of 180 degrees and a vertical field of view of 40 degrees. The projected image is generated at 60 Hz. An integrated 12 inch LCD screen behind the steering wheel provides the dashboard indicators and can be turned off or on depending on the experiment. An actuator can apply a haptic feedback force to the steering wheel with a controller data rate of up to 2500 Hz [17]. The vehicle in the simulation is a sedan with a 1.8 m width and simplified vehicle dynamics that were also used in numerous earlier experiments [9] [15] [17] [18] [19]. Figure 8 contains a picture of the experiment setup as seen from behind the driver seat when the simulation is running.

B. *Haptic Shared Control Implementation*

A haptic controller implementation based upon the four design choices architecture was used in the driving simulator, similar to the layout of the haptic controller used in the simulations (see Figure 4). The lateral position and heading feedback gains K_s and K_ψ were set to 0.08 and -0.03, respectively, in agreement with previous experiments. Upon initial testing of the HCR generated with the Van Paassen driver model two problems were found. Firstly, an offset existed in the nominal steering wheel angle. As a result, the vehicle ends up slowly driving off the road towards the left side. This was fixed by adding a small constant torque offset of -0.075 Nm to the haptic control torque loop which effectively evens out the steering wheel angle to the neutral position. Secondly, it was found that the amount of steering in the simulation did not fully translate to the generated amount of steering in the simulator environment. The FDCA controller would still complete the driving task for a LoHS of 1 but with weak curve negotiation instead of the expected moderate amount of curve-cutting. This discrepancy was attributed to modelling differences in components such as the steering wheel dynamics. To fix this issue, the simulator steering wheel mechanical properties were identified, see the results in Table VIII, and a correction factor was applied to the feedforward steering angle of the FDCA controller. The combination of a stiffness term for the simplified inverse steering wheel dynamics together with this correction factor increases the feedforward steering angle in the haptic controller by a factor of about 1.36. This value for the correction was obtained by iteratively testing the simulator with different correction factors and verifying the lateral trajectory output.

Figure 8: Car simulation running in the Human-Machine-Interaction Laboratory.

Table VIII: HMI Lab identified steering wheel properties.

J_{SW}	B_{SW}	K_{SW}
0.0269 kg·m^2	0.1082 Nms/rad	0.4869 Nm/rad

C. *Driving Task and Road*

The control task consists of steering the simulated vehicle along a winding road with six left and six right clothoidal corners with a curve radius of 205m at a speed of 80 kph, identical to a previous experiment [9]. As a result, the

amount of steering required in the curves is close to the upper limit of allowed lateral acceleration for road design rules [17]. The road consists of a single lane with clearly marked road edges and a road width of 3.2 m. Driving conditions are selected such that they are representative for a clear daylight driving environment without any road traffic. Trees are simulated along the road trajectory in order to provide some reference objects to the driver. A straight section of 240 m was included in between turns such that the driver is able to center the vehicle before the next turn.

D. Experiment Design

The manual driving condition is used as a baseline condition to compare the shared control conditions to and is achieved in the experiment by setting the LoHS and SoHF equal to zero. The experiment is conducted according to a within-subjects design with six conditions where the only independent variable is the LoHS. A balanced Latin square design is used to reduce the potential for detrimental effects related to learning, carry-over and fatigue. The resulting experiment design matrix is given in Table IX where the LoHS setting for each experimental condition is indicated. Before the start of the first run (R1) every subject got one training run in the manual driving condition and one training run at a LoHS of 0.5 to familiarize with the driving simulator and the haptic feedback. The driving task can be learned quickly as only steering input on the steering wheel is required. Gas and brake pedals are fixed and require no inputs.

Table IX: Experiment design matrix, S1 - S6 indicates subjects 1 through 6, R1 - R6 indicates experiment condition run 1 through 6.

	R1	R2	R3	R4	R5	R6
S1	0.5	0.75	0	0.25	0.92	1
S2	0.75	0.25	0.5	1	0	0.92
S3	0.25	1	0.75	0.92	0.5	0
S4	1	0.92	0.25	0	0.75	0.5
S5	0.92	0	1	0.5	0.25	0.75
S6	0	0.5	0.92	0.75	1	0.25

E. Participants and Instructions

Eighteen subjects were recruited into the experiment (6 women, 12 men) with ages ranging between 22 and 57 (median age = 25 years, interquartile range = 3.25 years). Due to the Latin Square design every row in the experiment matrix was performed by three subjects in total in an effort to balance the experiment. All subjects were in possession of a driver's license for at least one year (median license possession = 7 years, interquartile range = 3.68 years). Subjects participated voluntarily and were not paid any compensation. The participants were instructed to drive along the road as they would normally in real life and were asked to keep their hands on the steering wheel in the ten to two position. After every run with haptic feedback the subjects were asked to fill in a subjective assessment form. Any feelings of discomfort or nausea would be communicated to the experimenter. The experiment plan was approved by the Human Research Ethics Committee of Delft University of Technology.

F. Dependent Measures and Metrics

Throughout every experiment run data are collected in real time. The objective data consist of vehicle and environment states, steering wheel parameters and torque data. Torque data includes the driver torque T_{Driver}, haptic controller feedforward T_{FF} and feedback torques T_{FB} and the total torque on the steering wheel T_{total}. For each point in time the occurrence of conflict is checked for using the criteria in Equation (16).

$$O_{conflict} = \begin{cases} 1, & \text{if } T_{Driver} \cdot T_{FDCA} < 0 \\ & \text{and } |T_{Driver}| > 0.1 \cdot \max|T_{FDCA}| \\ 0, & \text{otherwise} \end{cases} \tag{16}$$

If the two controllers are in conflict the conflict torque is registered as the difference between the two absolute torques. If the two are in agreement the torque conflict is registered to be zero. The total conflict magnitude can then be computed for every condition by integrating the conflict torque over time, see Equation (17). This metric can be used as an indicator of objective acceptance.

$$M_{conflict} = \sum_{i=1}^{N} O_{conflict} \cdot |T_{Driver}(i) - T_{FDCA}(i)| \cdot dt \tag{17}$$

Secondly, the driver steering effort SEf [20] is computed by integrating the squared driver torque over time for each run of the experiment according to Equation (18). This metric gives an indication for the amount of effort that is required by the human to complete the steering task.

$$\text{SEf} = \int_0^{t_{run}} T_{Driver}^2 dt \tag{18}$$

A commonly used metric for steering activity is the steering wheel reversal rate (SWRR) [21] [22]. It is computed by counting the number of steering wheel reversals and averaging them over the runtime. A steering wheel reversal is counted if the steering wheel angle rate is opposite at two adjacent points in time. Only if a minimum threshold is exceeded the reversal is seen as large enough to be counted, see Equation (19).

$$O_{reversal} = \begin{cases} 1, & \text{if } \dot{\theta}(i+1) \cdot \dot{\theta}(i) < 0 \\ & \text{and } |\dot{\theta}(i+1) - \dot{\theta}(i)| > 0.006 \text{ deg/s} \\ 0, & \text{otherwise} \end{cases} \tag{19}$$

The steering wheel reversal rate is then computed by summing the total number of reversals and dividing them by

the total time for each experimental condition, see Equation (20).

$$\text{SWRR} = \frac{1}{t_{run}} \cdot \sum_{i=1}^{N} O_{reversal} \tag{20}$$

Moreover, the standard deviation of lateral position (SDLP) is computed as an indicator of the amount of lateral swerving along the road for each condition, see Equation (21). The lateral error in this formula is taken with respect to the centerline of the road.

$$\text{SDLP} = \text{SD}(e_{lat}) \tag{21}$$

With regards to the subjective data two questionnaires are completed by subjects after each experiment run with haptic feedback (i.e. not for the manual driving condition). Firstly, a Van der Laan questionnaire is used to obtain a satisfaction and usefulness score for each LoHS. This questionnaire consists of nine five-point rating-scale items which need to be ticked off by the subject [23].

The second questionnaire is known as the Controller Acceptance Rating Scale (CARS). In this flowchart type of questionnaire the subject is asked to rate the effectiveness of the haptic support on a scale from 1 (major deficiencies) to 10 (highly desirable). A confidence rating of either A (confident), B (somewhat confident) or C (not so confident) is also provided for every condition.

G. Statistical Analysis

Normality of the metrics is checked for using the Shapiro-Wilk test. The assumption of sphericity is checked for using Mauchly's test and a Greenhouse-Geisser correction is applied if sphericity is violated. The objective data are analysed with a one-way repeated measures ANOVA to test for significance of the LoHS independent variable. If an objective metric is not normally distributed a non-parametric Friedman test is used. The subjective data are analysed with a Friedman test as well to identify significance of the LoHS between the five haptic conditions. Post-hoc t-tests are performed for pairwise comparisons of normally distributed objective data and Wilcoxon signed-rank tests are done for the non-normally distributed and subjective metrics.

H. Hypotheses

The experiment is designed to help answer the research questions regarding driver acceptance, driver engagement and lateral performance for haptic shared control for car steering. The following three hypotheses are formulated for each aspect of the research question.

- *H.I*: Acceptance is assumed to increase for higher levels of haptic support. Driver acceptance can be objectively measured using the torque conflict magnitude ($M_{conflict}$) as a metric. A decreasing trend in conflict torques and frequency is predicted by the simulations as LoHS increases. Some subjects may prefer different LoHS settings. As a result, there may be a more optimal LoHS somewhere between 0.5 and 1 which optimizes the acceptance by minimizing the total torque conflict. Satisfaction with the haptic support should be high if the haptic feedback is perceived as supportive in completing the steering task. It is thus expected that the subjective ratings will improve for higher LoHS. This hypothesis is supported by findings in similar research by Mars et al. [20] and in studies that investigated implementations of the FDCA controller [17] [9].

- *H.II*: Driver steering effort (SEf) during execution of the task is expected to decrease for higher levels of haptic support as long as their intended steering path is aligned with that of the haptic support. This can be verified by inspecting the driven lateral trajectories in the manual driving condition compared to the conditions with haptic support. Subsequently, the human steering contribution to the total torque is hypothesized to decrease as well. Steering effort for lower LoHS values should be close to the manual driving baseline. These trends in the driver steering effort were also found in the HSC simulations. Previous research by Mars et al. found a decrease in steering effort and activity (steering wheel reversal rate) for low to medium support levels and a significant increase for the highest level of support as the drivers competed with the automation for control of the steering wheel [20]. Therefore, the steering wheel reversal rate (SWRR) is hypothesized to decrease for higher LoHS.

- *H.III*: The haptic shared control system is expected to be able to complete the steering task regardless of the LoHS as the human driver will adapt to the haptic support and supply the required amount of steering torque. This observation was also found in the HSC simulations. The lateral performance improved for higher LoHS in these simulations. It is therefore hypothesized that the variation in lateral performance (SDLP) decreases within the curvature sections as the LoHS increases. Variation in lateral performance along the straight sections is more dependent on the SoHF setting and is thus expected to remain more stable across the six experimental conditions. These expectations are further supported by a previous study that found a significant decrease in the variability of the lateral position as the degree of haptic support increased [20]. In this case the performance gains were obtained with diminishing returns up to medium to high levels of haptic support.

IV. RESULTS

The results section is divided into the subjective and objective datasets, after which the time trace overlay plots are given. Finally, the correlation between the subjective and objective data is shown.

A. *Subjective Data*

The median and interquartile range of the usefulness and satisfaction scores that were computed as a result of the Van der Laan questionnaire are shown in Figure 9 for every experimental condition. The medians are shown as well as the interquartile ranges per condition. A rating towards the upper right hand side of the plot indicates a higher subjective acceptance of the haptic support. A clear trend can be observed towards the higher LoHS settings which are rated as more useful and satisfactory by the subjects. A subjective optimum is achieved at a LoHS of 1. Usefulness ratings are observed to stabilize at around a LoHS of 0.75 while the satisfaction rating further improves even for the highest LoHS condition. Friedman tests reveal a significant effect of the LoHS on both the satisfaction ($\chi^2(4) = 28.683$, $p < 0.05$) and usefulness scores ($\chi^2(4) = 23.021$, $p < 0.05$).

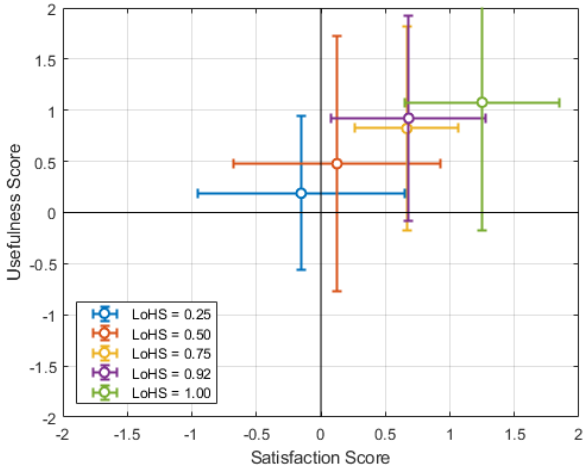

Figure 9: Van der Laan Usefulness and Satisfaction Scores for every condition.

The Controller Acceptance Rating Scale results for each experimental condition can be found in Figure 10. The medians are indicated using the dotted lines. A similar trend to the Van der Laan questionnaire is found in the CARS subjective rating dataset. The highest LoHS condition clearly received the highest subjective ratings with a median rating of 9 while the two LoHS values of 0.75 and 0.92 are rated very closely to each other at median ratings of 8. The lower two LoHS conditions were rated lower with median ratings of 7 and 6.5 for a LoHS of 0.5 and 0.25 respectively. A Friedman test reveals a significant effect of the LoHS on the CARS score ($\chi^2(4) = 26.618$, $p < 0.05$).

B. *Objective Data*

The objective data contains information regarding the torque conflict, steering effort, steering wheel reversal rate and lateral position.

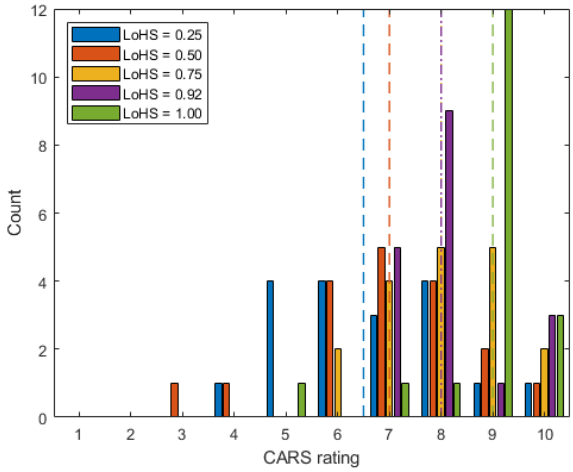

Figure 10: CARS rating distribution for every condition.

1. Torque Conflict

The torque conflict magnitudes for every condition are plotted in a boxplot in Figure 11. It is clear that as the LoHS increases the objective torque conflict decreases. For the highest two conditions (0.92 and 1.0) the torque conflict magnitude is the lowest, as expected. The torque conflict magnitude is decreased by 70% for LoHS values of 0.92 and 1 compared to the LoHS setting of 0.25. It also appears that the decreasing trend in conflict levels off somewhere between a LoHS of 0.75 and 0.92. This suggests that further increasing the LoHS does not alter the objective acceptance of the haptic support system. A one-way ANOVA confirms a significant effect of the LoHS independent variable on the conflict magnitude, $F(1,1.905) = 54.252$, $p < 0.05$. A more detailed scatter plot of the

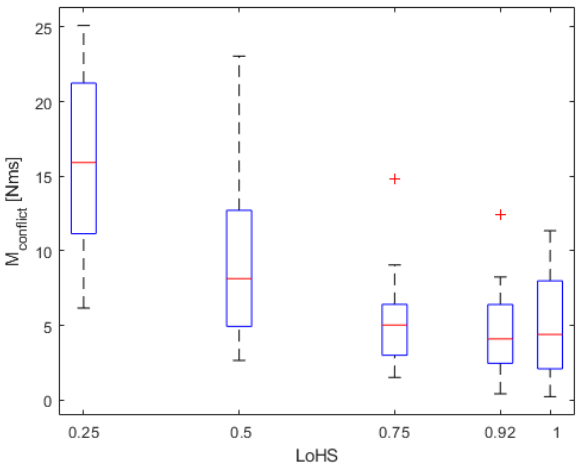

Figure 11: Torque conflict magnitude boxplot.

torque conflict magnitudes for all subjects per condition is given in Figure 12. The shaded area indicates the mean ± one standard deviation for every condition. There is clearly consistency between subjects with only a handful of outliers. As mentioned before, the improvement in ob-

jective acceptance as measured by torque conflict levels off for LoHS settings higher than 0.75.

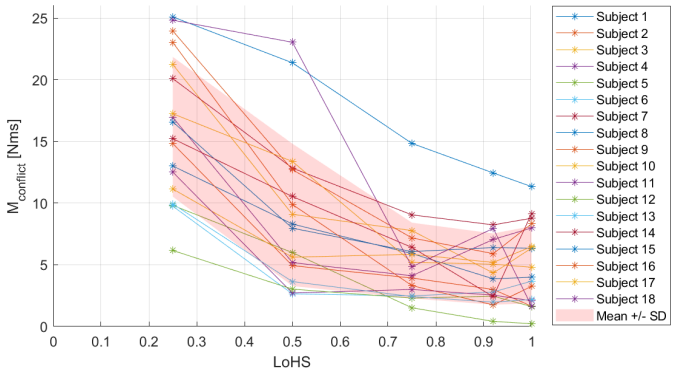

Figure 12: Torque conflict magnitude for every condition for all subjects.

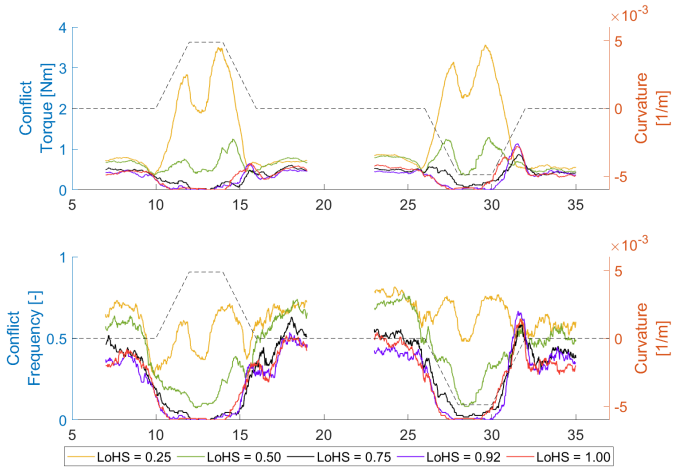

Figure 13: Average torque conflict and frequency for left and right curves. Firstly, an average left turn is shown for every LoHS condition and secondly, an average right turn.

Finally, the average conflict torque and frequency of conflict across all subjects at every point throughout the left and right curves is shown in Figure 13. At the lowest LoHS of 0.25 there is much conflict in the middle of the curvature sections. By inspecting the corresponding individual torque components in Figure 14 it can be concluded that in this case the driver is mainly in conflict with the haptic feedback torque (T_{FB}) while the haptic feedforward torque (T_{FF}) remains very small. As the LoHS increases the sign of the total haptic torque becomes more equal to that of the driver since the haptic feedforward torque becomes stronger. As a result, the conflict decreases in the middle curvature sections for higher LoHS. For higher LoHS the conflict torques are not only smaller but also occur for fewer subjects (as indicated by the conflict frequency). The remaining torque conflict at high LoHS is found in the curve entry and exit phases. In these road sections the haptic torque can sometimes oppose the driver torque. During the curve exit phase it appears that the driver torque decreases slightly more rapidly than the haptic feedforward. Finally, even though the haptic controller is able to drive the vehicle by itself at a LoHS of 1 the driver torque does not go down to zero. Instead the driver torque is reduced by 70% compared to the manual driving condition.

Figure 15 shows the time trace overlay plot for a LoHS of 0.25. In this plot every subject's conflict is indicated in transparent red and overlayed on top of each other for all eighteen subjects. The darker shaded red regions in this plot are the parts of the steering task where conflict occurs most frequently. For brevity only the time trace overlay plots for the lowest and highest LoHS conditions are shown. Notice that there are fewer patches of red conflict in the high LoHS condition while the colors are lighter as well indicating that the frequency of such conflict is also lower. Especially the dark conflict fringes close to curve entry and exit are mediated to a large extent due to the LoHS increase. A large part of the conflict takes place during the straight sections of the road when the feedback from the haptic controller attempts to keep the vehicle near the centerline. Note that the chosen definition for determining if the driver and FDCA controller are in conflict (see Equation (16)) means that it is easier to register conflict during the straights in lower LoHS conditions compared to a higher LoHS setting.

2. Steering Effort

The driver steering effort (SEf) per condition is plotted in Figure 17. An increase in steering effort is observed when comparing the LoHS setting of 0.25 to manual driving. This is not expected and may be an indication that the subjects are unable to effectively make use of the provided haptic support. For LoHS values higher than 0.25 the required driver steering effort is drastically reduced for every step towards a LoHS of 1. At a LoHS of 1 the driver steering effort is reduced by 81% compared to the manual driving condition. A significant effect of the LoHS on SEf is found using a Friedman test, $\chi^2(5) = 84.698$, $p < 0.05$.

3. Steering Wheel Reversal Rate

The steering wheel reversal rate for every condition is given by Figure 18. A slightly downwards trend can be found here when the LoHS increases. Less steering reversals are needed to complete the steering task as more steering is being done by the haptic controller which does so in a more steady manner compared to the humans. This also suggests that the drivers in this experiment comply with the guidance of the haptic support. A reduction in the SWRR of 52% is found for a LoHS of 1 compared to the manual driving condition. Furthermore, a significant effect of the LoHS on SWRR is found using a Friedman test, $\chi^2(5) = 42.997$, $p < 0.05$.

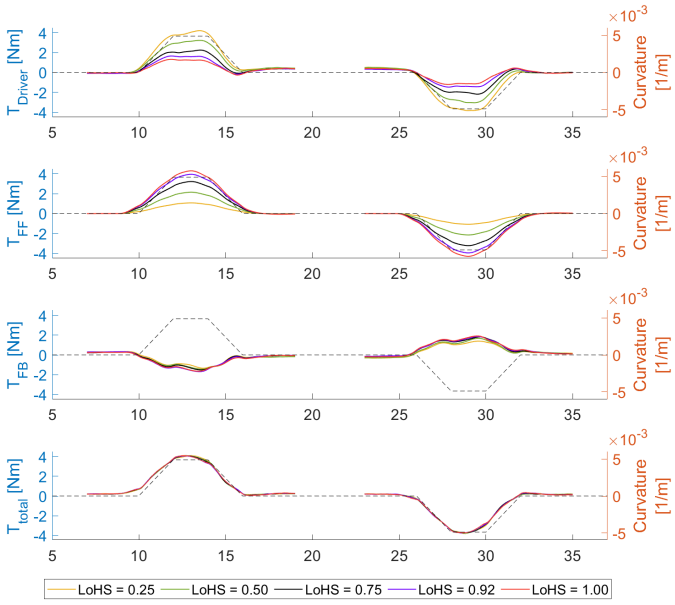

Figure 14: Average torque components and total torque for left and right curves.

4. Lateral Position

Figure 19 shows the SDLP for each experimental condition. The SDLP for all the haptic conditions decreases by 20% compared to the manual driving condition. Overall, no clear trend can be distinguished. A significant effect of the LoHS on SDLP is found using a Friedman test, $\chi^2(5) = 31.683$, $p < 0.05$.

Additionally, Figure 20 contains the average lateral position for every condition for left (L) and right (R) curves. It is clear that the higher the LoHS the more the lateral position exhibits the curve cutting of the HCR. However, the manual driving condition does not deviate from the haptic conditions which indicates that the selected HCR indeed matches the average driving style of the subjects quite well.

5. Pairwise Comparisons

Post hoc pairwise comparisons between LoHS conditions are made to find out whether changes in LoHS produce significant effects on the subjective/objective metrics. Wilcoxon signed rank tests are used for the subjective and non-normally distributed data. A t-test is used in case of the normally distributed conflict magnitude metric. For the steering effort, steering wheel reversal rate and standard deviation of lateral position pairwise comparisons are performed between each LoHS setting and the manual driving condition. For the objective torque conflict magnitude and the subjective ratings pairwise comparisons are made between the five LoHS conditions, see Table X. These results are confirmation that there are no significant improvements in the subjective metrics when increasing the LoHS from 0.25 to 0.5. Objectively, there is a significant improvement in terms of the torque conflict between these two LoHS settings. It can also be seen that the effect of LoHS on the subjective metrics becomes very significant when comparing higher LoHS values above 0.5 to the lowest support setting. Additionally, further increasing LoHS from 0.75 to 0.92 or 1 does not significantly improve the objective torque conflict. However, these final increments in the LoHS do significantly affect the subjective satisfaction score and to a lesser extent also improve the CARS rating.

A significant effect is found for the LoHS on the SEf, SWRR and SDLP in all haptic conditions compared to the manual driving baseline, see Table XI. The steering effort increase for a LoHS of 0.25 is significant compared to the manual driving case. Higher LoHS settings reduce the SEf very significantly. The steering wheel reversal rate is significantly lower for all haptic conditions compared to the baseline manual driving condition. Less steering wheel reversals occur as the driving task is more smoothly executed by the combination of the haptic support and the human. Finally, the amount of lateral swerving as indicated by the SDLP metric is lower for all haptic conditions compared to manually driving. The significant results for these objective metrics is an indication that the steering task is simplified for the human with the addition of haptic feedback.

C. *Subjective/Objective Correlation*

Figure 21 shows the relationship between the subjective usefulness scores and objective torque magnitude. Each experimental conditions is given a distinct color and the mean values for each condition are denoted with squares. A negative correlation of -0.3397 is found for the usefulness score and torque magnitude. Additionally, the relationship between the satisfaction scores and torque magnitude can be found in Figure 22. For these two parameters there is a negative correlation of -0.4235. A very similar plot can be obtained for the CARS scores and torque magnitudes with a negative correlation of -0.4368, see Figure 23. These correlations confirm that the results and trends from the survey data are similarly present in the objective torque conflict data. This means that higher subjective scores are accompanied by lower torque conflict.

V. DISCUSSION

The first hypothesis deals with the acceptance of the haptic support and assumes that acceptance becomes higher as the Level of Haptic Support is increased. As clearly seen in both the subjective and objective data this hypothesis can be accepted. The LoHS is shown to have a strong effect on the torque conflict magnitudes and subjective ratings. Moreover, it appears that LoHS values higher than a value of 0.75 do not yield further significant increases in objective torque conflict performance. For car steering under the circumstances in this scenario the LoHS can be increased up to a value of 1 to reach the highest subjective satisfaction. Acceptance also increased for a higher LoHS setting compared to an intermediate value

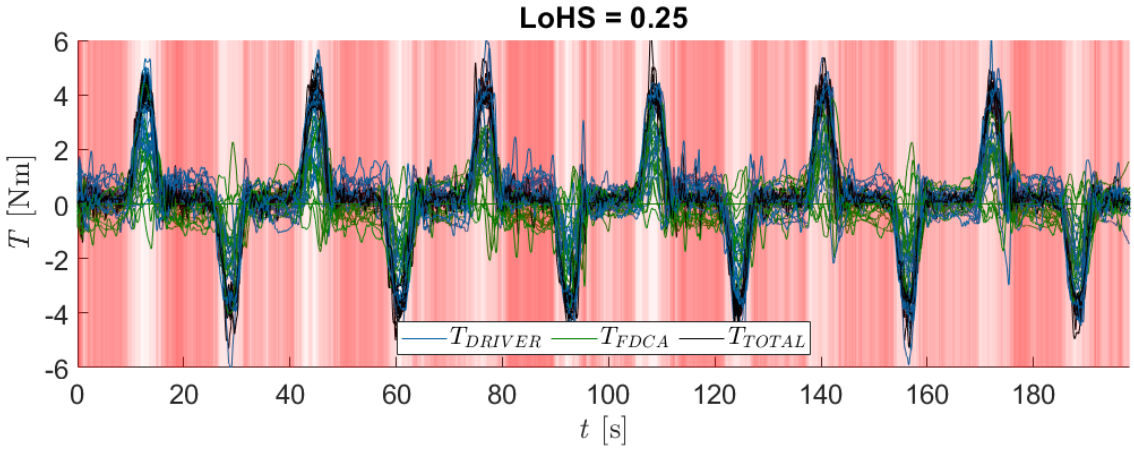

Figure 15: Time traces overlay plot for LoHS = 0.25.

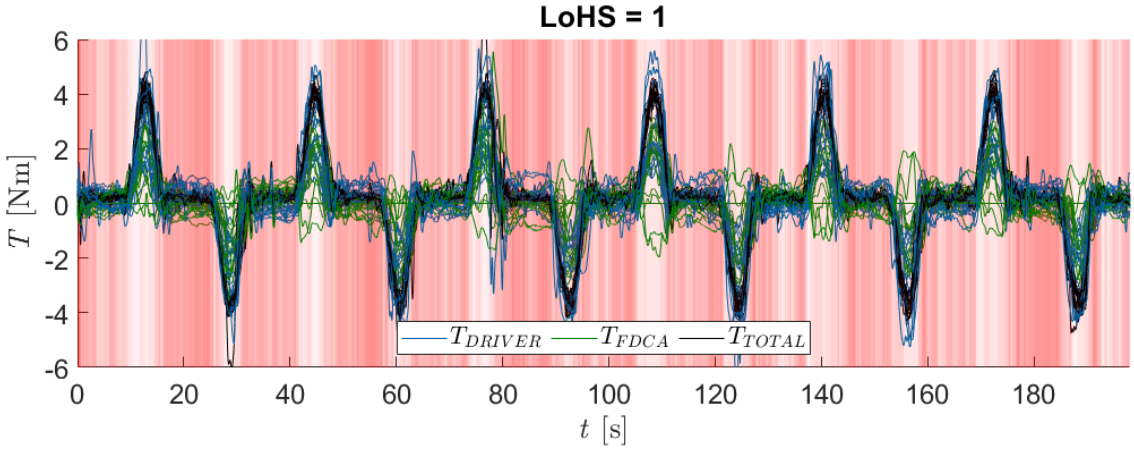

Figure 16: Time traces overlay plot for LoHS = 1.

in a previous study using the FDCA controller [9]. Another study found improvements in subjective ratings for low support settings but to a lesser extent for the highest level of support [20].

A core aspect for tuning the LoHS should be the preference of the driver. All subjects in this study preferred the higher LoHS settings over lower ones. However, some individuals preferred the LoHS setting of 0.75 while others rated the LoHS of 1 significantly higher. This interpersonal variability needs to be taken into account when choosing a LoHS. While the subjective ratings and objective torque conflict are certainly correlated this personal preference is impossible to predict with the metrics used in this analysis.

The current conflict definition seems like a good predictor for the subjective acceptance as proven by the correlation analysis. Moreover, conflict within curves is highly dependent on the LoHS. On the other hand, the conflict during straight sections is due to the haptic feedback of the FDCA controller. Thirdly, conflict during the prepositioning and curve exit phase is also dependent on the chosen HCR. Therefore, it makes sense to determine conflict torques for each of these road sections according to their own guidelines and metrics. In this HSC implementation, the remaining conflict instances are primarily found in the curve entry and exit phases. This can be attributed to the omission of individualized prepositioning in the HCR. Further advances in reducing the torque conflict are, therefore, likely to be made in this area of research. Several studies have proven that individualization can be effective in solving this issue [6] [9] [24] [25].

For the purposes of studying various LoHS settings it can be said that the implementation of a moderate curve-cutting reference under the aforementioned driving conditions is a relatively simple and efficient one size fits all solution. The selected HCR produces a lateral trajectory that closely resembles that of the manual driving condition. The Van Paassen driver model is found to be effective at creating a human-compatible reference. The EVP model can be utilized for achieving more individualized reference trajectories. The diversity in prepositioning maneuvers must carefully be taken into account when implementing this into the human-compatible references. This was shown to be possible by identifying an individual's driving style [9].

The second hypothesis states that driver steering effort is expected to decrease for higher levels of haptic support. This hypothesis can be accepted. From the data a very

Table X: Results for all pairwise comparisons for the conflict magnitude, usefulness, satisfaction and CARS scores. Significance values are given and a very significant ($p < 0.01$) effect is indicated using **, a significant effect ($p < 0.05$) with * and no significance is denoted by −.

	LoHS LoHS	0.25 0.50	0.25 0.75	0.25 0.92	0.25 1	0.5 0.75	0.5 0.92	0.5 1	0.75 0.92	0.75 1	0.92 1
$M_{conflict}$	Signif.	0.000 **	0.000 **	0.000 **	0.000 **	0.002 **	0.000 **	0.006 **	0.123 –	0.438 –	0.567 –
Usefulness	Signif.	0.177 –	0.003 **	0.003 **	0.001 **	0.063 –	0.019 *	0.003 **	0.568 –	0.117 –	0.127 –
Satisfaction	Signif.	0.336 –	0.012 *	0.004 **	0.001 **	0.063 –	0.049 *	0.001 **	0.950 –	0.015 *	0.009 **
CARS	Signif.	0.581 –	0.010 *	0.002 **	0.001 **	0.048 *	0.006 **	0.001 **	0.963 -	0.050 -	0.032 *

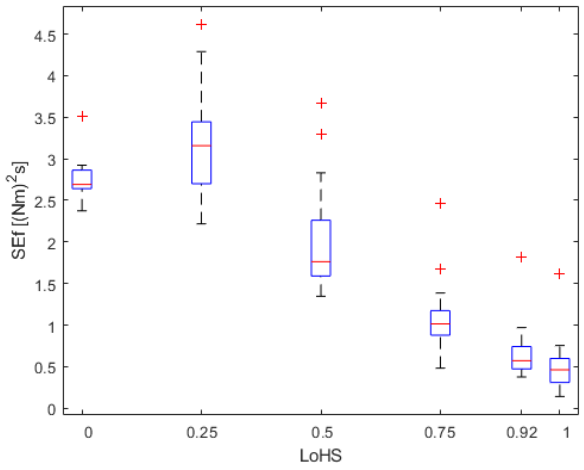

Figure 17: Steering effort for every condition.

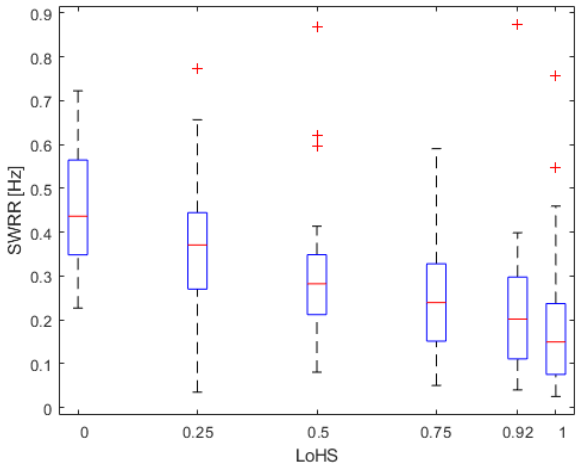

Figure 18: SWRR for every condition.

Table XI: Results for the pairwise comparisons between LoHS conditions and manual driving for SEf, SWRR and SDLP. Significance values are included and a very significant ($p < 0.01$) effect is indicated using **, a significant effect ($p < 0.05$) with * and no significance is denoted by −.

	LoHS	Manual 0.25	Manual 0.5	Manual 0.75	Manual 0.92	Manual 1
SEf	Signif.	0.012 *	0.001 **	0.000 **	0.000 **	0.000 **
SWRR	Signif.	0.031 *	0.004 **	0.000 **	0.000 **	0.000 **
SDLP	Signif.	0.000 **	0.001 **	0.000 **	0.000 **	0.000 **

clear trend is visible in the required driver torque needed to complete the steering task. The steering wheel reversal rate plot contains a similar trend albeit more conservatively as was also found in a similar HSC study by Mars et al. [20]. In conclusion, the amount of work required from the human driver appears to decrease significantly with increasing LoHS. Some subjects experienced the driving task as slightly boring and extremely easy, especially under the high LoHS settings. For high LoHS values it may become challenging to ensure that the driver remains in control and engaged in the driving task. A (nearly) supervisory role for the driver would come at great risks if such a steering system is not safely implemented [26].

The final hypothesis is concerned with the lateral performance of the HSC system and needs to be rejected. The standard deviation of lateral performance is marginally lower for the haptic conditions compared to the baseline manual driving condition. However, performance is not a very good metric in this driving scenario as the steering task was quite easy and only required completing the curves in a natural way. Higher LoHS values might be beneficial for achieving higher performance during more difficult tasks but this cannot be said for the driving experiment in this research.

This research is limited to investigating the effects of the LoHS setting. In order to find the optimal LoHS value for a given HSC implementation a different experiment design is needed. In such an experiment subjects are presented with two choices for the LoHS after which they indicate their preferred setting. This process is then repeated iteratively in order to refine the LoHS value with the highest subjective acceptance. More research is needed into how to properly select a combination of all FDCA parameters. An experiment varying both the SoHF and LoHS could

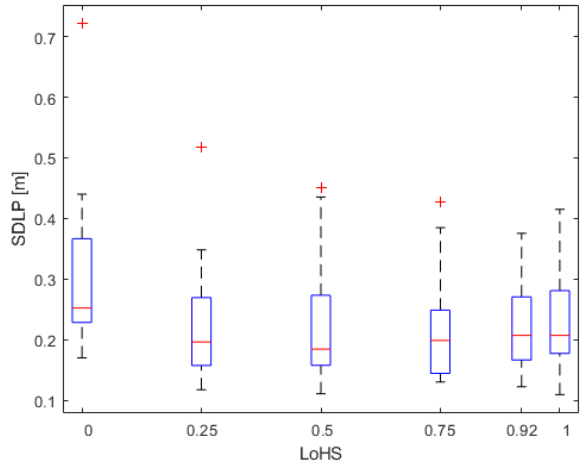

Figure 19: SDLP for every condition.

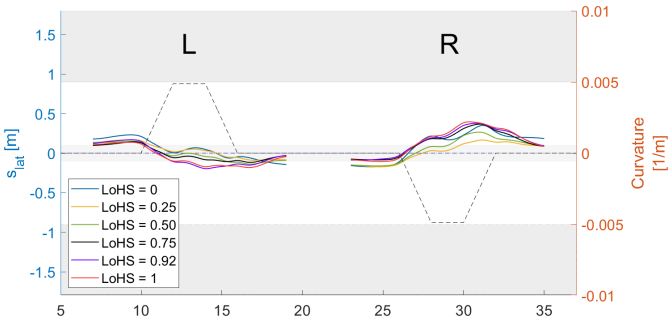

Figure 20: Average lateral position for left/right curves for every condition.

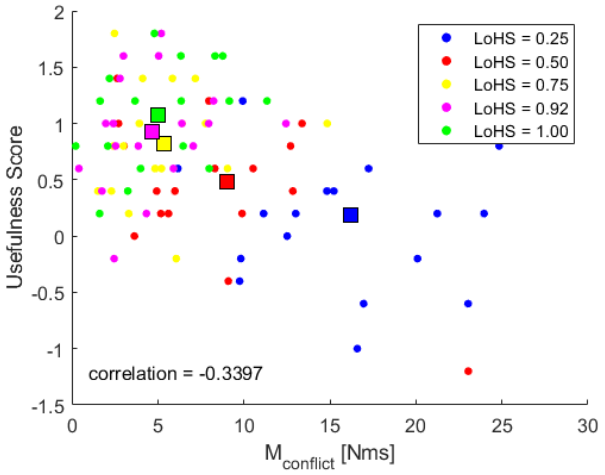

Figure 21: Correlation between usefulness score and conflict torque magnitude. Circles indicate the data for all subjects, squares indicate the mean for each experimental condition.

shed more light on how drivers perceive changes in the haptic controller. It is recommended to avoid a setting with high SoHF and low LoHS as this is known to cause a lot of conflict and instead increase both parameters simultaneously. Higher SoHF settings should be complemented

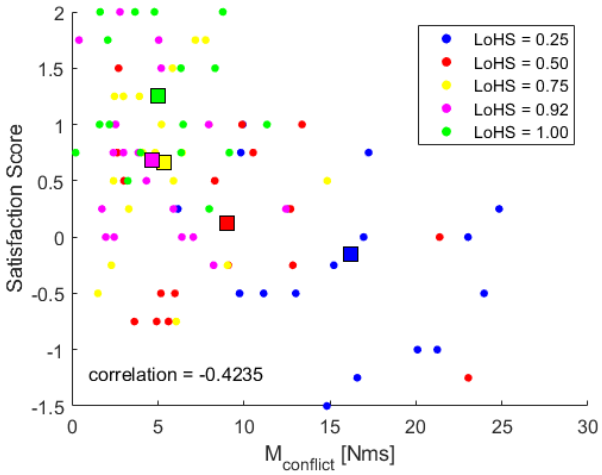

Figure 22: Correlation between satisfaction score and conflict torque magnitude.

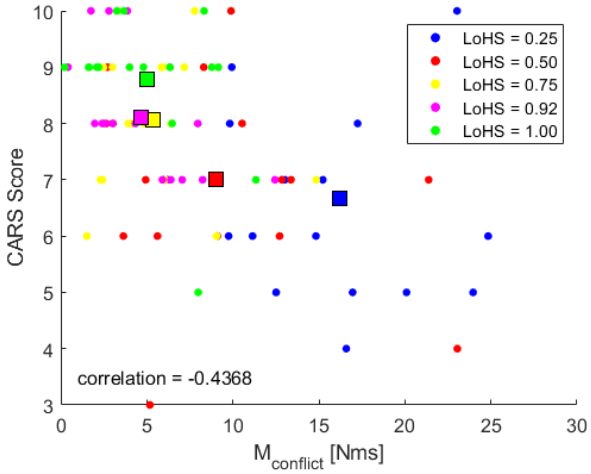

Figure 23: Correlation between CARS score and conflict torque magnitude.

by a higher LoHS. Furthermore, the exact impact of the LoHA parameter needs to be identified separately before it may be used in the haptic controller tuning process. This could be done using the same method as in this research where only one FDCA parameter was varied.

A selection of haptic settings may be found to work well for separate driving tasks. Haptic shared control has for example been shown to improve the skill level of novice drivers in rear parking [27]. Factors such as individual preference, road conditions and other external factors will likely complicate the inclusion of haptic steering support into the next generation of automated vehicles. Adaptive HSC solutions have the most potential to yield safety benefits without introducing torque conflict in safe driving conditions [24].

Finally, this study has shown the benefits of high LoHS settings for car steering. Torque conflict is reduced up to LoHS values in the range of 0.75 and 0.92 while better subjective ratings can be achieved for LoHS settings up

to 1. It is also shown that objective torque conflict and subjective ratings are correlated. A HCR with moderate curve cutting for implementation in the FDCA controller results in high acceptance amongst a group of 18 experienced drivers for a high LoHS.

VI. CONCLUSIONS

A gap in HSC research with regards to tuning of the LoHS of a FDCA type controller for car steering is addressed in this study. The goal of this research was to assess the acceptance of different design choices. The Van Paassen driver model is found to be effective at generating references with varying degrees of curve cutting. A current state-of-the-art HSC simulation was able to predict a reduction of torque conflict and driver steering effort for different LoHS settings. The model is less accurate at indicating the amount of conflict that may be expected across SoHF and LoHA settings. From a driving simulator experiment it was found that higher LoHS values for a FDCA type controller produce significantly higher levels of driver acceptance, both subjectively and objectively. The objective torque conflict metric and subjective Van der Laan and CARS ratings are correlated. Torque conflict is reduced by 70% for the highest LoHS compared to the lowest setting. Furthermore, the required driver steering effort was reduced strongly by up to 81% for the highest LoHS setting compared to manual driving. The law of diminishing returns becomes apparent for LoHS values around 0.75. However, no drawbacks were found when increasing the LoHS up to its highest setting. Small improvements are made past this point in terms of driver acceptance and steering effort. However, subjective satisfaction of the received support can still be enhanced by increasing the LoHS up to 1. A human-compatible reference with moderate curve-cutting is a promising starting point as evidenced by the closely matching lateral trajectories between the manual driving and haptic shared control conditions. Further reductions in conflict around the curve entry and exit phases can be achieved by updating the HCR to include prepositioning as long as this prepositioning type matches the driving style of the individual. This research has shown that all eighteen drivers in this study prefer a high LoHS setting between 0.75 and 1 for car steering in haptic shared control with a FDCA controller implementation.

References

[1] D. A. Abbink, M. Mulder, and E. R. Boer, "Haptic shared control: smoothly shifting control authority?," *Cognition, Technology & Work*, vol. 14, no. 1, pp. 19–28, 2012.

[2] D. A. Abbink, M. Mulder, F. C. Van der Helm, M. Mulder, and E. R. Boer, "Measuring neuromuscular control dynamics during car following with continuous haptic feedback," *IEEE Transactions on Systems, Man, and Cybernetics, Part B (Cybernetics)*, vol. 41, no. 5, pp. 1239–1249, 2011.

[3] R. Kondo, T. Wada, and K. Sonoda, "Use of haptic shared control in highly automated driving systems," *IFAC-PapersOnLine*, vol. 52, no. 19, pp. 43–48, 2019.

[4] M. Steele and R. B. Gillespie, "Shared control between human and machine: Using a haptic steering wheel to aid in land vehicle guidance," in *Proceedings of the human factors and ergonomics society annual meeting*, vol. 45, pp. 1671–1675, SAGE Publications Sage CA: Los Angeles, CA, 2001.

[5] D. A. Abbink, "Neuromuscular analysis of haptic gas pedal feedback during car following," tech. rep., TU Delft, 2006.

[6] R. Boink, M. M. Van Paassen, M. Mulder, and D. A. Abbink, "Understanding and reducing conflicts between driver and haptic shared control," in *2014 IEEE International Conference on Systems, Man, and Cybernetics (SMC)*, pp. 1510–1515, IEEE, 2014.

[7] M. M. van Paassen, R. Boink, D. A. Abbink, M. Mulder, and M. Mulder, "Four design choices for haptic shared control," *Advances in Aviation Psychology, Volume 2: Using Scientific Methods to Address Practical Human Factors Needs*, p. 237, 2017.

[8] N. Merat, A. H. Jamson, F. C. Lai, M. Daly, and O. M. Carsten, "Transition to manual: Driver behaviour when resuming control from a highly automated vehicle," *Transportation research part F: traffic psychology and behaviour*, vol. 27, pp. 274–282, 2014.

[9] E. P. Ghys, "Driver's acceptance of trajectory type in trajectory-driven haptic shared control," Master's thesis, Delft University of Technology, 2020.

[10] S. Barendswaard, *Modelling Individual Driver Trajectories to Personalise Haptic Shared Steering Control in Curves, Chapter 7: Four Design Choice Haptic Shared Controller to increase driver acceptance*. PhD thesis, Delft University of Technology, 2021.

[11] E. R. Boer, "Tangent point oriented curve negotiation," in *Proceedings of conference on intelligent vehicles*, pp. 7–12, IEEE, 1996.

[12] S. Barendswaard, D. M. Pool, E. R. Boer, and D. A. Abbink, "A classification method for driver trajectories during curve-negotiation," in *2019 IEEE International Conference on Systems, Man and Cybernetics (SMC)*, pp. 3729–3734, IEEE, 2019.

[13] S. Barendswaard, *Modelling Individual Driver Trajectories to Personalise Haptic Shared Steering Control in Curves, Chapter 6: Driver Prepositioning Modelling and Integration*. PhD thesis, Delft University of Technology, 2021.

[14] L. Saleh, P. Chevrel, F. Claveau, J.-F. Lafay, and F. Mars, "Shared steering control between a driver and an automation: Stability in the presence of driver behavior uncertainty," *IEEE Transactions on Intelligent Transportation Systems*, vol. 14, no. 2, pp. 974–983, 2013.

[15] S. Barendswaard, *Modelling Individual Driver Trajectories to Personalise Haptic Shared Steering Control in Curves*. PhD thesis, Delft University of Technology, 2021.

[16] F. Mars, M. Deroo, and C. Charron, "Driver adaptation to haptic shared control of the steering wheel," in *2014 IEEE International Conference on Systems, Man, and Cybernetics (SMC)*, pp. 1505–1509, IEEE, 2014.

[17] W. Scholtens, S. Barendswaard, D. Pool, M. M. Van Paassen, and D. A. Abbink, "A new haptic shared controller reducing steering conflicts," in *2018 IEEE International Conference on Systems, Man, and Cybernetics (SMC)*, pp. 2705–2710, IEEE, 2018.

[18] W. Vreugdenhil, "Complementing automotive haptic shared control with visual feedback for obstacle avoidance," Master's thesis, Delft University of Technology, 2019.

[19] V. Gruppelaar, M. van Paassen, M. Mulder, and D. A. Abbink, "A perceptually inspired driver model for speed control in curves," in *2018 IEEE International Conference on Systems, Man, and Cybernetics (SMC)*, pp. 1257–1262, IEEE, 2018.

[20] F. Mars, M. Deroo, and J.-M. Hoc, "Analysis of human-machine cooperation when driving with different degrees of haptic shared control," *IEEE transactions on haptics*, vol. 7, no. 3, pp. 324–333, 2014.

[21] G. Markkula and J. Engström, "A steering wheel reversal rate metric for assessing effects of visual and cognitive secondary task load," in *Proceedings of the 13th ITS World Congress*, Leeds, 2006.

[22] P. Choudhary and N. R. Velaga, "Analysis of vehicle-based lateral performance measures during distracted driving due to phone use," *Transportation research part F: traffic psychology and behaviour*, vol. 44, pp. 120–133, 2017.

[23] J. D. Van Der Laan, A. Heino, and D. De Waard, "A simple procedure for the assessment of acceptance of advanced transport telematics," *Transportation Research Part C: Emerging Technologies*, vol. 5, no. 1, pp. 1–10, 1997.

[24] H. M. Zwaan, S. M. Petermeijer, and D. A. Abbink, "Haptic shared steering control with an adaptive level of authority based on time-to-line crossing," *IFAC-PapersOnLine*, vol. 52, no. 19, pp. 49–54, 2019.

[25] S. M. Erlien, S. Fujita, and J. C. Gerdes, "Shared steering control using safe envelopes for obstacle avoidance and vehicle stability," *IEEE Transactions on Intelligent Transportation Systems*, vol. 17, no. 2, pp. 441–451, 2015.

[26] R. Parasuraman and V. Riley, "Humans and automation: Use, misuse, disuse, abuse," *Human factors*, vol. 39, no. 2, pp. 230–253, 1997.

[27] S. Tada and T. Wada, "Haptic shared control for backward parking and its effect on skill increase in novice drivers," in *2015 IEEE/SICE International Symposium on System Integration (SII)*, pp. 461–466, IEEE, 2015.

II

Literature Study Report

Graded separately for AE4020

1 Introduction

In the last decade the decreasing trend in the number of traffic accidents and fatalities has stagnated [1]. A significant contribution to this development is thought to be an increase in the number of elderly drivers due to the ageing European population. Innovative technologies such as haptic shared control could greatly benefit this demographic in realizing a safer and more accessible driving environment. Haptic shared control (HSC) is a new control paradigm that aims to improve shared control between human and automation by combining their inputs and providing the human with feedback on the control state that can be felt at the control device. This allows the human to effectively cooperate with the automation and achieve improved task performance while remaining actively involved in the control loop. In case of shared car driving systems the steering wheel and its dynamics shape the connection between a driver and the haptic support. The result is a novel means to inform the driver in addition to visual, auditory and vestibular cues. The integration of these signals in the central nervous system (CNS) allows drivers to react faster and more accurately to changes in the environment. Additional benefits include lower levels of control effort and reduced demand for visual attention [2]. Haptic interfaces have been studied extensively and are increasingly implemented in advanced driver assistance systems (ADAS) [3], [4], [5]. HSC has for example been effectively implemented in lane departure warning systems [6]. Furthermore, haptic interfaces have improved control system architectures such as those used for remote operating of UAVs [7] and training surgeons for minimally invasive surgeries [8]. Major advantages of haptic shared control include increased safety, situational awareness and the potential to reduce cognitive workload when implemented correctly.

Haptic support systems are an excellent candidate in the transition from manual to automated driving [9]. While the sophisticated cars of the future may not need any input from the driver in completing the required driving task, the present and near-future driving environment may involve intermediate automation levels that make use of control transitions between driver and automation [10] [11]. Significant advancements in areas such as vehicle-to-everything (V2X) communication, machine learning, artificial intelligence, sensing and computing are required to reach high levels of automation [12]. In the near future, these innovations will drive the development of advanced driver support systems that can adapt to the needs of various driver types [13] or even to the individual itself [14]. An important property of HSC systems is their ability to keep the human in the loop. As a result, they can help complete the transition from manual control to automated driving. Well-designed haptic shared control can greatly assist drivers in performing demanding tasks such as driving in heavily congested traffic, navigating narrow city streets and executing time-sensitive maneuvers [15]. Another area where haptic shared control systems can greatly benefit society is in supporting elderly [16], impaired [17] and novice drivers [18]. These groups often experience a low degree of mobility and can therefore potentially benefit the most. Finally, HSC systems can play a role in facilitating safe and effective driver lessons by educating the human-in-the-loop on the recommended steering input [17]. It is clear that HSC systems can benefit society in many ways.

A common indicator of successful cooperation between the driver and haptic support is the acceptance level [19] [20] [21]. High acceptance is realized when the intentions of the driver and haptic support agree throughout the duration of the steering task. Currently, little is known about how drivers' acceptance of the haptic support changes across the spectrum of haptic strength settings. An all-encompassing definition

of haptic strength does not exist as the term is used in different contexts between haptics shared control studies. This stems from the fact that the characteristics of the haptic support are highly dependent on the chosen architecture that generates the force and/or stiffness feedback. The four design choices architecture (FDCA) [22] defines haptic strength in terms of the identifiable components that together generate the haptic support. The four main design components in this innovative architecture enable the conception of a haptic shared control steering system which can be tuned ad hoc. A second metric for evaluating haptic shared control systems for car steering is the driver's engagement level in executing the steering task. It relates to the degree to which the human is actively involved in the steering task. Driver engagement levels are expected to change depending on the type and strength of the haptic support [23]. Evaluating how the human driver engages with each haptic setting may then provide an indication of the steering activity level of the human relative to the automation. Whenever the haptic support is unable to function normally (e.g. due to operational limits, failure or missing sensor data) an engaged driver is more likely to safely complete the driving task than an unengaged driver that is fully reliant on the automation to steer the vehicle [24]. This thesis attempts to address these knowledge gaps in the theory of haptic shared control. The research objective is thus as follows:

> *To evaluate haptic feedback strength settings in haptic shared control for car steering and their impact on acceptance and driver engagement.*

Nowadays, the strength of haptic feedback is often selected heuristically to achieve desirable properties of the shared control system. One of the few exceptions to heuristic tuning methods is the haptic support tuning philosophy for UAV teleoperation by Smisek et al. [25]. The knowledge gained on acceptance and driver engagement can be used in the design process of prospective haptic shared control systems. Such information is also valuable to predict how humans will use the HSC system in practice. Relevant human factors in haptic shared control such as workload and comfort will be considered as well. The goals of this research are achieved by answering the main research question:

> *How does haptic feedback strength affect driver acceptance and engagement in haptic shared control for car steering?*

The main research question can be divided into several sub-questions. By answering these sub-questions the main research question can be addressed in a stepwise manner. The following sub-questions are related to different aspects of this research topic:

1 Driver acceptance

- To what degree do steering wheel torques from the driver and haptic support agree?
- How satisfied are drivers with each haptic feedback strength?

2 Driver engagement

- How actively is the human involved in steering?
- How does the human steering contribution change across haptic feedback strengths?

3 Steering performance

- How well does the shared control system execute the steering task?
- How much variation in lateral performance occurs for different strengths of haptic feedback?

This thesis consists of two main parts. Part I is the scientific article that is written as a result of this research. Part II contains the thesis report and discusses (in order) the basics of HSC, haptic feedback strength settings, a literature review on haptic strength studies, a preliminary investigation using simulations, the HMI Laboratory experiment and results. The thesis report ends with a conclusion and some recommendations.

2

Haptic Shared Control Basics

This chapter starts by explaining the concept of haptic shared control in Section 2.1. Subsequently, Section 2.2 introduces design considerations for HSC systems as stated in the four design choices architecture. Hereafter, Section 2.3 contains a summary of the different haptic feedback settings and how they can be evaluated. A brief discussion on haptic shared control models for car steering is given in Section 2.4. Finally, Section 2.5 provides an overview of the key takeaways and conclusions based on the contents in this Chapter.

2.1. Concept of Haptic Shared Control

Haptic shared control can be defined as the cooperative control effort of a human and automation by continuously communicating forces on the control device [22]. A schematic representation of the haptic shared control concept is given in Figure 2.1. This overview illustrates how both parts of the shared control system contribute to the steering task. The human visual response to the road-vehicle environment produces a control torque on the steering wheel after being processed by the neuromuscular system. Secondly, the automation support generates a torque on the steering wheel based on a control law and the haptic controller settings. This haptic feedback torque actively guides the driver along the road. The torque contributions for each part are combined to produce a total torque that rotates the steering wheel which in turn results in a certain steering wheel angle.

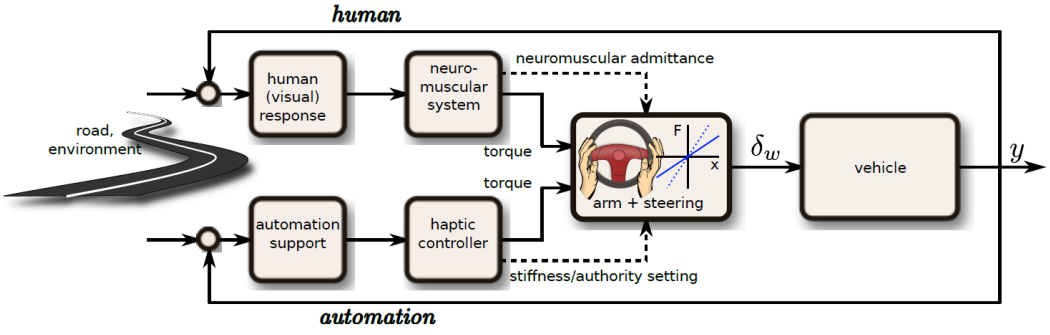

Figure 2.1: Schematic representation of haptic shared control [22]

The haptic shared control principle creates new characteristics that need to be considered by the engineers that design HSC systems. Firstly, the control input is no longer determined by just the human or automation but instead becomes the sum of both parts. A consequence of this control scheme is thus the necessity for the human and automation to understand each others' intentions. Secondly, interaction of the upper limb with the steering wheel couples the human neuromuscular system to the vehicle control system. As a result, any changes in steering dynamics or human admittance to steering wheel torques will affect the execution of the dynamic driving task. Therefore, the cooperative interaction between driver and

automation must be thoroughly investigated before haptic shared control systems can be implemented successfully. Additionally, the HSC paradigm requires the engineer to select a balance in control authority between the human controller and the haptic support. The strength of haptic feedback and the control law that governs it are major components in achieving the right balance. This can be achieved by following design considerations that have been established over the many years of haptics research, see Section 2.2.

Conceptually, haptic shared control relies on the driver to interpret the haptic feedback and perform the right control action. Significant mismatches between the driver and haptic support can limit the efficacy of the shared control system when the controller contributions oppose each other. As a result, the steering wheel torque from the driver can temporarily counteract the torque generated by the haptic support. In case of haptic shared control for car steering this phenomenon is known as torque interference. Conflicting torques are commonly found in HSC research [20] and their magnitude fluctuates throughout the duration of the steering maneuver. Torque interference can be the result of discrepancies between the driver model and real control behaviour. Another contributing factor is the selection of haptic controller gain settings. These settings tune the constituents (feedforward and feedback) that shape the steering torque support which is supplied to the steering wheel by the automation. As a result, the impact of these settings on the functioning of the shared control system is large [26]. Some underlying reasons for the aforementioned model discrepancies could be a limited understanding of human driving behaviour, neuromuscular adaptation to constant haptic feedback and modeling simplifications. Finally, a small but potentially significant source of torque interference may originate from the noise in the driver steering input inherited from the human motor system [27].

Early studies on a haptic steering wheel found improved path following performance and a significant reduction in visual demand [28]. Research on continuous haptic gas pedal feedback for longitudinal car following found effects similar to the lateral case: decreased physical control effort, increased or similar car following performance and the ability for haptic feedback to temporarily replace obstructed visual feedback [29]. It is also concluded that the design of haptic feedback is instrumental for developing a shared control system that poses benefits over the manual control case. Finally, haptic shared control has been proposed as a method to smoothly transfer control authority from automation back to the human [30]. This type of system evaluates the cooperative status between the human driver and automation such that the driver's intention to take over control can be detected. As a result, the occurrence of aggressive steering behaviour can be eliminated during a control transition from automated driving back to manual driving.

2.2. Four Design Choices Architecture

Paramount in successfully implementing a haptic support system is the design phase. Development of an aircraft autopilot requires knowledge on the different mission goals, aircraft dynamics, control surfaces and additional constraints and so forth. Analogously, a haptic shared control system designer must combine knowledge in several aspects such as: the goals of the haptic support and human controller, haptic feedback system settings and the corresponding shared controller qualities, interaction between human and automation. The four design choices architecture (FDCA) framework was developed as a result of lessons learned in evaluating haptic steering support with individualized references [22]. Figure 2.2 illustrates how the four design choices for the haptic feedback are linked to each other and combine to generate the haptic support.

This block diagram demonstrates how the FDCA allows the tuning of haptic feedback and feedforward to be performed separately. In a specific evaluation a haptic shared controller for steering that incorporates the FDCA framework was found to reduce the occurrence of conflicting torques by a factor of 2.3 compared to a conventional meshed haptic shared controller [21]. The FDCA can be used to streamline the design process of haptic shared control systems and consists of the following four design considerations:

- Defining a human-compatible reference (**HCR**) trajectory.
- Choosing the level of haptic support **LoHS**.
- Setting the strength of haptic feedback **SoHF**.
- Selecting the level of haptic authority **LoHA**.

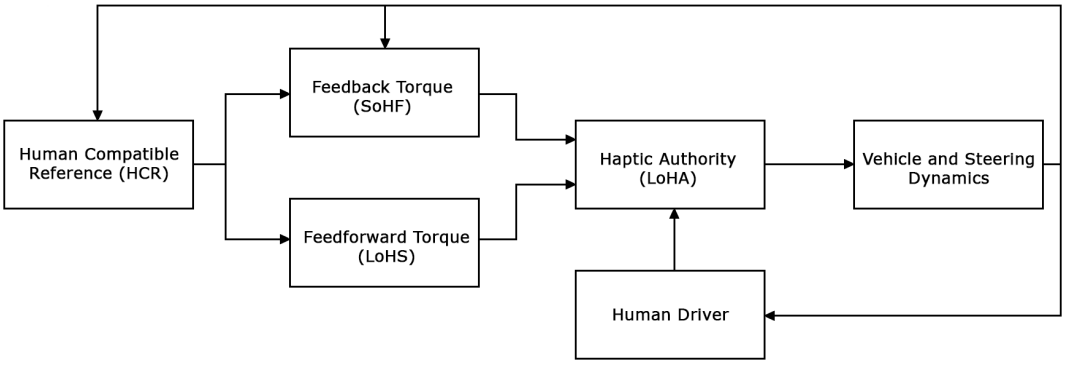

Figure 2.2: The four design choices architecture in relation to the haptic shared control system [21]

These design principles form the basis for the HSC steering model which is developed and discussed in this thesis.

2.2.1. Design Choice: HCR

An effective reference trajectory is essential in successful applications of HSC. The first rule states that the haptic support must follow a human-compatible reference trajectory. The reference trajectory for control of the vehicle must be perceivable to the driver such that this person can verify the integrity of the haptic support. Incongruence between the reference trajectories of the haptic support and the human will lead to an ineffective shared control system. This will lead to a significant amount of torque interference if the haptic feedback opposes the human part of the control input. Corner-cutting behaviour is observed for the majority of human drivers and must be taken into account in the design of a haptic steering support system. This can be done by generating a HCR trajectory that incorporates a realistic amount of corner cutting. The amount of corner cutting can even be personalized to account for different driving styles [31].

2.2.2. Design Choices: LoHS & SoHF

The feedforward part of the system models the human driver's capability to steer the car based on some preview of the road vehicle environment at a point in the future. The degree to which the haptic support adds to this feedforward control can be tuned using the level of haptic support (LoHS). As a result, a higher LoHS results in a haptic controller that places a larger emphasis on the feedforward part of the control loop. Furthermore, the feedback part of the HSC system corrects for lateral and heading errors between the reference trajectory and vehicle path. A design choice must be made in realizing a control law that effectively eliminates these errors. This haptic control setting is also called the strength and strategy of haptic feedback (SoHF). The combined working of the feedforward and feedback settings results in a haptic steering torque which is exerted on the steering wheel by the haptic controller. Consider the case where the haptic guidance is supposed to deliver the full steering input for completing the steering task. Additionally, assume that the human does not contribute any torque to the steering wheel. In this case, an incomplete feedforward steering torque (when LoHS < 1) is compensated for by the generated feedback torque as a result of setting the SoHF. The feedback loop generates the torque feedback over time based on the error with respect to the HCR. When the LoHS setting is decreased further the generated steering feedback will have to provide more torque to follow the HCR trajectory. Therefore, the setting for SoHF depends to some extent on the chosen value for LoHS.

2.2.3. Design Choice: LoHA

The level of haptic authority (LoHA) determines the balance between the human and the haptic support. The stiffness of the control device will impact its manipulability by the human driver. Consider a high level of haptic authority where a stiff steering wheel will barely rotate under a large torque from the driver. In this case very little control can be transferred from the human onto the system. As a result, the steering task functioning relies heavily on the control generated by the dominant haptic support. On the contrary is a lenient steering wheel that easily rotates under small torques produced by the driver's arm muscles. In this case the LoHA is set to a low value and the human can easily override the haptic support. Therefore, the LoHA selects the control balance somewhere in between the two extremes of manual control and fully

automated steering. The four design choices together are tuned in order to obtain a HSC system with desirable properties.

2.2.4. Additional Haptic Support Considerations

Another design requirement that remains of utmost importance in human-machine interface research is safety. Ensuring the safety of drivers within the HSC system can be accomplished in different manners such as through a control theoretic analysis of characteristic loci and M-circles [32] [33] and with robust control law designs [34] [35]. Dissipative (damping) elements are often included in haptic shared control systems to prevent unwanted oscillatory behavior due to phase lags. Co-contraction of muscles around the shoulder, elbow and wrist joints tightens the grip on the control device which can increase force loop gains [32]. Naturally, the stability loss due to this phenomenon is more pronounced for higher frequencies. Inherent operating limits of actuators and the potential occurrence of stiction can reduce the design space for HSC systems. Finally, to ensure that the HSC system remains within a stable operating region some tracking performance may need to be sacrificed [36].

Finally, the driver should always be able to override the additional torque imposed on the steering system by the haptic support. This is needed to ensure that in all cases the driver remains in charge of steering. Effectively, the human will thus always have the final authority to steer the vehicle. As a result, the role of the driver does not change to the role of supervising the automation, a control architecture which can cause a loss in awareness, complacency and skill degradation which can lead to a slow or inadequate response in case of an automation failure [37]. This also allows the driver to estimate whether the automation is still working as intended.

2.3. Haptic Feedback Generation

Haptics have been used in a large variety of applications and their haptic feedback settings are often designed heuristically. Haptic modality can be defined as the method through which the haptic design interacts with the human. A survey of haptic modalities for lane departure warning systems was performed by Beruscha et al. [6]. Their paper identifies two main groups of haptic warning signals: signals based on additional torque and signals induced by motors with eccentric weights. The first group works by exerting an additional torque on the steering wheel using an electric motor in the steering column. The addition of this steering torque can rotate the steering wheel if it is large enough and will then affect the trajectory driven by the car. The second group provides the driver with warning signals through vibrations which are generated with motors embedded within the steering wheel. These vibrations will not affect the steering wheel angle directly but can be used by the driver to make an informed steering decision. The remainder of this section and thesis will focus on the first group (steering wheel torque signals) because of their potential for haptic shared control in car steering.

The haptic feedback mechanism generates a haptic sensation at the steering wheel through force feedback, stiffness feedback or a mix of both. Note that force feedback on the steering wheel essentially amounts to torque feedback. Figure 2.3 illustrates the effect of force and stiffness feedback on steering wheel characteristics [38]. The driver can sense a change in these characteristics and as such be guided to apply an appropriate steering wheel input with the end goal being to safely complete the steering maneuver. The haptic support will then guide the driver along the reference trajectory which is some function of the road curvature κ. This reference trajectory depends on the chosen driver model and may include factors such as curve cutting, see Section 2.4.

The amount of torque feedback is a function of a performance criterion such as time-to-line crossing (TLC) or the amount of deviation from the reference trajectory. Deviation from the reference trajectory is often computed as a weighted sum of the heading and lateral deviations. In case of mixed force-stiffness feedback, a supportive torque will turn the steering wheel towards the desired steering wheel angle and a virtual stiffness is added around the desired steering angle. This stiffness contributes to the Level of Haptic Authority (LoHA) setting in the four design choices architecture. A higher stiffness will reduce the driver's ability to deviate from this steering angle as more torque is required. This may lead to improved steering performance at the risk of negatively affecting the human acceptance of the support and their feeling of being in control [39]. Another possibility is to design adaptive haptic feedback that operates at a low stiffness when the driver stays within specified margins of safety and switches to high stiffness in dangerous situations. A study on situation-adaptive LoHA during lane-keeping based on TLC found that compared to

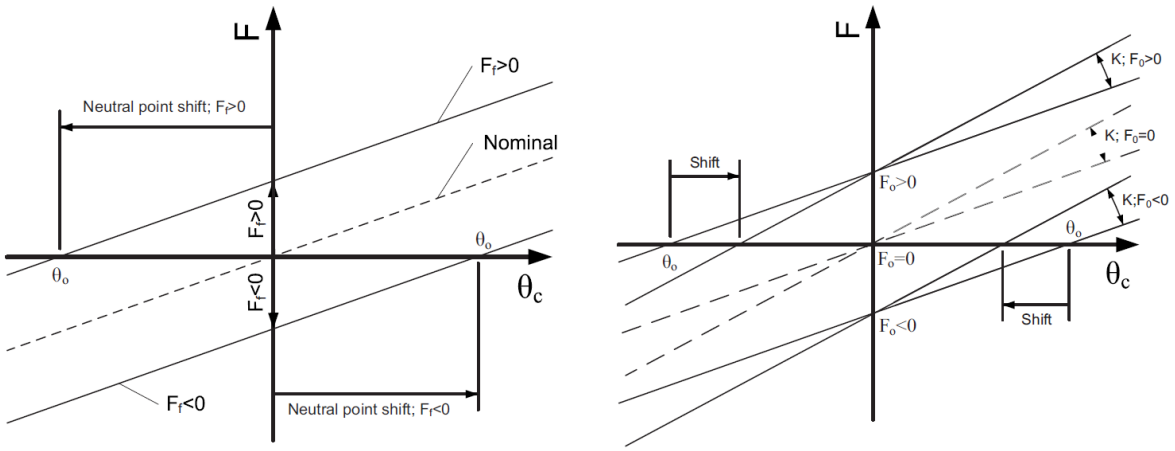

Figure 2.3: Force and stiffness feedback mechanisms for a steering wheel. Positive force feedback F_f translates the force-position curve upwards and shifts the neutral point to the left, vice versa for negative F_f. Stiffness feedback K rotates the force-position characteristic around the zero-force axis and shifts the neutral point θ_0 when an offset force F_0 is present. [38]

a high LoHA controller adaptive LoHA controller designs resulted in similar safety margins and decreased conflict torques [39]. A conventional (unadaptive) haptic feedback design can be made unobtrusive to the human by selecting a low torsional stiffness and a maximum for the haptic steering wheel torque. This will limit the haptic control authority and allow the driver to steer away from the suggested steering angle if desired without requiring too much muscular effort. This type of haptic design was studied by Griffiths et al. with a torsional stiffness of 1.2 Nm/rad and a maximum haptic torque of 0.82 Nm [40]. A drawback of such a design is the limited improvement in steering performance.

The amount of torque should be above a lower limit such that it is consciously felt by the driver. Additionally, the torque feedback should not be too high such that driver input becomes too difficult or uncomfortable. A study on driver perception of steering feel revealed that drivers have a better sense of steering wheel force and steering wheel angle rather than steering wheel torque and steering wheel displacement [41]. Human internal estimation of torque relies on force estimates and knowledge of the distance between the hands and centre of the steering wheel. The steering wheel radius will thus scale force perception and change the steering feel. Furthermore, to judge steering wheel displacement humans are required to combine joint angle estimates with limb length [41]. Consequently, the authors of [41] attribute their findings to the fact that estimation of torque and distance requires more information and greater processing than the estimation of force and angle. Other research indicates that steering wheel force perception depends on the steering wheel angle and the direction of the load [42]. A second experiment by Newberry et al. [41] revealed that a difference of 15% and 14% for steering wheel force and angle, respectively, was required in order for those differences to be detected. This just noticeable difference in physical magnitude of a stimulus is known as a Weber fraction [43]. The steering force perception was also independently found in [42] to follow the Weber-Fechner law [44]. Other research has found Weber fractions of 7% for forces in the elbow flexor muscles [45] and 13% for torque sensitivity of the hands [46]. Stiffness was harder for humans to discern with their wrist at a Weber fraction of 22% [47]. A third experiment by Newberry et al. showed that neither the perception of steering wheel force nor the perception of steering wheel angle is linear [41]. The rate of growth of sensation for steering wheel force was 1.39 and 0.93 for angle. As a result, when the applied steering wheel force is doubled the sensed force increases by a factor of 2.62. Knowledge on how humans perceive haptic feedback and what differences can just be noticed will be very useful for designing an experiment that can be used to evaluate haptic steering feedback settings.

The natural adaptability of the human neuromuscular system (NMS) is an area that is often omitted in the design of HSC systems. Multiple studies have found the presence of a human frequency bandwidth for energy-efficient reflexive responses [48] [49]. Instantaneous muscle co-contraction is possible for higher frequencies than indicated by this bandwidth at a high energy usage cost [50]. The reflexive response depends on several factors including task instruction, amount of steering rotation, steering force, haptic feedback force bandwidth and muscle co-contraction [48]. As a result, investigating the effects of haptic feedback on the driver's neuromuscular dynamics is of key interest to HSC research. Higher levels of haptic

feedback can result in more NMS adaptation to external torques which can be measured as a smaller admittance. The amount of adaptation will also depend on how accepting the human is of the haptic support. Haptic feedback forces that are perceived as being too strong result in nuisance and fatigue after some time. A driver can resist the haptic feedback by increasing their limb stiffness, give way to the haptic feedback force, ignore it or let go of the steering wheel altogether [51]. Throughout this spectrum of responses it is found that grip force also changes depending on the human where the grip force varies inversely with the admittance [52]. This grip force can be measured with sensors in the steering wheel in order to adapt the stiffness of the haptic support (i.e. the level of control authority). Such a grip-adaptable HSC system was found to increase performance over unassisted control and weak guidance systems while reducing the operator physical control effort needed to cope with disturbances [25].

2.4. Driver Steering Models for HSC

Models of human steering control can be conveniently partitioned into the categories of pursuit, preview and optimal control [53]. Contemporary models are not as easily classified and often choose a control strategy which relies on some combination of feedback and feedforward control. In these models the feedback control loop is responsible for correcting short-term deviations from an operating point such as the centerline or road surface markings in a turn. Additionally, the feedforward part of the control scheme determines the required steering angle for a given preview time based on the steering system and a disturbance in the environment. In case of steering models this disturbance is the road curvature κ at a future point in the turn. Naturally, within a set of humans different driver types can be identified with varying control strategies [26].

The efficacy of HSC systems can be adversely affected by significant interference between human and automation control inputs. Reducing torque interference is crucial in developing haptic systems that are accepted by the complete spectrum of driver types. A typical example of conflicting human-machine intentions is the case of a steering task in which the driver opts to cut a corner while the automation prefers to steer the vehicle more along the road centerline. The resulting haptic support may then be negatively perceived by the driver as intrusive and ineffective if its control authority is large enough. Human drivers are not strictly optimal controllers but rather controllers which accomplish tasks in a subjectively satisfactory manner [54] where a multitude of safe trajectories are possible [38]. It is known that drivers strive to stay within certain safety margins and only accept limited risk [55]. The remainder of this section discusses steering models for HSC systems and how they attempt to replicate human steering behaviour.

The first driver models were based on the seminal work on the crossover model introduced by McRuer [56] who introduced a dedicated driver model based on his findings [57]. The theory behind the crossover model combined with verbal adjustment rules gave rise to a practical way of modelling a large variety of manual control systems. However, the crossover model only captures a small part of human driving behaviour due to the simplified model structure and the fact that it is only valid around the crossover frequency. Another shortcoming of the crossover model is the absence of preview control. More recently, two-point visual driver models were developed to explicitly make use of the notion that drivers use information from near and far viewpoints on the road to steer the vehicle [58]. The near point is slightly in front of the car and is used for feedback control. Additionally, the far point is located at or near the tangent point and is used for anticipatory preview control. However, the explicit manner in which the driver switches between the two viewpoints is not well-defined and also needs to be modelled [59]. An example of a two-point steering model is the model developed by Sentouh et al. [60], also sometimes referred to as the Mars model [19]. A block diagram of this model is given in Figure 2.4.

The addition of the preview point sparked research into multipoint models which use a set of preview points distributed over a finite interval on the future trajectory. A cost function is then minimized in order to determine the optimal path through these preview points. These optimal steering control models have been developed by Sharp et al [61]. Optimal control have been combined with robust control by Saleh et al. to obtain a so-called H2-preview control model for car steering [62].

Research efforts by Van Paassen [22] and Barendswaard et al. [63] culminated in a driver steering model with explicit feedforward control based on the four design choices architecture. A block diagram of the Van Paassen model is given in Figure 2.5. In the remainder of this thesis this driver model is referred to as the Van Paassen model. Feedforward control generates a steering input based on the curve cutting distance

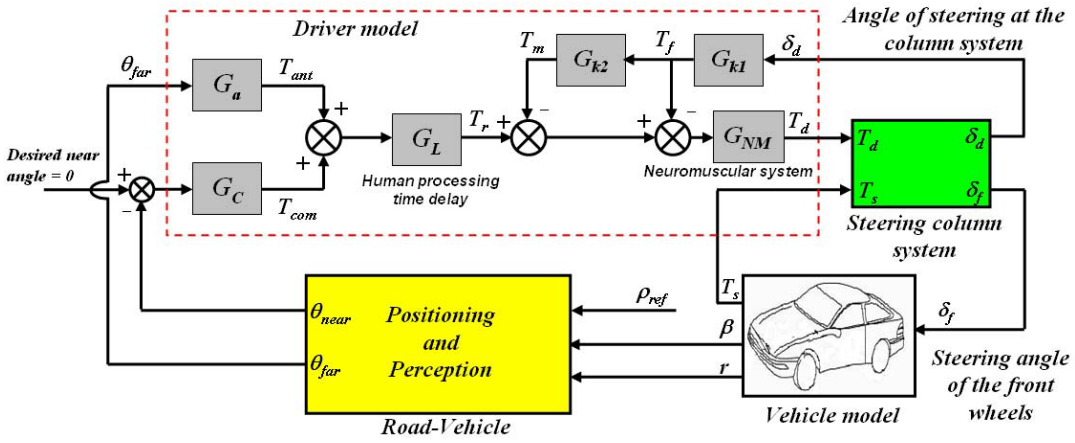

Figure 2.4: Sentouh two-point driver model [60]

at a lookahead time τ_{LH}. The curve cutting distance y_{cc} is computed with the filtered road curvature at this preview point. Road curvature is filtered with a second order filter with a break frequency at T_{hs} to ensure smooth transitions between straight roads and curve driving. The feedback control loop corrects for lateral deviation from a predicted position at the prediction lookahead time τ_p. This predicted position is computed by linear approximation and uses the curve cutting distance as a reference. The prediction lookahead time should be calibrated to the filter break frequency and lookahead time such that the lateral position error is compensated: $\tau_p = \tau_{LH} - T_{hs}$. This lateral position error from the curve cutting reference is then magnified by the feedback gain K_{FB} and scaled by K_δ (identified human curve negotiation parameter) and K_w (steering wheel stiffness) to convert the lateral error into a guidance force. Filtered road curvature is amplified by a feedforward gain K_{FF} and scaled by K_w, the effective steering ratio K_{eff}, the wheel base L_{wb} and the velocity V to produce a steering angle proportional to the yaw rate in the curve. The human neuromuscular dynamics are given by the transfer function H_{nm}. A driver model assessment found that the Van Paassen model is the most suitable driver model for generating individualized steering behaviour [64]. Curve cutting is found to be stronger in experienced drivers (independent of age) while younger inexperienced drivers tend to drive the car closer to the road centerline [16].

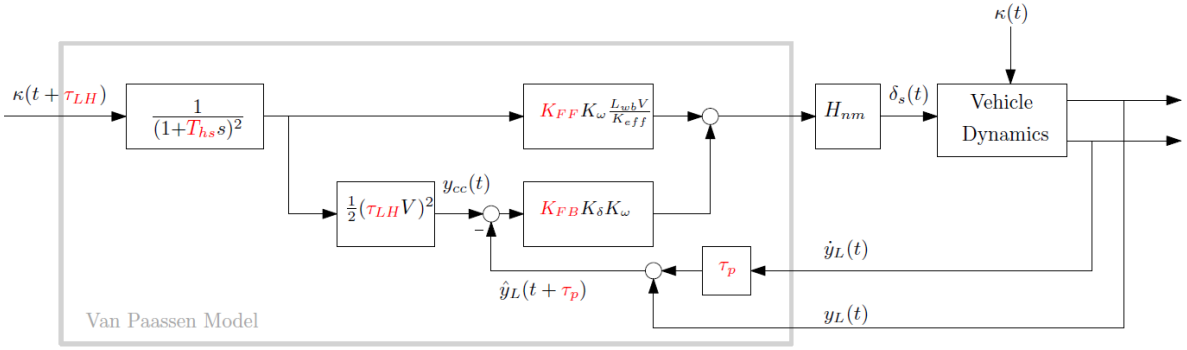

Figure 2.5: Van Paassen driver model [22]

Inoue et al. [65] developed a shared control steering assistance system which combines haptic steering guidance torques with direct yaw-moment control for enhanced path tracking performance and good human-machine cooperative characteristics. The system employs a first order preview-predictive expert driver model combined with an independent direct yaw-moment control input. Furthermore, a control law governing the haptic steering torque is based on the steering wheel angle deviation from the reference (expert driver) steering wheel angle for a preview time T_{ps}. The addition of direct yaw control compensates for the effect of the self-aligning torque term. As a result, the gain on the haptic steering guidance torque could be set to a comparatively lower level. This ensures that the driver can still intervene with the system and torque interference in the inner-loop is reduced. The effectiveness of the system was evaluated in

an elderly driver experiment and resulted in good path tracking performance and a small reduction in torque interference between driver and automation. In conclusion, this research found a work-around that mitigates the effect of torque disagreement between human and automation by adding a secondary independent steering input. However, as stated by Abbink et al. [51] the neuromuscular response of drivers to haptic feedback must be well-understood to prevent subtle conflicts between driver and shared controller. Development of a HSC system must include this principle in order to be applied successfully.

The apparent stiffness of the steering wheel due to self-aligning torque on the front wheels is often included in driver models for a more realistic feel of the steering dynamics. Mass and damping properties of the steering wheel also contribute to dynamic characteristics and are generally set close to their real values. Lateral vehicle dynamics are commonly simulated with a linear bicycle model that can be obtained by decoupling longitudinal and lateral dynamics and only keeping the lateral and yaw dynamics. This kind of bicycle model assumes small steering angles and a linear tire model. Neuromuscular dynamics can be modelled as a first- or second-order system and are sometimes lumped together with the steering wheel dynamics.

2.5. Key Conclusions for Chapter 2

This section contains a summary of the key takeaways and conclusions based on the contents in Chapter 2. The conclusions are given in bullet point form within boxes that follow the order of the topics as presented in this Chapter. Finally, a statement is made on how all the information gathered here will contribute to shaping the research project contained within this thesis.

Concept of HSC and Knowledge Gap

- Haptic shared control for car steering is a novel control architecture that enables the human to steer a car together with an automated agent. A knowledge gap in HSC research exists with regards to how human acceptance varies for haptic steering support systems with different settings.
- HSC systems can offer improved path following performance and reductions in the driver's visual demand and control effort. Simultaneously, torque interference is commonly found to occur between the driver and the haptic support which can affect the human acceptance of the overall HSC system.

Four Design Choices Architecture

- The four design choices architecture (FDCA) summarizes design considerations for the identified adjustable components of HSC systems. The FDCA stipulates that the basis for the trajectory of the haptic support should be compatible to the reference of the human. This is known as the human-compatible reference (HCR). Additionally, the haptic guidance consists of a feedforward and a feedback component which are generated based on the selected HCR. The feedforward component is scaled by the level of haptic support (LoHS) and the feedback component is scaled by the strength of haptic feedback (SoHF). Finally, the level of haptic authority (LoHA) sets the control authority of the haptic automation by adjusting the steering wheel stiffness.
- Inherently, the four design choices shape the feel of the haptic feedback on the steering wheel as perceived by the human. Acceptance and driver engagement are hypothesized to change depending on the different settings selected for these four components.

Haptic Force Generation

- Haptic force generation can consist of force, stiffness or a mixed force stiffness feedback principle. Compared to the force or stiffness principles there is less research specifically dedicated to studying the intricacies of mixed force stiffness feedback.
- The human perception of forces, torques and angles on the steering wheel have been studied extensively and estimates for internal estimation limits of these parameters are available. The interconnected nature of the HSC system implies that the human neuromuscular system and adaptation could be linked to the type and strength of the haptic steering support. Depending on the individual a driver may choose to accept, ignore or reject the haptic steering support in addition to removing their steering input if the haptic support is deemed as satisfactory.

Driver Steering Models for HSC

- Humans steer their vehicle in different ways through a corner. Some people exhibit prepositioning while others do not. Simultaneously, curve cutting has been found in a large proportion of experienced drivers as opposed to more novice drivers that tend to steer closer to the road centerline. The human control strategy is somewhat of a black box where areas such as task complexity, efficiency, satisfactory performance and safety margins intersect each other as part of the decision making process.
- Driver steering models attempt to simulate the human steering response to a given road trajectory. Some models only include feedback loops while others use a combination of feedback and feedforward loops. Several types of steering models can be identified including: two-point angle-based models, curvature based feedback and feedforward models, yaw rate control and torque feedback models, multipoint models and optimal control models.
- In order to simulate a complete HSC implementation it is necessary to integrate the driver steering model with the haptic control generation logic, the neuromuscular dynamics, steering wheel dynamics and vehicle dynamics.

Implications for Research

- Findings from previous research suggest that the Van Paassen model is the most suitable steering model for generating individualized human-compatible references [64]. The haptic support will be generated according to the design considerations as detailed in the four design choice architecture. Through this method it becomes possible to evaluate how a change in one or multiple FDCA parameters impacts human acceptance and engagement levels. Using the limits on human internal estimation of steering force in the literature it is possible to design experimental conditions with several discernable levels of haptic support that are within the perceivable and acceptable limits.

3

Effects of Haptic Feedback

This chapter starts with a discussion on how humans accept various levels of haptic feedback, see Section 3.1. Hereafter, driver engagement in the haptic shared control environment is discussed in Section 3.2. Subsequently, the steering performance and its relation to haptic feedback settings will be discussed in Section 3.3. Section 3.4 summarizes several complicating factors that are inherent to haptic shared control research. Finally, in Section 3.5 an overview is provided of the key conclusions from the present Chapter.

3.1. Acceptance of Haptic Feedback Settings

The importance of acceptance is evident from the way in which humans interact with machine systems. Humans are unlikely to utilize systems if they fail to effectively support completion of the task at hand. As a result, *acceptance* is a key indicator for evaluating how satisfied users are with the haptic feedback that is presented to them. The concept of acceptance is not consistently defined throughout human-machine research and has been measured in terms of safety, comfort, trust, ease of use or efficiency [66]. Throughout this thesis the following definition of acceptance of HSC systems will be used: acceptance is the degree to which an individual intends to use a system and, when available, to incorporate the system in his/her driving [26]. As driver acceptance of the haptic support increases, the benefits of HSC become more prevalent. A higher acceptance should be related to improved cooperation between human and automation. Acceptance will vary depending on the haptic feedback settings. Therefore, evaluation methods and metrics are needed to determine the acceptance level for a given haptic feedback condition.

Acceptance can be measured objectively and subjectively. Humans are known to be imperfect at making subjective assessments of human-machine systems. Subjective metrics can lose some of their value due to issues related to (confirmation) bias, experience level, individual differences and sensitivity to the used subjective scale. Some of these problems can be partially accounted for thanks to thorough experiment design and scientific procedures. Subjective assessments may still present interesting findings since human perceptions are almost certainly deeper, more complex and more subtle than external observations [67]. An approach to ensure the validity of collected acceptance data is the concept of convergent validity. By combining two independent methods of measuring acceptance it is possible to assume validity of the data if the same results are found in both metrics. Combining objective and subjective acceptance metrics is thus an excellent way to obtain reliable results.

Subjective assessments can be obtained using several principles such as ranking, rating, questionnaires, interviews or checklists. A common method for measuring acceptance in driving systems research is the Van der Laan questionnaire [68]. This questionnaire consists of nine five-point rating-scale items which need to be ticked off by the subject, see Figure 3.1. The responses are then used to generate satisfaction and usefulness scores which can be statistically analyzed [26] [21] [69]. Mars et al. [19] evaluate subjective acceptance indirectly using a combination of four metrics of comfort, safety, control and attention. Another rating scale that can be used in subjective evaluation is the controller acceptance rating scale (CARS) [70]. This is essentially a modified inverse version of the Cooper-Harper scale [71] where a score of 1 indicates a haptic controller with major deficiencies and a score of 10 indicates a highly desirable and excellent haptic

controller.

My judgements of the (...) system are... (please tick a box on every line)		
1	useful	useless
2	pleasant	unpleasant
3	bad	good
4	nice	annoying
5	effective	superfluous
6	irritating	likeable
7	assisting	worthless
8	undesirable	desirable
9	raising alertness	sleep-inducing

Figure 3.1: Contents of a Van der Laan questionnaire [68]

Objective acceptance metrics are usually defined with regards to the amount of torque interference. The occurrence of torque conflict can be quantified as the time percentage for which the two torques are opposed. Alternatively, agreement between operator and haptic support can be based on a magnitude and sign comparison which are calculated in discrete time. The magnitude is computed as the root mean square error if the driver and haptic torque are of opposite sign, see Equation 3.1, and the sign is time-averaged with a range from 0 (total disagreement) to 1 (perfect agreement), see Equation 3.2. Consequently, the sign comparison indicates the frequency of torque conflict (identical to the time percentage of conflict) while the magnitude comparison reveals how much the torque disagrees on average.

$$M_{\text{rms}} = \sqrt{\frac{1}{N}\sum_{i=1}^{N}(|T_{Driver}(i)| - |T_{Haptic}(i)|)^2} \tag{3.1}$$

$$M_{\text{sgn}} = \frac{1}{N}\sum_{i=1}^{N}\text{eql}(\text{sgn}(T_{Driver}(i)), \text{sgn}(T_{Haptic}(i))) \tag{3.2}$$

Finally, objective acceptance can be evaluated by the amount of torque conflict occurrences that meet criteria such as a minimum duration and magnitude to be registered as a conflict.

3.2. Driver Engagement in HSC

An advantage of HSC systems over highly or fully automated driving systems is that the driver remains actively involved in the control loop [19]. Research on cooperative steering revealed that human drivers are highly able to successfully negotiate in ambiguous obstacle evasion scenarios using only haptic communication [72]. Similar research found that drivers were able to interpret simple trajectory intentions conveyed by an external human acting as a driving agent [73]. Driver engagement can be used as a means to capture changes in human control behaviour and strategy. This information can then be used to design HSC systems that keep the driver sufficiently involved in the execution of the steering task.

Driver engagement can be measured objectively with metrics related to control activity such as the standard deviation of steering wheel angle or steering rate. Another common metric for driver engagement is the steering wheel reversal rate (SWRR). It is known that the SWRR is affected by task difficulty and its demand on human cognitive abilities [74]. Furthermore, the SWRR is known to be a metric which is very sensitive to different steering conditions [75], [19], [76]. Subjective assessments related to workload may provide an indication of the perceived level of engagement. Driver engagement in low levels of haptic feedback should be similar to manual driving. On the other hand, when the amount of haptic feedback increases the level of engagement may either increase if the human disagrees with the automation or decrease if a large part of the steering task execution is transferred to the haptic support. It is, therefore, difficult to predict driver engagement.

Cnossen et al. measured driver engagement, referred to as invested effort, in car following as a function of task demands, driving speed and mental effort [77]. Car following was investigated in a simulator for three conditions: normal driving, driving in a hurry and accurate driving. In this study heart rate and heart

rate variability were used as measures of mental effort. Heart rate variability is more sensitive to cognitive processed involved with information manipulation in working memory. Furthermore, a subjective measure of invested mental effort was based on a rating scale for mental effort. The results indicated that heart rate variability is affected substantially by the car following condition and resulting workload. Therefore, driver engagement was significantly higher in the fast driving condition.

3.3. Steering Performance

The effects of HSC on steering performance have been investigated extensively in recent research [78] [38] [19] [65] [79] [26] [69]. A major potential benefit of HSC is reduced control effort with similar or even increased task performance [2]. For example, a haptic gas pedal design for active car-following resulted in a reduction in control effort and increased car-following performance [80]. Similarly, in the lateral case Mars et al. [19] found that all settings that included haptic support improved the lateral steering error except for the highest intrusive setting where an increase in lateral standard deviation (SDLP) occurred which indicated the presence of significant human-machine conflict. Literature indicates that reduced control effort and increased task performance can be achieved for car steering in a HSC environment [40], [19]. Steering task performance can be evaluated with a number of metrics such as: mean lateral position (MLP) [19] [28], standard deviation of lateral position (SDLP) [19] [76], root mean square of lateral error [40] or safety-related metrics such as time-to-line crossing (TLC) [21] [39]. Steering performance can be enhanced by adaptively increasing the authority level of the haptic controller in safety critical situations [39]. This will come at the cost of reduced driver acceptance if the driver perceives the haptic feedback as too intrusive. The inherent result is that tuning the strength of the haptic controller becomes a trade-off between steering performance and driver acceptance.

While performance benefits of HSC systems have been found as summarized in this Section there is also a number of risks that come with the implementation of the HSC structure. An obvious risk is a malfunction in the logic that generates the haptic steering support. Assume in this case that the haptic steering torque will steer the car off the road. Such errors are then likely to be noticed by the driver at the steering wheel. This could lead to extremely dangerous events if the driver is not properly engaged in the control task and cannot be the fallback mechanism needed to properly steer the vehicle. In such an event, a higher LoHA (e.g. larger than 1) will be particularly problematic for the driver as their required steering force is larger than in the manual driving case. It is known from human factors research that other risks are present which are associated with the human nature [81]. These include misuse due to over-reliance or a loss in steering skills due to reduced task demand [2]. The extent to which these risks are present may change depending on the haptic support settings and the control authority allocation between the human and the automation. Attempts have been made to establish a generalizable driver model (i.e. a unified theory that can explain human driving behaviour for different driving scenarios) based on a safety-related risk metric [82]. However, no precise data is available on the risks associated with HSC as a function of HSC settings in the literature at the time of writing this report.

3.4. Complicating Factors

Haptic shared control research is inherently complex due to the intricate nature of the human response and interaction with the automated part of the control system. This section discusses some prevalent factors that complicate this research project.

3.4.1. Human Adaptability

Completing a car steering task requires the human to actuate the pedals and steering wheel properly. An essential element for completing such tasks is the sense of body position, movement and acceleration. These measurements are collected in the human body by a sense known as proprioception: the sense of self-movement and body position. Proprioception can occur due to the integration of information from the vestibular system in the inner ear (motion and orientation) and stretch receptors in muscles (stance). Proprioceptive control depends on proprioceptors which are mechanosensory neurons located within muscles, tendons and joints. Proprioceptor neurons are distributed throughout the human body and comprise of three types. The first type are muscle spindles which are embedded in skeletal muscle fibers. These neurons sense a limb's velocity and its movement by detecting changes in length of the muscle fibres. The second type are Golgi tendon organs at the interface of muscles and tendons. Their role consists of

detecting the load on a limb and become active once a given threshold in muscle force is reached. A third type of proprioceptor neurons are joint receptors which are low-threshold mechanoreceptors embedded in joint capsules. These receptors activate when a joint is in an extreme position.

The proprioceptors play an important role in reflexive movements in the human body. The Golgi tendon reflex prevents muscles and tendons from damage and may help to spread load on the muscle throughout its muscle fibres. This effect is obtained through a negative feedback mechanism that activates upon reaching a tension limit in a muscle or joint. According to Abbink [29] the force feedback functionality of the Golgi tendon organ reflex is expected to play in important role in interaction with haptic driver support systems. Information from the proprioceptors is, however, also passed to the central nervous system (CNS). The CNS combines this information with vision and the vestibular system to generate an internal representation of the body position, movement and acceleration. Proprioceptive sense adapts to a continuously present stimulus which is called habituation, desensitization or adaptation. Subsequently, proprioceptive feedback becomes unnoticed in the human mind and disappears to the background. This should alleviate a human's attention such that its focus can shift to other concerns or tasks at hand.

Admittance is a measure of the causal dynamic relationship between force inputs and the resultant displacement and it can describe neuromuscular mechanisms that occur in motion control. The inertial, elastic and viscous properties that characterise the dynamic neuromuscular settings of the human body can adapt to changing environments through muscle co-contraction and reflexive activity. An advantage of using admittance as an overarching measure of neuromuscular activity is that it can be estimated by frequency response functions. Frequency-domain estimates of admittance allow measuring a driver's frequency response at the frequencies where the disturbing force(s) contain power. For example, Abbink et. al. [83] computed the admittance relationship between driver torque (input) T_c and gas pedal rotation (output) θ_c at the force disturbance frequencies f_t according to Equation 3.3 for classical tasks (rest, position or force task). The computation uses estimates of the cross-spectral density of disturbance and pedal rotation ($\hat{S}_{T_{dist}\theta}$) and the cross-spectral density of disturbance and driver torque ($\hat{S}_{T_{dist}T_c}$).

$$\hat{H}_{adm}(f_t) = \hat{H}_{T_c\theta_c}(f_t) = \frac{\hat{S}_{T_{dist}\theta_c}(f_t)}{\hat{S}_{T_{dist}T_c}(f_t)} \tag{3.3}$$

Admittance models are often second-order transfer functions and have been applied in human driver research projects that aim to investigate the neuromuscular dynamics [84], [85], [86].

Neural adaptation is defined as a gradual decrease over time in the responsiveness of the sensory system to a constant stimulus. The adaptability of the human to external forces will, therefore, play an important role when haptic support forces are continuously communicated at a significant magnitude. A NMS-based analysis of the upper limb should be included to understand human perception of haptic steering wheel torque. The complex joints in human arms can change their axes of rotation during movement. Using the following rigid-body assumptions a pragmatic model of the human arm can be developed [87]:

1. The deformation of soft tissues does not significantly affect the mechanical properties of the limb segment as a whole.
2. Within each segment (forearm and upper arm), bones and connective tissues have similar rigid-body motions.

3.4.2. Interpersonal Variability

It is common knowledge that humans respond to novel situations differently. This is significant since the variety in haptic feedback preferences will complicate data analysis and selection of a haptic feedback setting during the design phase. As a result, recent studies have sought to identify differences between drivers and adapt the haptic feedback to the individual's needs [31]. In a study on force perception of the foot on a gas pedal [88] it was found that with increasing amplitude, forces were reported to be felt more often. Furthermore, with increasing frequency, forces were reported to be felt at a lower amplitude. These results contained a significant variability within experiment participants. Similar conclusions are likely to be found for human hands on a steering wheel. This can be seen by the fact that even though feet are known to contain more nerve endings than hands, the usage of hands in our daily lives means that they are more trained to handle forces, disturbances and precise movements.

As people age their skeletal muscles decrease in volume which leads to a progressive decrease in strength [89]. High-resistance physical exercise can partially reverse this muscular weakening. Additionally, muscle contraction time increases with age for both plantarflexors and dorsiflexors of the ankle joint. These results suggest that older drivers may not be able to respond as accurately and swiftly to haptic feedback. One solution may be to increase the haptic authority such that the amount of human control required is reduced. Alternatively, the haptic control loop could be modified to allow for less aggressive corner-cutting or driving closer to the reference. It is likely that a range of haptic feedback settings will suffice to complete the goals of the haptic support. However, moving from heuristic tuning to a more methodical approach should allow the haptic feedback to be adapted based on the needs of the driver.

3.4.3. Modelling Uncertainties

The HSC modelling process comes with some uncertainties. Firstly, some modelling deficiencies will always be present in the selected driver model that will be incorporated into the HSC model. Namely, the Van Paassen driver model assumes that the human driver executes a turn with a certain amount of curve-cutting. As a result, it is very impractical to obtain a reference trajectory that exhibits the opposite of curve-cutting. The opposite of curve-cutting will be referred to in this thesis as *curve-slacking* and is defined as: a successful completion of a road curvature section where the driver steers the vehicle on the side of the road which is towards the outside of the curve. In this case the driver steering response would be slightly too weak at the start of the curve but sufficient to complete the curve without exceeding any road boundaries. While this type of curve driving strategy does not frequently occur [26] it cannot be ruled out completely. Due to the aforementioned curve-cutting modelling assumption the Van Paassen driver model is not very suitable for these kinds of trajectories. As a result, it is more functional to only use the Van Paassen driver model for generating various curve cutting reference trajectories or (near) centerline references. However, the Van Paassen driver model is known to score the highest in terms of descriptiveness and realistic identifiability [64] compared to the Mars model [60] and Van der El model [90]. Therefore, it is decided to use the Van Paassen driver model for generating the results in the preliminary analyses, see Chapter 5.

Another uncertainty stems from the fact that all results in this report will be based on a road section with a fixed road radius for the curves and a constant vehicle speed. It is established that the type of steering behaviour, as shown by a driver class identification method, is sensitive to a change in the velocity [91]. Consequently, it cannot be ruled out that a different combination of speed and curvature will lead to seemingly different results when evaluating the HSC model settings.

3.5. Key Conclusions for Chapter 3

This section contains a summary of the key takeaways and conclusions based on the contents in Chapter 3. The conclusions are given in bullet point form within boxes that follow the order of the topics as presented in this Chapter.

Acceptance of Haptic Feedback Settings

- Acceptance is a key indicator for evaluating how satisfied drivers are with the haptic feedback presented to them. It should be evaluated through a combined subjective and objective assessment.
- Acceptance is correlated in some way to the amount of torque conflict which occurs in the haptic shared control implementation. Several post hoc methods exist to objectively quantify torque conflict between the driver and the haptic support. Subjective ratings of acceptance are commonly derived from questionnaires such as the Van der Laan acceptance questionnaire or the Controller Acceptance Rating Scale (CARS).

Driver Engagement in HSC

- Driver engagement can be measured and used as an indicator for changes in human control behaviour. It can be measured objectively in terms of a control activity metric such as the steering wheel reversal rate or the steering wheel angle standard deviation. No general methods are available for obtaining subjective measurements of driver engagement although research specific attempts have been made to obtain some meaningful results using simplistic questionnaires.

Steering Performance

- Steering performance improvements have been found in research on HSC models when compared to the manual driving case. When the haptic steering support is accepted by the driver this may be accompanied by a reduction in driver control effort.
- Steering performance is measured objectively in a number of ways. The most commonly used and effective metrics for evaluating steering performance are: the standard deviation of lateral position (SDLP), mean lateral position (MLP), root mean square of lateral position or time-to-line crossing (TLC).
- Tuning the haptic support inherently becomes a trade-off between steering performance and acceptance. A perfectly followed HCR trajectory with good steering performance can still be deemed as intrusive by the driver. Therefore, steering performance should only be considered as a metric to verify that the shared control system completes the task in an expected and realistic manner.
- While performance benefits are documented in the literature there are also considerable risks associated with the implementation of HSC systems. These risks are related to haptic support system malfunctioning and human factor issues such as misuse and over-reliance. The degree to which these risks manifest themselves for a specific HSC setting is extremely difficult to predict.

Complicating Factors

- Three important factors that complicate research in the HSC domain are related to human adaptation, interpersonal variability and modelling uncertainties. The impact of these factors should be assessed during the design and test phases of a HSC implementation such that their confounding impact on the results can be minimized.
- Human adaptation to haptic feedback will occur naturally and cannot be fully negated. The experiment can be designed in such a way that the effects of human adaptation are minimized. Keeping the following aspects into account may prove beneficial in the end: the presence and amount of training, the task instruction and ensuring that the torque feedback magnitude is within acceptable limits.
- Interpersonal variability is always present and cannot be accounted for. In case of outliers in the measured data it is possible to discard this data in the end. Alternatively, it has been shown to be possible to group drivers into different driver classes depending on their steering behaviour using machine learning. Doing so may help to explain some of the variance in the results.
- Modelling uncertainties arise for a number of reasons. Firstly, a driver model should only be used for generating a HCR if it is validated for the steering task. Furthermore, all assumptions that apply to the chosen driver model should hold for this specific scenario. The best driver model for implementation into HSC is found to be the Van Paassen driver model. This means that the HCRs which are generated with this model are practically limited to include only those trajectories that exhibit centerline driving or some degree of curve-cutting.

4

Methodology of Haptic Strength Studies

This chapter starts with an overview of the methods used by previous studies that investigated the strength of haptic feedback, see Section 4.1. Secondly, Section 4.2 contains a synthesis of the results that were found in these studies. This chapter is then continued with a technical feature comparison between established haptic strength studies in Section 4.3. Finally, in Section 4.4 an overview is provided of the key conclusions from the present Chapter.

4.1. Methods Used in Established Research

Over the past few decades a large variety of haptic applications have been studied, creating an extensive body of research [38] [40] [92]. Simultaneously, many design approaches exist with a variety in methodologies that have been applied in these studies [19] [21] [22] [28] [39] [69]. Kirkpatrick et al. suggest to define the link between applications and haptic devices in terms of the haptic modes that they use [93]. A haptic mode is a distinct style of using the haptic system that depends on the human and the task that needs to be completed. The suitability of a haptic interface can then be evaluated for every haptic mode that is needed for the application. Moreover, metrics for interaction techniques must be defined in terms of percepts meaningful to the human user. Performance metrics should not just focus on the haptic device but be aligned with the way in which the human uses the haptic feedback. The following subsections discuss the methods used by existing HSC strength studies and gives a summary of their haptic feedback design, evaluation methods and main findings.

4.1.1. Abbink et al. (2009)

Abbink et al. investigated different combinations of haptic force and stiffness feedback on the steering wheel for a second order system disturbance-rejection task [38]. A baseline condition without haptic feedback was investigated in addition to the following four haptic feedback settings: weak and strong force feedback, both with and without additional stiffness feedback. Haptic feedback was generated depending on the sign of the error such as to help the human steer in the direction that reduces the error. A human-in-the-loop experiment tasked a total of nine participants to use the steering wheel to minimize the error between two squares on a screen which indicated the control system state relative to a target state. For each haptic condition subjects were tested with and without visual feedback and for two bandwidth levels of a multisine disturbance signal. Data analysis was done in the time domain for control activity, control effort and task performance and in the frequency domain for an estimate of the disturbance rejection transfer function to assess control behavior. Control activity is measured by the standard deviation of the measured steering wheel angle while control effort is estimated by the standard deviation of the measured steering wheel force. Task performance is determined by the standard deviation of the control error.

The results indicated that compared to the baseline manual control condition participants improved their task performance significantly and substantially for the weak and strong force feedback conditions respectively, see Figure 4.1. Stiffness feedback was shown to be only beneficial when the force feedback controller produces similar control behaviour to that of the human. Manual control without visual feedback was possible with the right amount of haptic feedback. Increasing the force feedback gain lead to a smaller

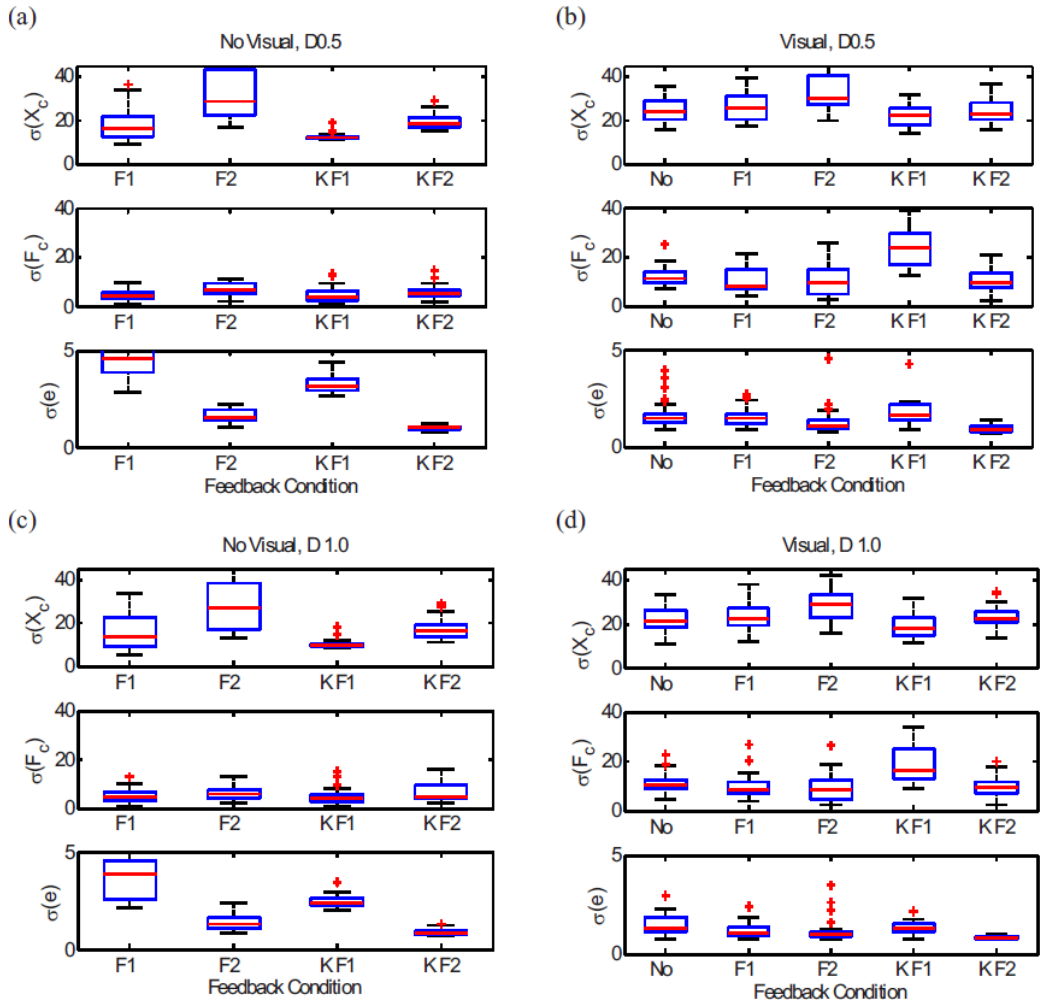

Figure 4.1: Time-domain results by Abbink et al. for control activity (top), control effort (middle) and performance (bottom) for: a) no visual FB and low disturbance, b) visual FB and low disturbance, c) no visual FB and high disturbance, d) visual FB and high disturbance. [38]

improvement in task performance as the bandwidth of the disturbance signal increased. Control activity was highest for the strong force feedback condition and significantly reduced with the addition of stiffness feedback. Visual feedback significantly increased control activity compared to conditions without a visual on screen. Increased disturbance signal bandwidth resulted in reduced control activity. Finally, control effort only increased significantly in the visual conditions for weak force feedback combined with stiffness. Therefore, high control activity did not necessarily lead to high control effort.

4.1.2. Jamson et al. (2013)

Jamson et al. investigated the design of haptic gas pedal feedback to support eco-driving [94]. A total of six different haptic feedback conditions were evaluated: low/high force feedback, low/high stiffness feedback and low/high adaptive stiffness feedback. Adaptive stiffness feedback in the context of this study refers to a force-position profile identical to the stiffness feedback with the addition of lower stiffness feedback as the gas pedal transitions from cruise to accelerate. The low and high force feedback conditions required the driver to exert an extra force of 20N and 40N, respectively, to further increase the gas pedal travel beyond the ideal position. In the low and high stiffness feedback conditions the standard stiffness gradient of 0.2N per percent pedal travel was increased to 1.45N and 2.9N, respectively. Twenty drivers took part in an experiment in a high-fidelity driving simulator. The driving task involved a 30s scenario that required the subjects to cruise at 40mph (64km/h), accelerate and return to cruising at 60mph (97km/h). Root mean squared pedal error was used as an objective measure of task performance. A one-way repeated-measures

ANOVA with the six levels of haptic feedback systems was used to analyze this data. Subjective preference data was collected by asking which of two haptic feedback systems (conditions were presented in pairs) presented the best gas pedal position guidance.

Results indicated a clear preference towards the high feedback systems as opposed to low feedback systems. High force feedback was significantly more popular compared to high adaptive stiffness feedback but not significantly more preferable when compared to the high stiffness feedback. No significant preference effect was found when comparing the low feedback systems. Of the low feedback conditions force feedback resulted in significantly better objective task performance compared to both low stiffness and low adaptive stiffness. With respect to the high feedback conditions force feedback again resulted in significantly better task performance compared to stiffness feedback but not compared to the adaptive stiffness feedback. In conclusion, the result showed that force feedback was preferred over adaptive stiffness feedback. Finally, the authors note that the studied high pedal forces could lead to fatigue over longer periods of driving.

4.1.3. Mars et al. (2014)

Mars et al. investigated different degrees of haptic shared control by comparing five steering assistance settings to unassisted steering [19]. The haptic support system uses a control law based on an optimal preview control law with H2 optimization and preview of the road curvature [62]. Steering wheel torque was limited to 5Nm with a maximum variation of 3Nm/s. As a result, the driver was always able to overrule the haptic feedback torque. The level of shared control was defined by how much of the torque computed by the control law was applied on the steering column. The following six shared control levels were investigated 0% (unassisted driving), 1%, 11%, 21%, 31%, 100%. The 1% condition represented a type of subliminal haptic support that would only be noticed if the lateral deviation is large or the steering wheel is held lightly. The 11%, 21% and 31% conditions represent light, medium and strong settings of shared control. Initial tests showed that the 21% level was perceived as a condition in which the human and the haptic support contributed equally to steering. Finally, the 100% condition was included for being very uncooperative (i.e. intrusive) with the driver by compensating for any centerline deviation and not allowing for any curve cutting. Stiffness feedback was not considered in this study.

Twenty-one subjects took part in a fixed-base driving simulator experiment and were tasked to complete a lap on a 2.5km long road in a rural environment and adhere to the speed limit of 70 km/h. Three visibility conditions were tested: good visibility, heavy fog (up to 50m of road visible) and visual demand (a wiper press would show the simulator screen for 1 second). Performance indicators such as the steering wheel reversal rate (SWRR), steering effort, mean lateral position (MLP) and standard deviation of lateral position (SDLP) were used to assess the effects of different haptic assistance settings in conjunction with subjective assessments. Steering effort is computed by integrating the square of the steering torque over the duration of one lap. The frequency of visual request was the only metric used for evaluating the visual demand condition. The subjective assessment was done with a brief questionnaire after every experimental condition that asked participants to evaluate the effect of shared control on comfort, safety, feeling of being in control and attention allocated to driving.

The results indicate that the best human-machine cooperation was achieved with systems of relatively low-level haptic authority (11% condition). The weakest level of haptic support (1%) did not significantly affect steering performance. Low and medium levels of shared control significantly reduced SWRR, SDLP and steering effort while MLP values were not significantly changed, see Figures 4.2 and 4.3. Subjectively, drivers felt that they were in complete control and rated their driving experience to be safer and more comfortable compared to unassisted driving. Further increasing the level of shared control (31% condition) attenuated the benefits of the haptic support, especially in the good visibility conditions. The resulting values for SWRR and steering effort were similar to those in the unassisted condition whereas the SDLP was as low as in the 11% and 21% conditions. The subjects chosen trajectory started to conflict with the haptic support. This was also found in the subjective metrics with reduced comfort and feeling of being in control. The aforementioned cooperation issues were even more prominent in the 100% condition. Furthermore, it is noted that more steering assistance may be preferable in scenarios with poor road visibility due to fog or self-controlled visual occlusions. Increasing haptic authority beyond the low level of shared control did not yield higher benefits in terms of steering behaviour, visual demand or subjective feeling. Finally, it is concluded that an optimal division of control in terms of human-machine cooperation can be determined through the analysis of several variables, with the SWRR indicator being particularly sensitive.

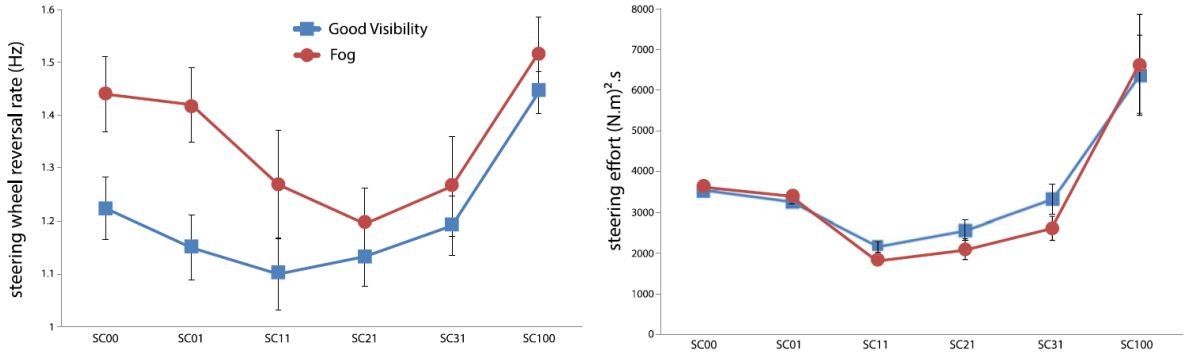

Figure 4.2: SWRR and steering effort results by Mars et al. [19]

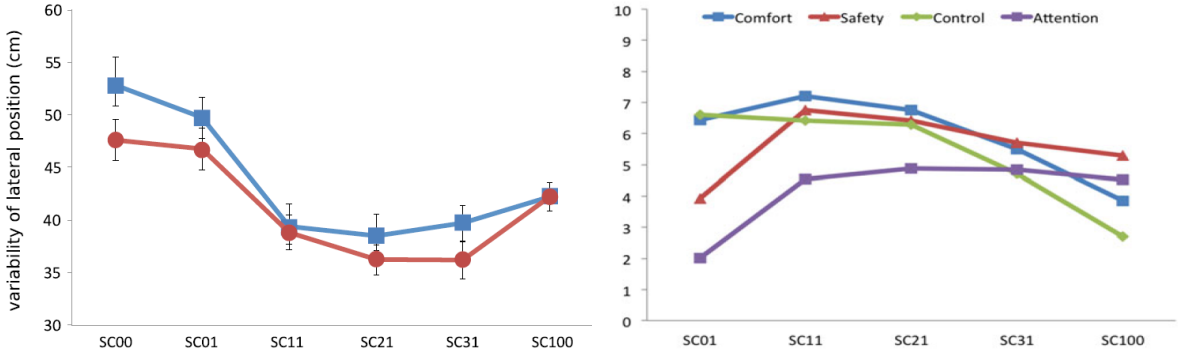

Figure 4.3: SDLP and subjective assessment results by Mars et al. [19]

4.1.4. Smisek et al. (2016)

Smisek et al. studied NMS-based tuning of haptic guidance forces for collision avoidance in UAV teleoperation [95]. The haptic feedback is designed to induce minimal physical workload by operating around the NMS operating point that is typical for a relax-task (RT). Ten subjects took part in the first experiment to identify the average admittance for thirteen different stick bias moments. The stick bias moment varies in magnitude and direction to cover a range of conditions to which the NMS may adapt differently. This information can then be used for tuning the haptic shared controller as the admittance depends on the magnitude and direction of manual control inputs. A collision avoidance system computes the optimal flight trajectory based on the UAV state in the environment and scales the required stick input by the inverse arm/stick dynamics. The haptic feedback scaling is tuned to the intrinsic NMS stiffness that was found for the thirteen distinct regions of stick moment and direction.

A second experiment in a fixed-base flight simulator presented twelve different subjects with a UAV navigational task in an urban environment with obstacles. The haptic controller tuning profile was used as independent variable with the following four conditions: no haptic feedback, under-tuned (weak) HSC that is half as strong as the RT tuning, HSC tuning based on relax task admittance, over-tuned (strong) HSC that is twice as strong as RT tuning. These haptic controller settings were evaluated with metrics for six categories: safety, performance, control activity, haptic activity, haptic controller agreement, subjective assessment. Safety is measured by the number of collisions while performance is determined by the mean velocity and minimum distance to waypoints. Control activity in pitch and roll axes is defined as the standard deviation of stick deflection rate. Furthermore, haptic activity is given by the standard deviation of haptic guidance moment in both pitch and roll axes. Haptic controller agreement is determined in discrete time by comparing the magnitude and angle of the pilot and haptic moment on the stick. Finally, the subjective assessment consists of a NASA-TLX questionnaire to measure workload and surveys with a five-point Likert scale for situational awareness and haptic feedback acceptance.

The total number of collisions reduced when the haptic controller strength increases. Furthermore, the mean velocity and minimum distance to waypoints was unaffected by the haptic feedback strength. Control activity increased for stronger haptic feedback while the difference between the under-tuning (weak)

and relax-task tuning (intermediate) was not significant. Haptic activity increased with haptic controller strength, especially in the longitudinal axis. Moreover, the lowest haptic agreement in terms of magnitude was found for the over-tuned haptic feedback profile, particularly in the longitudinal direction. Directional agreement deteriorated with increasing haptic feedback strength and was highest for under-tuned feedback and lowest for the over-tuned feedback. The subjective assessments reveal low levels of workload for the under-tuning and relax-task tuning. Alternatively, the no haptic feedback and over-tuned conditions are perceived as high workload. Situational awareness was highest for relax-task tuning and lowest for no haptic feedback. Acceptance levels were high for under-tuning and relax-task tuning (i.e. low to medium levels of haptic feedback). However, acceptance was significantly lower for the high haptic feedback condition (over-tuning). Finally, it is noted that under-tuning the haptic controller may be the best strategy for car driving since the driver needs to actively agree and engage with the haptic guidance to follow a trajectory.

4.1.5. Benloucif et al. (2017)

Benloucif et al. investigated online adaptation of the level of haptic authority for a lane-keeping assistance system. Three driving conditions are considered: manual driving, continuous haptic feedback and adaptive haptic feedback. In this last condition the LoHA is adapted in real time based on how distracted the driver is by a secondary task. The driver state depends on fatigue and visual attention measurements. Fatigue is based on gaze and blinking measurements while visual attention is determined by head position and orientation. The driving systems are evaluated with objective performance and control effort measures as well as subjective ratings of comfort, safety, control quality and workload. Lane keeping performance is evaluated with the following four metrics: standard deviation of lateral position (SDLP), steering wheel reversal rate (SWRR), mean lateral position (MLP) and the root-mean-square of the lateral position error (RMSE). Steering effort is computed as the integral of the squared driver torque over the duration of the experimental condition. Participants were asked to provide subjective ratings ranging from 0 to 100. The lane keeping system consists of a weighted sum of a lane keeping controller with high stiffness that provides good performance and a driver assistance controller which minimizes torque conflict with the driver. Fifteen experienced drivers took part in an experiment in a moving-base driving simulator.

When subjects were tasked with normal driving conditions (no secondary task) the continuous haptic feedback resulted in the lowest SWRR with a slightly higher but insignificant value for the adaptive feedback. The addition of a secondary task showed that the adaptive feedback produced significantly lower SWRR compared to the other two systems. Similar results were found for the SDLP and RMSE metrics with an even stronger effect when a secondary task was added. The MLP decreased significantly in the secondary task conditions for the continuous haptic feedback and substantially for the adaptive feedback. Steering effort was reduced by about 50% for both the continuous and adaptive feedback systems in the nominal driving condition. The addition of a secondary task produced a slightly lower but insignificant steering effort in the continuous haptic feedback condition compared to manual driving. However, this reduction in steering effort was significant when comparing the continuous haptic feedback to the adaptive feedback. Secondary task performance was best when drivers used the adaptive feedback system. Continuous haptic feedback significantly improved subjective feelings of comfort, safety and control quality. Adaptive haptic feedback further enhanced these subjective metrics and also significantly improved subjective workload.

It is concluded that the high LoHA adaptive system provides the best performance at the cost of increased driver steering effort and being perceived as intrusive when the need for lane-keeping assistance is low. Therefore, for normal driving conditions the continuous haptic feedback is most effective. When the driver is paying attention to lane-keeping the adaptive feedback should be tuned such that its lower bound equals that of the continuous haptic feedback. Finally, it is stated that some of the variability in results for the adaptive system may be due to differences in trust of the haptic support.

4.1.6. Scholtens et al. (2018)

Scholtens et al. studied a new haptic shared controller to reduce steering conflicts [21]. The haptic feedback design is based on the four design choices architecture and is compared to the previously used meshed haptic shared controller as well as manual driving. As detailed in Section 2.2 the haptic torque is a combination of feedforward and feedback control. Firstly, the average manual driving steering behaviour was measured in order to fit a human-compatible reference trajectory that can be used by the haptic shared controller. Subsequently, sixteen subjects participated in a fixed-base driving simulator experiment and were tasked to perform a curve negotiation task at a speed of 24 m/s with five left and five right turns of

300m radius. Conflict between driver and the haptic support is quantified by the occurrence of conflicts which is 0 if the controls are in agreement and -1 or 1 depending on the direction of driver torque if there is disagreement. The resulting conflict metric is averaged over the duration of the steering task and ranges from 0 (complete agreement) to 1 (complete disagreement). Subjective acceptance is evaluated with usefulness and satisfaction scores as part of a Van der Laan questionnaire. Workload is quantified by the mean driver torque.

The results indicated that the FDCA haptic shared controller can significantly reduce the frequency of torque conflict for both left and right curves by an average factor of 2.3. Simultaneously, the FDCA controller reduced driver torque by a factor of 3.2 and 2.8 for respectively left and right curves, see Figure 4.4. Subjective usefulness of the new FDCA controller was rated similarly to manual driving and significantly

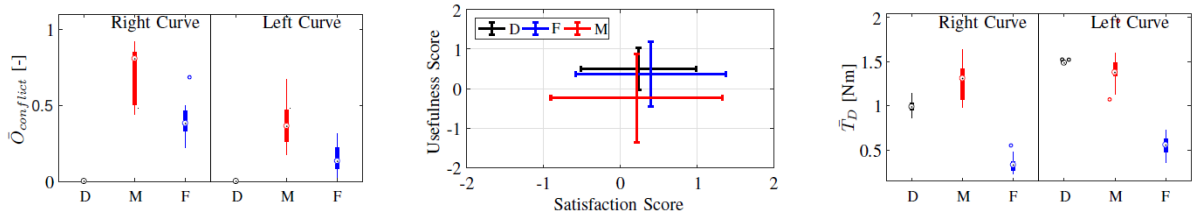

Figure 4.4: Conflict, satisfaction and driver torque results by Scholtens et al. for manual driving (D), meshed controller (M) and the FDCA controller (F). [21]

higher compared to the meshed controller. Satisfaction with the steering system was rated slightly higher for the FDCA controller in comparison to manual driving and the meshed controller. The dominant factors in conflict reduction are the addition of a feedforward haptic torque and a reference trajectory that supports future driver intentions. Finally, it is noted that less conflicts occur for left curves as opposed to right curves. This is attributed to the fact that the subjects are more accepting of left curve guidance which is in the direction of curve cutting due to left curve entry offset. Supporting the initial direction of intention of the driver is thus instrumental to reduce conflicts.

4.1.7. Zwaan et al. (2019)

Zwaan et al. investigated haptic shared steering control for lane keeping with an adaptive level of authority based on time-to-line crossing [39]. Adapting the LoHA based on the driving situation has the potential to reduce trivial conflicts when the driver is within safety margins. A total of five different driving conditions were tested: manual driving, low LoHA, high LoHA, symmetrical adaptive LoHA and asymmetrical adaptive LoHA. Adaptive LoHA can be implemented either symmetrically or asymmetrically. In the symmetrical case the steering wheel stiffness is increased in both steering directions when the TLC metric drops below a design threshold. Alternatively, asymmetric adaptation of the LoHA only increases steering wheel stiffness in the direction of low TLC (i.e. the side of the road lane that is at risk of being exceeded). Two road widths (3.6m and 2.2m) are used as an independent variable to study the system for different TLC scenarios. Fourteen subjects participated in a fixed-base driving simulator experiment and were asked to perform a lane keeping task on a road with eight left and eight right curves of 500m radius at a fixed speed of 24m/s.

The mean minimum 10% of the TLC is used to indicate the level of hazard in the most safety critical parts of the drive. Moreover, mean conflict torque is used as a metric to evaluate cooperation between human and haptic support. The mean minimum 10% TLC results showed no significant differences between the different haptic feedback systems. As expected significantly lower safety margins were observed for the narrow road section when compared to the wider road parts. The high LoHA controller caused significantly stronger torque conflict compared to the other systems. Compared to the high LoHA controller, both adaptive LoHA controllers designs resulted in similar safety margins, but at decreased conflict torques.

4.1.8. Ghys (2020)

Ghys et al. studied how driver's acceptance varies for different trajectory types in trajectory-driven HSC. The measured driver trajectories in a driving simulator were used to classify participants into one of seven driver classes. Additionally, the most efficient curve-cutting group and a group of drivers with the most popular driving style were compared. The reference that is used for the force feedback generation algorithm is either personalized to the individual, personalized to the average of the corresponding driver class, personalized

to the average of the other driver group or (as a baseline) centerline driving. The implemented driver model used to generate the HCRs is the Mars model [96], see also Section 2.4. In addition to the references the level of haptic support is varied between a value of 0.5 and 0.92. The HSC implementation is based upon the FDCA design guidelines and a combination of subjective acceptance and objective torque conflict metrics is recorded in a human-in-the-loop experiment with a road with 6 left and 6 right curves. After classification more variation was found in the resulting driver class allocation for left curves compared to right curves. Furthermore, the vast majority of drivers was found to have a consistent preference for a certain driver class.

It is concluded that the amount of conflict between driver and haptic support is strongly dependent on whether the driver adapts to the driven trajectory. If the driver chooses to cooperate with the given HCR, meaning he/she is willing to follow the haptic guidance, low conflict was found. Alternatively, high conflict occurred if the driver ended up fighting the guidance by forcibly attempting to follow their own desired trajectory. Acceptance was concluded to not be linked to optimal trajectories as they are experienced as nuisance and produce high torque conflict and low subjective ratings. Moreover, centerline reference as a guidance offered a good middle ground even though it is a driving style that did not occur frequently at all in the participants. The higher level of haptic support of 0.92 reduces conflict torque and results in better subjective scores according to Van der Laan and CARS ratings. Finally, it is found that some drivers ended up adapting their driving style when submitted to HSC. The occurrence of this phenomenon is thought to be lie in the classification algorithm as some drivers need complete individualisation while others only required individualisation to the driver class average. In conclusion, not every driver needed complete individualisation of their haptic guidance trajectory (i.e. the HCR). However, doing such individualisation for each driver guaranteed high levels of acceptance across the board.

4.2. Synthesis of Results from Haptics Literature

Common throughout HSC research is the notion of increased task performance as the level of haptic support is increased [4], [38], [94]. This often comes at the cost of increased conflict torques and potentially reduced levels of comfort. Additionally, when the human is no longer actively involved in the control loop his/her role may become supervisory to an extent in case of highly automated HSC systems [97]. The result can be that humans become over-reliant on the haptic steering support system and their driving skills degrade. However, haptic shared control systems that are calibrated properly contain the beneficial property to keep the human engaged in the driving task at all times. Striking the right balance in control authority between human and automation is thus one key problem in HSC research for car steering. Mars et al. advocate that designers should determine how much guidance is just enough to assist the driver instead of converging to a level of haptic feedback that can be tolerated [19]. High steering performance can be achieved for adaptive HSC systems while reducing the physical workload as compared to fixed authority HSC systems [25].

The human acceptance of HSC systems is an important indicator for evaluating different haptic feedback designs [19]. Acceptance can be measured objectively and subjectively and is dependent on the level of cooperation between human and automation. Acceptance appears to be at least partially related to the strength of the haptic feedback as high levels of corrective steering feedback are perceived as punishing by drivers [26]. Individual preferences for certain levels of haptic feedback can cause significant differences in acceptance of the haptic support between drivers. Systems that restrict driver behaviour or enforce a behavioural change are most likely going to be less accepted [68]. Ensuring that the haptic support acts on the reference trajectory of the driver is a design principle that can lead to increased acceptance. In a realistic driving scenario it is likely that a driver will disagree with the automation at some point. Therefore, humans will be accepting of haptic support up to a certain level of haptic authority. At this point, increasing the level of haptic control authority leads to a reduction in acceptance, comfort and feeling of control. The adaptability of the human NMS and the transient nature of steering a vehicle through a series of curves complicate the design of the haptic support system. Adapting the haptic authority setting based on the needs of the driver has been shown to be a promising solution [21]. Adaptive systems tend to increase acceptance compared to their non-adaptive counterparts by reducing torque conflicts [39] or by alleviating their impact on the steering behaviour.

Keeping the human engaged in the driving task is critical to ensure road safety and situational awareness [98]. Driver engagement is an indicator for how actively the driver is involved with the steering task. This

measure can be used as a proxy for the role of the human and can reveal underlying changes in driver behaviour. The precise definition of driver engagement depends on the context within it is used. In some research engagement refers to the awareness state of the driver which is relevant for distracted driving scenarios [99]. Other studies investigate engagement in a scenario where the subject is required to react to a potential collision for automated and manual driving [24]. In the context of HSC driver engagement refers to the steering activity level of the driver which is some function of the shared control system and steering task. Results from studies on HSC systems indicate that, as expected, engagement reduces with increasing levels of haptic support. This is only true if the driver's intention is in agreement with that of the automation. In case of conflicting intentions the level of engagement can, conversely, increase since the driver is now fighting the haptic support. The driver's control effort will then increase as conflicts become more frequent and severe in magnitude. Ideally, driver engagement for HSC systems is kept at a moderate level that is comparable to manual driving to prevent reliance on the haptic support.

Another common finding of HSC research for car steering is a reduction in visual demand of 29% and a faster reaction time [40]. However, differences in literature exist on how much of a reduction can be achieved in visual demand and whether or not it decreases even more as the level of haptic support is increased. Mars et al. found that visual demand decreased by 10% for a low haptic support setting compared to manual driving [19]. Increasing the strength of the haptic support did not lead to a further reduction in visual demand. Muscle fatigue may only become an issue if the haptic forces are perceived as too strong or experienced for a long time. Passive fatigue due to a reduction in task load is not expected to be an issue in this research due to the active torques on the steering wheel [100]. Driving comfort can only be measured subjectively and is therefore subject to large personal variability. Mars et al. measured subjective comfort levels across different levels of haptic support and concluded an insignificant effect. Only the intrusively strong haptic support was perceived as uncomfortable by the subjects. Driving comfort is expected to increase when the automation can fulfill the needs of the individual. Overall, the benefits gained from HSC for car steering will vary from person to person and depend on the driving scenario.

4.3. Research Comparison Table

Research on haptic feedback is not straightforward to compare as there are differences in various aspects. An overview of studies that have investigated different levels of haptic feedback can be valuable for this research project. Such an overview is obtained by comparing the important technical features. The following features are identified: type of driving task, modes of haptic feedback (force-based, stiffness-based or mixed), controller elements, adaptability of haptic feedback (individualised haptic feedback settings) and driving experience level of experiment participants. Table 4.1 summarizes established studies on the effects of haptic feedback strength in the following chronological order: Abbink et al. [38], Jamson et al. [94], Mars et al. [19], Smisek et al. [95], Benloucif et al. [79], Scholtens et al. [21], Zwaan et al. [39], Ghys [26].

Table 4.1: Comparison of studies on the strength of haptic feedback

Authors	**Task Type**	**Modes**	**Controller**	**Adaptive**	**Experience**
Abbink et al. (2009)	Positioning a 2nd-order system	F, S, M	FB	No	Competent
Jamson et al. (2013)	Eco-driving	F, S	-	No	Expert
Mars et al. (2014)	Steering	F	FB & FF	No	Expert
Smisek et al. (2016)	Position tracking	M	FB	Yes	-
Benloucif et al. (2017)	Lane keeping	F	FB & FF	No	Expert
Scholtens et al. (2018)	Steering	M	FB & FF	No	Competent
Zwaan et al. (2019)	Steering	M	FB & FF	Yes	Competent
Ghys (2020)	Steering	F	FB & FF	Yes	Competent

It can be observed that haptic shared control research has become more advanced with respect to the feedback modes, controller architectures, tuning methods and realism of the steering task. The haptic feedback modality and whether it is adapted to different driver types is the most notable difference. Recent research efforts increasingly include individualised haptic feedback that can adapt to the needs of different driver types. Results seem to indicate this can be a good method for reducing the occurrence of torque conflicts. Furthermore, stiffness tuning is not always combined with force feedback even though promising

results have been attributed to adaptive mixed stiffness-force feedback [101].

4.4. Key Conclusions for Chapter 4

This section contains a summary of the key takeaways and conclusions based on the contents in Chapter 3. The conclusions are given in bullet point form within boxes that follow the order of the topics as presented in this Chapter.

Current Knowledge in HSC Research

- Torque conflict is a reoccurring finding in all studies on HSC for car driving. The amount of conflict varies depending on the haptic feedback generation logic and strength, the selected control authority balance between human and automation and the references on which the human and automation act.
- Driver engagement with the steering control task changes significantly across different HSC conditions. The highest engagement occurs when the human ends up fighting the haptic guidance. Slightly lower than average driver engagement is found for low to intermediate levels of haptic support where the human driver still needs to deliver a very substantial part of the total steering torque required to complete the task.
- Task performance slightly increases once haptic support is added compared to the manual driving case. However, the trend in performance gains seems to follow a trajectory of diminishing returns.
- It appears from the literature that strong corrective forces are accepted much less so by the driver than a moderate or strong feedforward haptic control signal.
- Attempts to minimize the torque conflict problem are at the heart of many HSC car driving studies. There is a number of methods that have been proven to reduce the frequency and/or amount of conflict. One strategy is to tune the haptic controller gains such that the haptic support is perceived as useful and comfortable. Additionally, the alignment of the human and haptic references is an effective method to alleviate the torque problem. Finally, making the haptic controller adaptable to the human needs or the driving situation has been shown to reduce conflict.

Knowledge Gap and Implications for this Research

- No accurate and specific methods exist for predicting driver's acceptance and engagement of a given HSC implementation a priori.
- A combination of subjective and objective metrics for acceptance is expected to provide more insight than either a subjective or objective metric by themselves.
- The haptic controller can be implemented and tuned according to the four design choices architecture. This framework streamlines the process of studying the separate identifiable components of the haptic controller, namely: the HCR, LoHS, SoHF and LoHA.
- Due to the large number of potential independent variables and endless variations in the structure for the haptic controller, a choice must be made for the experiment on what haptic modes will be used, which FDCA parameters will be varied and whether the haptic guidance is adapted to the individual.
- Interpersonal variability and preferences will have an effect on the results from the experiment. This can only be dealt with during or after the experiment by identifying potential outliers or groups of driver types.

5

Preliminary Investigation

This chapter discusses preliminary research that is carried out to predict what effects may arise across haptic feedback settings. Firstly, Section 5.1 summarizes the prepositioning behaviour in human drivers and its implementation in the Van Paassen driver model. Section 5.2 details the development of a HSC steering model which is used in a simulated haptic shared steering scenario. The results of the preliminary HSC simulations are treated in Section 5.3 with a sensitivity analysis for each FDCA parameter. Finally, the verification of the HSC model is discussed in Section 6.1.

5.1. Prepositioning Behaviour

A reference trajectory is needed to which the vehicle state can be compared by the haptic support system in order to determine the haptic feedback on the steering wheel. For the purposes of the preliminary simulations this human-compatible reference (HCR) will be generated with a driver model. Once the HCR trajectory is available it can be imported into the complete FDCA simulation which is then able to compute the human and automation responses in the haptic shared control environment. When humans encounter an upcoming curve in the road some anticipatory steering behaviour occurs even before the road curvature starts. This phenomenon is known as prepositioning. The following subsections will treat the importance of prepositioning, the method used to add prepositioning to the Van Paassen driver model and the resulting reference trajectories for each parameter of the extended Van Paassen model.

5.1.1. The Importance of Prepositioning

From the four design choices architecture it is clear that a human-compatible reference is of great importance in achieving successful cooperation between the human and the automation. This raises the need for a realistic driver model that can simulate several commonly found curve driving styles. The lateral vehicle state before curve entry is assumed to be steady centerline driving in some driver models. However, in real life prepositioning behaviour occurs due to human anticipation of the road curvature. As a result, the driver moves the vehicle to a lateral position on the road which may not coincide with the centerline. Experienced drivers may for example position the vehicle towards the outer side of the road with respect to the upcoming turn such as to minimise the lateral accelerations. This part of the steering problem is often neglected but can be added to the driver model in an attempt to simulate a more realistic steering response. The amount of prepositioning inherently depends on the driver and road curvature profile and is affected by other factors such as car handling properties, weather conditions and so forth. In the following simulations most of these variables can be controlled which leaves the amount of prepositioning to vary with the driver settings. The inclusion of prepositioning behaviour will thus result in the generation of a reference that is more compatible with realistic human driving behaviour in the corner anticipation phase. Prepositioning will also have an effect on the future trajectory in the curve.

5.1.2. Extending the Van Paassen Model with Prepositioning

Before the Van Paassen driver model can be extended it is necessary to formalize the concept of prepositioning and provide some definitions. Firstly, a curve negotiation maneuver can be divided into the following

sections: initial straight, prepositioning, curve and exit to final straight. The human steering behaviour in each road section can be characterized by estimation, anticipation, execution and normalization. During the initial straight the human driver estimates the upcoming curvature and adjusts their speed accordingly. Subsequently, the driver anticipates on the observed curvature by moving the car to his/her preferred lateral position on the road ahead of the curve entry point. Hereafter, the curve negotiation is executed for a suitable path through the curve. Finally, a transition takes place from active steering towards nominal straight line driving. The concept of extending a driver model with prepositioning is illustrated in Figure 5.1 where the overall dimensions are exaggerated for clarity. This shows how the addition of prepositioning affects the trajectory that may be obtained from the driver model. Note that in addition to the prepositioning section also a change can be observed in the future trajectory throughout the curvature section.

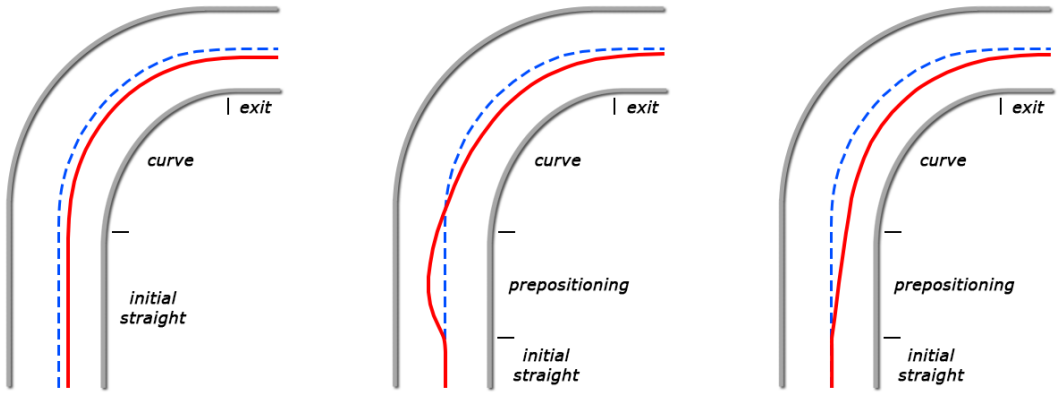

Figure 5.1: The concept of adding prepositioning to a driver model. A model with curve cutting and a centerline bias but without prepositioning (left), one with outwards prepositioning and no centerline bias (middle) and one with inwards prepositioning and no centerline bias (right). Blue dotted line indicates the road centerline, red line indicates (top-down) vehicle trajectories.

After defining the concept of prepositioning driver behaviour it must be expressed mathematically such that it can be added to the standard Van Paassen model. A prepositioning-path model for the Van Paassen model was derived geometrically by Barendswaard et al. [63]. In this implementation the prepositioning path geometry is quantified by the following metrics (see Figure 5.2): straight section bias (y_b), maximum prepositioning distance (y_{max}), curve entry position (y_e), maximum prepositioning distance relative to the straight section bias (Δy_{max}), the curve entry position relative to the straight section bias (Δy_e), turn in time (τ_{in}) and, finally, the prepositioning time (τ_{pre}). The straight section average bias y_b, prepositioning time τ_{pre} and prepositioning displacement relative to straight section bias Δy_{max} are the most important for modelling prepositioning behaviour in different types of drivers. Before the prepositioning phase begins the driver is following the straight road with a constant lateral bias of y_b. At the prepositioning time the driver will start to drift from the straight section bias towards y_{max} by an increase in lateral position of Δy_{max}. The prepositioning time varies strongly between drivers but for the purposes of this model is assumed to be seven seconds.

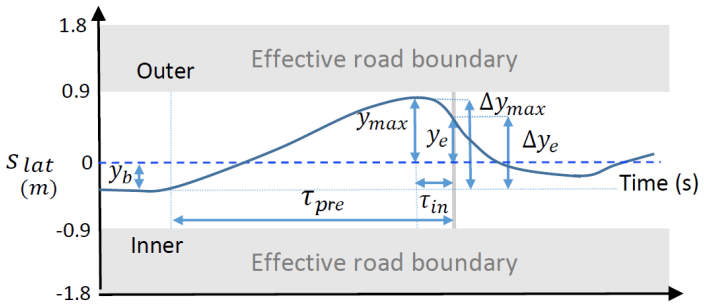

Figure 5.2: Geometric definition of prepositioning for the Van Paassen model [63].

Smooth transitions from the initial straight section to prepositioning and from the prepositioning to the

curve driving phase are achieved with two sigmoidal functions according to Equations 5.1. The first sigmoid activates around the prepositioning time τ_p and has a time shift τ_1 near the middle of its slope a_1. The second sigmoid activates as soon as the curve is detected around τ_2 and smoothly but quite rapidly reduces the prepositioning response to zero such that the curve driving phase can begin.

$$y_{prep} = y_b + \frac{g_1}{1+e^{-a_1(t-\tau_1)}} - \frac{g_1+y_b}{1+e^{-a_2(t-\tau_2)}} \tag{5.1}$$

For modelling the values of a_2 and τ_2 are fixed to 2 m/s and 0.5 respectively produce a fast yet smooth transition at the end of the prepositioning phase. This leaves g_1, a_1 and τ_1 as the degrees of freedom for modelling a prepositioning path. These parameters have been identified in previous research [69] for three driver classes (outer, middle, inner) based on the curve entry position y_e and are listed in Table 5.1.

	g_1		τ_1		a_1	
	R	L	R	L	R	L
Outer	0.25	-0.44	5.6	3.3	0.33	0.38
Middle	0.20	-0.07	2.1	3.0	0.42	1.6
Inner	0.07	-0.03	0.03	0.01	0.14	1.1

Table 5.1: Identified sigmoid parameters for each prepositioning category for a right curve (R) and left curve (L). [63]

As a result, the degrees of freedom in the prepositioning model are the driver class and the straight section bias which together determine the complete prepositioning trajectory. In order to extend the Van Paassen model the prepositioning position y_{prep} is added to the curve cutting reference in the feedback loop to generate the so-called future position reference y_{fr}. Additionally, a corresponding prepositioning curvature κ_{prep} is added as an independent component to the feedforward loop. This prepositioning curvature is computed using the second derivative of the prepositioning position, see Equations 5.2 - 5.3. The result of both components is an improved response that exhibits less overshoot and lag when compared to either component by itself.

$$a_{lat}(t) = \frac{d^2 y_{prep}(t)}{dt^2} \tag{5.2}$$

$$\kappa_{prep}(t) = \frac{a_{lat}(t)}{V^2} \tag{5.3}$$

An overview of the extended Van Paassen model with the addition of prepositioning can be found in the block diagram in Figure 5.3. The extended Van Paassen model contains seven degrees of freedom for modelling curve driving behaviour: feedforward gain K_{FF}, feedback gain K_{FB}, lookahead time τ_{LH}, filter time constant T_{hs}, prediction time τ_p, driver class and straight section bias y_b. These seven degrees of freedom will be referred to as the parameters of the extended Van Paassen driver model.

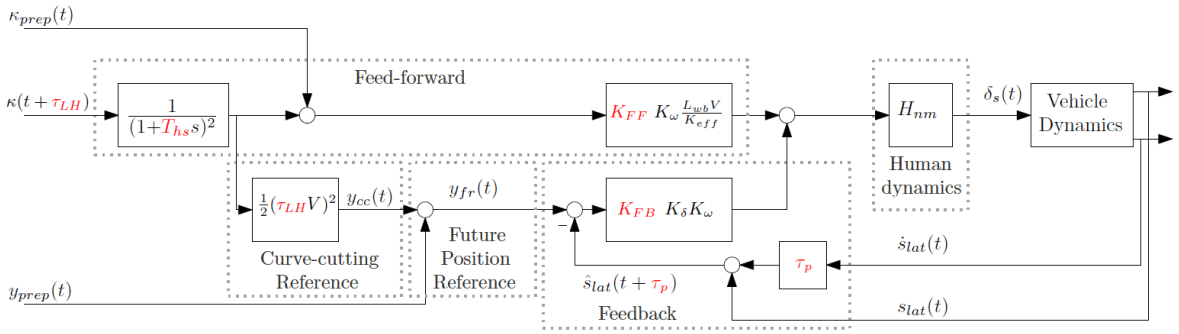

Figure 5.3: Block diagram of the extended Van Paassen model with the addition of the prepositioning curvature feedforward contribution k_{prep} and the prepositiong distance feedback contribution y_{prep}. [63]

For the preliminary simulations the human neuromuscular dynamics are simplified and given by the transfer function from Equation 5.4, where the neuromuscular time delay T_N is set to 0.1.

$$H_{nm} = \frac{1}{T_N s + 1} \tag{5.4}$$

The vehicle dynamics, see Equation 5.5, consist of a simplified linear bicycle model which is obtained from the lateral dynamics detailed by Saleh et al. [102]. The inputs are the curvature κ and steering angle δ_s while the prepositioning lateral position y_{pre} is added to the system as a bias in the output equation. Furthermore, the state vector includes the side slip angle β, yaw rate r, heading angle ψ_L and lateral distance from centerline s_{lat}. The coefficients in Equation 5.5 are defined according to Equations 5.6 - 5.11.

$$\begin{bmatrix} \dot{\beta} \\ \dot{r} \\ \dot{\psi}_L \\ \dot{s}_{lat} \end{bmatrix} = \begin{bmatrix} a_{11} & a_{21} & 0 & 0 \\ a_{12} & a_{22} & 0 & 0 \\ 0 & 1 & 0 & 0 \\ V & l_s & V & 0 \end{bmatrix} \begin{bmatrix} \beta \\ r \\ \psi_L \\ s_{lat} \end{bmatrix} + \begin{bmatrix} 0 & a_{15} \\ 0 & a_{25} \\ -V & 0 \\ -l_s V & 0 \end{bmatrix} \begin{bmatrix} \kappa \\ \delta_s \end{bmatrix} \tag{5.5}$$

$$a_{11} = -\frac{2(c_f + c_r)}{MV} \tag{5.6}$$

$$a_{12} = \frac{2(c_r l_r + c_f l_f)}{MV^2} - 1 \tag{5.7}$$

$$a_{15} = \frac{2c_f}{MVR_s} \tag{5.8}$$

$$a_{21} = \frac{2(c_r l_r - c_f l_f)}{I_Z} \tag{5.9}$$

$$a_{22} = -\frac{2(c_r l_r^2 + c_f l_f^2)}{I_Z V} \tag{5.10}$$

$$a_{25} = \frac{2c_f l_f}{I_Z R_s} \tag{5.11}$$

5.1.3. Influence of Driver Model Parameters on HCR

In these preliminary simulations the Van Paassen driver model simulates the curve driving response for a road section plotted in Figure 5.4. The vehicle drives at a constant speed of 80 kph (≈ 22.2 m/s) on a 3.6m wide road that consists of initial and final straights that take 3 seconds each and a curve that takes 10 seconds. The complete simulation is thus 16 seconds long. At the start of the curve the curvature increases gradually for 2 seconds to $4.9 * 10^{-3}$ [1/m] (which equals a radius of 205m), remains constant for 6 seconds, and decreases back to zero in 2 seconds. The gradual changes in curvature ensure a smooth steering response by preventing an unrealistic step response to an instantly strong curve. These curvature sections connect straights to curves and are known as clothoids. The application of clothoids is very common in road design.

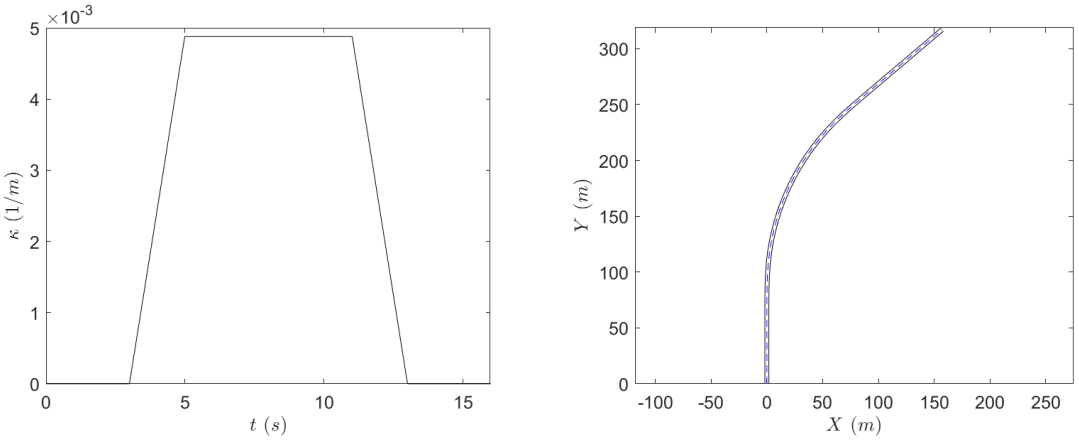

Figure 5.4: Curvature plot and 2D road section for preliminary simulations

In order to gain an understanding of the extended Van Paassen driver model the influence of each parameter must be investigated. This is done by running the driver model for a range of values and investigating the lateral position and steering angle plots. Firstly, the addition of prepositioning will be compared to the standard Van Paassen model in order to demonstrate the efficacy of the prepositioning path model. The plot in Figure 5.5 is obtained for a fixed set of parameter values and compares the standard to the extended Van Paassen model with a driver class that prepositions near the outside of the curve and a straight section

bias of 0.2 m. It can be seen that the addition of this type of prepositioning has a clear effect on the lateral position which remains slightly closer to the centerline in the curve. The trajectory within the curve section is affected especially near the start of the curve due to the curve entry point shifting outwards with prepositioning. Furthermore, the plot in Figure 5.6 compares the standard Van Paassen model to the extended Van Paassen model with a driver class that prepositions near the inside of the curve and a straight section bias of -0.2 m. The trajectories are more similar in this case since the inner prepositioning is not as aggressive as the outer prepositioning driver class. Furthermore, in this case the curve entry point is almost the same for the standard and extended model.

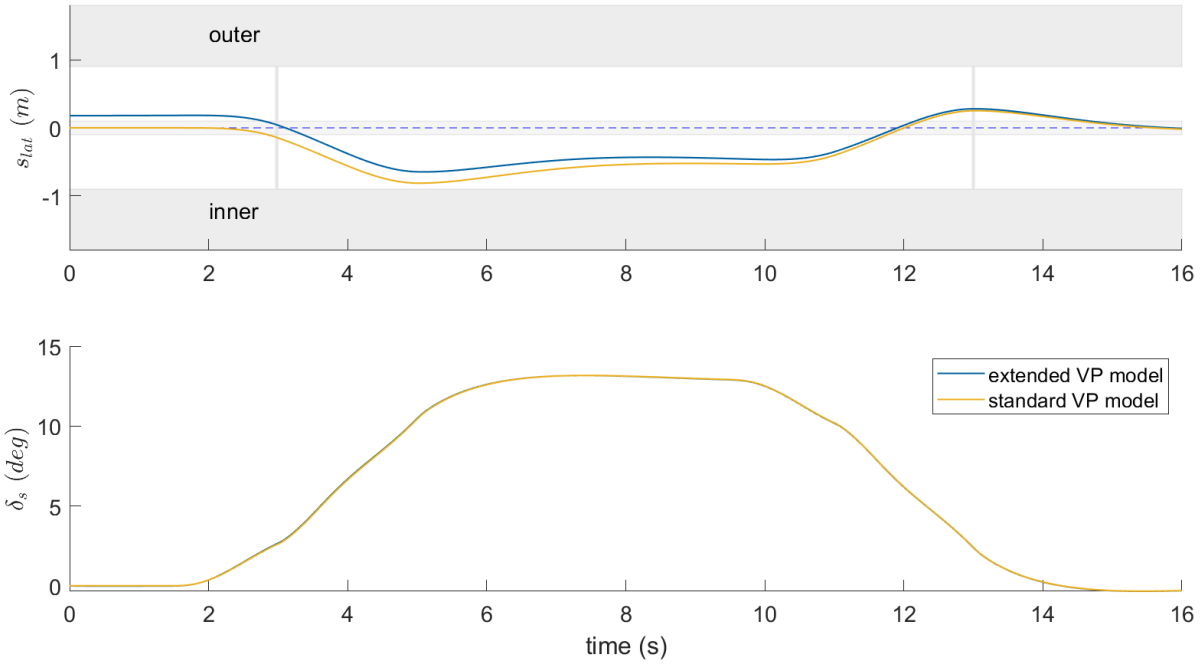

Figure 5.5: Comparison of model with outwards prepositioning to standard Van Paassen model

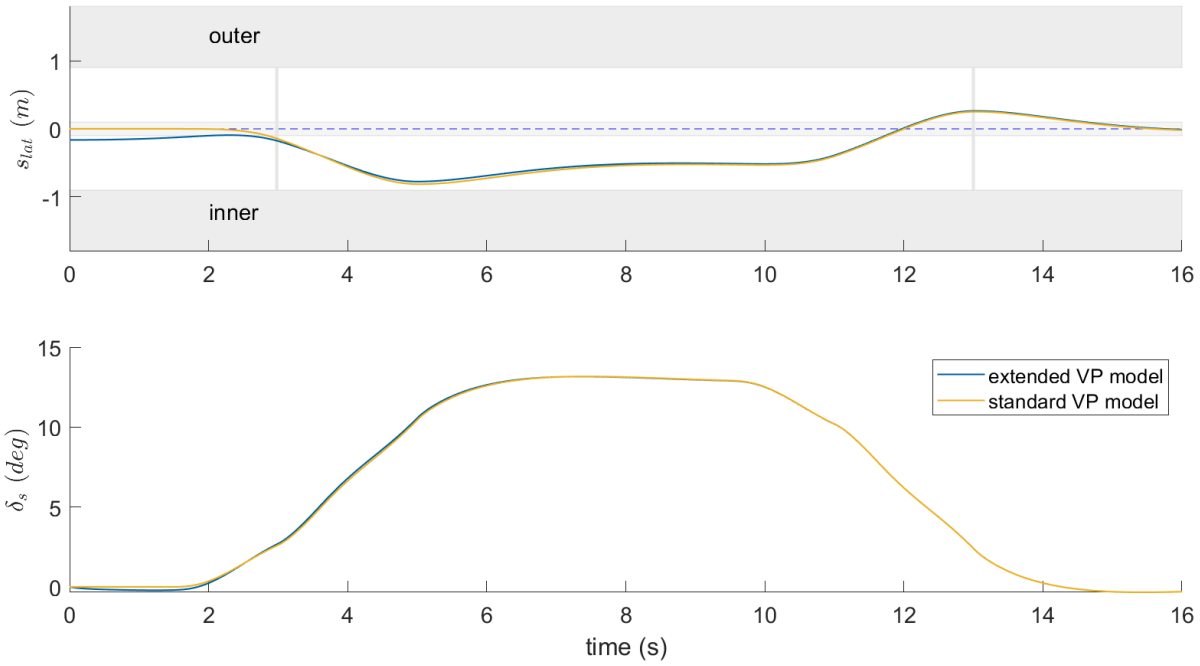

Figure 5.6: Comparison of model with inwards prepositioning to standard Van Paassen model

The following plots will compare different settings of the extended Van Paassen model. In Table 5.2 an overview is given of the baseline parameter values that are used to generate the preliminary results. These

driver_class	y_b	K_{FF}	K_{FB}	T_{hs}	τ_{LH}	τ_p
outer	0	0.21	0.07	0.45	1.5	1.3

Table 5.2: Extended Van Paassen model baseline parameter set for preliminary simulations

values are selected for the preliminary road section as they result in a moderate amount of curve cutting which remains stable throughout the maximum curvature portion of the curve. In human drivers it is reasonable to expect this kind of cornering behaviour. Furthermore, the selected steering wheel mechanical properties for the simulations are matched to those of the driving simulator in the Human-Machine Interaction Laboratory at Delft University of Technology. These values can be found in Table 5.3.

J_{SW}	B_{SW}	K_{SW}
0.005	0.03	1

Table 5.3: Preliminary simulation settings for the steering wheel mechanical properties

In Figure 5.7 the effect of the driver class parameter is illustrated for the baseline set of parameters of the extended Van Paassen (EVP) model. As expected the driver class setting mainly affects the prepositioning section and subsequently slightly affects the in-curvature section due to the shift in lateral road position at curve entrance. Additionally, in case of the outwards prepositioning driver class the lateral position in the curve section shifts towards the centerline the most compared to the middle and inwards driver classes. The different curve entry point is the underlying reason for this result. With regards to the steering angle it is more difficult to discern any differences due to the minor changes in steering behaviour. The main difference in steering angle can as expected be found in the first three seconds (i.e. prepositioning section) as a result of changing the type of prepositioning behaviour.

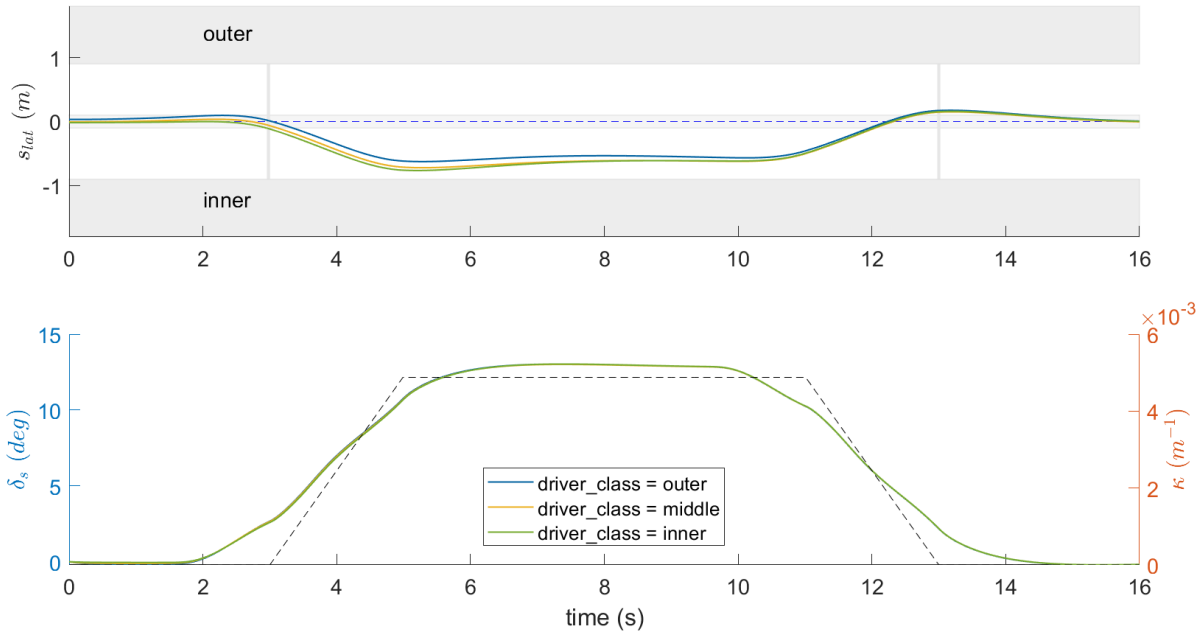

Figure 5.7: Effect of driver class on lateral position and steering angle for the extended Van Paassen model

Figure 5.8 shows the effect of changing the straight section bias (y_b). It is apparent that a change in y_b significantly affects the offset from the centerline in the prepositioning section. The driving behaviour in the curvature section remains almost completely independent of the straight section bias setting. Finally, the y_b and driver class settings should be selected together to match the individual's preferred way of prepositioning before the curve.

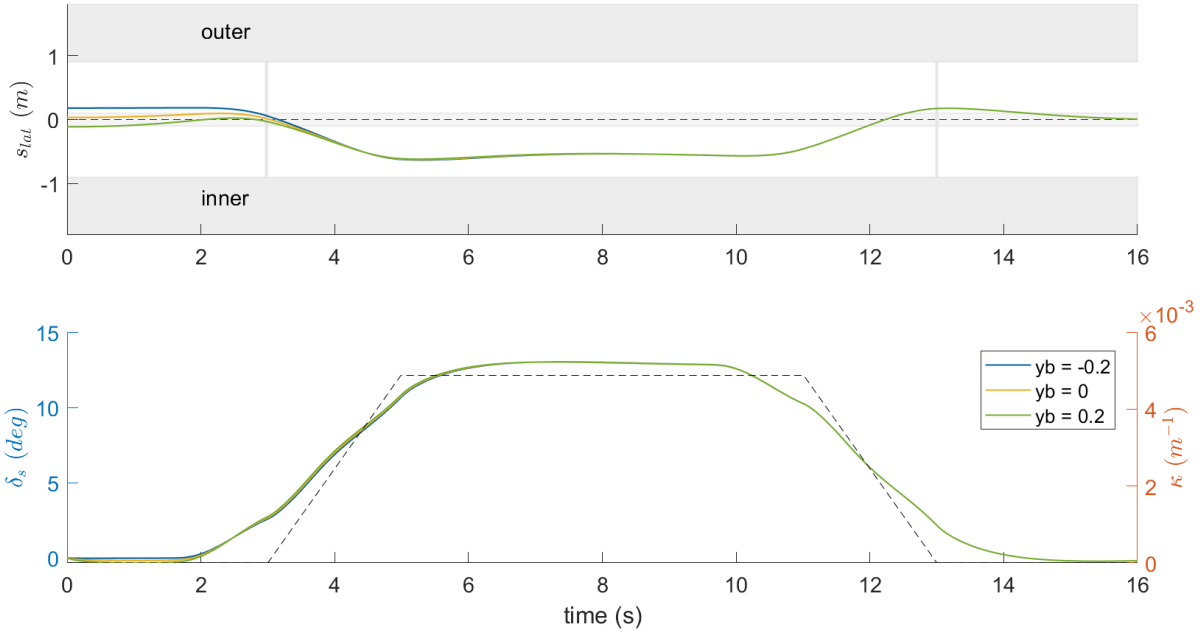

Figure 5.8: Effect of y_b on lateral position and steering angle for the extended Van Paassen model

Figure 5.9 depicts the results for different settings of the driver feedforward gain parameter K_{FF}. It is clear that a higher feedforward gain produces more aggressive corner cutting behaviour within the curvature section. The amount of lateral offset due to the corner cutting appears to stabilize around 5s into the simulation as the curvature reaches its peak value at 5s. At this point the amount of curvature has been linearly increasing for 2s since the start of the curve as a clothoid. Due to the small delay introduced by filtering the curvature input the steering angle can be seen to stabilize slightly later at 6s to a maximum value of around 13 degrees. Another effect that can be derived from these plots is that a higher feedforward yields less overshoot from the centerline at the curve exit point. This is mainly due to the vehicle starting the corner exit clothoid closer to the inside of the curve while the steering contribution steadily decreases. The stronger feedforward response in that case has more leeway before swerving back across the centerline at which point the feedback loop can only bring the vehicle back to the centerline since the curvature has decreased back to zero.

Figure 5.10 shows the effect of changing the feedback gain parameter K_{FB}. The results follow a similar pattern to changing the feedforward gain parameter K_{FF}. This is a direct result of the fact that both the feedforward and feedback loops use the filtered road curvature as input. The addition of lateral position feedback causes the model to follow the curve cutting reference more closely. It is clear that a stronger feedback gain produces more curve cutting. However, the lateral position within the curve is more consistent with higher feedback gains and varies more across the lane width with lower feedback gains. The overall curve driving behaviour should match the expected real driving behaviour in humans. In order to achieve this both the feedforward and feedback gains should be tuned simultaneously since their contributions together determine the total amount of curve cutting generated by the driver model. Subsequently, the feedback gain can be altered to change how much variation from the curve cutting reference is present within the curve section.

Figure 5.11 details the influence of the lookahead time and filter time constant parameters. These settings should be matched in order to ensure that the vehicle does not enter the curve too late or too early. This is an implication from the structure of the Van Paassen model as the lag due to T_{hs} must be compensated for by τ_{LH}. As a general rule of thumb this means that the lateral error from the curve cutting reference is ideally compensated by K_{FB} when $\tau_p = \tau_{LH} - T_{hs}$. Since the combinations of both parameters are matched the vehicle enters the curve at the same time for all three simulation conditions. A low value for T_{hs} will result in more aggressive turning behaviour when changes in road curvature are encountered. However, this is largely compensated for by a lower value for the lookahead time parameter. This can be seen in the lateral plot as the trajectories are nearly identical around the curve entry point. Once the curvature reaches

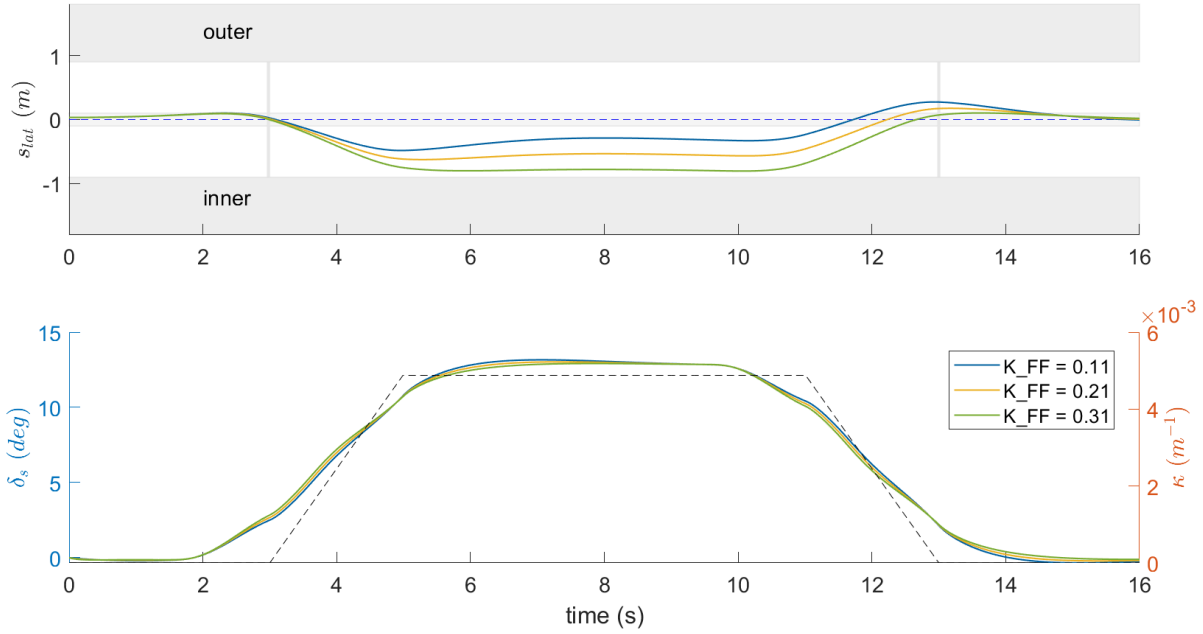

Figure 5.9: Effect of K_{FF} on lateral position and steering angle for the extended Van Paassen model

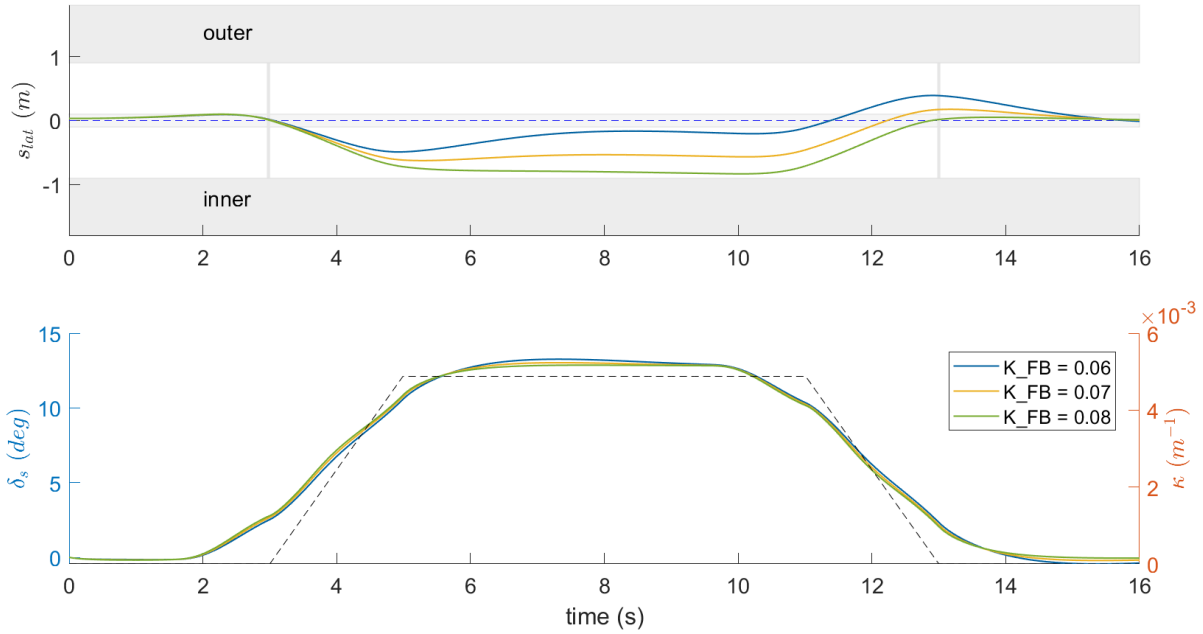

Figure 5.10: Effect of K_{FB} on lateral position and steering angle for the extended Van Paassen model

its maximum value the effect of the filter time constant diminishes and the higher lookahead time value produces a slightly stronger curve cutting response. Finally, it can be seen that different combinations of lookahead and filter time can also affect the lateral positioning at the end of the curve since the curve exit is entered differently due to changes in the amount of curve cutting.

Finally, Figure 5.12 shows how different values for the prediction time parameter τ_p affect the output of the extended Van Paassen driver model. The results are as expected since the prediction time parameter has a direct effect on the feedback loop of the driver model. The largest differences are found around the time where the curvature has reached its maximum value or has finished reducing to its baseline value. This makes sense as it is at these locations in the curve that the steering torque contribution from the feedforward loop becomes stable or reduces back down to zero. The feedback loop then reduces the error

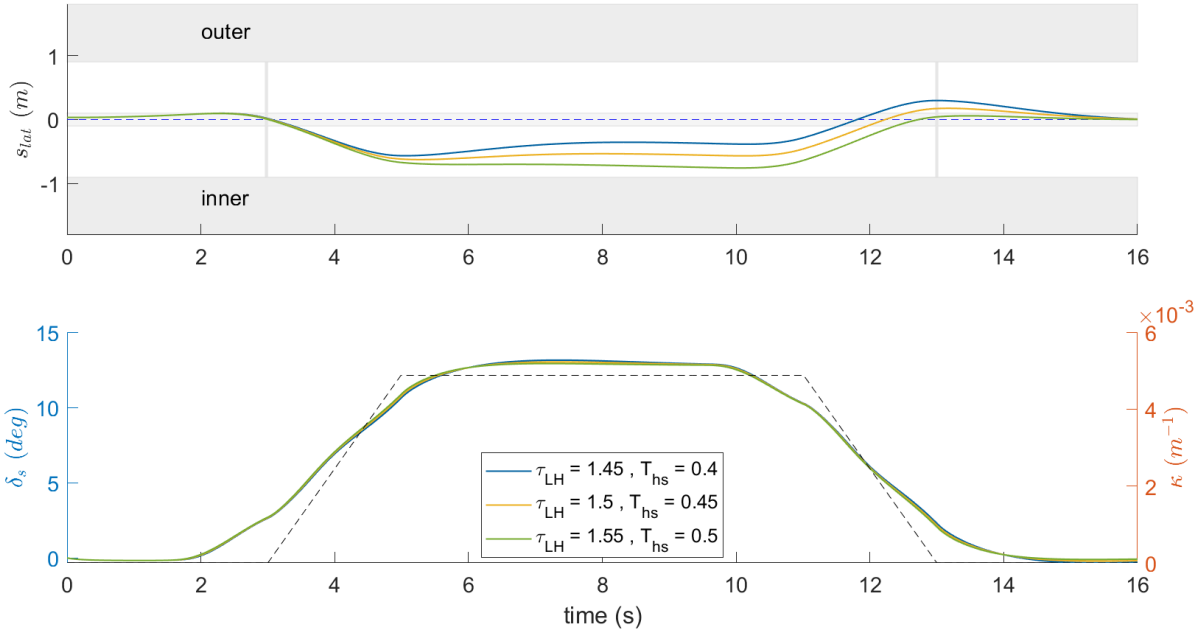

Figure 5.11: Effect of τ_{LH} and T_{hs} on lateral position and steering angle for the extended Van Paassen model

with respect to the curve cutting reference which is done more effectively with a higher gain in the feedback loop (i.e. higher τ_p) as is also clear from the difference between the three settings in the lateral position plot.

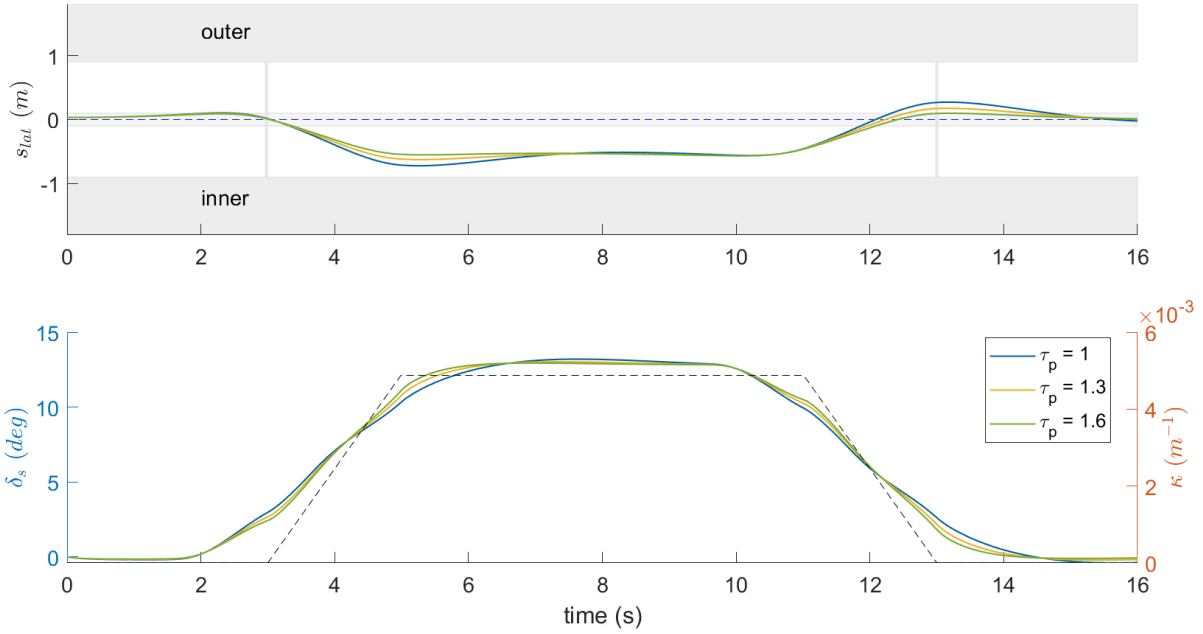

Figure 5.12: Effect of τ_p on lateral position and steering angle for the extended Van Paassen model

5.2. Building the HSC Steering Model

This section will detail the process of building the complete haptic shared control simulation model. Firstly, the generation of the human and haptic references with the use of the extended Van Paassen model will be discussed. These reference trajectories are referred to as the human-defined reference (HDR) and human-compatible reference (HCR). Subsequently, the process of combining the human and haptic steering torques

will be explained in addition to the rationale for the required conversions.

5.2.1. Haptic Part of the HSC Simulation

The haptic support part of the FDCA simulation generates a steering torque based on a combination of feedforward and feedback. The feedforward torque is generated with respect to a steering angle reference while the feedback is based on the heading and lateral deviation from the used reference path. In the FDCA framework the human-compatible reference (HCR) is generated with the extended Van Paassen driver model and then imported into the FDCA simulation. Finding the closest reference point to the current vehicle position at time i results in the nearest global point (NGP). The selected reference steering angle, δ_r, at this point is then obtained and used as a feedforward in the haptic path. However, this steering angle needs to be converted back to a torque first such that it can be combined with the haptic feedback torque. The conversion method is based on an approximation of the inverse steering wheel dynamics. The steering wheel is modelled as a rotational mass-spring-damper system under a torque τ with the following mechanical properties: inertia (J_{SW}), friction coefficient (B_{SW}) and stiffness (K_{SW}). The steering wheel dynamics are given by Equation 5.12, where θ denotes the steering wheel angle.

$$T_{SW} = J_{SW}\ddot{\theta} + B_{SW}\dot{\theta} + K_{SW}\theta \tag{5.12}$$

While the steering wheel angle is known its derivatives are needed as well to complete the conversion from steering angle to torque. These derivatives can be computed numerically at the downside of being sensitive to sudden changes in curvature and skips in the NGP index. This effect stems from the steering wheel dynamics in which the torque significantly leads the steering angle in phase for higher frequencies over the corner frequency. A NGP skip will occur when the next closest reference point does not advance by one entry in comparison to the previous one. Such an additional backwards or forward NGP step will cause the derivatives to locally decrease or increase with respect to derivatives at adjacent points. A more robust method for computing these derivatives is by approximating their values in the Laplace domain with the transfer function from Equation 5.13 as was proven to be effective by Ghys et al. [26]. Once the first derivative is obtained the second derivative can be obtained subsequently by substituting the value of the first derivative.

$$\frac{\dot{\theta}(s)}{\theta(s)} = \frac{s}{\frac{s}{20}+1} \tag{5.13}$$

Using the above method the required steering torque at every point in the curve can be reconstructed using the respective steering angle at the closest point on the HCR. As a result, a complete feedforward of the steering torque should then result in the FDCA simulation exactly following the HCR. However, the derivative approximation introduces a small amount of lag to the computation of the currently required steering torque. As a result, over time the FDCA simulation drifts slowly but only slightly away from the HCR trajectory. This can be seen in Figure 5.13 by comparing the yellow line (FDCA simulation without adjustment to fix this drift) to the blue line (HCR). Additionally, the steering angle that is required at each point in the curve is shifted forward either 0, 1 or 2 datapoints forward in an effort to compensate for the lag in approximating the derivatives. The resulting plot shows that the FDCA simulation can be tuned to correctly follow the HCR by shifting the steering angle obtained from the HCR forward one datapoint in time (i.e. dt = 0.01s). For the curve used in these simulations this setting produces a steering response that is nearly identical to the HCR.

The haptic feedback is generated by comparing the vehicle state at each point in time to the state at the closest point on the HCR. The states used to correct for deviations from the reference trajectory are the heading angle and lateral position on the road. This results in a heading error, $\Delta\psi$, and a lateral position error Δs_{lat}. These are then scaled by a heading error gain K_ψ and a lateral error gain K_s respectively before being combined together. The initial values for these gains are set to match those used in previous haptic shared control experiments within the HMI laboratory at Delft University of Technology. These gains can be optimized for iteratively with a cost function based on the total lateral error between the simulation and the HCR, see Equation 5.14.

$$J_{cost} = \frac{1}{2m}\sum_{i=0}^{m}[s_{lat}(i) - s_{lat_{HCR}}(i)] \tag{5.14}$$

This optimization is performed with a handful of different initial values for the gains to ensure that a convergent solution is obtained. Once a set of gain parameters is found they can be inserted into the

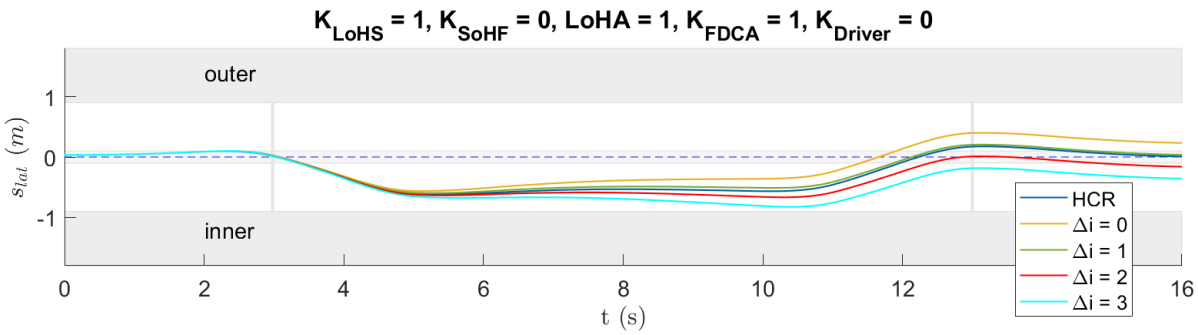

Figure 5.13: Lateral position plots for different time shifts of the steering angle

simulation to check that they produce a steering response that is suitable for usage in the HSC model. This means the steering feedback torque is present when needed but does not become too strong with respect to the feedforward torque. Furthermore, the steering behaviour should be smooth as is the case in natural driving and not for example oscillatory or transient. One set of gain values that was found to work well in these preliminary simulations is: $K_s = 0.1$ N and $K_\psi = 2$ N/rad. These values are suitable for simulation purposes but may be perceived as too aggressive for usage in the real driving simulator of the HMI lab. In this case their values can be lowered accordingly. Similar slightly lower values are used by Ghys et al. for a HSC driving simulator experiment ($K_s = 0.08$ N and $K_\psi = -0.03$ N/deg) [26]. Note that there is a minus sign for the heading gain due to different axes conventions in the HMI laboratory simulator compared to the MATLAB implementation. In conclusion, selecting these gains for the HSC experiment will have to be done heuristically and care must be taken to ensure that the chosen setting is appropriate.

5.2.2. Human Part of the HSC Simulation

The human part of the haptic shared control model uses the human-defined reference generated with the EVP model. As a result, it can be set equal to the haptic reference (i.e. the HCR) or set to a different reference trajectory in order to investigate the effect of conflicting references on the shared steering control behaviour. The human torque consists of a feedforward component that is computed with the filtered road curvature and a feedback component dependent on the error from the human-defined curve cutting reference. The exact computation is identical to the one described in detail for the extended Van Paassen driver model. As a result, the human feedforward torque is scaled by the selected HDR human feedforward gain setting (K_{FF}) while the human feedback torque is scaled by the human feedback gain setting in the HDR reference (K_{FB}). Subsequently, the total human torque is passed through the human neuromuscular dynamics which are approximated by the first order transfer function from Equation 5.4. The result is the human contribution to the steering angle which needs to be converted back to a torque such that it can be combined with the haptic torque in the end. This conversion is done identically to the method detailed before for the haptic steering angle to torque conversion (see Equations 5.12 and 5.13).

5.2.3. Torque Combination Process

Once the torque components from both agents of the HSC simulation are computed it is possible to determine the net effect on the steering angle. The obtained steering angle is then fed back into the vehicle dynamics to advance the state of the system to the next point in time. If the human and haptic torques were summed together without any adjustment the total torque acting on the steering wheel will be larger than the amount of torque generated by the human driver model for making the HCR. As a result, so-called collaboration gains are added to ensure the steering torque will be around the same level as used for generating the references with the EVP driver model. The values of these two collaboration gains range from 0 to 1 and are kept constant throughout these preliminary simulations. A collaboration gain value of 0.63 is assigned to the haptic torque contribution while a value of 0.37 is set for the human steering torque. This is in line with previous work done in the area of HSC for car steering [26]. The scaling of these torque contributions is then simply given by Equation 5.15.

$$T_{total} = K_{FDCA} \cdot T_{FDCA} + K_{Driver} \cdot T_{Driver} \tag{5.15}$$

To some extent these collaboration gains set the human and haptic steering authority levels in the sim-

ulations. As these collaboration gains are not present in the experiment it is important to find a way to compare the preliminary simulations to the experiment. Firstly, a LoHA setting may be implemented that is in line with a collaboration gain balance of 0.63 and 0.37. While this solution does not guarantee strict equivalence a LoHA that increases the steering wheel stiffness by a factor of 1.70 (= 0.63/0.37) should result in a close match between the experiment and simulation implementations. Additionally, some preliminary simulations will be run with equal collaboration gains (0.5) to ensure both the human and haptic support have equal steering authority. These can then be compared to the collaboration gains mentioned above to assess their impact on the results.

Due to the direct linkage between the human limbs and the steering wheel and their interaction it is sensible to lump the neuromuscular and steering wheel mechanical properties into one. A transfer function of the combined system is given by Equation 5.16. In order to compensate for the increased inertia, damping and stiffness the torque conversion method (Equations 5.12 and 5.13) must be updated. The steering wheel mechanical properties will now have to include the neuromuscular contributions as well which will lead to the updated steering wheel dynamics, see Equation 5.17.

$$H_{SW+NMS}(s) = \frac{1}{(J_{SW} + J_{NMS})s^2 + (B_{SW} + B_{NMS})s + (K_{SW} + K_{NMS})} \tag{5.16}$$

$$T_{SW} = (J_{SW} + J_{NMS}) \cdot \ddot{\theta} + (B_{SW} + B_{NMS}) \cdot \dot{\theta} + (K_{SW} + K_{NMS}) \cdot \theta \tag{5.17}$$

In addition to the above changes required to combine the torques it is now possible to include the Level of Haptic Authority (LoHA) into the haptic shared control simulation. The chosen LoHA implementation effectively sets the authority level of the haptic support by scaling the stiffness of the steering wheel based on its default stiffness value K_{SW_0}, see Equation 5.18. A LoHA setting of 1 is thus the default steering wheel stiffness while a LoHA value of 2 for example doubles the stiffness.

$$K_{SW} = LoHA * K_{SW_0} \tag{5.18}$$

Finally, this change in the steering wheel stiffness will produce some shift in the control authority balance between the human and the haptic support. The human parameters will not be adjusted to account for this change in steering wheel stiffness. With the torque combination process complete the steering dynamics can be computed for every steering input and the loop is closed. Figure 5.14 provides a block diagram overview of the complete HSC simulation and its components.

5.3. FDCA Parameter Sensitivity Analysis

In order to investigate the effects of the FDCA parameter settings on the haptic shared control steering output a sensitivity analysis is performed. Each FDCA parameter will be varied in order to study the effects on the driving behaviour and to form some hypotheses in preparation for the driving simulator experiment. Additionally, conflict between the two parts of the HSC simulation will be modelled and discussed.

5.3.1. Effect of Changing K_{LoHS}

In order to investigate the sensitivity of the HSC simulation to a change in the level of haptic support gain (K_{LoHS}) it is necessary to establish a baseline set of parameters to start from. This set of parameters is chosen such that they are in line with previous research and produce suitable steering behaviour as explained in Subsection 5.2.1. The baseline values for these parameters are given in Table 5.4. Additionally, the baseline values used for the steering wheel and NMS mechanical properties as well as the driver model settings used for the human driver model part of the simulation are given in Table 5.5 and 5.6.

Table 5.4: Baseline values for important parameters of preliminary HSC simulations

K_{LoHS}	K_{SoHF}	$LoHA$	K_{FDCA}	K_{Driver}	K_s	K_ψ
0.92 [-]	1.5 [-]	1 [-]	0.63 [-]	0.37 [-]	0.1 [N]	2 [Nm/rad]

Throughout Subsection 5.3.3 the human and haptic references (i.e. HCR & HDR) that will be used for the HSC simulation are generated with the extended Van Paassen model and the corresponding baseline values

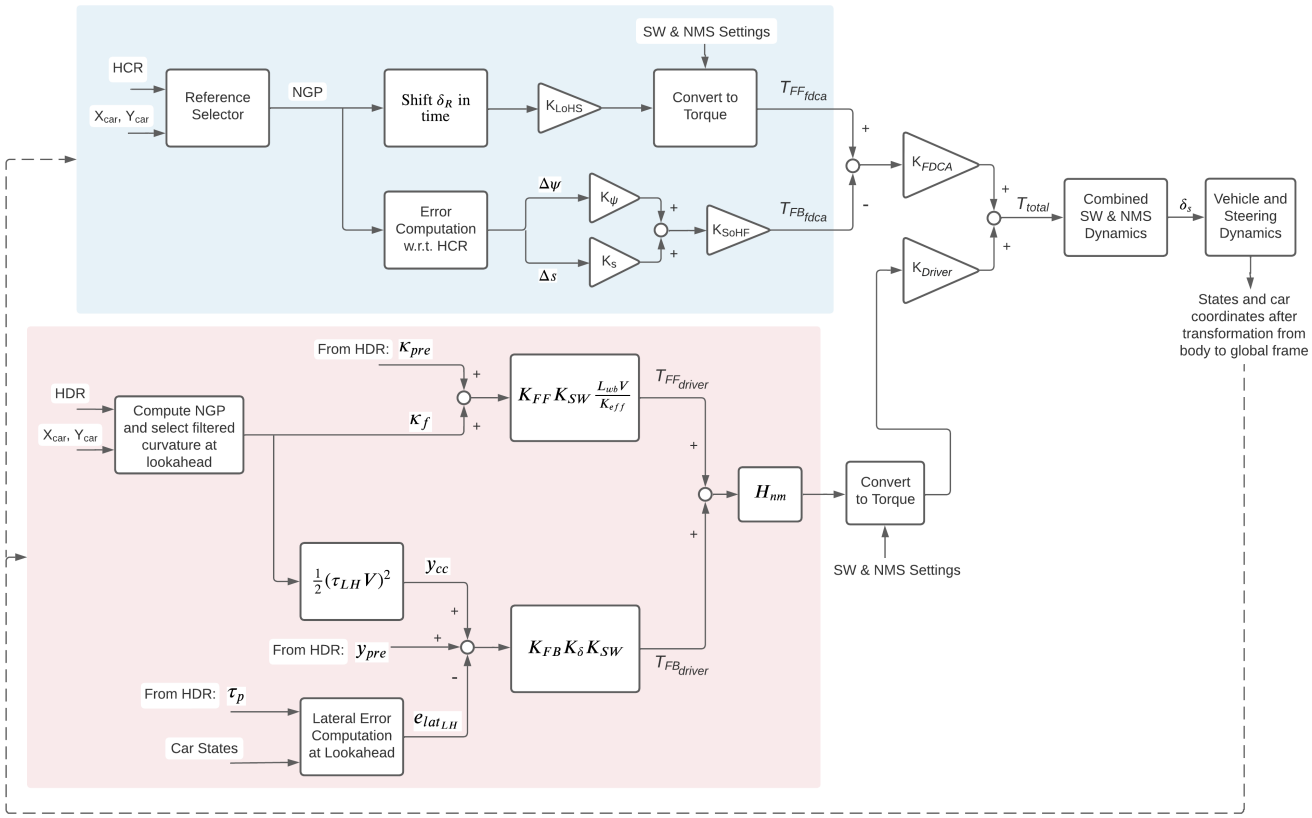

Figure 5.14: Block diagram of the HSC simulation. Top blue is the haptic controller and bottom red is the human controller.

Table 5.5: Baseline values for steering wheel and NMS mechanical properties

J_{SW}	B_{SW}	K_{SW}	J_{NMS}	B_{NMS}	K_{NMS}
0.005 [kg·m^2]	0.03 [N·ms/rad]	1 [Nm/rad]	0.064 [kg·m^2]	0.1 [N·ms/rad]	1 [Nm/rad]

Table 5.6: Baseline values for EVP driver model settings

K_{FF}	K_{FB}	T_{hs}	τ_{LH}	τ_p
0.21 [-]	0.07 [-]	0.45 [s]	1.5 [s]	1.3 [s]

from Table 5.5. These references include a moderate amount of curve cutting that can be expected in human drivers [31]. The human and haptic parts of the simulation will act based on the same reference: HCR = HDR. What happens when the references are not the same will be discussed at a later stage in Subsection 5.3.4. A slight amount of outwards prepositioning is added such that the model makes a small lateral adjustment towards the outside of the curve. This kind of steering behaviour can be seen especially in racing drivers as it leads to the fastest and most efficient way to take a turn. However, the very minor amount of prepositioning added in this case is unexpected to lead to different results for the different FDCA settings that will be treated here.

Due to the large number of variables contained within the complete HSC simulation it is very time consuming to get a complete view of the model. Therefore, for each FDCA parameter a handful of typical simulations cases will be discussed that accurately portray the sensitivity of the haptic shared control model. Changing FDCA parameters independently is useful for a preliminary analysis. However, in real life applications it is necessary to employ a cohesive method to tune all parameters simultaneously or to dynamically update parameters as needed by the individual driver.

Figure 5.15 shows how the model output changes depending on different levels of haptic support. The top part details the lateral position on the road over time while the middle and lower part provide the corresponding steering angle and steering torque. As expected a complete feedforward of the steering angle

($K_{LoHS} = 1$) in the haptic part of the simulation causes the shared control system to exactly follow the haptic reference (HCR). As the level of haptic support is reduced the degree to which the model exhibits curve cutting reduces. More steering torque is required from the human driver as LoHS decreases. It can also be concluded that a minimal LoHS of about 0.4 is needed for the car to stay within the lane boundaries for the full road section. Alternatively, a lower value for LoHS could be used if the collaboration gains are weighted more in favor of the human. It also appears that around a LoHS of 0.7 the model ends up producing a near centerline type of curve negotiation. This observation may be useful for implementing a HSC model based on the EVP driver model for human drivers that prefer staying near the center of the road for the given type of curve. Looking at the steering angle plot it can be seen that a high level of haptic support produces an almost ideal response to the road curvature. The steering angle gradually rises around 1s before the curvature starts increasing similar to how humans would anticipate corners in real life. Moreover, a lower LoHS means that a small overshoot in the steering angle will occur just after the curvature has reached its peak value. Simultaneously, it can be argued that this overshoot is only small and very smooth which indicates that the resulting steering behaviour will be stable and likely also acceptable to the human. As a result, it appears that for the given single curve problem the range of possible values for LoHS is between 0.4 and 1 provided the collaboration gains are fixed. Also note that the steering torque in the HCR reference case is lower compared to the total steering torques in the HSC simulations. This is due to lumping the neuromuscular and steering wheel dynamics in the HSC model whereas the neuromuscular dynamics in the EVP driver model consist of a first order lag transfer function. The method used to reconstruct the torque from the steering angle introduces this increase in torque which is then compensated for by the lumped steering wheel and neuromuscular dynamics.

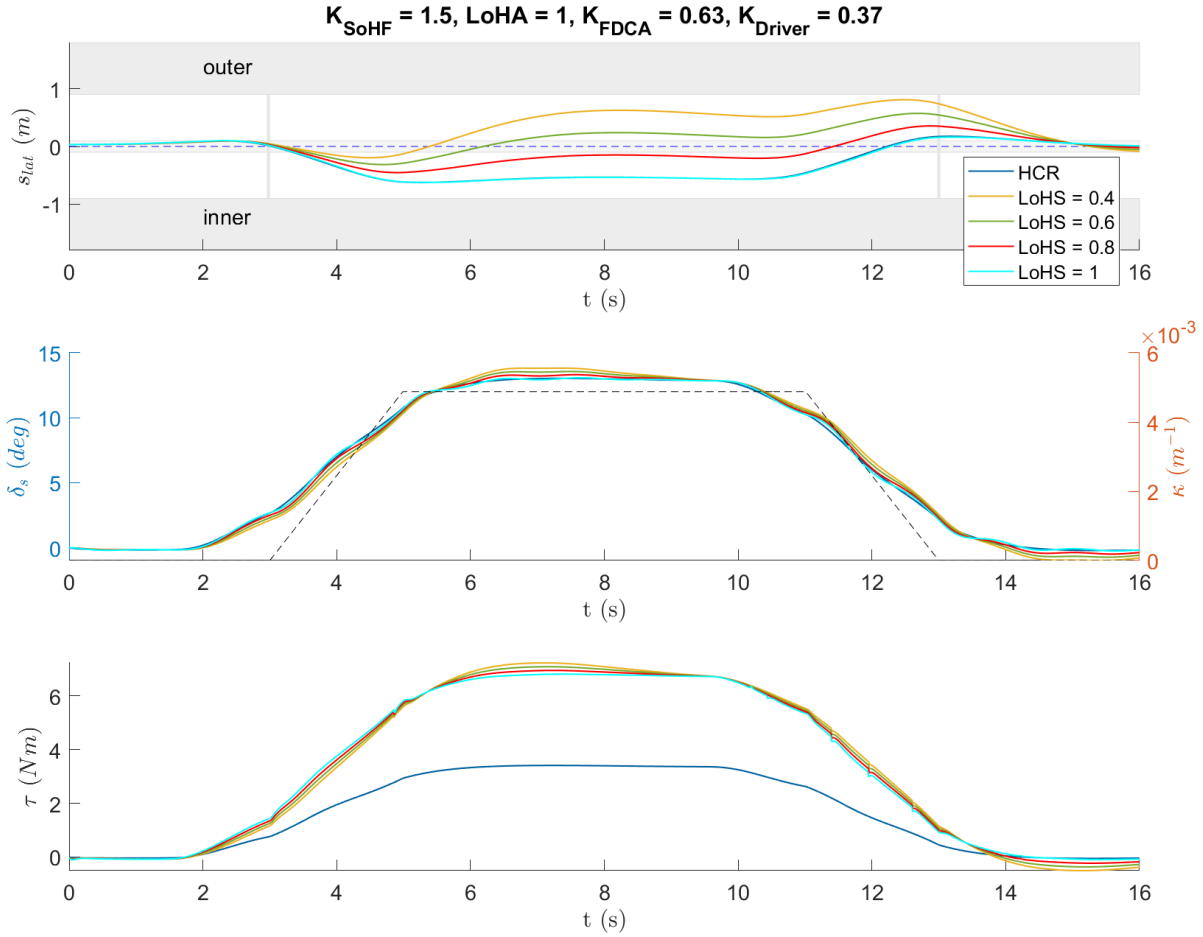

Figure 5.15: Sensitivity plot for the level of haptic support

Figure 5.16 illustrates how a lower level of haptic support below 0.4 can produce sufficient steering behaviour by shifting the collaboration gain balance towards the human. As a result of the larger importance placed on the human by the collaboration gain the lines in the plot are now closer together. Therefore, it is clear that

the impact of the LoHS setting on the resulting trajectory has now diminished significantly. As the haptic collaboration gain is decreased from 0.63 towards a lower value the lateral variation within the trajectories for the respective LoHS settings will decrease. As a result, the lateral plot for equal collaboration gains (0.5 for both the human and the haptic support) shows lateral trajectories which are slightly more grouped together compared to the default setting, see Figure 5.17. However, the differences compared to Figure 5.15 are not striking as the collaboration gain balance was only shifted slightly from 0.63 and 0.37 to 0.5 and 0.5. In the limiting case where the collaboration gain for the haptic support goes to an infinitesimally small value the resulting lateral plot will converge to the lateral trajectory of the human reference.

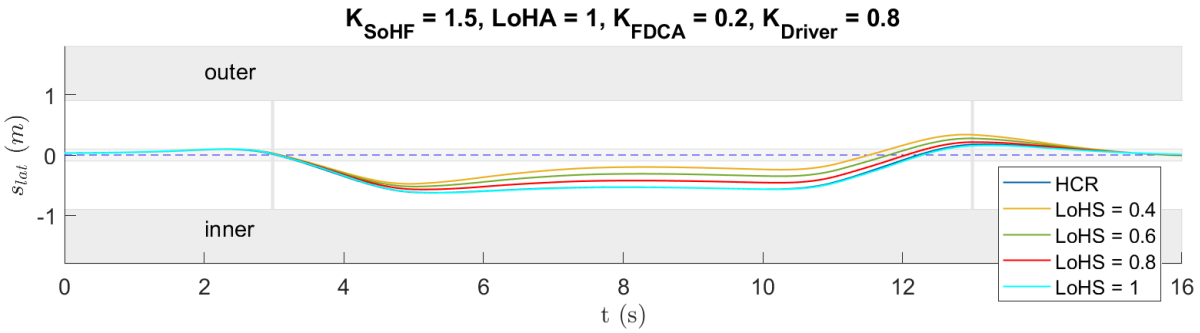

Figure 5.16: Sensitivity plot for the level of haptic support with a higher collaboration gain for the human

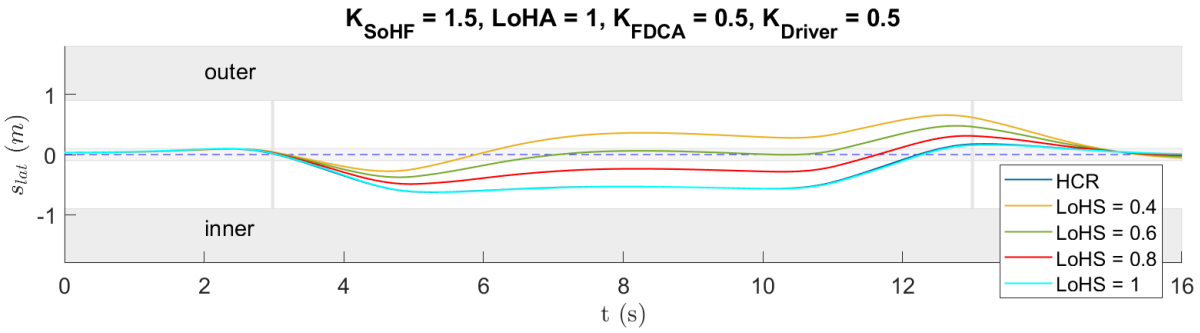

Figure 5.17: Sensitivity plot for the level of haptic support with equal collaboration gains for the human and the haptic support

Table 5.7 summarizes the resulting values for the metrics that can be computed for the preliminary simulations. These metrics are for simulations using the baseline values mentioned in Tables 5.4 - 5.6 except for K_{LoHS} which is varied. The torque conflict magnitude has been computed by checking if the driver and haptic support torques are of opposite sign for every point in time. No minimum threshold is used for which conflict will be registered and as a result even the smallest opposing torques will be counted. If there is a conflict the absolute of the difference between the two torques then gives the conflict torque at that instant. The average of all the torque conflicts is then obtained and reported as the torque conflict magnitude in these results. As expected the amount of torque conflict and its frequency decrease as the LoHS is increased towards full feedforward of the steering angle in the haptic loop. The human torque contribution is computed as the median of the human torque fraction of the total torque for the complete time series. It is clear that a higher LoHS results in a smaller relative human torque contribution. Moreover, after checking the individual human torques for the different settings it is concluded that when the LoHS is decreased the human torque naturally goes up to compensate for the extra torque needed to make the turn. Furthermore, the HSC performance is computed as the lateral position error (e_{lat}) with respect to both the HCR and HDR. The averages of the absolute errors are taken and then combined to obtain a mean and standard deviation for the performance metric, see Equation 5.19.

$$\mu_e = \frac{\mu(|e_{lat_{HCR}}|) + \mu(|e_{lat_{HDR}}|)}{2} \tag{5.19}$$

$$\sigma_e = \frac{\sigma(e_{lat_{HCR}}) + \sigma(e_{lat_{HDR}})}{2} \tag{5.20}$$

Consequently, this allows to compute a composite measure of performance in case the HCR and HDR are not aligned (see Subsection 5.3.4). Higher values for LoHS result in better performance metrics. Furthermore, the performance seems to decrease linearly as the LoHS is reduced. Finally, the human steering effort is computed as the work done by the human torque on the steering wheel. Numerically this is computed as the work done by human torque over the change in steering angle in between two time steps, see Equation 5.21. As LoHS increases the steering effort goes down in line with the reduction in human steering torque.

$$W_h = \sum_{i=1}^{N} T_d(i) \cdot (\theta(i+1) - \theta(i)) \tag{5.21}$$

Table 5.7: Resulting metrics for LoHS simulations

HSC Settings	Torque Conflict	Human Contribution	Performance	Steering Effort
HCR = HDR LoHS = 0.4	0.0616 Nm 1.374%	0.521	0.548 m (μ) 0.464 m (σ)	0.920 Nm
HCR = HDR LoHS = 0.6	0.0556 Nm 1.124%	0.471	0.364 m (μ) 0.308 m (σ)	0.801 Nm
HCR = HDR LoHS = 0.8	0.0332 Nm 0.874%	0.422	0.181 m (μ) 0.153 m (σ)	0.690 Nm
HCR = HDR LoHS = 1	0.0128 Nm 0.937%	0.370	0.00503 m (μ) 0.00706 m (σ)	0.590 Nm

5.3.2. Effect of Changing K_{SoHF}

For the sensitivity analysis of the strength of haptic feedback the same baseline values will be used, see Table 5.4. The only change that is made here considers the LoHS value. In order to investigate the effect of changing SoHF it is not possible to use a complete feedforward of the steering angle (i.e. LoHS = 1) as the lateral plot would be on top of the HCR line regardless of the haptic feedback setting. Therefore, a choice is made to set LoHS to 0.7 for the remainder of the SoHF sensitivity analysis. In Figure 5.18 the results are shown for different strengths of haptic feedback. It can be seen that a higher feedback gain results in a lateral trajectory that is increasingly closer to the reference. This effect is most prominent in the second half of the curvature section.

The torque conflict seems to be decrease for higher values of the strength of haptic feedback gain, see Table 5.8. From previous experiments it is known that this is generally not the case. Therefore, it is concluded from this simulation that it is very difficult to model torque conflict and hence acceptance of the HSC system for a range of SoHF gain values. The human torque contribution meanwhile reduces as SoHF increases since the human torque as a fraction of the total torque decreases. Furthermore, it is also clear that performance gains from increasing SoHF are nonlinear. For example: increasing the SoHF from a low to intermediate value provides a significant increase to performance whereas an increase in SoHF from intermediate to high only adds a further small increase in lateral performance. It may thus be more practical to keep the haptic feedback as low as possible while maintaining smooth steering qualities even in absence of or a lack of human steering torque. Finally, human steering effort is slightly affected by changing the SoHF. However, as explained before the human steering effort may increase if the haptic support is experienced as incompatible with the control goals of the driver.

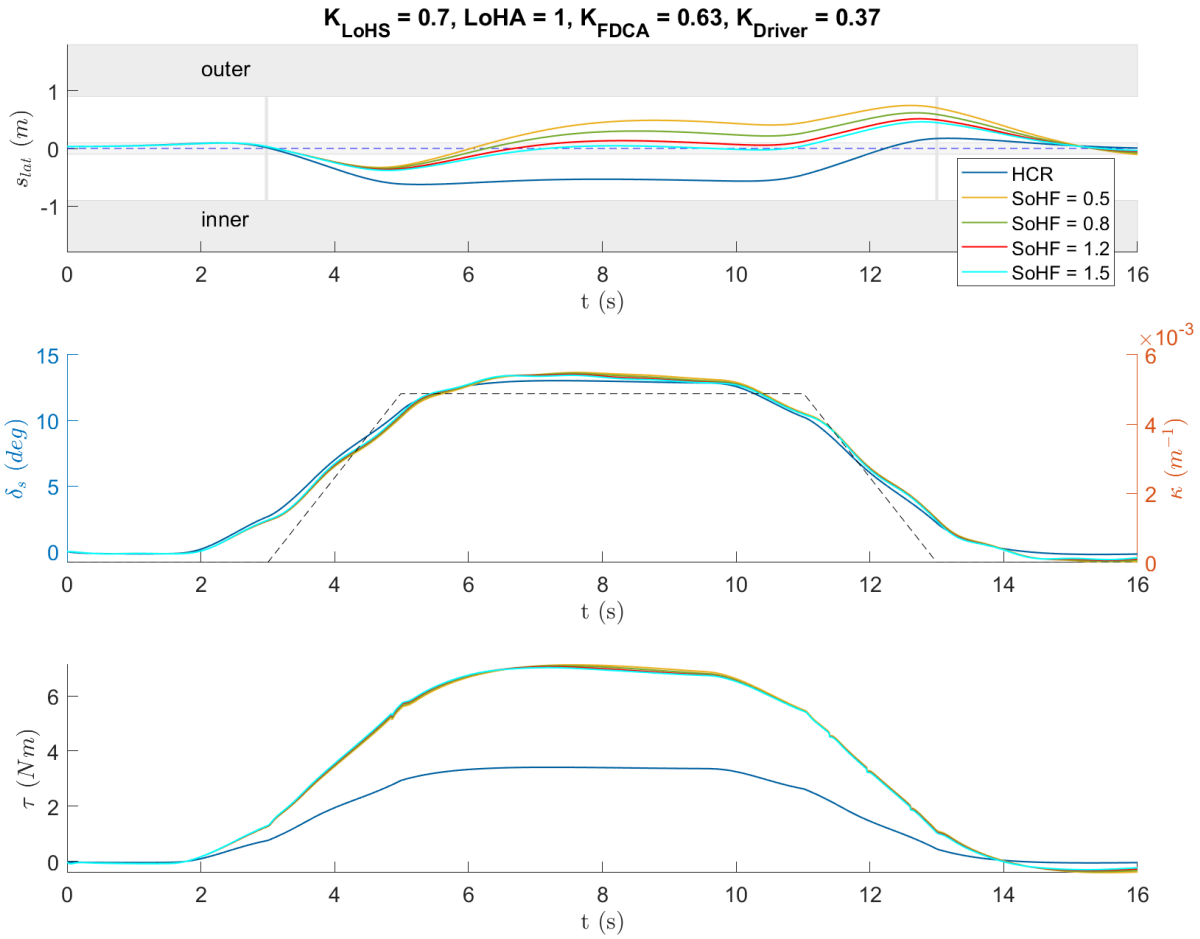

Figure 5.18: Sensitivity plot for the strength of haptic feedback

Table 5.8: Resulting metrics for SoHF simulations

HSC Settings	Torque Conflict	Human Contribution	Performance	Steering Effort
HCR = HDR SoHF = 0.5	0.0910 Nm 1.999%	0.527	0.464 m (μ) 0.403 m (σ)	0.848 Nm
HCR = HDR SoHF = 0.8	0.0773 Nm 1.624%	0.498	0.384 m (μ) 0.330 m (σ)	0.806 Nm
HCR = HDR SoHF = 1.2	0.0631 Nm 1.187%	0.471	0.311 m (μ) 0.265 m (σ)	0.765 Nm
HCR = HDR SoHF = 1.5	0.0447 Nm 1.062%	0.462	0.273 m (μ) 0.231 m (σ)	0.744 Nm

In order to investigate what happens when the SoHF is increased even more an additional set of simulations is done. The results are shown in Figure 5.19. It is clear that the steering behaviour becomes unstable somewhere in the range of 2.5 to 5 for the SoHF setting. This must be prevented at all cost and as such the SoHF gain should be kept below 2.5. The exact value for which stability can be guaranteed depends on the other HSC settings and particularly on the NMS and steering wheel mechanical properties.

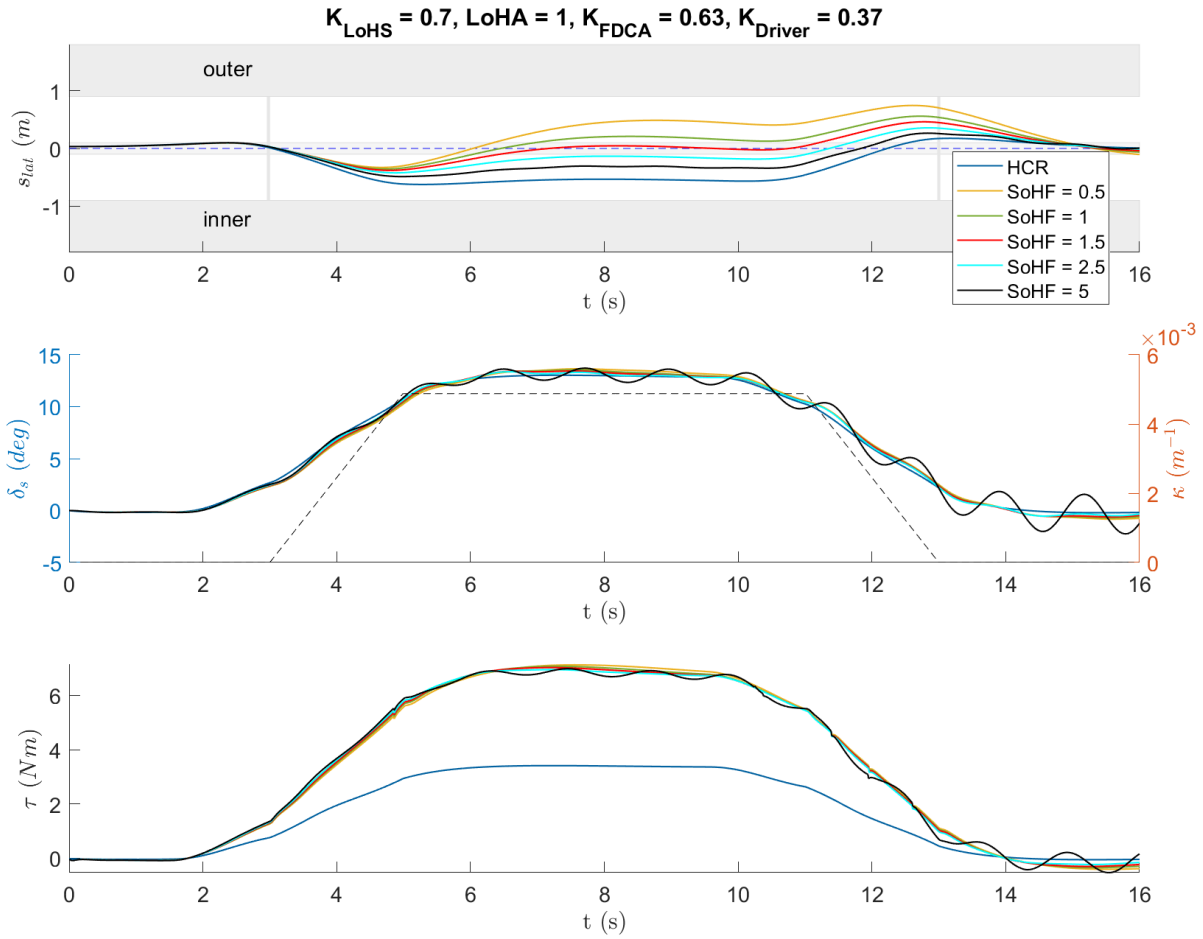

Figure 5.19: Sensitivity plot for the strength of haptic feedback for a bigger range of gain settings

5.3.3. Effect of Changing LoHA

The third FDCA parameter concerns the level of haptic authority (LoHA). In this implementation the LoHA value influences the control authority by setting the steering wheel stiffness to a value which is some factor of the intrinsic steering wheel stiffness. A value of 1 is the default setting which does not alter the steering wheel stiffness. It therefore makes sense to investigate what happens in case of LoHA settings lower, higher and equal to 1. Figure 5.20 provides the sensitivity plots for LoHA values ranging from 0.5 to 3.

An increase in the steering wheel stiffness produces changes in two locations of the HSC model. Firstly, the lumped NMS and steering wheel dynamics are updated with the new steering wheel stiffness. Secondly, the updated steering wheel stiffness directly affects the feedforward part of the human torque computation loop. A value of 2 for the LoHA then doubles the human FF steering torque in the HSC simulation. The first effect cancels out since the torque generation increase is compensated for by the updated NMS and steering wheel dynamics. Consequently, a change in the human steering torque causes the differences in the sensitivity plots for different values of the level of haptic authority. It can be noted that a low LoHA only slightly reduces the amount of curve cutting. At the other side of the spectrum an increase in steering wheel stiffness (i.e. a higher LoHA) enforces the HSC model to follow a stronger curve cutting trajectory due to the increase in human feedforward torque. Due to the way the LoHA can slightly tune the steering behaviour towards more or less aggressive curve cutting in these simulations it might be suitable for achieving a steering feel that is comfortable to the individual driver.

By inspecting the metrics for all LoHA settings it can be seen that a change in LoHA towards either side of the spectrum increases conflict, reduces performance and significantly affects the required human steering effort, see Table 5.9. More specifically, a high LoHA setting yields more conflict torques than a low setting while also inducing the need for the human to apply more torque to the steering system. In conclusion, as long as performance and acceptance permit a change to the LoHA setting it is possible to adapt its setting

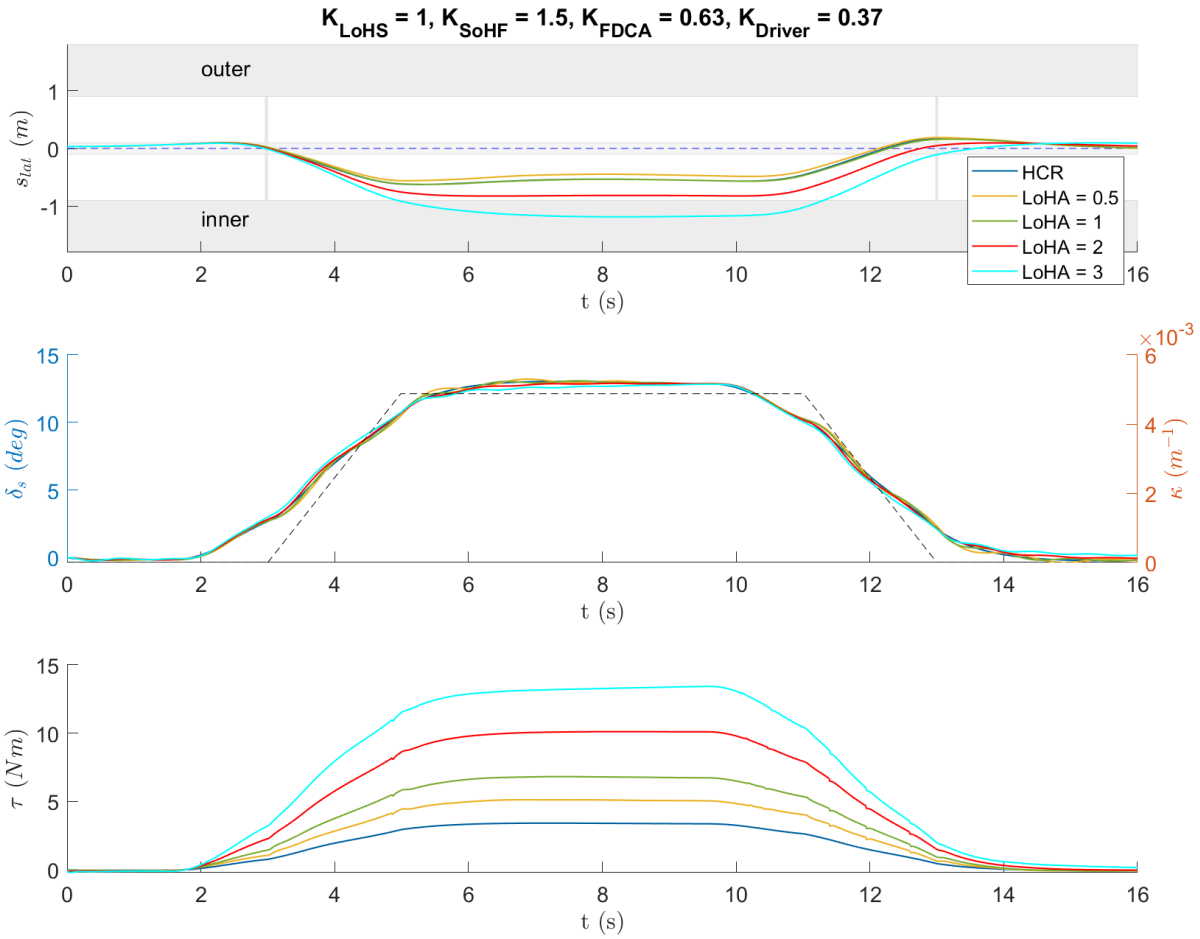

Figure 5.20: Sensitivity plot for the level of haptic authority

to meet the individual's needs and preferences for steering wheel handling qualities.

Table 5.9: Resulting metrics for LoHA simulations with LoHS = 1

HSC Settings	Torque Conflict	Human Contribution	Performance	Steering Effort
HCR = HDR LoHA = 0.5	0.0160 Nm 0.687%	0.347	0.0407 m (μ) 0.0350 m (σ)	0.426 Nm
HCR = HDR LoHA = 1	0.0128 Nm 0.937%	0.370	0.00503 m (μ) 0.00706 m (σ)	0.590 Nm
HCR = HDR LoHA = 2	0.0433 Nm 7.495%	0.405	0.135 m (μ) 0.116 m (σ)	0.929 Nm
HCR = HDR LoHA = 3	0.0910 Nm 1.874%	0.429	0.306 m (μ) 0.266 m (σ)	1.309 Nm

In order to get a more detailed idea of how the LoHA parameter affects the HSC model output another set of simulations is done with a lower value of haptic support of 0.6. The results are shown in Figure 5.21. Once again an increase in LoHA adds some curve cutting by increasing the human feedforward torque, especially around the middle section of the curve. It is also clear that the system appears to be stable for the full LoHA range of values regardless of the level of haptic support. This was verified by running the simulations for low LoHS values such as 0.3, see Figure 5.22. Finally, it is concluded that the effect of LoHA on the curve cutting diminishes as LoHS becomes smaller since the lack of feedforward in the haptic loop can not be fully compensated for by increasing the LoHA.

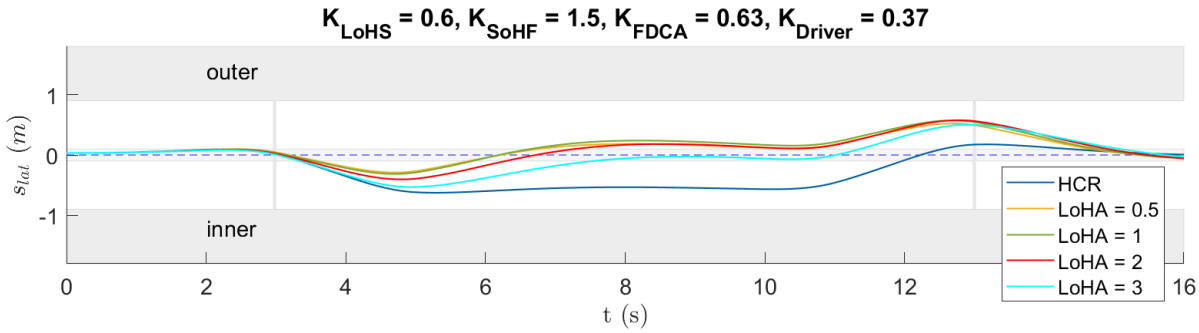

Figure 5.21: Sensitivity plot for the level of haptic authority for a lower baseline value of LoHS

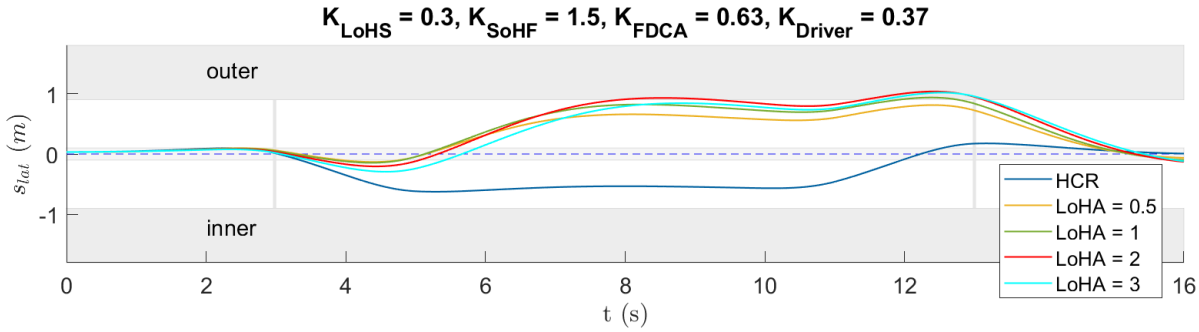

Figure 5.22: Sensitivity plot for the level of haptic authority for the lowest baseline value of LoHS

5.3.4. Effect of Dissimilar References

The results of the simulations in this Subsection are obtained for a fixed level of haptic support of 0.92 in accordance to previous research on this topic [26]. In order to investigate what happens when the HCR and HDR are not aligned several scenarios are investigated. In the first scenario, either the HCR or HDR remains equal to the baseline reference (see Table 5.4) while the other reference now contains slightly weaker curve cutting (obtained by decreasing K_{FF} from 0.21 to 0.14). In the second scenario a strong curve cutting reference (K_{FF} increased to 0.28) is combined with a reference where the "opposite" of curve cutting is generated with the EVP driver model. This will be referred to as curve slipping and is obtained by lowering K_{FF} from the baseline value of 0.21 to 0.03 while simultaneously decreasing K_{FB} from the baseline of 0.07 to 0.06. The corresponding steering response is just strong enough such that the curvature is navigated successfully at the outer side of the curve (i.e. the road half opposite of where the car would be in the curve cutting scenario). This is done in an attempt to maximise the disagreement between the two references. The resulting metrics are summarized in Table 5.10 for every scenario which are compared to a baseline simulation where the references are equal (see top row). Curve cutting is abbreviated here as CC.

It can be concluded that the amount and frequency of torque conflict increases for every scenario except for one (weak HCR & default HDR) compared to the ideal situation where both references are equal. Furthermore, a reference that exhibits weaker curve cutting compared to the other one produces more conflict when the HDR is less aggressive in cornering compared to the HCR. The mirrored scenario (HCR has weaker CC than HDR) does not cause as much and frequent torque conflict in this case and is close to the baseline level in terms of conflict with slightly worse lateral performance. This result may be counter intuitive considering the fact that the HCR is associated with the higher collaboration gain. However, a change in the HDR flows through to both the feedforward and feedback torque paths of the human driver model whereas in the HCR case only the feedforward torque path is affected. The net result is that a mismatch in the HDR causes the biggest magnitude of torque conflict. On the other hand, a similar mismatch in the HCR causes a relatively smaller amount of torque conflict which is more frequent in occurrence. This is due to the higher collaboration gain for the haptic support even though the amount of conflict is more pronounced when the human reference is mismatched since both the feedforward and feedback paths in the HSC model are affected. Lateral performance only decreases slightly when small mismatches occur between the two references. When large mismatches are present the lateral performance

will be affected significantly. This notion may prove that a HSC model based on the FDCA and the EVP driver model is quite robust to misaligned references in terms of lateral performance. Finally, it must be indicated that the human contribution to the steering task as well as the steering effort are impacted significantly in case of large mismatches between references. Mismatches must therefore be minimized as much as possible such that FDCA parameter settings can be independently tested without interference from HCR/HDR misalignment(s).

Table 5.10: Resulting metrics for simulations with different combinations of human and haptic references

HSC Settings	Torque Conflict	Human Contribution	Performance	Steering Effort
HCR = HDR LoHS = 0.92	0.0122 Nm 0.625%	0.391	0.0708 m (μ) 0.0594 m (σ)	0.628 Nm
HCR default HDR weak CC	0.0194 Nm 0.812%	0.377	0.0637 m (μ) 0.0542 m (σ)	0.609 Nm
HCR weak CC HDR default	0.00884 Nm 0.437%	0.404	0.0784 m (μ) 0.0657 m (σ)	0.656 Nm
HCR default HDR strong CC	0.0764 Nm 5.684%	0.410	0.0944 m (μ) 0.0804 m (σ)	0.667 Nm
HCR strong CC HDR default	0.0716 Nm 7.995%	0.372	0.0777 m (μ) 0.0684 m (σ)	0.583 Nm
HCR strong CC HDR slipping	0.0830 Nm 9.557%	0.307	0.290 m (μ) 0.232 m (σ)	0.490 Nm
HCR slipping HDR strong CC	0.0904 Nm 5.934%	0.481	0.290 m (μ) 0.232 m (σ)	0.814 Nm

Figure 5.23 shows the lateral position plot for the baseline parameter set. Note that the HCR and HDR reference trajectories are the same and as a result overlap in this case. The lateral position output of the total HSC system is indicated as well and it contains slightly less curve cutting as the level of haptic support does not provide full feedforward (0.92). Subsequently, investigate Figure 5.24 and compare with the baseline plot to see the effect of a HCR with weaker curve cutting. Notice how the HSC simulation output contains slightly less curve cutting. When the HDR has weaker curve cutting the resulting plot is found in Figure 5.25. In this plot the HSC simulation produces a similar plot with less curve cutting and slightly more lateral deviation than when HCR was changed, analogous to the performance results found earlier.

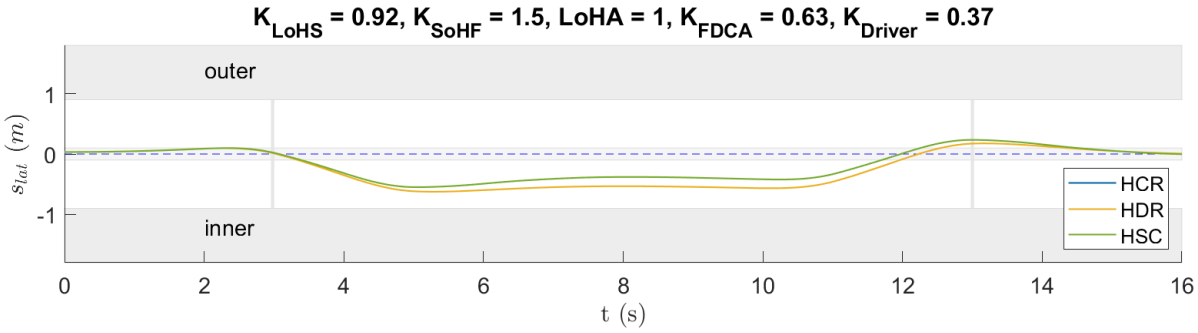

Figure 5.23: Lateral position plot for HCR equal to HDR with LoHS set to 0.92

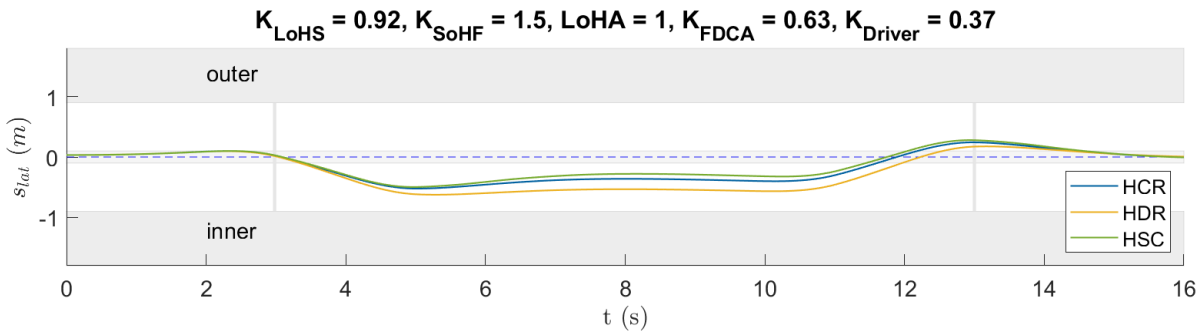

Figure 5.24: Plots for HCR with weaker curve cutting compared to HDR

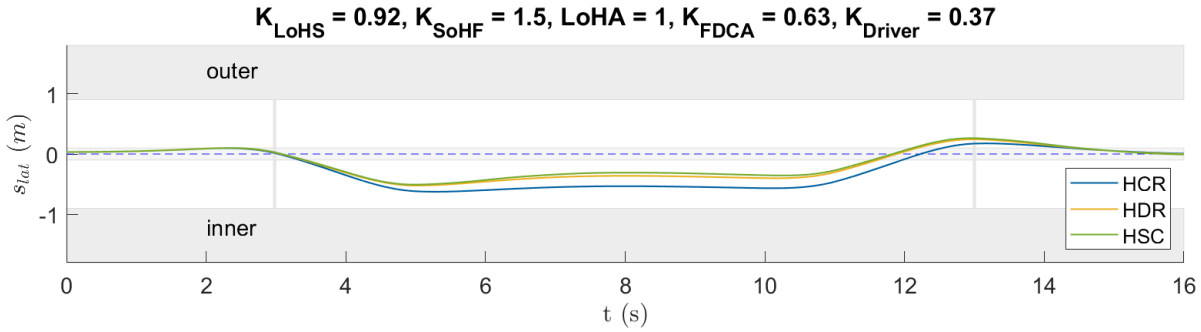

Figure 5.25: Plots for HDR with weaker curve cutting compared to HCR

Figure 5.26 and 5.27 provide the lateral position plot in case either the HCR or HDR respectively includes significantly stronger curve cutting compared to the default reference. As expected the HSC system produces a stronger steering response in both cases compared to the standard case. A small difference between the two cases can be seen at the start of curve section where the lateral position reaches its minimum value. When the HCR is stronger the system cuts the corner slightly more at the start of the maximum curvature than when the HDR is stronger. Apart from this, the resulting lateral trajectory through the curve is very similar with minor differences in the conflict and performance metrics as discussed before.

Figures 5.28 and 5.29 detail how the HSC output changes when big mismatches between the two references occur. Notice that in this case the largest change to the HSC output occurs for the case where the HCR contains curve slipping. This may be due to the higher collaboration gain for the haptic part of the simulation which generates torque with respect to the HCR. Finally, it is important to note that this analysis cannot indicate how the acceptance of the HSC system degrades as the references are dissimilar. This can be illustrated by the fact that high levels of conflict are found when a strong curve cutting reference is combined with a curve slipping reference on both sides of the spectrum irrespective of which reference is the curve cutting or curve slipping one. However, from the human point of view a scenario where they are required to deliver a strong contribution which is in conflict with the automation will likely be perceived as more obtrusive compared to a scenario where they need to supply only a small contribution to the total steering input.

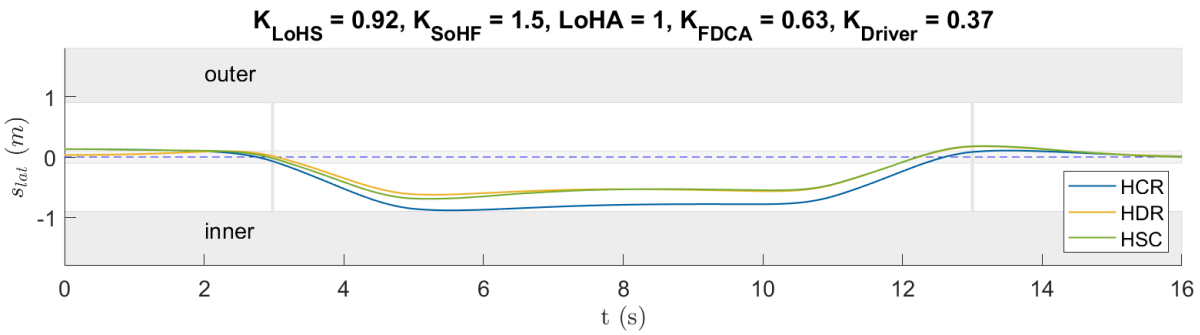

Figure 5.26: Lateral position plot for HCR with stronger curve cutting and HDR with default curve cutting

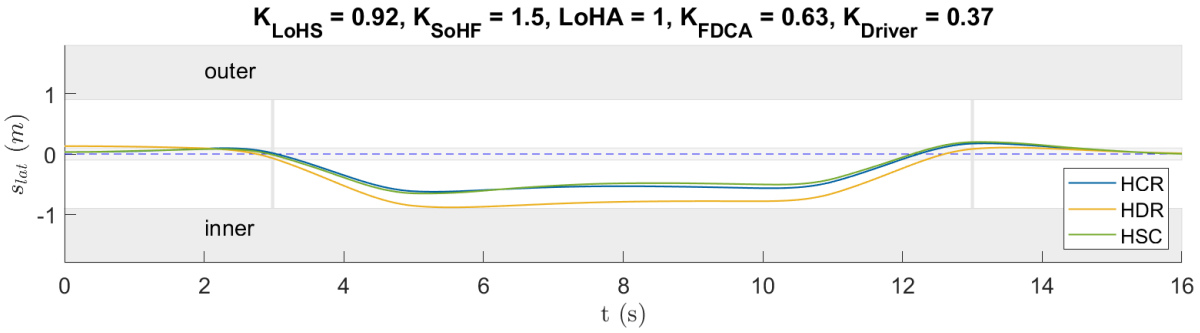

Figure 5.27: Lateral position plot for default HCR and HDR with stronger curve cutting

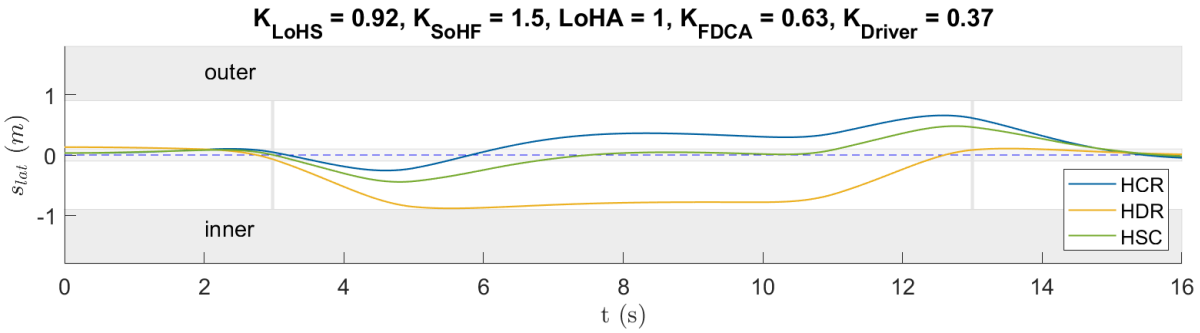

Figure 5.28: Lateral position plot for HCR with curve slipping and HDR with strong curve cutting

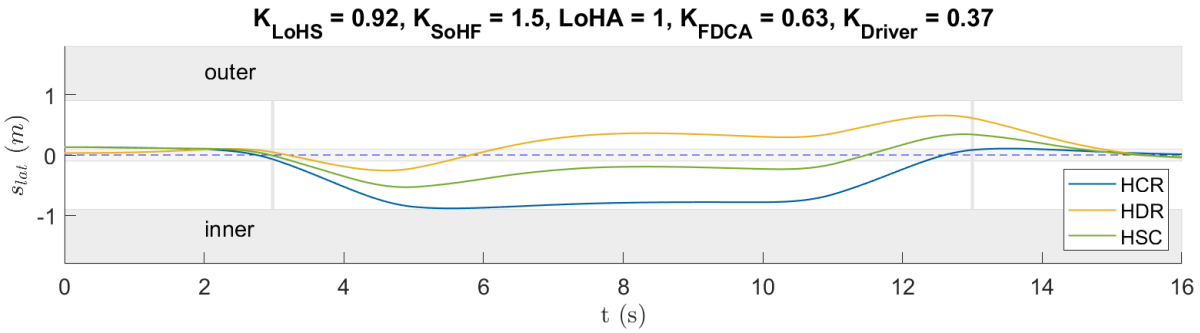

Figure 5.29: Lateral position plot for HDR with curve slipping and HCR with strong curve cutting

5.4. Key Conclusions for FDCA Parameter Sensitivity Analysis

This section contains a summary of the key takeaways and conclusions based on the FDCA parameter sensitivity analysis in Section 5.3. The conclusions are given in bullet point form within boxes for each of the FDCA parameters which were investigated in the sensitivity analysis.

LoHS Sensitivity Analysis

- In the preliminary simulations the LoHS setting has a large effect on the trajectory that is driven. The impact on the collective steering response changes depending on the degree to which the haptic support is able to contribute steering torque to the shared control system. As the LoHS reduces the steering feedforward becomes increasingly incomplete. As a result, the vehicle trajectory in the curve goes from curve cutting at high LoHS values (> 0.75) to more sloppy curve negotiation where the curve is driven closer to the outer edge at intermediate LoHS values (0.4 - 0.6). For low LoHS values the vehicle may exceed the road boundaries, especially towards the end of the curve.
- As long as the human and haptic references match, increasing the LoHS reduces the amount of torque conflict while increasing lateral steering performance. Furthermore, the necessary human steering torque decreases significantly as the LoHS is increased.
- Due to the strong effects of the selected LoHS on the vehicle trajectory, the corresponding conflict and the required human steering effort it should be considered as the first and most prominent parameter to tune once a HCR has been established that matches the human reference.

SoHF Sensitivity Analysis

- Increasing the SoHF from a low to intermediate value provides a significant increase to performance whereas an increase in SoHF from intermediate to high only adds a further small increase in performance. According to these simulations there is thus no need for increasing the SoHF past intermediate values of around 1.2.
- This HSC model is unsuited for making realistic predictions on the amount of torque conflict across SoHF settings. However, from literature and previous experiments it is known that jerky steering feedback can be perceived as obtrusive. Therefore, instead of focusing on the SoHF setting it is probably more beneficial to find a good setting for the LoHS of a suitable HCR which only requires the addition of a little feedback (i.e. small SoHF).
- To keep the simulated HSC system within safety margins it can be said that SoHF values above 2 should not be used as too high gain settings can cause lateral instability of the steering system.

LoHA Sensitivity Analysis

- The LoHA setting in these simulations directly impacts the amount of curve cutting that occurs in the shared control case. This effect originates from the human loop of the shared control system since the computation for the amount of human steering torque includes two steering wheel stiffness terms. A LoHA value of 0.5 which sets the steering wheel stiffness to half its original value only reduced the amount of curve cutting by a very small margin. A higher LoHA value of 2 increased the amount of curve cutting significantly at the cost of requiring the human to exert just over 50% more torque compared to the default setting. Exceedingly high LoHA values such as 3 ended up steering the car too strongly in the middle section of the curve which results in the vehicle driving off the road temporarily.
- The chosen simulation setup does not account for changes in the human neuromuscular system which are to be expected when the steering feel changes as a result of a LoHA setting unequal to 1. This makes it difficult to predict how acceptance and individual LoHA settings are related. From the simulations results, however, it is clear that the amount of torque conflict increases drastically when the LoHA setting increases. In conclusion, small changes to the LoHA setting can be used to adapt the HSC system to the individual's preference for an acceptable control authority level.

Dissimilar References Analysis

- It is evident that any mismatch between the human and haptic reference will inherently result in torque conflict and a reduction in steering performance. From the simulations it appears that a mismatch from the human side increases the conflict slightly more compared to the same mismatch from the haptic support side of the system. Although conflict degrades rapidly when reference dissimilarity increases it can be concluded that a HSC model using the EVP driver model is comparably less sensitive in terms of lateral performance as the overall curve cutting steering response prevails.
- When the misalignment between references increases the severity of torque conflict increases non-linearly. In this analysis two types of extreme reference misalignment are studied: a strong curve cutting reference combined with normal curve cutting (1) and a normal curve cutting reference with anti curve cutting (2). By comparing these two it is interesting to note that an overly strong curve cutting reference is nearly as bad as a lackluster one which is too weak and would individually end up steering the vehicle near the outer side of the road. As a result, it may be important to ensure that a reference is implemented which includes a conservative amount of curve cutting (i.e. no excessive amount of curve cutting).

6

Model Verification

This chapter discusses the verification procedure and its results in order to ensure that the preliminary simulations are working as intended. Firstly, Section 6.1 discusses the verification of the HSC model. Subsequently, the HCRs that are generated using this model are verified in Section 6.2. Finally, an overview of these references is provided in Section 6.3 as well as the method used to implement them into the simulator environment.

6.1. HSC Model Verification

Verifying the Van Paassen driver model and the corresponding FDCA implementation is crucial in order to obtain results that may provide a representative indication of the human-machine cooperation characteristics. While the preliminary simulation is implemented verification procedures take place in parallel. The first step in this process consists of checking the written MATLAB code for errors. Once these errors are all resolved the used inputs and generated output signals for all models are checked and inspected for any inconsistencies or irregularities. The first step in the full FDCA simulation is the generation of the road data which is created by a separate function using the curvature vector as an input. From this function several outputs are obtained such as road coordinates, road heading and a reference heading and trajectory. The road curvature vector follows the shape of a step input if no clothoids are present. Once the curvature was adjusted to include these clothoids it steadily ramps up over time and decreases again after staying constant for a certain amount of time. The inclusion of these clothoids was easily verified by checking the curvature over time in a plot. Subsequently, this part of the FDCA simulation is verified if the curvature vector and generated road match. Additionally, the generated road is cross verified with previous research to ensure that the road generation process is correct and that the same road is obtained.

The road heading output obtained from the road generator is used at a later stage to compute the car heading with respect to the road. After transformation of the body frame coordinates to the global frame it is possible to plot the car trajectory in a top-down 2D plot. In doing so it was found that a sudden excessive jump in the vehicle position was present under for a road set up with long corners that exceeded π. This error occurred as a result of using the basic arc tangent function in MATLAB to compute the road heading reference. This function does not properly handle sign changes in the $\frac{x}{y}$ coordinates contribution to the heading estimation. A solution for this issue was implemented that makes use of the *atan2* robust computation function for the arc tangent. This resolved a discontinuity in the generated road reference heading angle in the road generator script.

Second in the verification procedure is the process of checking the generated driver model output which is handily done with the lateral position and steering angle plots. The main input to the extended Van Paassen driver model is the curvature vector which has been verified before. Alternatively, the selected seven EVP driver model parameters are the driver class, straight section bias, feedforward and feedback gains, curvature filter time constant, lookahead time and prediction time. The influence of each setting has been investigated in Section 5.1.3 and their values are adjusted until a satisfactory amount of curve cutting is generated by the driver model. Satisfactory in this case implies a steady lateral position plot which shows

a degree of curve cutting which is consistent (no sudden or significant fluctuations) and naturalistic, i.e. similar to how real drivers may cut corners on real roads. As a result of these preliminary simulations it is possible to generate human-compatible references which exhibit strong, moderate or weak curve cutting behaviour. Additionally, a reference was generated which follows the road centerline as well as one with a small degree of curve slacking (curve is completed but on the opposite side of the road compared to the curve cutting trajectories). Such a curve slacking trajectory would be representative of a driver that prefers to complete the curve towards the outside of the curve as opposed to the inside of the curve for the curve cutting group. The generation process of these HCRs is discussed further in Section 6.3. The driver model implementation is subjected to different roads with varying curvatures in a further effort to remove any shortcomings or bugs in the code.

Finally, the model is run with a noisy curvature vector input to check the sensitivity and the resulting steering behaviour. A noisy curvature vector is equivalent to letting the model simulate driving on a jittery road with sudden changes in geometry which is not realistic for simulating human driving behaviour. This analysis is performed purely to investigate how the main model outputs for the HCR (i.e. road position, heading and steering angle) are affected by a stochastic input to the EVP model. The result can be seen in Figure 6.1 where two levels of noise for the curvature input vector k are compared to the case without noise. A high noise level corresponds to an additional amount of noise on the curvature vector that is equal to 75% of the mean of the curvature, see Equation 6.1. Similarly another noisy curvature vector is generated with a low noise level of 25% of the mean of the curvature.

$$\kappa_n(i) = \kappa(i) + 0.75 \cdot \mu(\kappa) \cdot \mathrm{R(i)} \tag{6.1}$$

It is clear that the generated lateral road position over time stays relatively close to the curve cutting

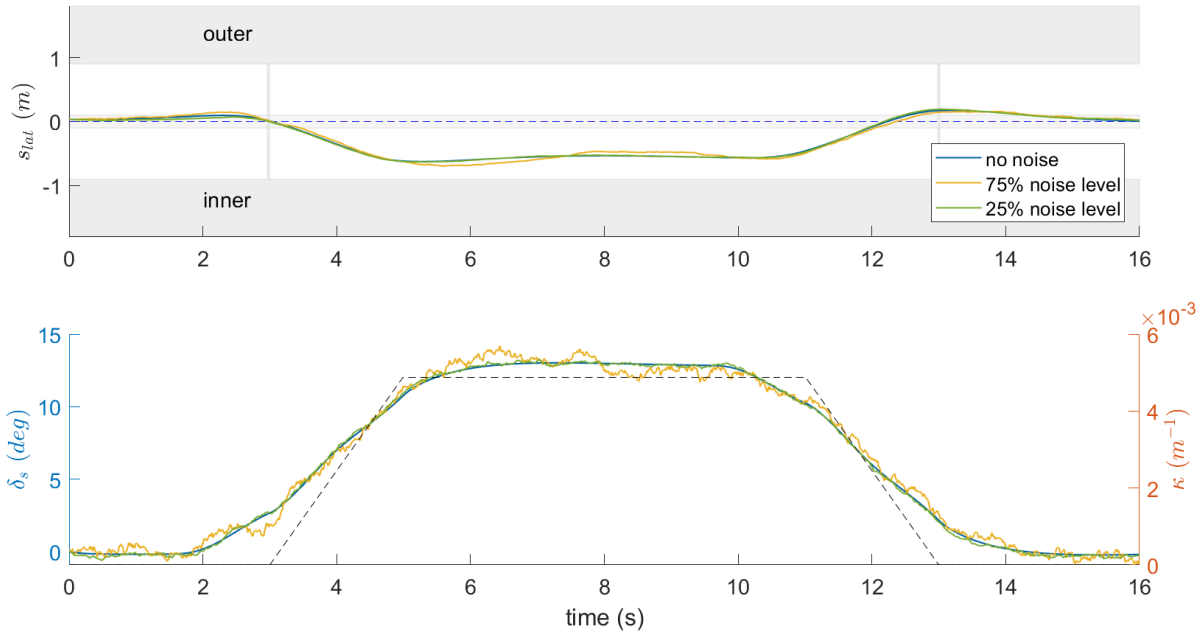

Figure 6.1: Extended Van Paassen driver model lateral position and steering angle output for two levels of noise applied to the road curvature vector.

references without any noise for the low level of noise. In case of the higher noise level the lateral road position swerves slightly around the deterministic lateral position. A larger effect can be seen in the steering angle. The resulting steering angle of the vehicle is affected significantly in case of the high level of noise. Contrarily, a low noise level results in only a very minor departure from the deterministic case. To get a better view of how the noise impacts the system the errors with respect to the no noise case are plotted in Figure 6.2 for the lateral road position and the steering angle. As noted before the lateral road position increases for higher noise levels but remains easily within the road width boundaries of +/- 0.9m. Additionally, the steering angle is clearly affected the most when the noise increases due to the way the vehicle steering dynamics make use of the road curvature input. In the feedforward loop the road curvature

noise directly contributes to an additional change in the steering angle while simultaneously the feedback loop will also generate an extra steering angle contribution based on the dynamic states from the vehicle steering dynamics which take the road curvature as an input. This produces a more pronounced effect on the steering angle compared to the lateral road position which is only impacted once by the road curvature which goes into the vehicle dynamic states.

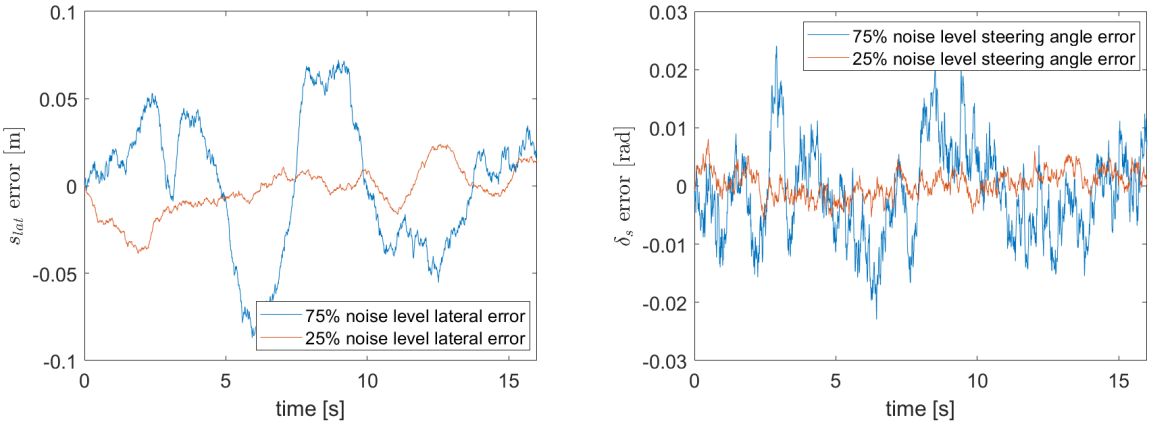

Figure 6.2: Extended Van Paassen driver model lateral position and steering angle errors with respect to the no noise case for a high and a low level of noise.

This short analysis shows that the EVP model remains stable even when the curvature vector contains a significant amount of noise. Especially the lateral road position output remains useful for both levels of noise. Alternatively, the steering output becomes quite noisy which may prove problematic when used as a reference in the HSC implementation. Some filtering or smoothing of the steering angle signal might be required for high levels of noise. The deterministic nature of the preliminary simulations means that this noise problem does not need to be investigated thoroughly in this thesis project. However, applications where the stochastic road curvature is measured in real-time, such as with a sensing system in an automated vehicle, would have to deal with this issue accordingly. This importance of minimizing the effects of noise in the HSC implementation stem from the fact that the steering angle from the HCR is directly used as a feedforward input to the generated haptic steering torque.

6.2. HCR Verification

The output from the extended Van Paassen driver model can be used as a human-compatible reference in a haptic shared control system. For the haptic support to function as intended it is therefore critical that the HCR is properly set. The obtained HCR is verified here by plotting it against a reference that was derived from measurements in a simulated manual driving environment in a HSC research project by Ghys et al. [26]. These references are based on the same road data with 6 left and right 205m radius curves, see Figure 6.3.

Since the sampling interval of the old HCR derived from simulator measurements is not constant the references are plotted against the x and y coordinates. Firstly, Figure 6.4 compares the default HCR obtained with the EVP driver model to the HCR that was generated for a preceding research project by Emma Ghys [26]. It is apparent that the reference heading angles match closely. Small differences can be found at curve entry and exit, where the EVP model reacts to the curvature changes just slightly slower than the HCR derived from the manual driving measurements.

Figure 6.5 illustrates how the steering angle for both HCRs changes across the x and y coordinates. Similar to before it can be seen that the steering angle for the EVP driver model (Kelsey HCR) ramps up and decreases back to zero at a slightly later point on the road compared to the HCR derived from measurements (Emma HCR). Additionally, there is a discrepancy with regards to the extreme steering angle values between the two HCRs. The HCR obtained from the driver model contains about 15% less steering at the maximal and minimal steering angles. This difference can be attributed to the fact that the EVP driver model uses simplified car dynamics compared to the driving simulator used to measure the other HCR. As a result, the HCR from the driver model may not produce enough steering feedforward when applied in the HSC system

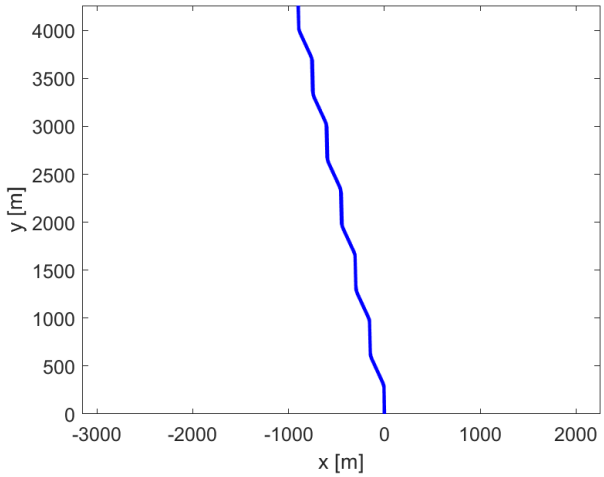

Figure 6.3: Experiment road used for generating the HCRs.

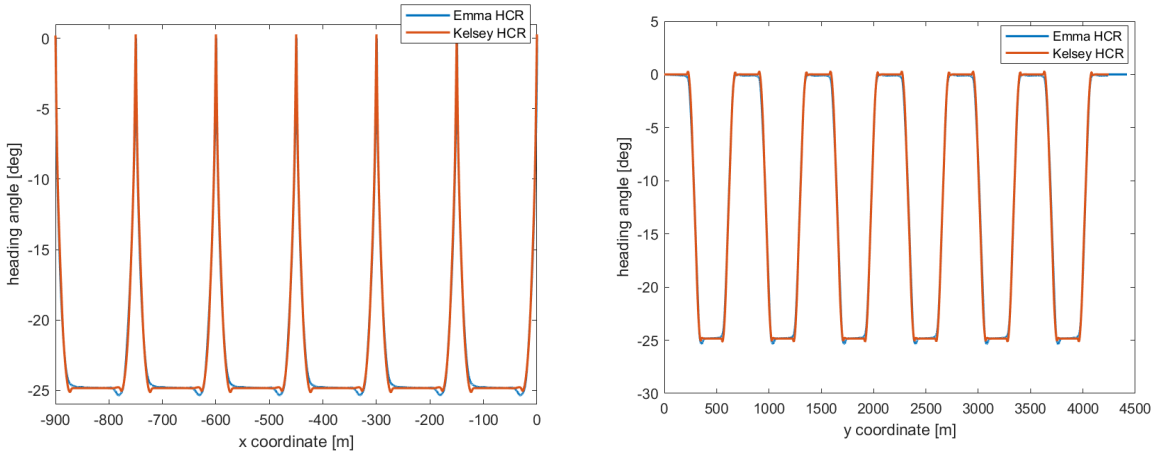

Figure 6.4: Emma HCR heading angle compared to Kelsey HCR heading angle.

of a driving simulator. This needs to be checked for during testing of the HSC system. A straightforward fix for this issue could be to implement a correction factor that scales the steering angle to achieve a complete feedforward steering signal.

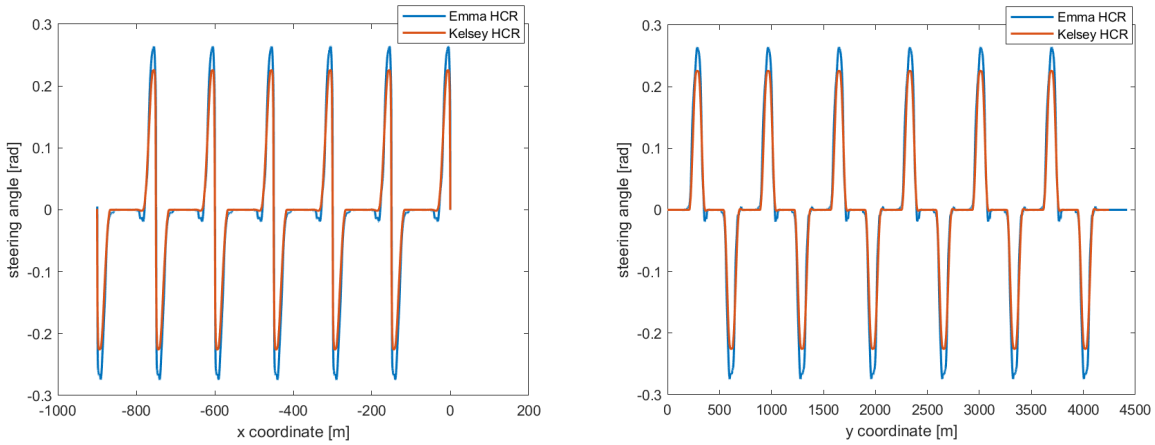

Figure 6.5: Emma HCR steering angle compared to Kelsey HCR steering angle.

6.3. HCR Generation Process

Several HCR variations are generated such that they can be tested in the HMI Lab simulator. Figure 6.6 gives an example of the lateral position range for which the EVP model can generate a HCR. For this plot only K_{FF} and K_{FB} are varied. By trying out different combinations for all EVP model parameters it is possible to

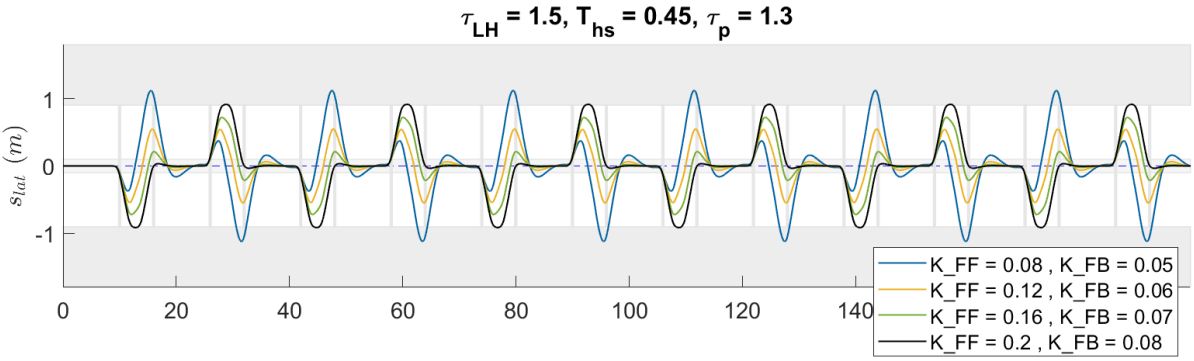

Figure 6.6: Lateral position range for full experiment road for different values of K_{FF} and K_{FB}.

achieve even more variation in output trajectories. This manual trial and error process lead to the selection of several references that are realistic and representative for different steering behaviour found in humans. These can then be imported into the HMI Lab simulator to get a feel for each of them during the experiment design phase such that one can be selected for use in the experiment. Table 6.1 lists the four variations that are investigated and the EVP model parameter selection for each HCR type. The HCRs discussed in this Section are compared to each other without the inclusion of prepositioning.

	K_{FF} [-]	K_{FB} [-]	T_{hs} [s]	τ_{LH} [s]	τ_p [s]
1. default CC	0.21	0.07	0.45	1.5	1.3
2. smoother CC	0.21	0.10	0.40	1.3	0.9
3. near centerline CC	0.30	0.12	0.35	1.0	0.8
4. anti CC	0.21	0.07	0.40	1.2	0.8

Table 6.1: EVP driver model settings for all generated HCRs

The full experiment road data is the input to the EVP model and the output HCR contains the x and y coordinates for the vehicle trajectory as well as the corresponding steering and heading angles. The default HCR is the same reference that was used throughout the preliminary simulations to study the driver model parameter sensitivities. Secondly, the smoother curve cutting HCR includes a nearly equal amount of curve cutting as the default reference. However, in this case the lateral position throughout the middle section of the curve is more constant while there is also less overshoot away from the centerline near the curve exit point. This can be seen when the two HCRs are compared in a lateral position and steering angle plot, see Figure 6.7. The third HCR type exhibits a very small amount of curve cutting close to the centerline. Finally, the fourth HCR type contains anti curve cutting where the curves are driven on the outer half of the road. The lateral position plot for these last two HCR types is given in Figure 6.8. This Figure clearly shows the small amount of curve cutting for the near centerline CC type in addition to the anti curve cutting response of the last HCR type. Furthermore, due to an axis change for the steering angle the plot appears to be quite different compared to the ones before even though it is very similar.

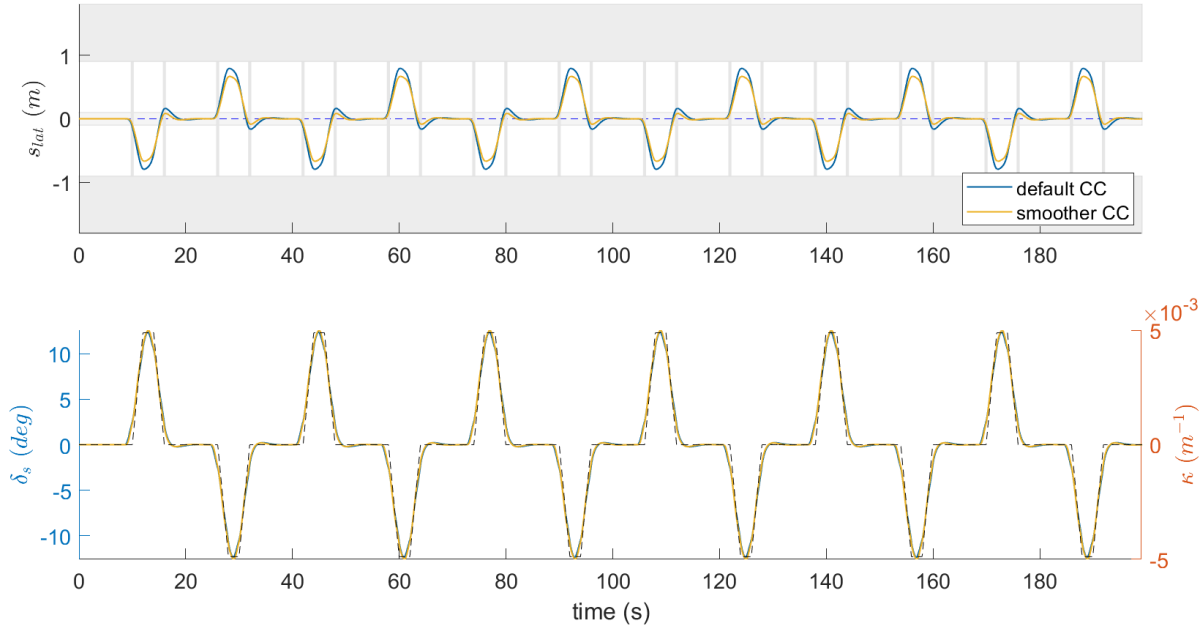

Figure 6.7: Lateral position and steering angle output for full experiment road for default and smoother CC HCRs.

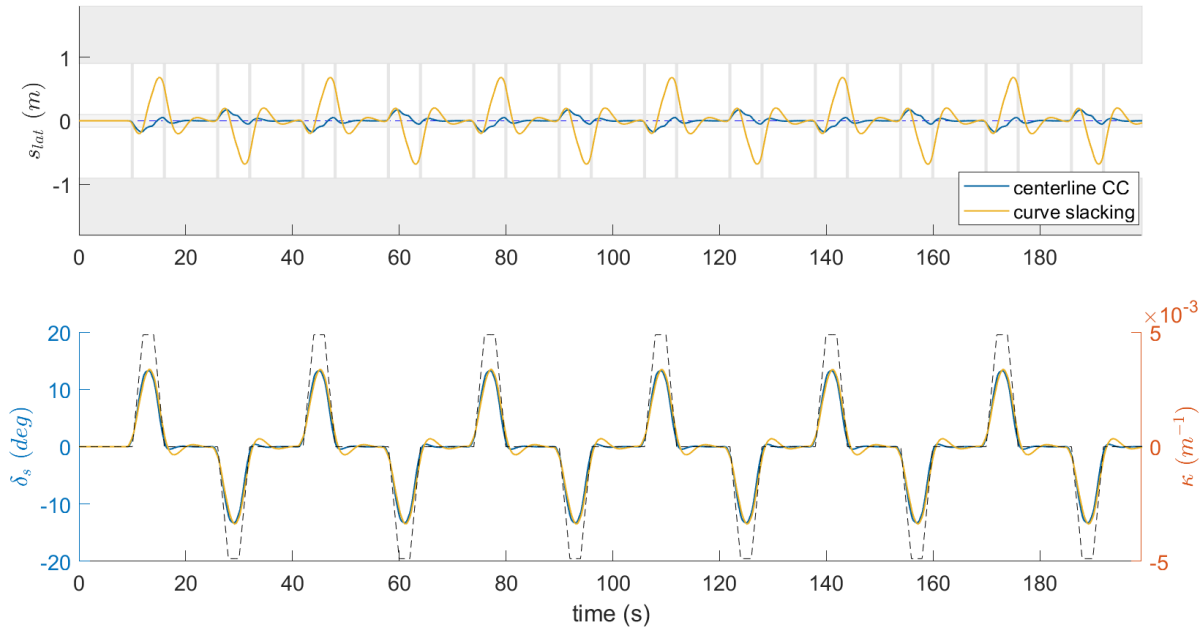

Figure 6.8: Lateral position and steering angle output for full experiment road for near centerline CC and anti CC HCRs.

For each HCR type four variations are made which include either no, inner, center or outer prepositioning as explained in Section 5.1. Figure 6.9 depicts how the addition of prepositioning affects the lateral position plot for the default HCR type. Note that the inner prepositioning variation is not included here as it almost overlaps with the no prepositioning variation.

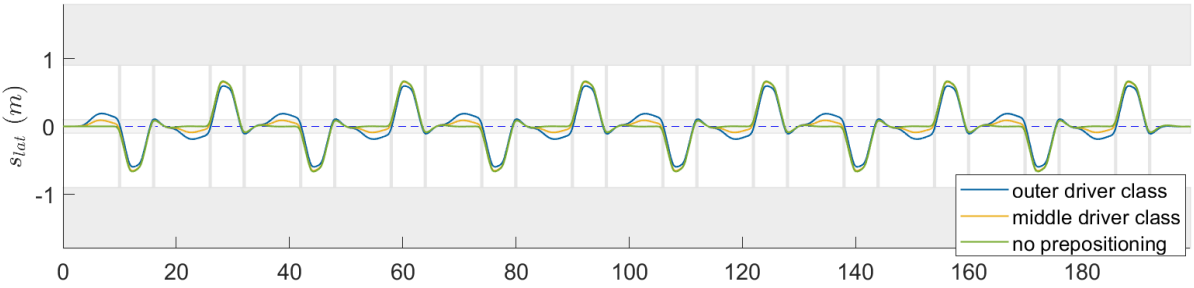

Figure 6.9: Lateral position output for full experiment road for default HCR with no, middle or outer prepositioning.

The above references are loaded unto the computers that generate the simulation. More specifically, access to the selected HCR is provided to the modules which determine the vehicle state and the haptic feedback forces. In order to verify that the haptic controller can steer the vehicle along the supplied reference some test runs are executed for the complete force feedback setting (LoHS = 1 and SoHF = 1.5).

7

Experiment Proposal

This chapter discusses the experiment performed in the human-machine interaction laboratory at the aerospace engineering faculty of TU Delft. Sections 7.1 - 7.5 detail the HMI laboratory equipment, the experiment design and hypotheses.

7.1. Apparatus

The HMI Laboratory at the Aerospace Engineering faculty of Delft University of Technology consists of a fixed-base platform that can be used for aircraft or car simulation. In case of the driving simulator the participant is seated on the left side whereas for the flight simulator the subject takes place on the right seat, see Figure 7.1. The car controls include a control-loaded steering wheel, a control-loaded gas pedal and a passive spring loaded brake pedal. For this experiment, the gas pedal and brake pedal are unused as the vehicle speed is kept fixed at 80 kph. The image is projected in front of the car seat onto a three-sided projection screen at a resolution of 800 x 600 which enables a horizontal field of view of 180 degrees and a vertical field of view of 40 degrees. The projected image is generated at 50 Hz. An integrated 12 inch LCD screen behind the steering wheel provides the dashboard indicators and can be turned off or on depending on the experiment. An actuator can apply a haptic feedback force to the steering wheel at a rate of up to 2500 Hz [21]. The vehicle in the simulation is a sedan with 1.8 m width and simplified vehicle dynamics [103]. Figure 7.1 also contains a picture of the experiment as seen from behind the driver seat when the simulation is running.

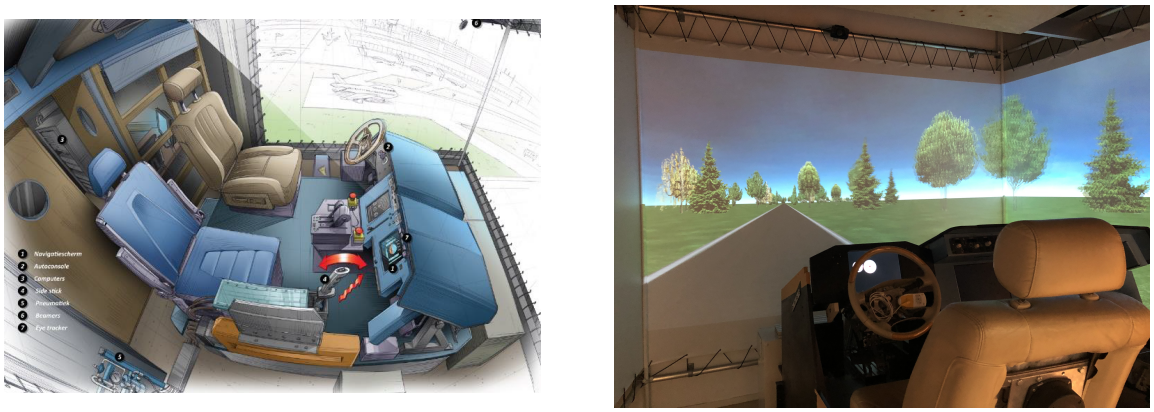

Figure 7.1: Overview of the human-machine interaction laboratory and a picture of the car simulation running.

7.2. Control Task

The control task consists of steering the simulated vehicle along a winding road with six left and six right clothoidal corners with a curve radius of 205m at a speed of 80 kph. As a result, the amount of steering

required in the curves is close to the upper limit of allowed lateral acceleration for road design rules [21]. The road consists of a single lane with clearly marked road edges and a road width of 3.2 m. Driving conditions are selected such that they are representative for a clear daylight driving environment without any road traffic. Trees are simulated along the road trajectory in order to provide some reference objects to the driver. However, the fidelity of the simulation graphics is set to a satisfactory level to prevent the potential occurrence of motion sickness. In between turns the driver is able to center the vehicle during a straight road section. To complete the driving task the driver will be supported by a haptic force controller that actuates the steering wheel at a selected level of strength. The amount of force produced by the control logic is tuned by the LoHS and SoHF settings and depends on the error with respect to the chosen HCR. The LoHA setting is fixed to 1 for this experiment to investigate the effects of the LoHS parameter.

7.3. Subjects and Instructions

Subjects are required to be in possession of a driver's license for at least one year. This should exclude any novice drivers who may be too inexperienced as the vehicle completes the road curves at a relatively high lateral acceleration. The subjects will consist of young adults to adults up to intermediate age. Any age differences within this range are not expected to produce any significant changes in the results. The total number of subjects will be in the range of 12 to 24 and preferably in a multiple of six in order to balance the experimental conditions. The subjects are instructed to complete the driving task as they normally would in the real world with their hands on the steering wheel in the ten to two position. In order to adhere to regulations related to the outbreak of the COVID-19 pandemic a protocol set up by the aerospace engineering faculty of TU Delft is followed throughout the entirety of the experiment.

7.4. Experiment Design

From the preliminary investigation it is found that the LoHS has a strong effect on the torque conflict and the amount of driver torque needed. As relatively more knowledge is currently available with regards to the HCR, it is chosen to focus on the LoHS as the independent variable for this experiment. Previous research suggested to investigate the impact of the LoHS at six different levels ranging from manual driving to full support [69] using a HSC system based on the FDCA. Additionally, this is in line with the study done by Mars et al. [96] which provides a good candidate for comparing findings even though their HSC system is not based on the FDCA.

Keeping the SoHF fixed at a satisfactory level should make interpretation of the results more straightforward as compared to when both are varied simultaneously. Preliminary tests in the simulator indicated that a SoHF value equal to 1.5 is reasonable for the feedback loop of the haptic controller. This is equal to the value used in an earlier experiment by Ghys et al. [26]. The manual driving condition is represented by setting the LoHS and SoHF equal to zero. The LoHS settings of 0.5 and 0.92 were included in the aforementioned experiment by Ghys and may be used to compare results between research studies. Finally, the remaining settings of 0.25, 0.75 and 1 are chosen such that the whole range of LoHS settings is covered.

The selected HCR contains a moderate amount of curve cutting which is distributed smoothly along the road curvature sections. This reference is representative for experienced drivers and contains no unexpected transients which should elicit a natural steering feel. The lateral position and steering angle for this reference were plotted in Figure 6.7 and the extended Van Paassen driver model settings that were used for generating this HCR can be found in the second row of Table 6.1. Finally, the LoHA implementation in the HMI Laboratory simulator simply scales the steering wheel stiffness. However, it has been shown that adaptive LoHA solutions outperform such a basic implementation [39]. Additionally, setting the LoHA to a value larger than 1 inherently raises the human force required to control the steering wheel which may impact their feeling of being in control. As a result, the LoHA value is fixed to a value of 1 for this experiment. The experiment is conducted according to a within-subjects design with six conditions where the independent variable is the LoHS. A balanced Latin square design is used to reduce the potential for detrimental effects related to learning, carry-over and fatigue. The resulting experiment design matrix is given in Table 7.1 where the LoHS setting for each experimental condition is indicated. Before the start of the first run every subject will get one training run in the manual driving condition to familiarize with the driving simulator. Only one training run is needed since the driving task can be learned quickly.

	Run 1	Run 2	Run 3	Run 4	Run 5	Run 6
Subject 1	0.5	0.75	0	0.25	0.92	1
Subject 2	0.75	0.25	0.5	1	0	0.92
Subject 3	0.25	1	0.75	0.92	0.5	0
Subject 4	1	0.92	0.25	0	0.75	0.5
Subject 5	0.92	0	1	0.5	0.25	0.75
Subject 6	0	0.5	0.92	0.75	1	0.25

Table 7.1: Experiment design matrix

7.5. Hypotheses

The following hypotheses are made for the results of the experiment. These are divided into the three groups for which research questions were established.

- Acceptance is assumed to increase for higher levels of haptic support. Some subjects may prefer higher LoHS values than others. As a result, there may be a more optimal LoHS setting somewhere between 0.5 and 1 which optimizes the acceptance by minimizing the total torque conflict. Satisfaction with the haptic support should be high if the haptic feedback is perceived as supportive in completing the steering task. This hypothesis is supported by findings in similar research by Mars et al. [19] and in studies that have investigated implementations of the FDCA controller [21] [26]. However, higher LoHS settings may be perceived as more intrusive compared to lower LoHS settings and are thus more likely to cause changes in the satisfaction level of the haptic support.
- Driver engagement in terms of human involvement in the steering task is expected to decrease for higher levels of haptic support as long as their intended steering path is aligned with that of the haptic support. Subsequently, the human steering contribution is hypothesized to decrease as well. Engagement levels for lower LoHS values should be close to the manual driving baseline. Previous research by Mars et al. found a decrease in steering effort and activity (steering wheel reversal rate) for low to medium support levels and a significant increase for the highest level of support as the drivers competed with the automation for control of the steering wheel [19].
- The shared control system is expected to be able to complete the steering task regardless of the LoHS as the human driver will adapt their steering force based on their perception and senses. Furthermore, it is hypothesized that the variation in lateral performance decreases slightly within the curvature sections as the LoHS increases. Variation in lateral performance along the straight sections is more dependent on the SoHF settings and are thus expected to remain more stable across the six experimental conditions. These expectations are supported by a previous study that found a significant decrease in the variability of the lateral position as the degree of haptic support increased [19]. In this case the performance gains were obtained with diminishing returns up to medium to high levels of haptic support.

8

Conclusion

This report contains a research proposal that will help to investigate the effects and acceptance of haptic shared control settings for car steering. Previous research indicates that the level of haptic support setting for the feedforward part of the force generation loop is important in the perception and acceptance of a haptic shared control system. Therefore, six different LoHS settings will be tested in a driving simulator in which the subjects are tasked with driving along a winding road with left and right curves. The results of this research will shine some light on the importance of setting the LoHS value for a haptic controller that uses the four design choices architecture.

Preliminary simulations were conducted for the Van Paassen driver model which is able to generate reference trajectories which exhibit centerline driving or some level of curve cutting. Furthermore, it is shown that this model can be extended to include the prepositioning phase for curve negotiation. Although it is difficult to predict the exact interaction between the human and the haptic support using this model some general trends are observed which indicate that higher support levels can reduce the required human steering torque significantly. Furthermore, in these simulations it is found that the magnitude of torque conflict rises drastically as the human and haptic references are more dissimilar. This is in accordance to findings from previous research studies on this topic.

Bibliography

[1] European Road Safety Observatory. Annual accident report 2019. Technical report, European Commission, 2019.

[2] D. A. Abbink, M. Mulder, and E. R. Boer. Haptic shared control: smoothly shifting control authority? *Cognition, Technology & Work*, 14(1):19–28, 2012.

[3] CORDIS. Using haptic technology to prevent distracted driving, February 2020.

[4] T. Brandt, T. Sattel, and M. Bohm. Combining haptic human-machine interaction with predictive path planning for lane-keeping and collision avoidance systems. In *2007 IEEE intelligent vehicles symposium*, pages 582–587. IEEE, 2007.

[5] M. Mulder, D. A. Abbink, and E. R. Boer. The effect of haptic guidance on curve negotiation behavior of young, experienced drivers. In *2008 IEEE International Conference on Systems, Man and Cybernetics*, pages 804–809. IEEE, 2008.

[6] F. Beruscha, K. Augsburg, and D. Manstetten. Haptic warning signals at the steering wheel: A literature survey regarding lane departure warning systems. *Haptics-e, The electronic journal of haptics research*, 4(5), 2011.

[7] T. M. Lam, H. W. Boschloo, M. Mulder, and M. M. van Paassen. Artificial force field for haptic feedback in uav teleoperation. *IEEE Transactions on Systems, Man, and Cybernetics-Part A: Systems and Humans*, 39(6):1316–1330, 2009.

[8] S. S. Nudehi, R. Mukherjee, and M. Ghodoussi. A shared-control approach to haptic interface design for minimally invasive telesurgical training. *IEEE Transactions on Control Systems Technology*, 13(4):588–592, 2005.

[9] C. Lv, Y. Li, Y. Xing, C. Huang, D. Cao, Y. Zhao, and Y. Liu. Human-machine collaboration for automated driving using an intelligent two-phase haptic interface. *Advanced Intelligent Systems*, 3(4), 2021.

[10] Z. Lu, R. Happee, C. D. D. Cabrall, M. Kyriakidis, and J. C. F. de Winter. Human factors of transitions in automated driving: A general framework and literature survey. *Transportation research part F: traffic psychology and behaviour*, 43:183–198, 2016.

[11] K. Okada, K. Sonoda, and T. Wada. Transferring from automated to manual driving when traversing a curve via haptic shared control. *IEEE Transactions on Intelligent Vehicles*, 6(2):266–275, 2020.

[12] D. Watzenig and M. Horn. *Automated driving: safer and more efficient future driving*. Springer, 2016.

[13] M. V. Martínez, I. Del Campo, J. Echanobe, and K. Basterretxea. Driving behavior signals and machine learning: A personalized driver assistance system. In *2015 IEEE 18th International Conference on Intelligent Transportation Systems*, pages 2933–2940. IEEE, 2015.

[14] Z. Wang, Z. Yan, and K. Nakano. Comfort-oriented haptic guidance steering via deep reinforcement learning for individualized lane keeping assist. In *2019 IEEE International Conference on Systems, Man and Cybernetics (SMC)*, pages 4283–4289. IEEE, 2019.

[15] X. Ji, K. Yang, X. Na, C. Lv, and Y. Liu. Shared steering torque control for lane change assistance: a stochastic game-theoretic approach. *IEEE Transactions on Industrial Electronics*, 66(4):3093–3105, 2018.

[16] M. Mulder and D. A. Abbink. Sharing control with elderly drivers: Haptic guidance during curve negotiation. *IFAC Proceedings Volumes*, 43(13):310–315, 2010.

[17] J. Fan, J. W Wade, A. P. Key, Z. E. Warren, and N. Sarkar. Eeg-based affect and workload recognition in a virtual driving environment for asd intervention. *IEEE Transactions on Biomedical Engineering*, 65(1):43–51, 2017.

[18] T. Wada, K. Sonoda, and S. Tada. Simultaneous achievement of supporting human drivers and improving driving skills by shared and cooperative control. *IFAC-PapersOnLine*, 49(19):90–95, 2016.

[19] F. Mars, M. Deroo, and J. Hoc. Analysis of human-machine cooperation when driving with different degrees of haptic shared control. *IEEE transactions on haptics*, 7(3):324–333, 2014.

[20] R. Boink, M. M. van Paassen, M. Mulder, and D. A. Abbink. Understanding and reducing conflicts between driver and haptic shared control. In *2014 IEEE International Conference on Systems, Man, and Cybernetics (SMC)*, pages 1510–1515. IEEE, 2014.

[21] W. Scholtens, S. Barendswaard, D. M. Pool, M. M. van Paassen, and D. A. Abbink. A new haptic shared controller reducing steering conflicts. In *2018 IEEE International Conference on Systems, Man, and Cybernetics (SMC)*, pages 2705–2710. IEEE, 2018.

[22] M. M. van Paassen, R. Boink, D. A. Abbink, M. Mulder, and M. Mulder. Four design choices for haptic shared control. *Advances in Aviation Psychology, Volume 2: Using Scientific Methods to Address Practical Human Factors Needs*, page 237, 2017.

[23] N. Merat, A. H. Jamson, F. C. H. Lai, M. Daly, and O. M. J. Carsten. Transition to manual: Driver behaviour when resuming control from a highly automated vehicle. *Transportation research part F: traffic psychology and behaviour*, 27:274–282, 2014.

[24] T. Louw, G. Kountouriotis, O. Carsten, and N. Merat. Driver inattention during vehicle automation: How does driver engagement affect resumption of control? In *4th International Conference on Driver Distraction and Inattention (DDI2015), Sydney: proceedings*. ARRB Group, 2015.

[25] J. Smisek, W. Mugge, J. B. J. Smeets, M. M. van Paassen, and A. Schiele. Haptic guidance on demand: A grip-force based scheduling of guidance forces. *IEEE transactions on haptics*, 11(2):255–266, 2017.

[26] E. P. Ghys. Driver's acceptance of trajectory type in trajectory-driven haptic shared control. Technical report, TU Delft, 2020.

[27] R. Osu, N. Kamimura, H. Iwasaki, E. Nakano, C. M. Harris, Y. Wada, and M. Kawato. Optimal impedance control for task achievement in the presence of signal-dependent noise. *Journal of Neurophysiology*, 92(2):1199–1215, 2004.

[28] M. Steele and R. B. Gillespie. Shared control between human and machine: Using a haptic steering wheel to aid in land vehicle guidance. In *Proceedings of the human factors and ergonomics society annual meeting*, volume 45, pages 1671–1675. SAGE Publications Sage CA: Los Angeles, CA, 2001.

[29] D. A. Abbink. Neuromuscular analysis of haptic gas pedal feedback during car following. Technical report, TU Delft, 2006.

[30] T. Wada, K. Sonoda, T. Okasaka, and T. Saito. Authority transfer method from automated to manual driving via haptic shared control. In *2016 IEEE International Conference on Systems, Man, and Cybernetics (SMC)*, pages 002659–002664. IEEE, 2016.

[31] S. Barendswaard, D. M. Pool, E. R. Boer, and D. A. Abbink. A classification method for driver trajectories during curve-negotiation. In *2019 IEEE International Conference on Systems, Man and Cybernetics (SMC)*, pages 3729–3734. IEEE, 2019.

[32] E. de Vlugt, A. C. Schouten, F. C. T. van der Helm, P. C. Teerhuis, and G. G. Brouwn. A force-controlled planar haptic device for movement control analysis of the human arm. *Journal of neuroscience methods*, 129(2):151–168, 2003.

[33] A. C. Schouten, E. de Vlugt, B. J. J. van Hilten, and F. C. T. van der Helm. Design of a torque-controlled manipulator to analyse the admittance of the wrist joint. *Journal of neuroscience methods*, 154(1-2):134–141, 2006.

[34] J. Van Oosterhout. Robustness of haptic shared control against model inaccuracies during telemanipulation. *TU Delft Repository*, 2012.

[35] B. Pano, F. Claveau, P. Chevrel, C. Sentouh, and F. Mars. Systematic h2/h∞ haptic shared control synthesis for cars, parameterized by sharing level. In *2020 IEEE International Conference on Systems, Man, and Cybernetics (SMC)*, pages 4416–4423. IEEE, 2020.

[36] P. R. Culmer, A. E. Jackson, S. Makower, R. Richardson, J. A. Cozens, M. C. Levesley, and B. B. Bhakta. A control strategy for upper limb robotic rehabilitation with a dual robot system. *IEEE/ASME Transactions on Mechatronics*, 15(4):575–585, 2009.

[37] R. Parasuraman, T. B. Sheridan, and C. D. Wickens. A model for types and levels of human interaction with automation. *IEEE Transactions on systems, man, and cybernetics-Part A: Systems and Humans*, 30(3):286–297, 2000.

[38] D. A. Abbink and M. Mulder. Exploring the dimensions of haptic feedback support in manual control. *Journal of Computing and Information Science in Engineering*, 9(1), 2009.

[39] H. M. Zwaan, S. M. Petermeijer, and D. A. Abbink. Haptic shared steering control with an adaptive level of authority based on time-to-line crossing. *IFAC-PapersOnLine*, 52(19):49–54, 2019.

[40] P. G. Griffiths and R. B. Gillespie. Sharing control between humans and automation using haptic interface: primary and secondary task performance benefits. *Human factors*, 47(3):574–590, 2005.

[41] A. C. Newberry, M. J. Griffin, and M. Dowson. Driver perception of steering feel. *Proceedings of the Institution of Mechanical Engineers, Part D: Journal of Automobile Engineering*, 221(4):405–415, 2007.

[42] J. Sato, K. Takemura, N. Yamada, A. Kishi, K. Nishikawa, T. Nouzawa, T. Tsuji, and Y. Kurita. Investigation of the subjective force perception based on the estimation of the muscle activities during a steering operation. In *Proceedings of the 2013 IEEE/SICE International Symposium on System Integration*, pages 76–81. IEEE, 2013.

[43] K. H. Norwich. On the theory of weber fractions. *Perception & Psychophysics*, 42(3):286–298, 1987.

[44] S. Dehaene. The neural basis of the weber–fechner law: a logarithmic mental number line. *Trends in cognitive sciences*, 7(4):145–147, 2003.

[45] L. A. Jones. Matching forces: constant errors and differential thresholds. *Perception*, 18(5):681–687, 1989.

[46] B. Woodruff and H. Helson. Torque sensitivity as a function of knob radius and load. *The American journal of psychology*, 80(4):558–571, 1967.

[47] L. A. Jones and I. W. Hunter. A perceptual analysis of stiffness. *Experimental Brain Research*, 79(1):150–156, 1990.

[48] W. Mugge, D. A. Abbink, A. C. Schouten, J. P. A. Dewald, and F. C. T. Van Der Helm. A rigorous model of reflex function indicates that position and force feedback are flexibly tuned to position and force tasks. *Experimental brain research*, 200(3):325–340, 2010.

[49] D. A. Abbink and M. Mulder. Neuromuscular analysis as a guideline in designing shared control. In *Advances in haptics*. IntechOpen, 2010.

[50] A. J. Pick and D. J. Cole. A mathematical model of driver steering control including neuromuscular dynamics. *Journal of dynamic systems, measurement, and control*, 130(3), 2008.

[51] D. A. Abbink, D. Cleij, M. Mulder, and M. M. van Paassen. The importance of including knowledge of neuromuscular behaviour in haptic shared control. In *2012 IEEE International Conference on Systems, Man, and Cybernetics (SMC)*, pages 3350–3355. IEEE, 2012.

[52] H. Nakamura, D. A. Abbink, and M. Mulder. Is grip strength related to neuromuscular admittance during steering wheel control? In *2011 IEEE International Conference on Systems, Man, and Cybernetics*, pages 1658–1663. IEEE, 2011.

[53] E. C. Hildreth, J. M. H. Beusmans, E. R. Boer, and C. S. Royden. From vision to action: Experiments and models of steering control during driving. *Journal of Experimental Psychology: Human Perception and Performance*, 26(3):1106, 2000.

[54] E. R. Boer. Satisficing curve negotiation: Explaining drivers' situated lateral position variability. *IFAC-PapersOnLine*, 49(19):183–188, 2016.

[55] J. J. Gibson and L. E. Crooks. A theoretical field-analysis of automobile-driving. *The American journal of psychology*, 51(3):453–471, 1938.

[56] D. McRuer and D. H. Weir. Theory of manual vehicular control. *Ergonomics*, 12(4):599–633, 1969.

[57] D. T. McRuer, R. W. Allen, D. H. Weir, and R. H. Klein. New results in driver steering control models. *Human factors*, 19(4):381–397, 1977.

[58] D. D. Salvucci and R. Gray. A two-point visual control model of steering. *Perception*, 33(10):1233–1248, 2004.

[59] J. Steen, H. J. Damveld, R. Happee, M. M. van Paassen, and M. Mulder. A review of visual driver models for system identification purposes. In *2011 IEEE international conference on systems, man, and cybernetics*, pages 2093–2100. IEEE, 2011.

[60] C. Sentouh, P. Chevrel, F. Mars, and F. Claveau. A sensorimotor driver model for steering control. In *2009 IEEE International Conference on Systems, Man and Cybernetics*, pages 2462–2467. IEEE, 2009.

[61] R. S. Sharp. Driver steering control and a new perspective on car handling qualities. *Proceedings of the Institution of Mechanical Engineers, Part C: Journal of Mechanical Engineering Science*, 219(10):1041–1051, 2005.

[62] L. Saleh, P. Chevrel, and J. Lafay. Optimal control with preview for lateral steering of a passenger car: Design and test on a driving simulator. In *Time delay systems: Methods, applications and new trends*, pages 173–185. Springer, 2012.

[63] S. Barendswaard, D. M. Pool, M. M. van Paassen, E. R. Boer, and D. A. Abbink. A pre-curve prepositioning model to enhance the descriptiveness of specific control-theoretic driver steering models. *Unpublished*, 2020.

[64] S. Barendswaard, D. M. Pool, and D. A. Abbink. A method to assess individualized driver models: Descriptiveness, identifiability and realism. *Transportation research part F: traffic psychology and behaviour*, 61:16–29, 2019.

[65] S. Inoue, T. Ozawa, H. Inoue, P. Raksincharoensak, and M. Nagai. Cooperative lateral control between driver and adas by haptic shared control using steering torque assistance combined with direct yaw moment control. In *2016 IEEE 19th International Conference on Intelligent Transportation Systems (ITSC)*, pages 316–321. IEEE, 2016.

[66] S. Comte, M. Wardman, and G. Whelan. Drivers' acceptance of automatic speed limiters: implications for policy and implementation. *Transport Policy*, 7(4):259–267, 2000.

[67] M. A. Sinclair. Subjective assessment. *Evaluation of human work-a practical ergonomics methodology*, pages 69–100, 1995.

[68] J. D. Van Der Laan, A. Heino, and D. De Waard. A simple procedure for the assessment of acceptance of advanced transport telematics. *Transportation Research Part C: Emerging Technologies*, 5(1):1–10, 1997.

[69] S Barendswaard. Modelling individual driver trajectories to personalise haptic shared steering control in curves. *TU Delft*, 2021.

[70] K. Lee, K. Kerns, R. Bone, and M. Nickelson. Development and validation of the controller acceptance rating scale (cars): Results of empirical research. In *Proceedings of the 4th USA/Europe Air Traffic Management R&D Seminar*, 2001.

[71] W. W. Wierwille and J. G. Casali. A validated rating scale for global mental workload measurement applications. In *Proceedings of the human factors society annual meeting*, pages 129–133. Sage Publications Sage CA: Los Angeles, CA, 1983.

[72] S. Rothfuss, F. Grauer, M. Flad, and S. Hohmann. A steering experiment towards haptic cooperative maneuver negotiation. In *2018 IEEE International Conference on Systems, Man, and Cybernetics (SMC)*, pages 3207–3212. IEEE, 2018.

[73] M. Johns, B. Mok, D. Sirkin, N. Gowda, C. Smith, W. Talamonti, and W. Ju. Exploring shared control in automated driving. In *2016 11th ACM/IEEE International Conference on Human-Robot Interaction (HRI)*, pages 91–98. IEEE, 2016.

[74] Wendy A Macdonald and Errol R Hoffmann. Review of relationships between steering wheel reversal rate and driving task demand. *Human Factors*, 22(6):733–739, 1980.

[75] G. Markkula and J. Engström. A steering wheel reversal rate metric for assessing effects of visual and cognitive secondary task load. In *Proceedings of the 13th ITS World Congress*. Leeds, 2006.

[76] P. Choudhary and N. R. Velaga. Analysis of vehicle-based lateral performance measures during distracted driving due to phone use. *Transportation research part F: traffic psychology and behaviour*, 44:120–133, 2017.

[77] F. Cnossen, T. Rothengatter, and T. Meijman. Strategic changes in task performance in simulated car driving as an adaptive response to task demands. *Transportation Research Part F: Traffic Psychology and Behaviour*, 3(3):123–140, 2000.

[78] M. K. O'Malley, A. Gupta, M. Gen, and Y. Li. Shared control in haptic systems for performance enhancement and training. *Dynamic Systems, Measurement, and Control*, 128(1), 2006.

[79] M. A. Benloucif, C. Sentouh, J. Floris, P. Simon, and J. Popieul. Online adaptation of the level of haptic authority in a lane keeping system considering the driver's state. *Transportation research part F: traffic psychology and behaviour*, 61:107–119, 2019.

[80] M. Mulder, D. A. Abbink, M. M. van Paassen, and M. Mulder. Design of a haptic gas pedal for active car-following support. *IEEE Transactions on Intelligent Transportation Systems*, 12(1):268–279, 2010.

[81] R. Parasuraman and V. Riley. Humans and automation: Use, misuse, disuse, abuse. *Human factors*, 39(2):230–253, 1997.

[82] S. Kolekar, J. de Winter, and D. A. Abbink. Human-like driving behaviour emerges from a risk-based driver model. *Nature communications*, 11(1):1–13, 2020.

[83] D. A. Abbink, M. Mulder, F. C. T. Van der Helm, M. Mulder, and E. R. Boer. Measuring neuromuscular control dynamics during car following with continuous haptic feedback. *IEEE Transactions on Systems, Man, and Cybernetics, Part B (Cybernetics)*, 41(5):1239–1249, 2011.

[84] D. A. Abbink, M. Mulder, and M. M. van Paassen. Measurements of muscle use during steering wheel manipulation. In *2011 IEEE International Conference on Systems, Man, and Cybernetics*, pages 1652–1657. IEEE, 2011.

[85] D. I. Katzourakis, D. A. Abbink, E. Velenis, E. Holweg, and R. Happee. Driver's arms' time-variant neuromuscular admittance during real car test-track driving. *IEEE Transactions on Instrumentation and Measurement*, 63(1):221–230, 2013.

[86] T. Yang. A new control framework of electric power steering system based on admittance control. *IEEE Transactions on Control Systems Technology*, 23(2):762–769, 2014.

[87] W. Maurel and D. Thalmann. A case study on human upper limb modelling for dynamic simulation. *Computer methods in biomechanics and biomedical engineering*, 2(1):65–82, 1999.

[88] D. A. Abbink and F. C. T. van der Helm. Force perception measurements at the foot. In *2004 IEEE International Conference on Systems, Man and Cybernetics (IEEE Cat. No. 04CH37583)*, volume 3, pages 2525–2529. IEEE, 2004.

[89] M. M. Porter, A. A. Vandervoort, and J. Lexell. Aging of human muscle: structure, function and adaptability. *Scandinavian journal of medicine & science in sports*, 5(3):129–142, 1995.

[90] K. van der El, D. M. Pool, M. M. van Paassen, and M. Mulder. A unifying theory of driver perception and steering control on straight and winding roads. *IEEE Transactions on Human-Machine Systems*, 50(2):165–175, 2019.

[91] S. Barendswaard, L. Van Breugel, B. Schelfaut, J. Sluijter, L. Zuiker, D. M. Pool, E. R. Boer, and D. A. Abbink. Effect of velocity and curve radius on driver steering behaviour before curve entry. In *2019 IEEE International Conference on Systems, Man and Cybernetics (SMC)*, pages 3866–3871. IEEE, 2019.

[92] V. Hayward, O. R. Astley, M. Cruz-Hernandez, D. Grant, and G. Robles-De-La-Torre. Haptic interfaces and devices. *Sensor review*, 2004.

[93] A. E. Kirkpatrick and S. A. Douglas. Application-based evaluation of haptic interfaces. In *Proceedings 10th Symposium on Haptic Interfaces for Virtual Environment and Teleoperator Systems. HAPTICS 2002*, pages 32–39. IEEE, 2002.

[94] A. H. Jamson, D. L. Hibberd, and N. Merat. The design of haptic gas pedal feedback to support eco-driving. In *Proceedings of the Seventh International Driving Symposium on Human Factors in Driver Assessment, Training, and Vehicle Design*, pages 264–270. University of Iowa, 2013.

[95] J. Smisek, E. Sunil, M. M. van Paassen, D. A. Abbink, and M. Mulder. Neuromuscular-system-based tuning of a haptic shared control interface for uav teleoperation. *IEEE Transactions on Human-Machine Systems*, 47(4):449–461, 2016.

[96] F. Mars, M. Deroo, and C. Charron. Driver adaptation to haptic shared control of the steering wheel. In *2014 IEEE International Conference on Systems, Man, and Cybernetics (SMC)*, pages 1505–1509. IEEE, 2014.

[97] E. A. Byrne and R. Parasuraman. Psychophysiology and adaptive automation. *Biological psychology*, 42(3):249–268, 1996.

[98] M. Blommer, R. Curry, D. Kochhar, R. Swaminathan, W. Talamonti, and L. Tijerina. The effects of a scheduled driver engagement strategy in automated driving. In *Proceedings of the Human Factors and Ergonomics Society Annual Meeting*, volume 59, pages 1681–1685. SAGE Publications Sage CA: Los Angeles, CA, 2015.

[99] B. Donmez, L. N. Boyle, and J. D. Lee. Mitigating driver distraction with retrospective and concurrent feedback. *Accident Analysis & Prevention*, 40(2):776–786, 2008.

[100] Z. Wang, R. Zheng, T. Kaizuka, K. Shimono, and K. Nakano. The effect of a haptic guidance steering system on fatigue-related driver behavior. *IEEE Transactions on Human-Machine Systems*, 47(5):741–748, 2017.

[101] F. Bufalo, M. Olivari, S. Geluardi, C. A. Gerboni, L. Pollini, and H. H. Bülthoff. Variable force-stiffness haptic feedback for learning a disturbance rejection task. In *2017 IEEE International Conference on Systems, Man, and Cybernetics (SMC)*, pages 1517–1522. IEEE, 2017.

[102] L. Saleh, P. Chevrel, F. Claveau, J. Lafay, and F. Mars. Shared steering control between a driver and an automation: Stability in the presence of driver behavior uncertainty. *IEEE Transactions on Intelligent Transportation Systems*, 14(2):974–983, 2013.

[103] W. Vreugdenhil. Complementing automotive haptic shared control with visual feedback for obstacle avoidance. Technical report, TU Delft, 2019.

III

Paper Appendices

A

Individual Driver Results - Torque Data Averages for Left and Right Curves

This appendix contains the torque data averaged over the six left and six right curves for all eighteen participants in the experiment. The torque components as well as the conflict torque are shown for the three lowest and three highest LoHS conditions in two plots per subject.

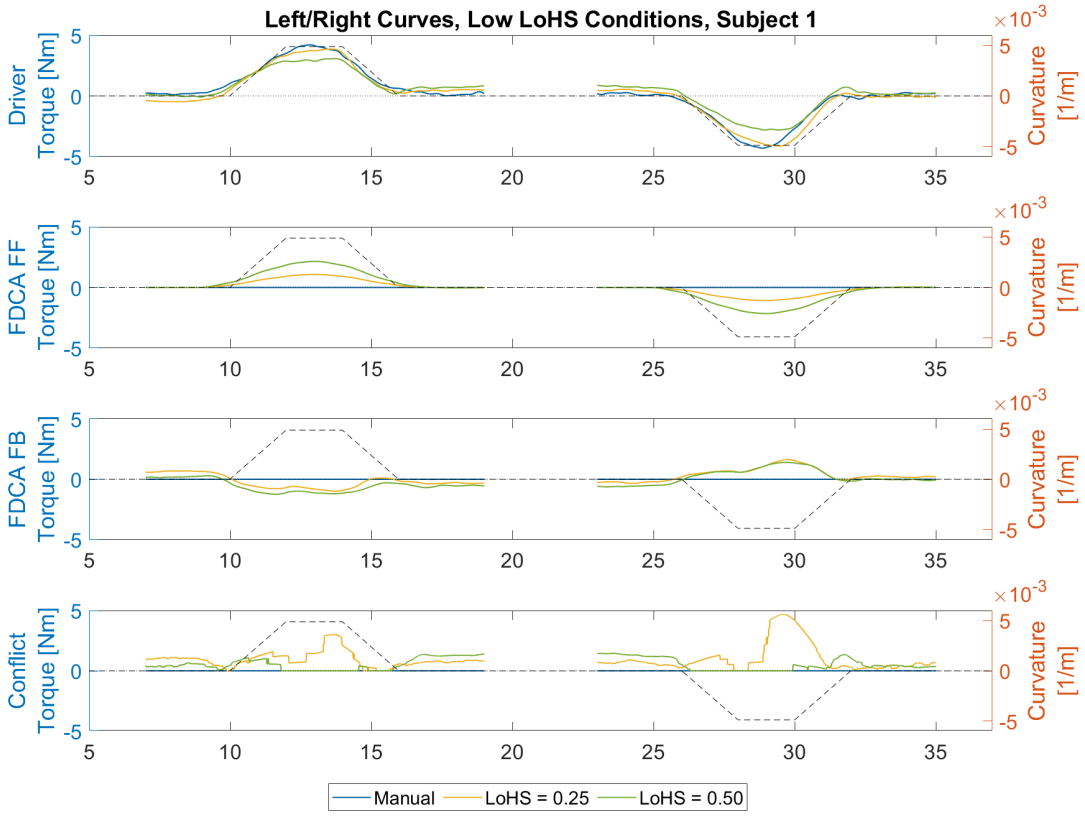

Figure A.1: Torque data averaged for left and right curves for subject 1 for the three lower LoHS conditions

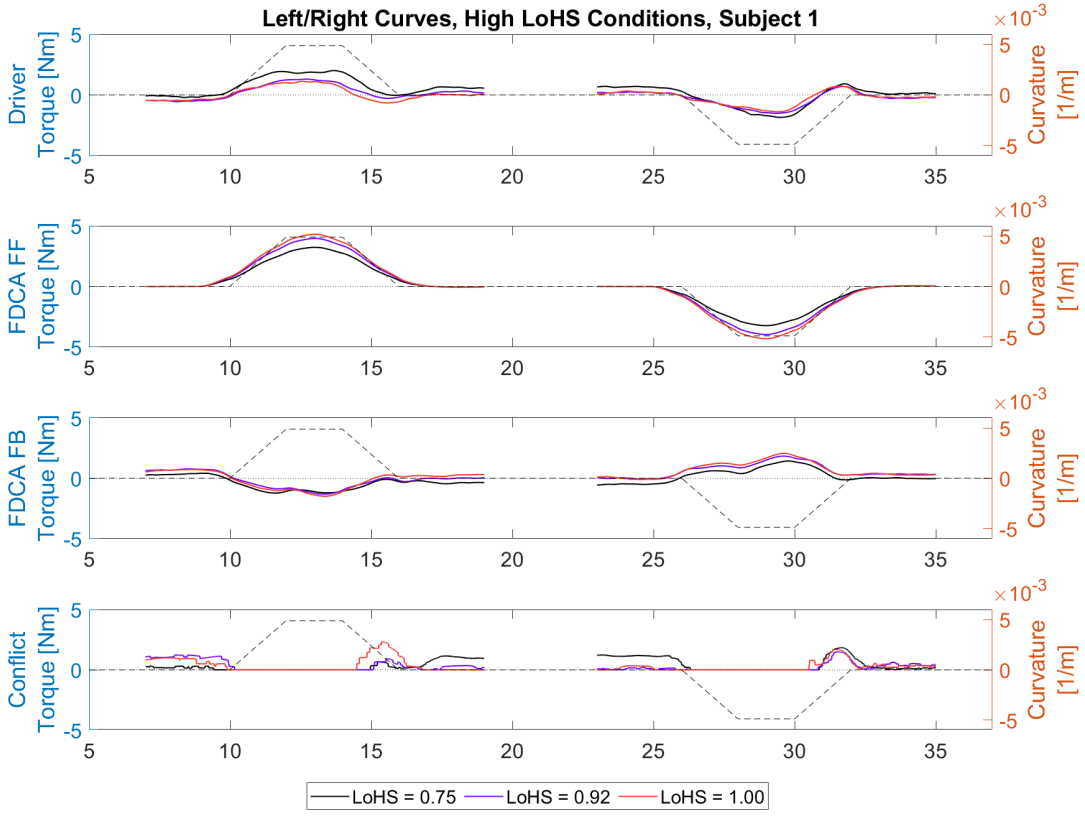

Figure A.2: Torque data averaged for left and right curves for subject 1 for the three higher LoHS conditions

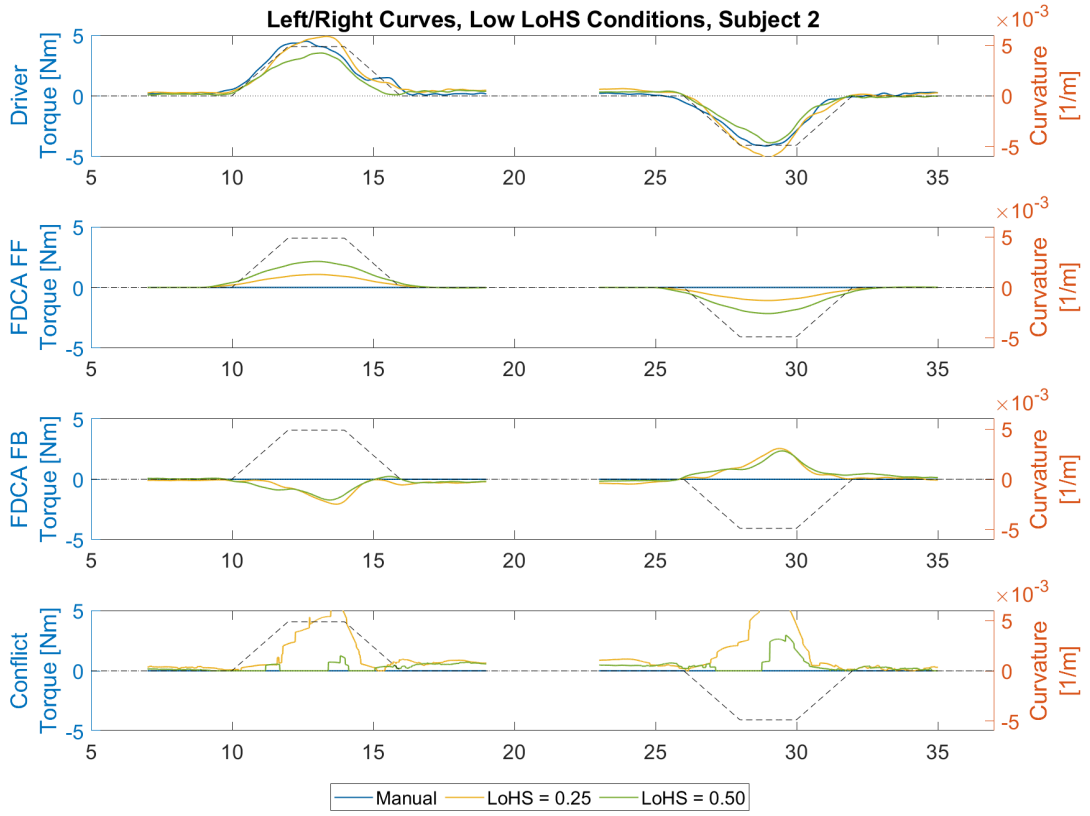

Figure A.3: Torque data averaged for left and right curves for subject 2 for the three lower LoHS conditions

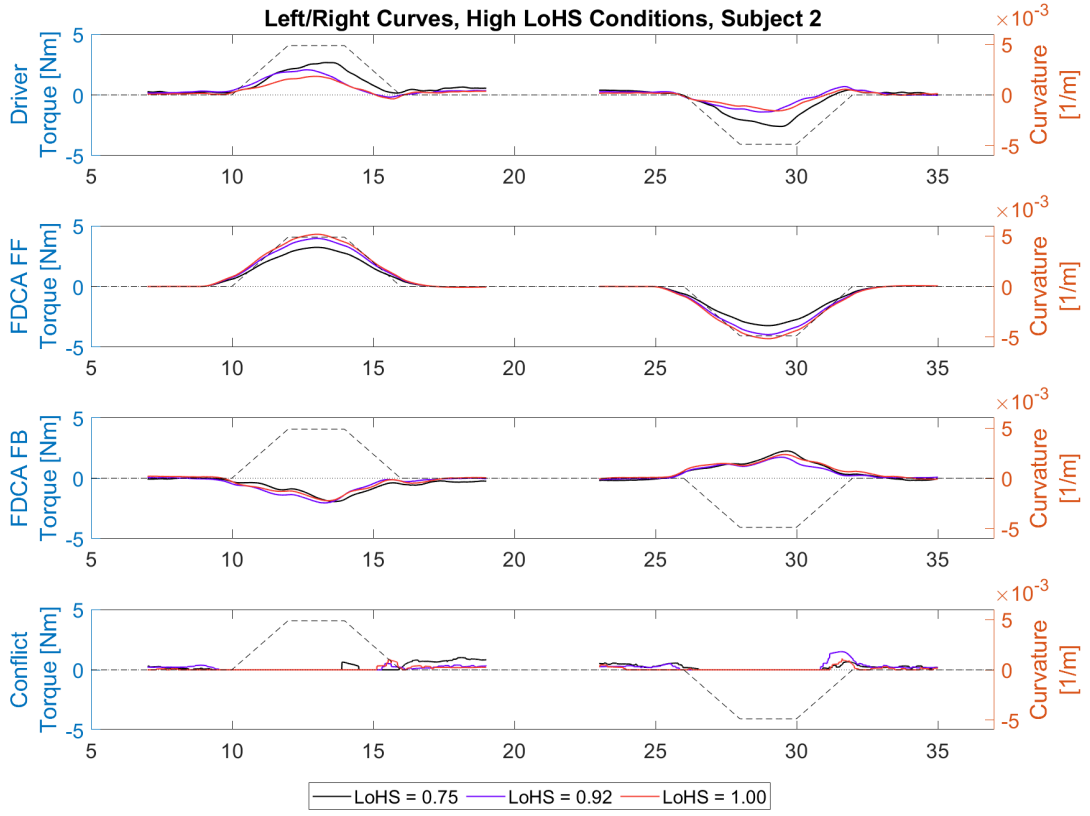

Figure A.4: Torque data averaged for left and right curves for subject 2 for the three higher LoHS conditions

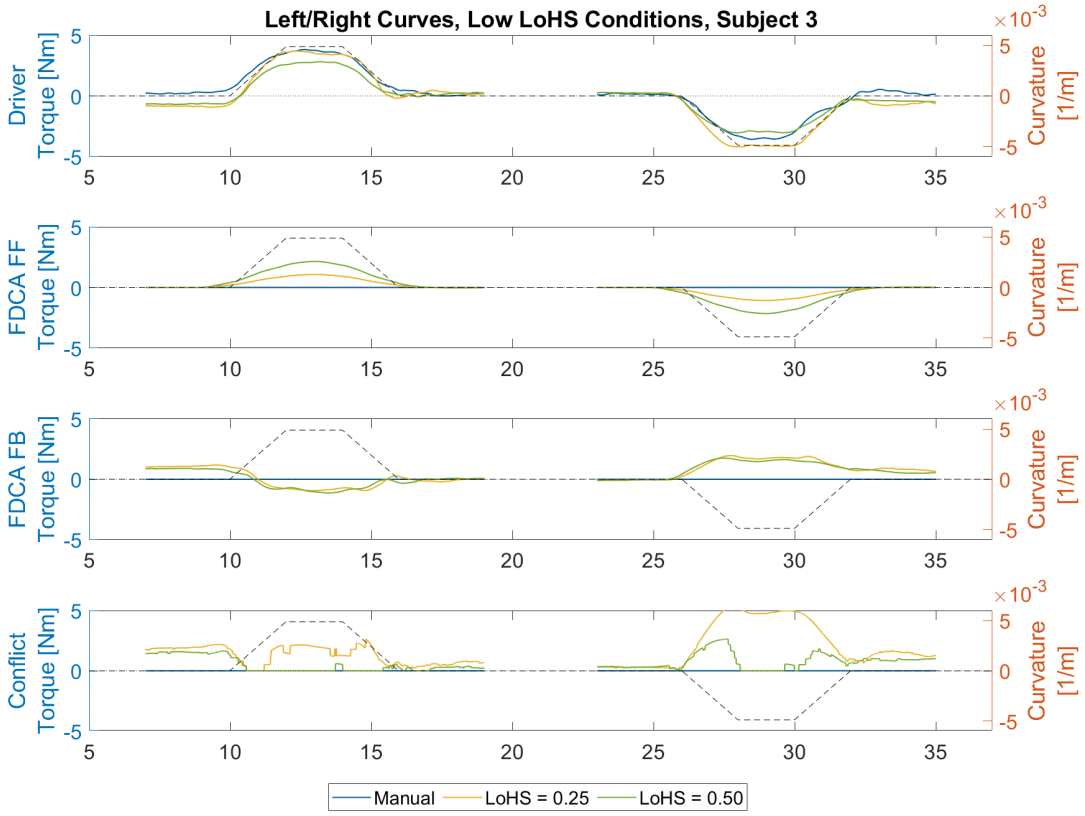

Figure A.5: Torque data averaged for left and right curves for subject 3 for the three lower LoHS conditions

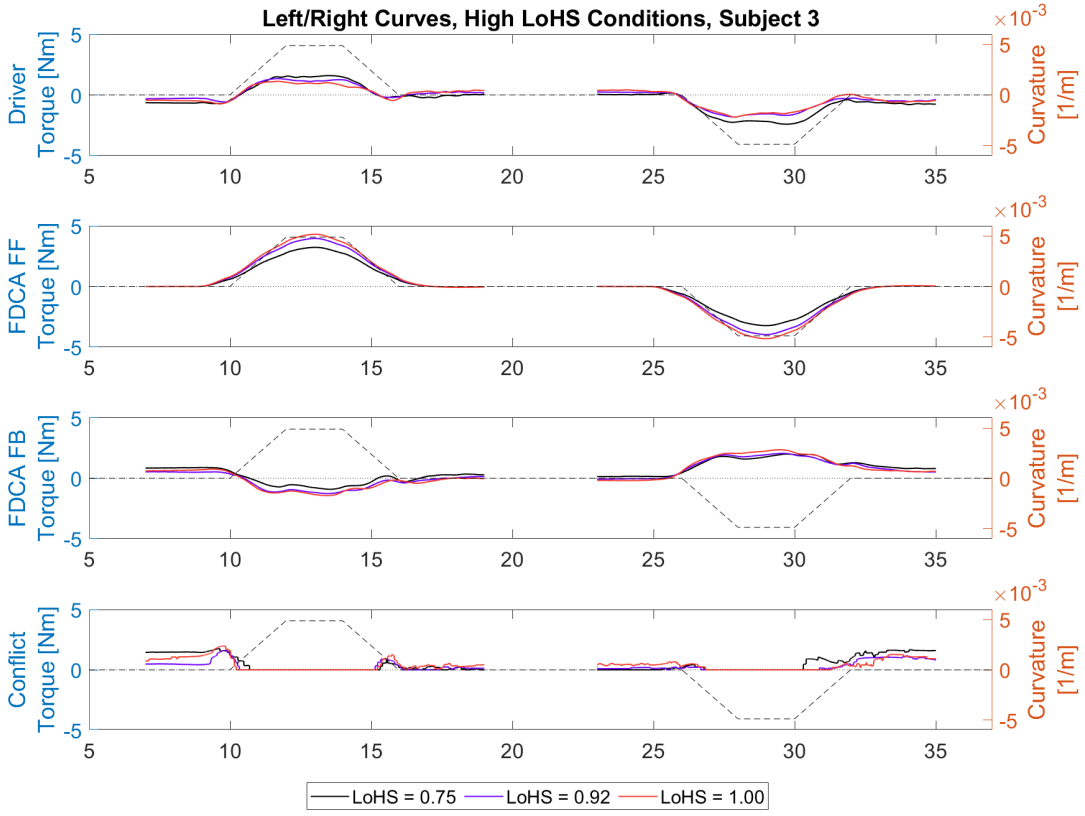

Figure A.6: Torque data averaged for left and right curves for subject 3 for the three higher LoHS conditions

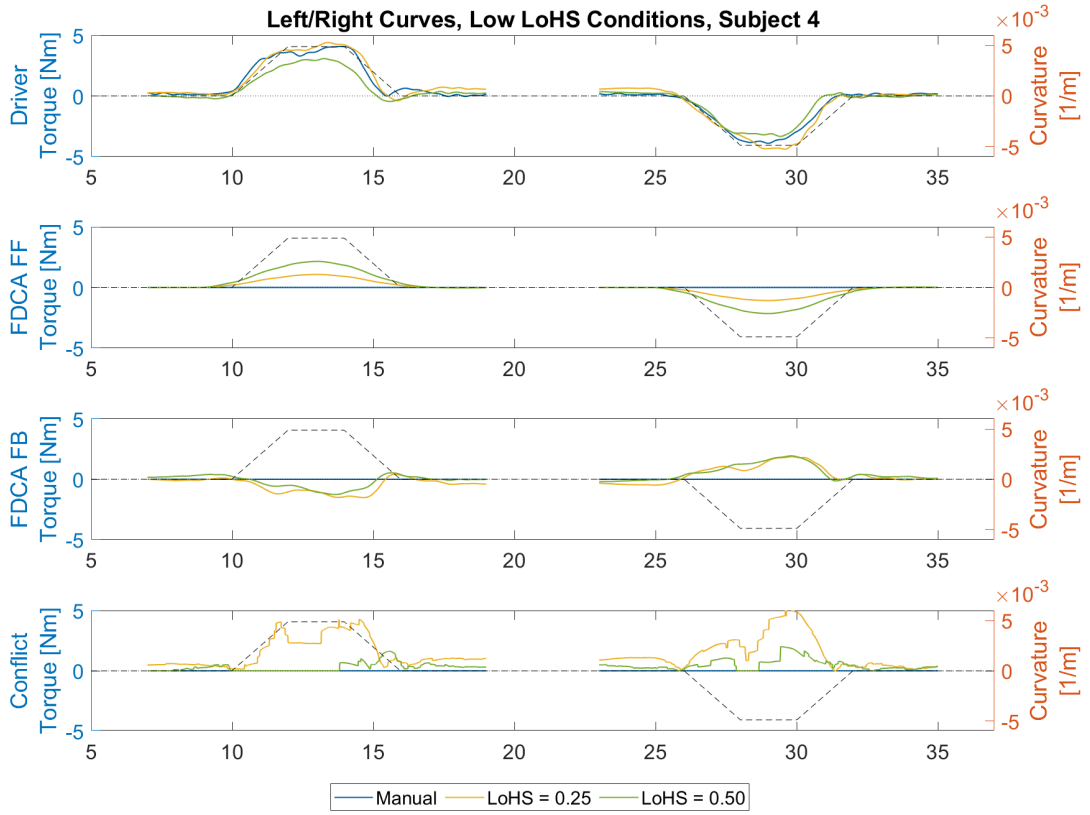

Figure A.7: Torque data averaged for left and right curves for subject 4 for the three lower LoHS conditions

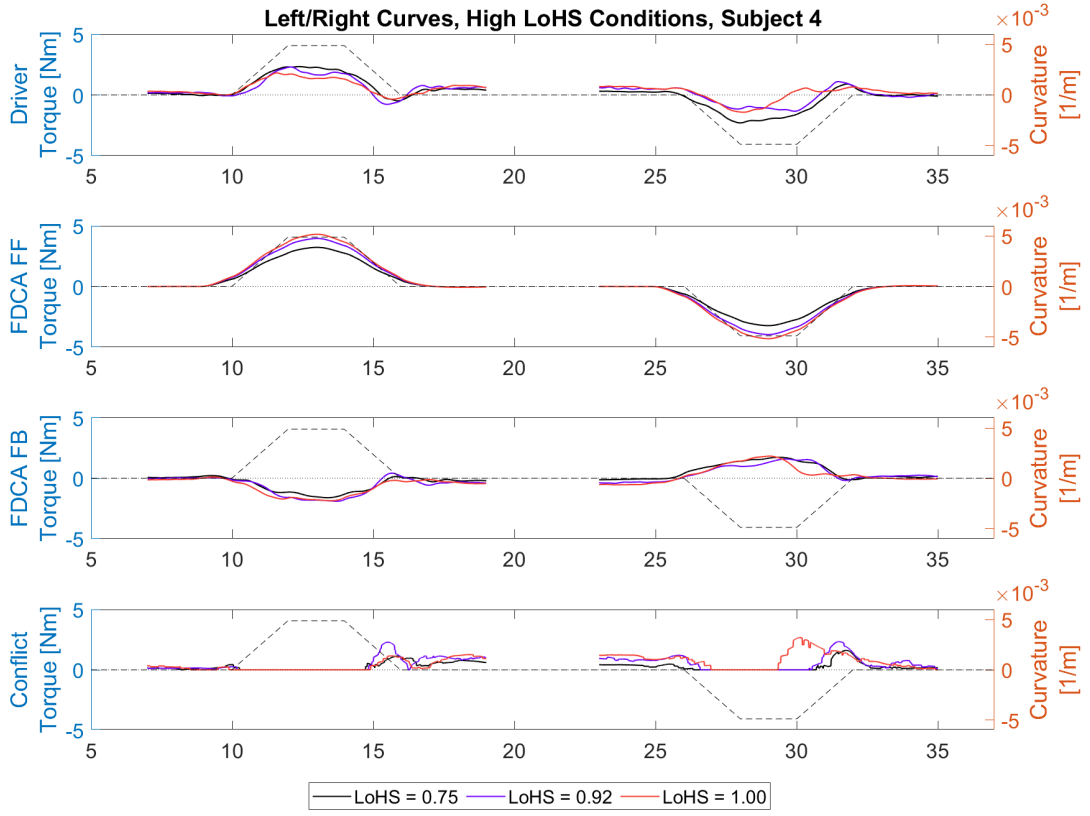

Figure A.8: Torque data averaged for left and right curves for subject 4 for the three higher LoHS conditions

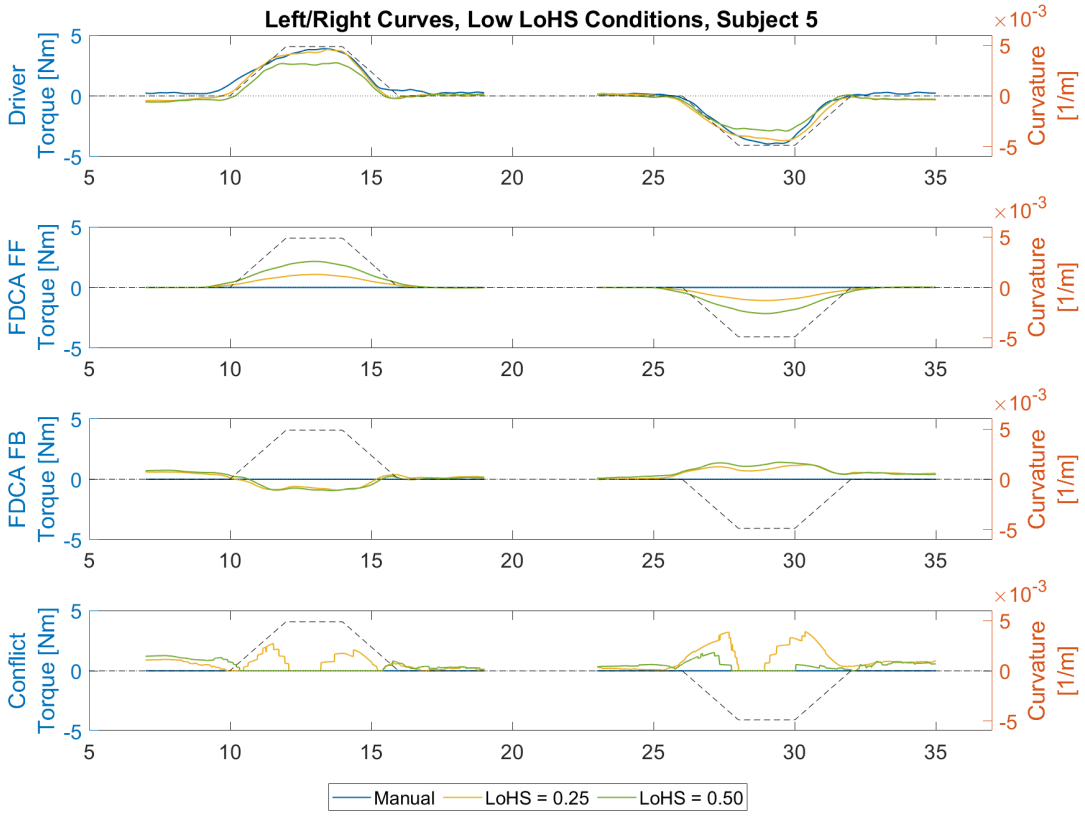

Figure A.9: Torque data averaged for left and right curves for subject 5 for the three lower LoHS conditions

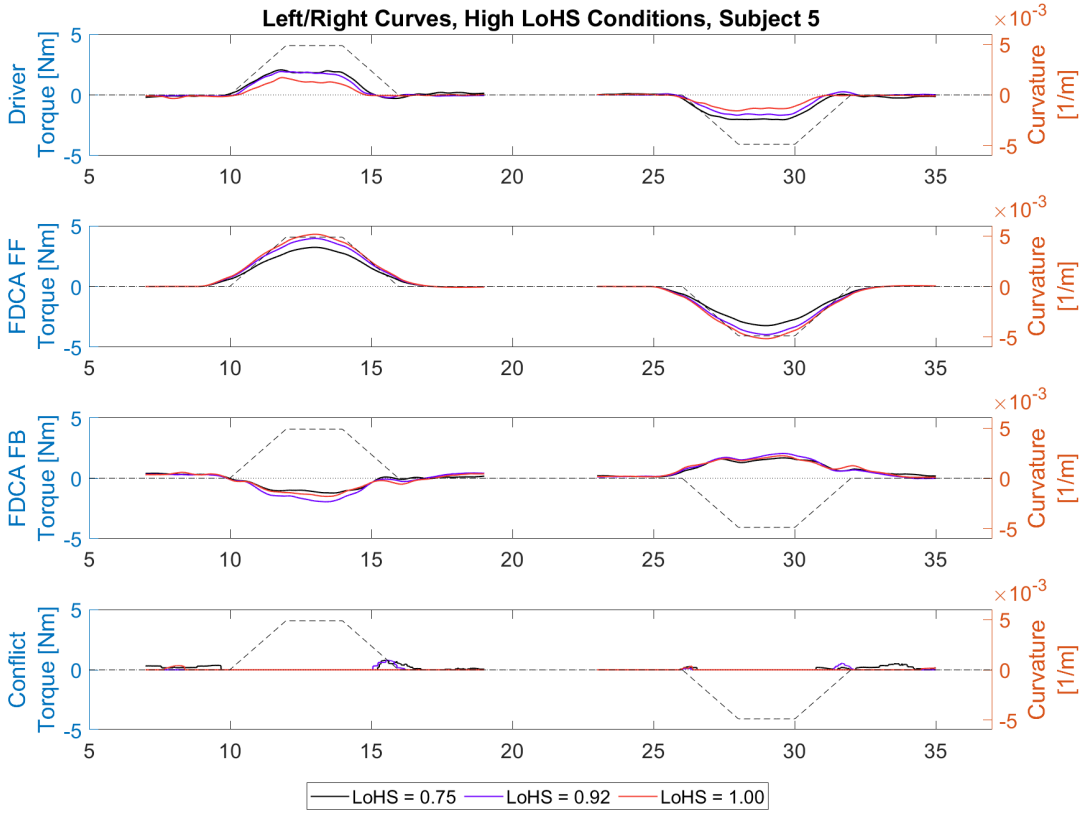

Figure A.10: Torque data averaged for left and right curves for subject 5 for the three higher LoHS conditions

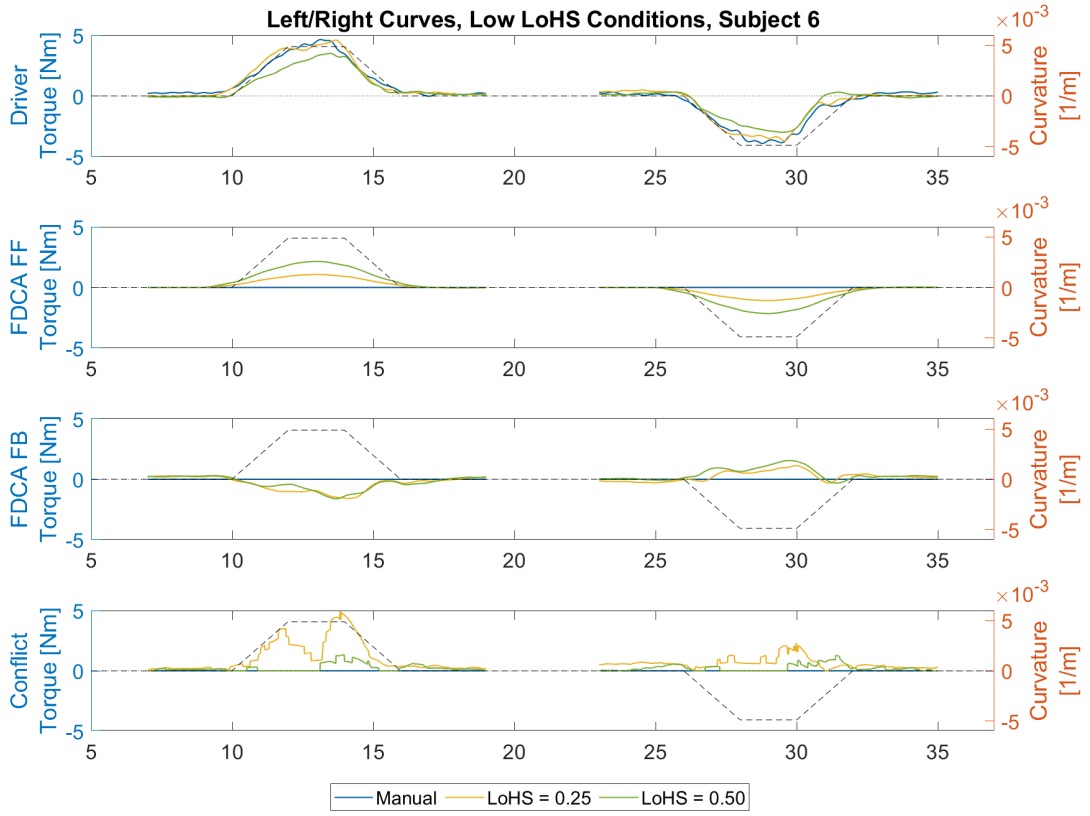

Figure A.11: Torque data averaged for left and right curves for subject 6 for the three lower LoHS conditions

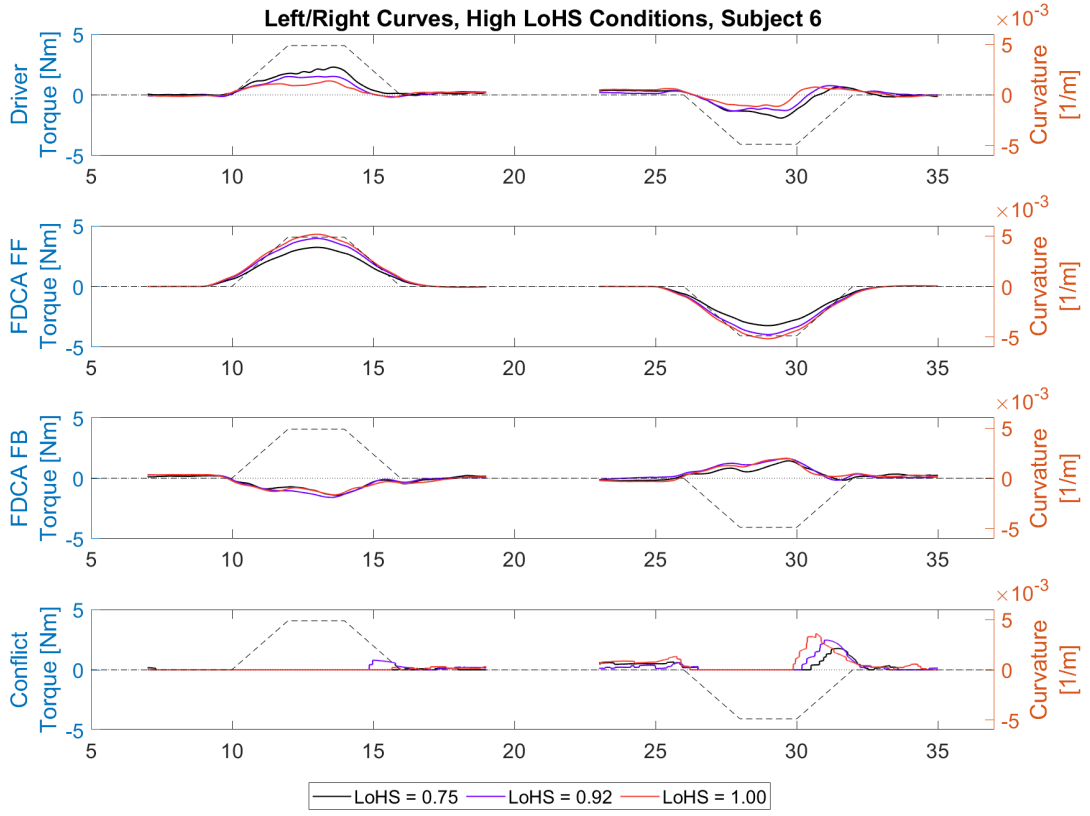

Figure A.12: Torque data averaged for left and right curves for subject 6 for the three higher LoHS conditions

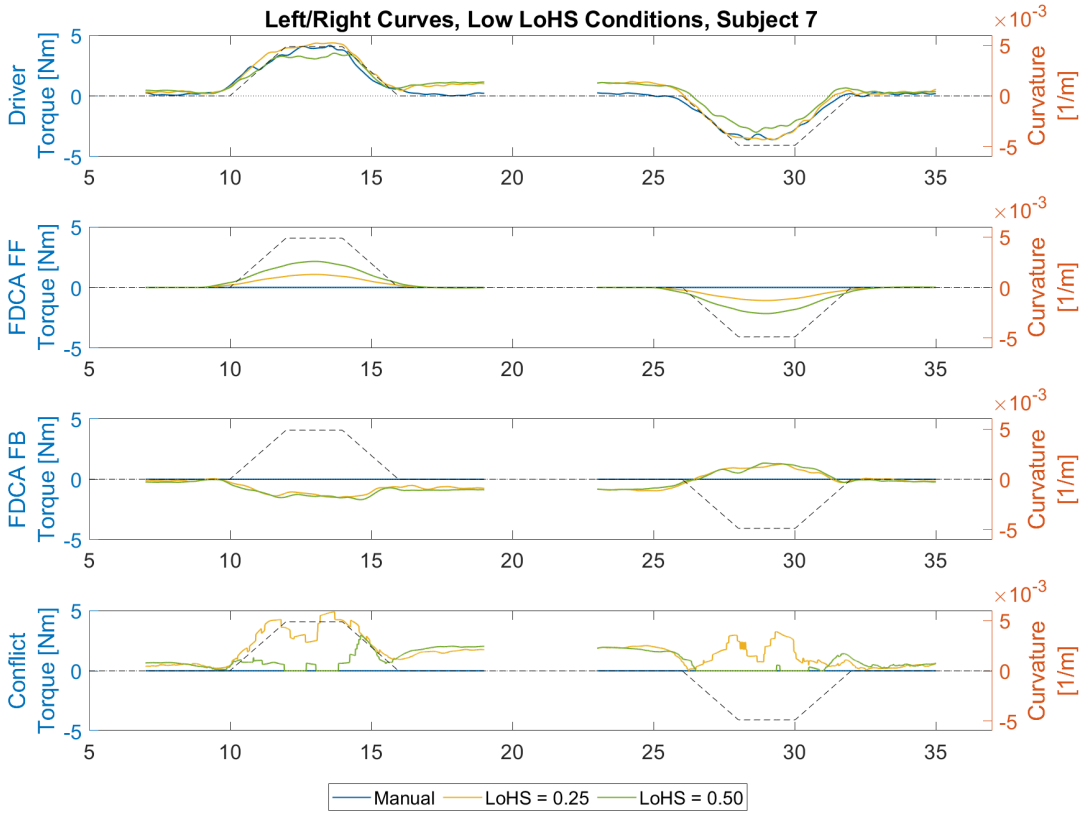

Figure A.13: Torque data averaged for left and right curves for subject 7 for the three lower LoHS conditions

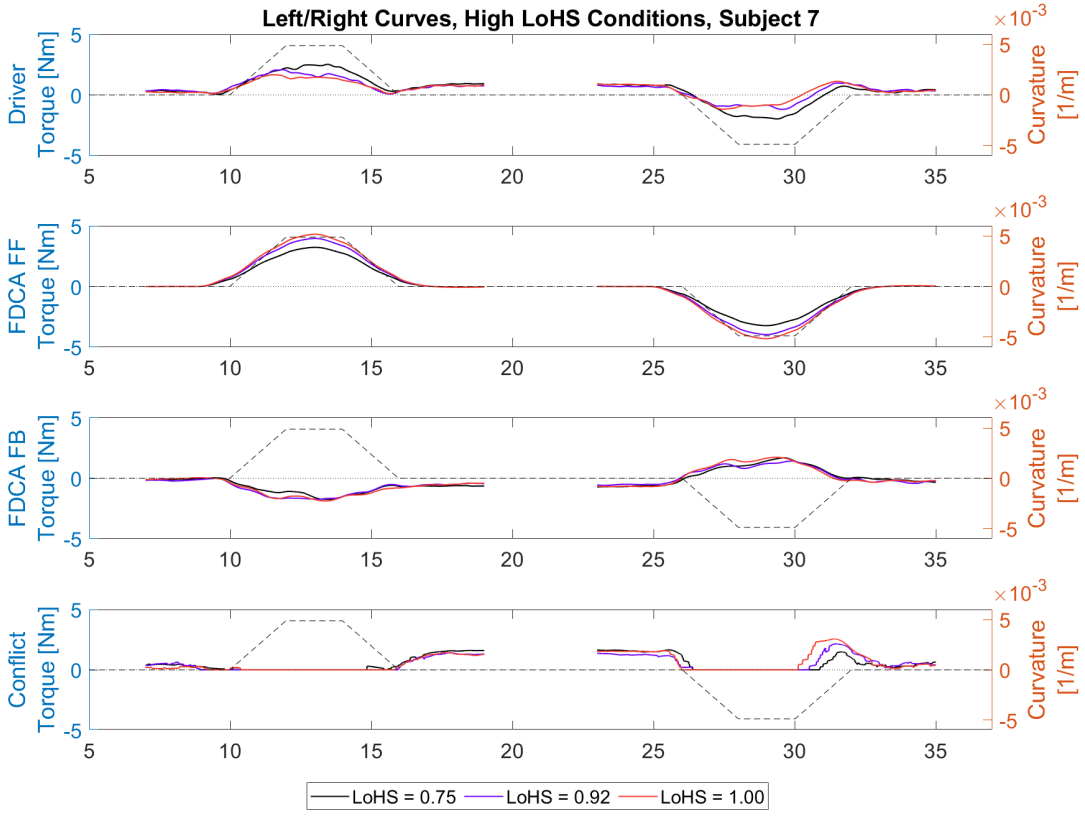

Figure A.14: Torque data averaged for left and right curves for subject 7 for the three higher LoHS conditions

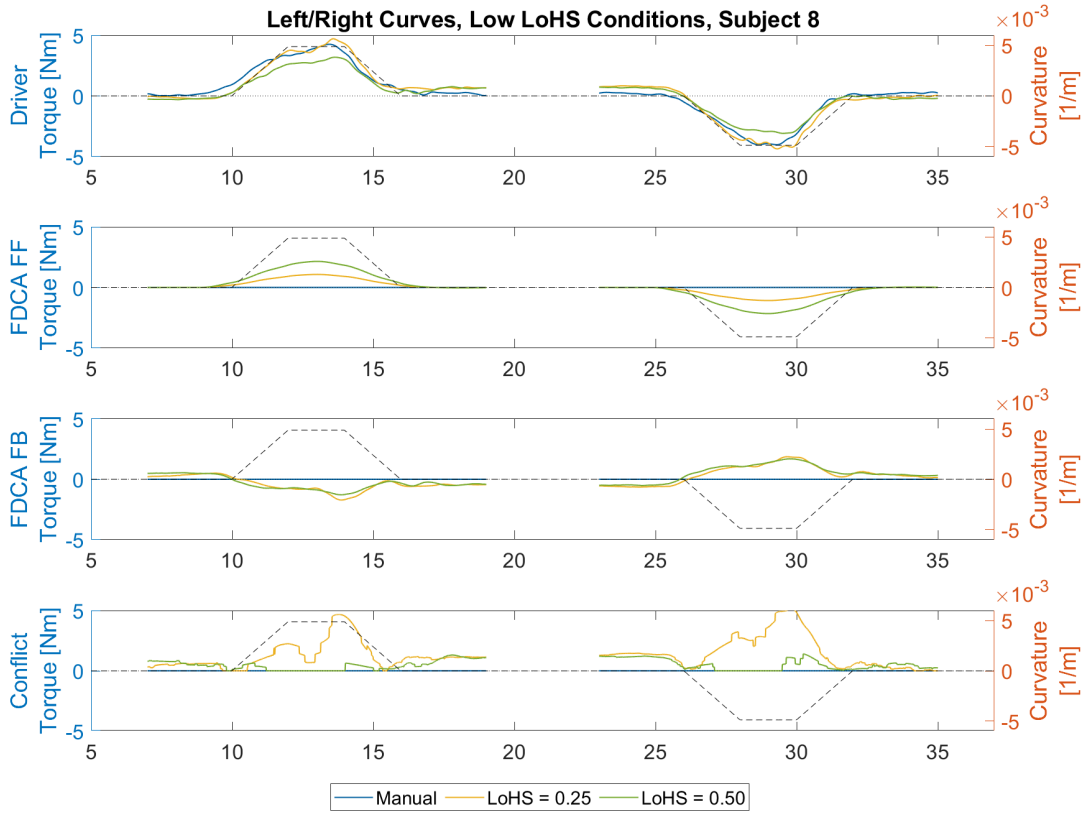

Figure A.15: Torque data averaged for left and right curves for subject 8 for the three lower LoHS conditions

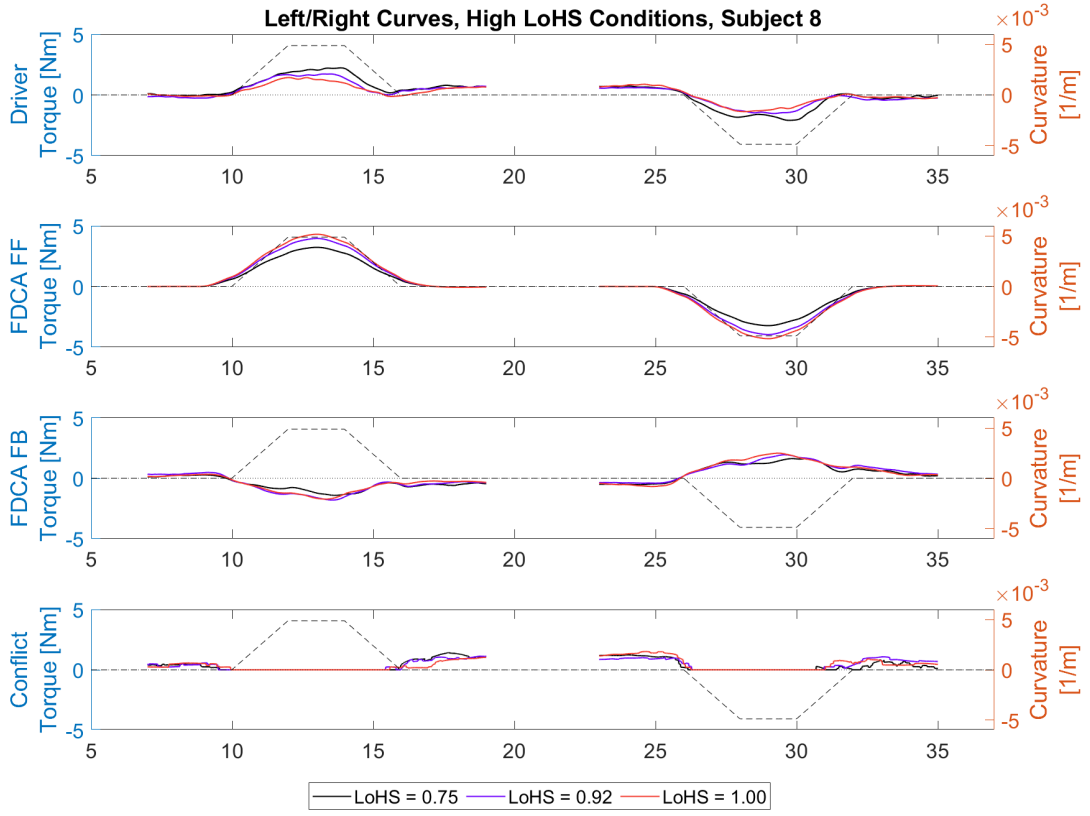

Figure A.16: Torque data averaged for left and right curves for subject 8 for the three higher LoHS conditions

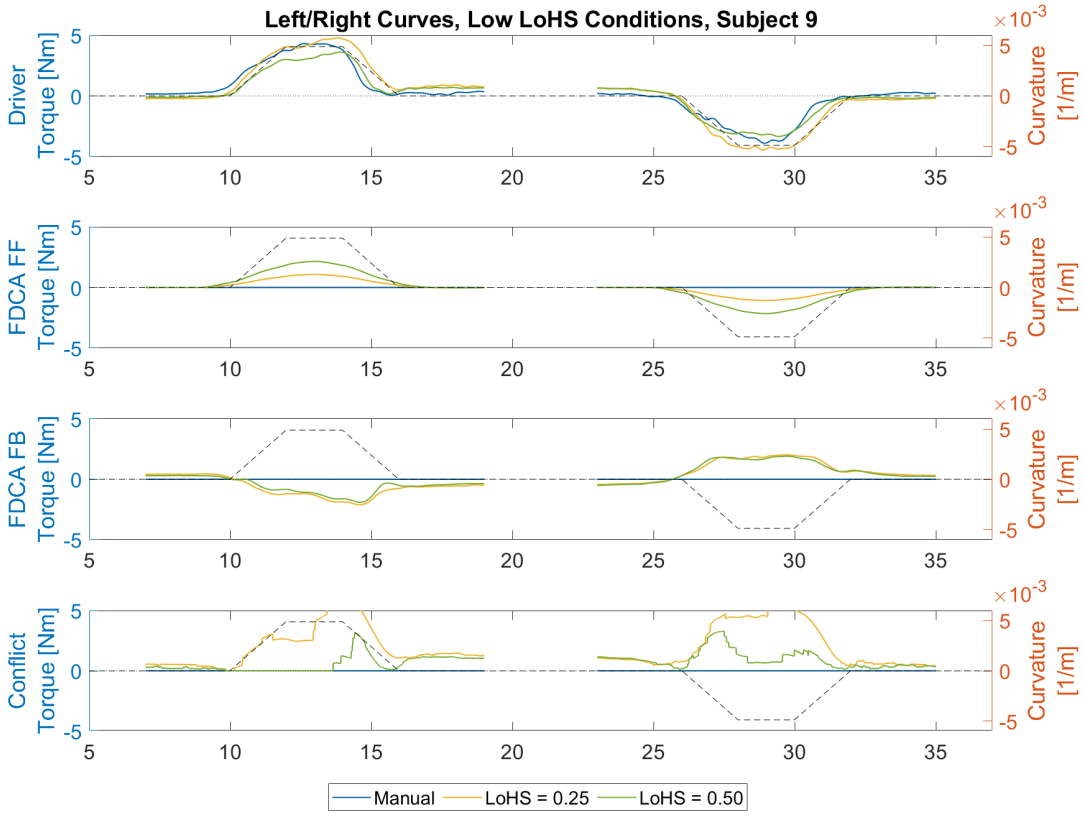

Figure A.17: Torque data averaged for left and right curves for subject 9 for the three lower LoHS conditions

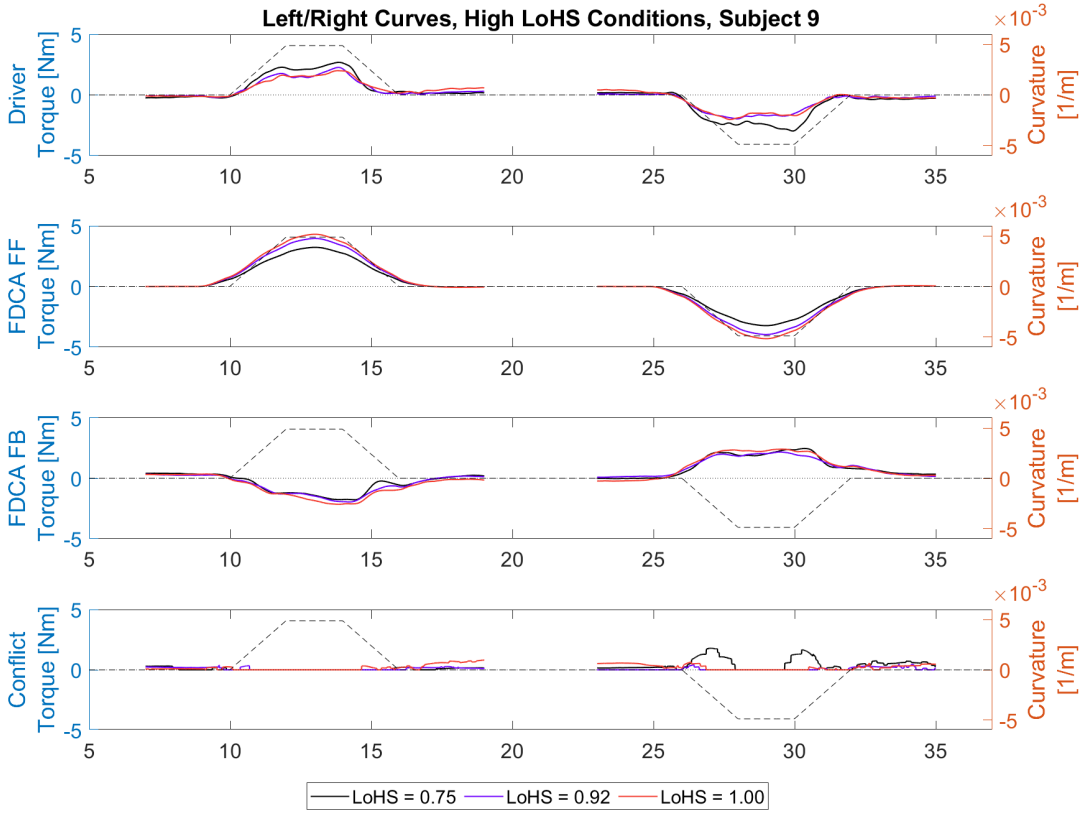

Figure A.18: Torque data averaged for left and right curves for subject 9 for the three higher LoHS conditions

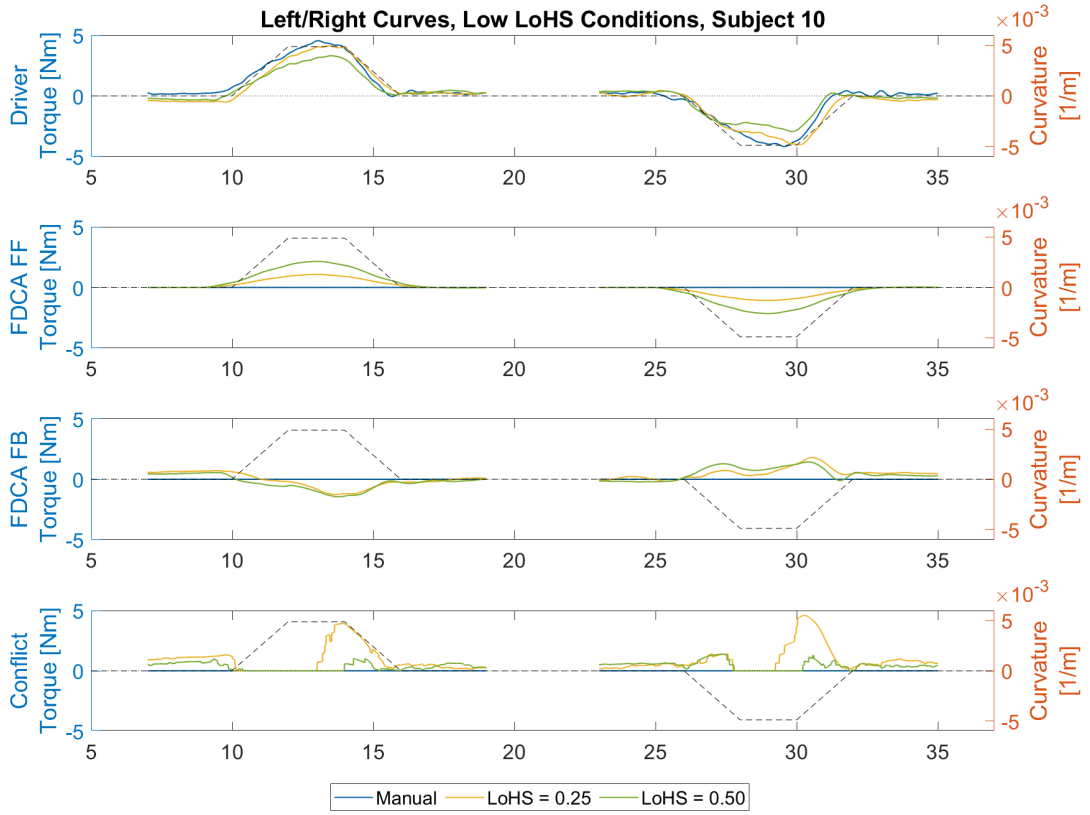

Figure A.19: Torque data averaged for left and right curves for subject 10 for the three lower LoHS conditions

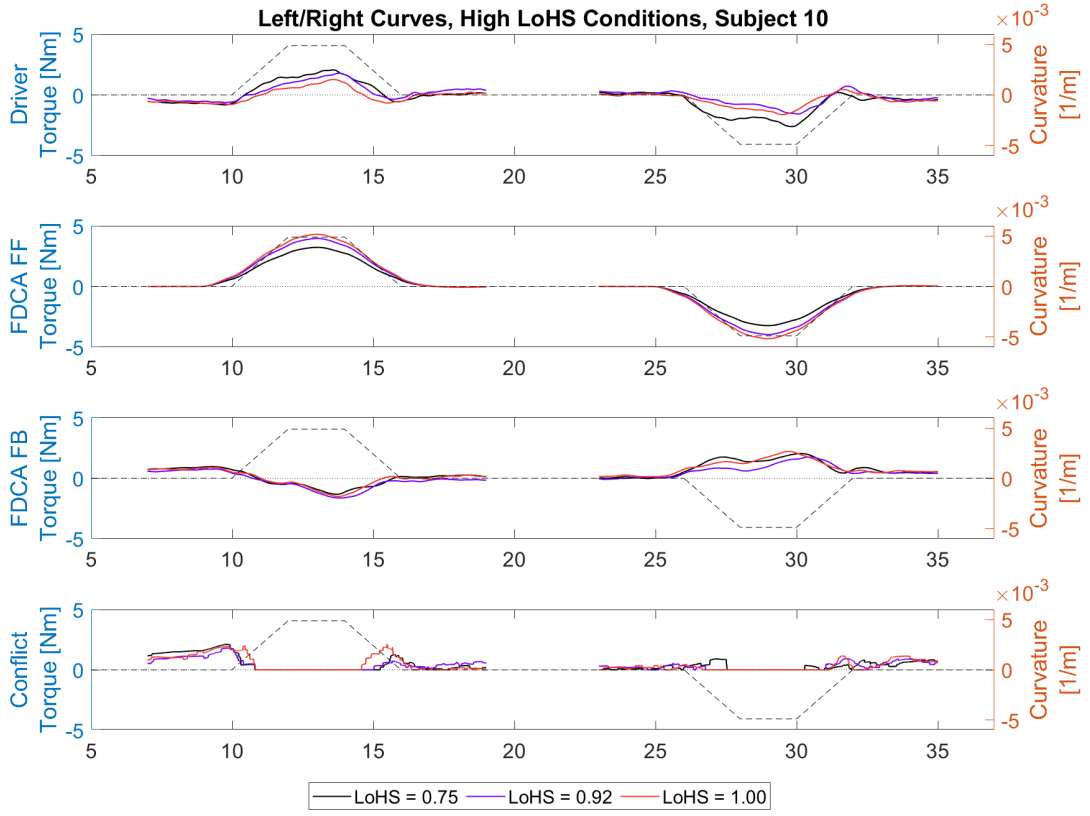

Figure A.20: Torque data averaged for left and right curves for subject 10 for the three higher LoHS conditions

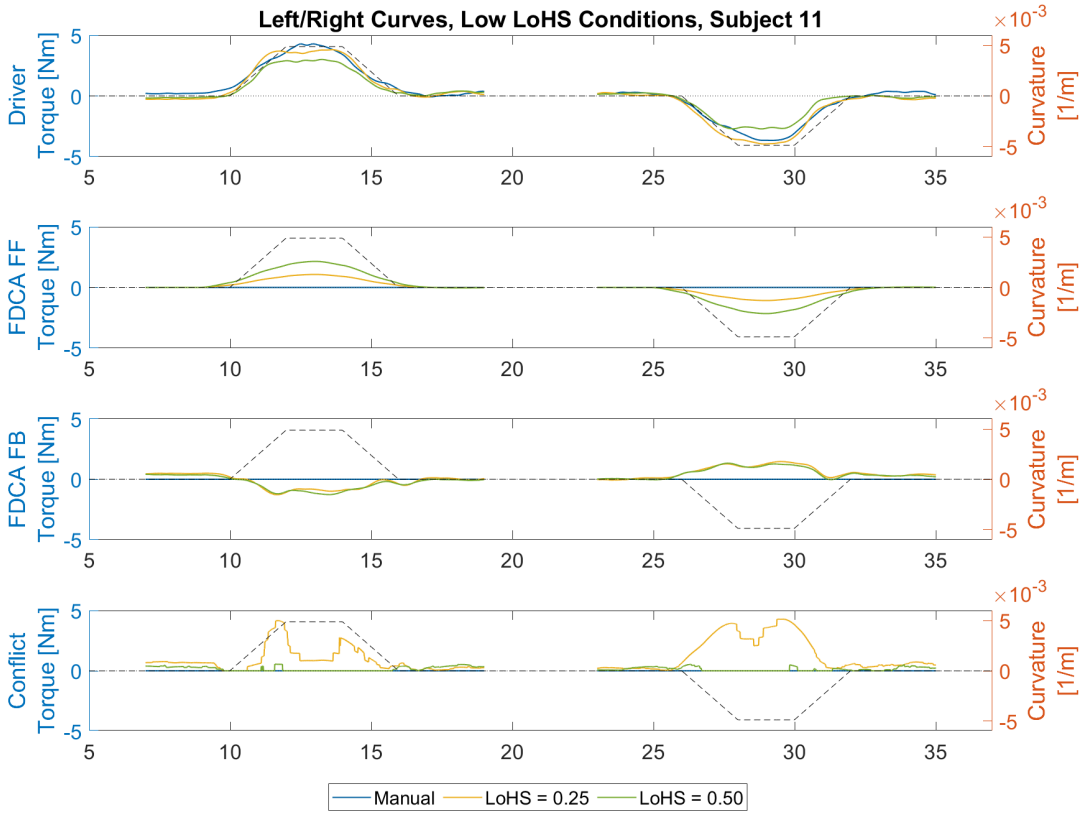

Figure A.21: Torque data averaged for left and right curves for subject 11 for the three lower LoHS conditions

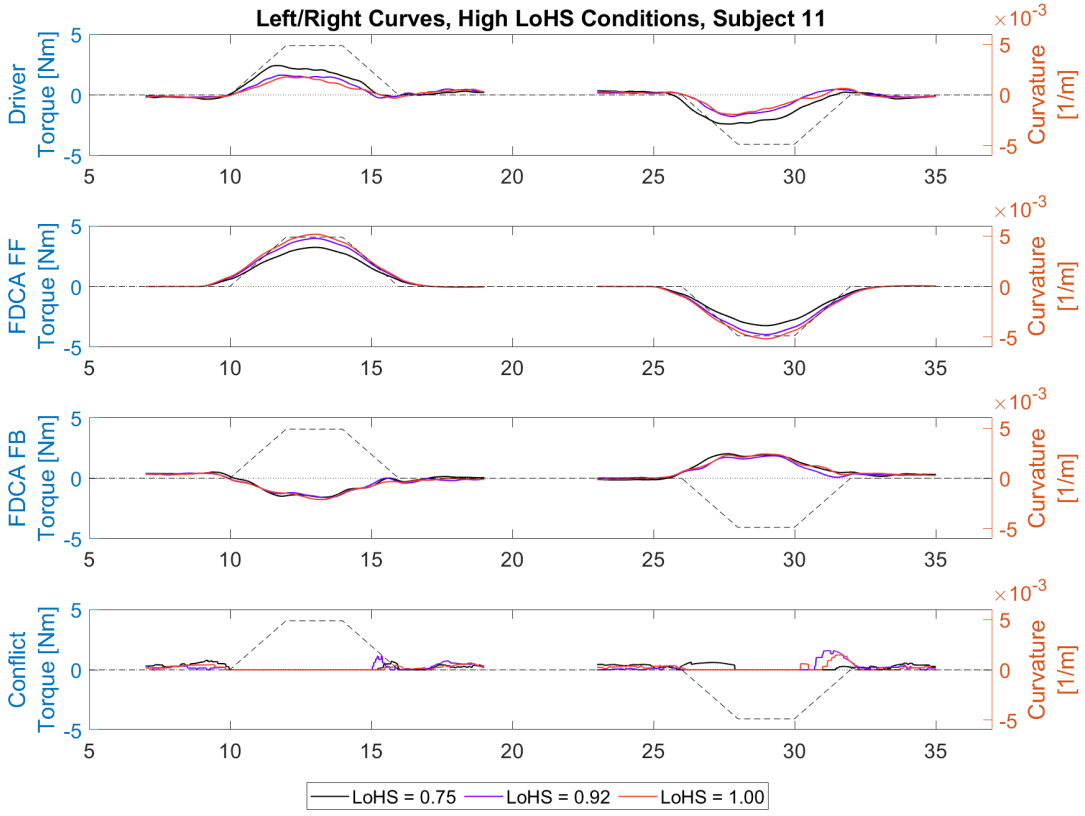

Figure A.22: Torque data averaged for left and right curves for subject 11 for the three higher LoHS conditions

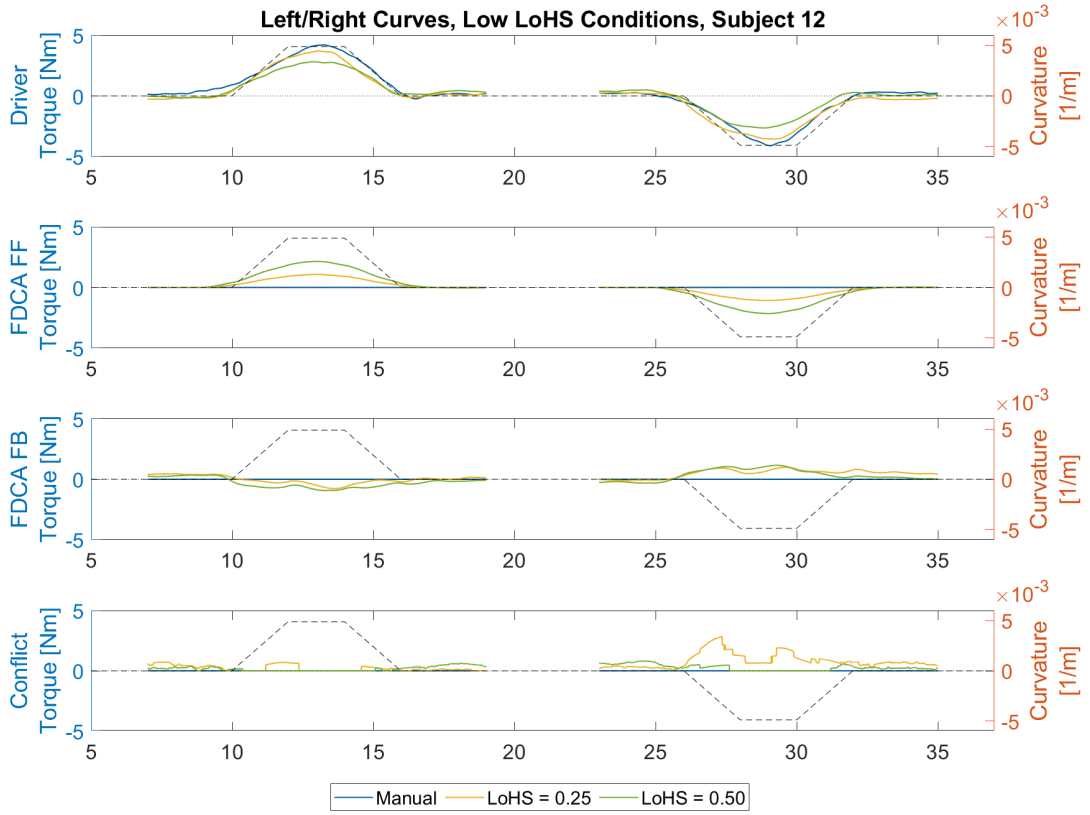

Figure A.23: Torque data averaged for left and right curves for subject 12 for the three lower LoHS conditions

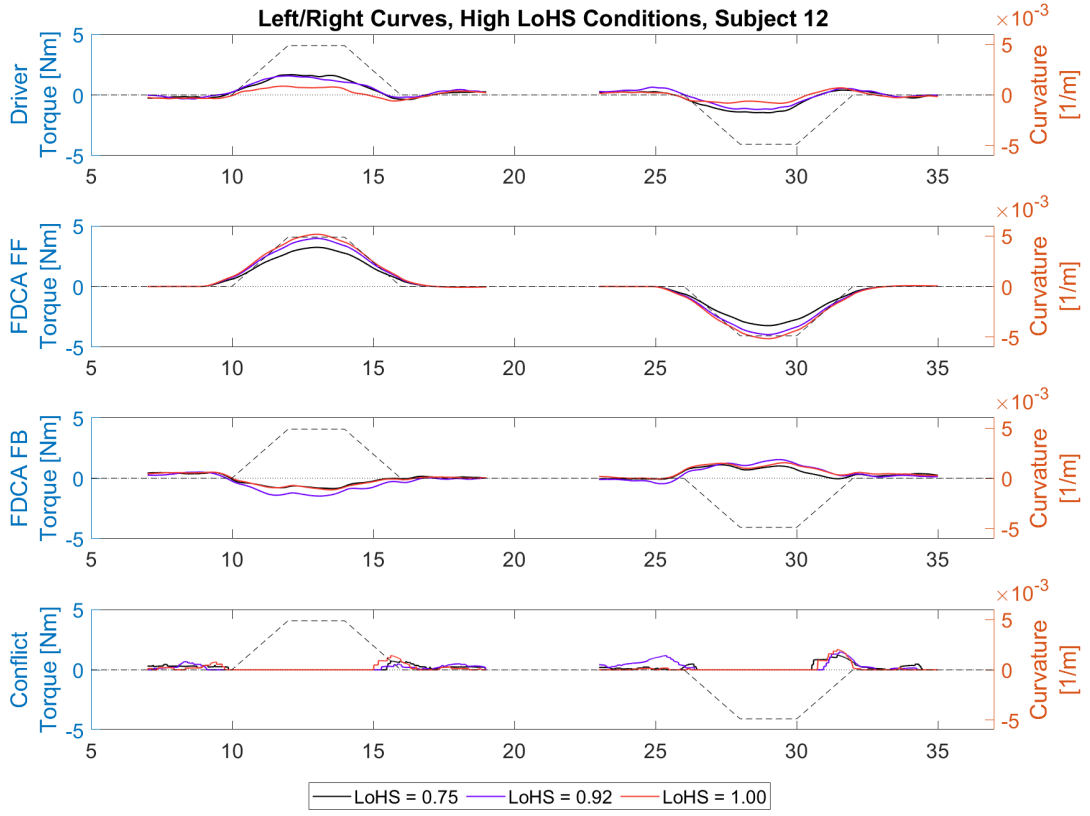

Figure A.24: Torque data averaged for left and right curves for subject 12 for the three higher LoHS conditions

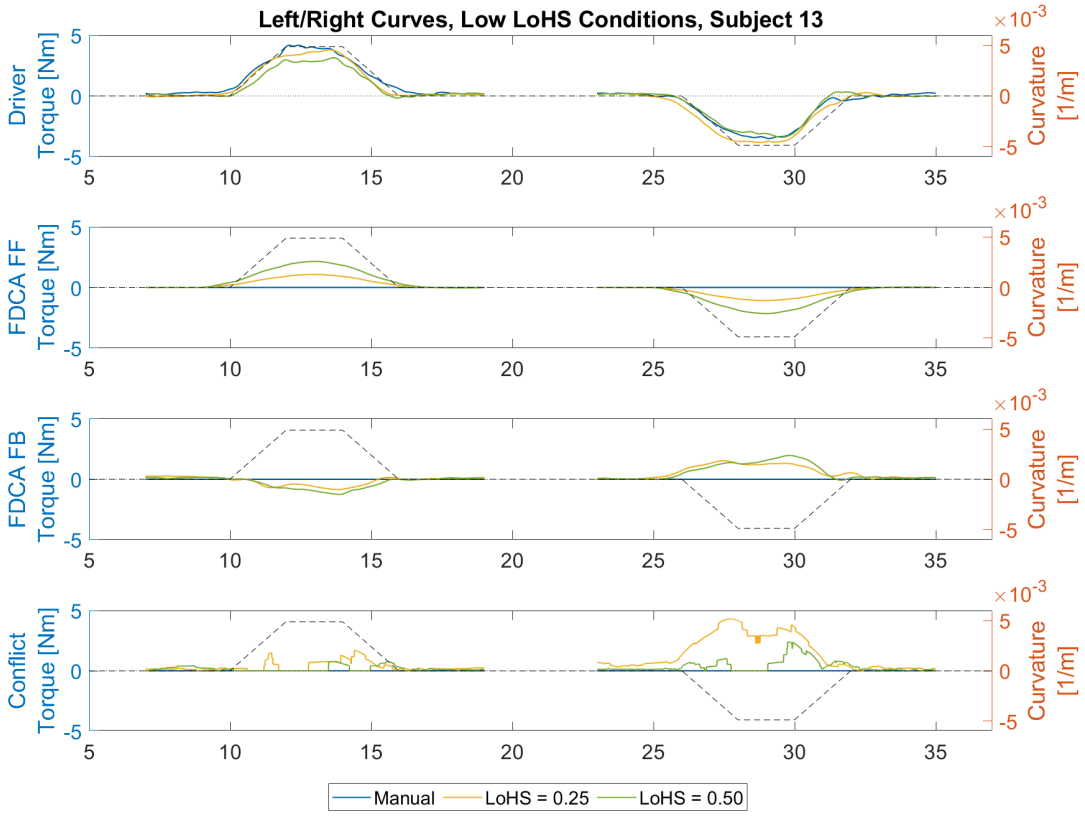

Figure A.25: Torque data averaged for left and right curves for subject 13 for the three lower LoHS conditions

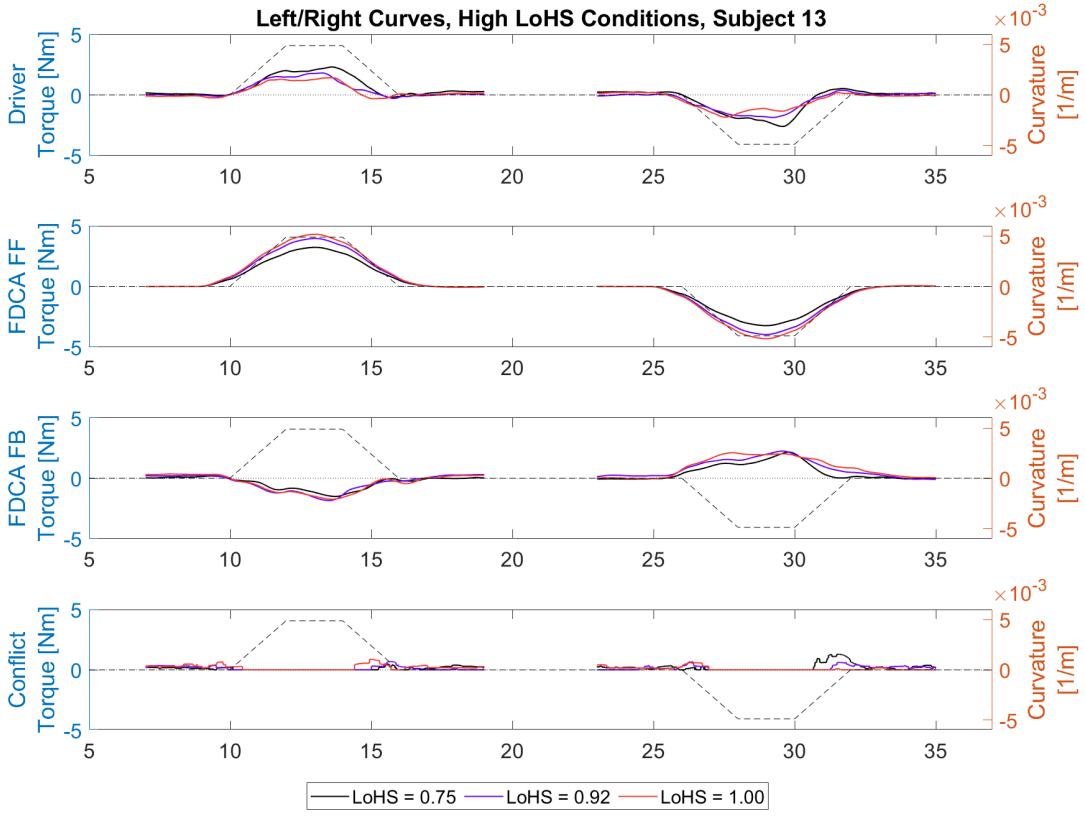

Figure A.26: Torque data averaged for left and right curves for subject 13 for the three higher LoHS conditions

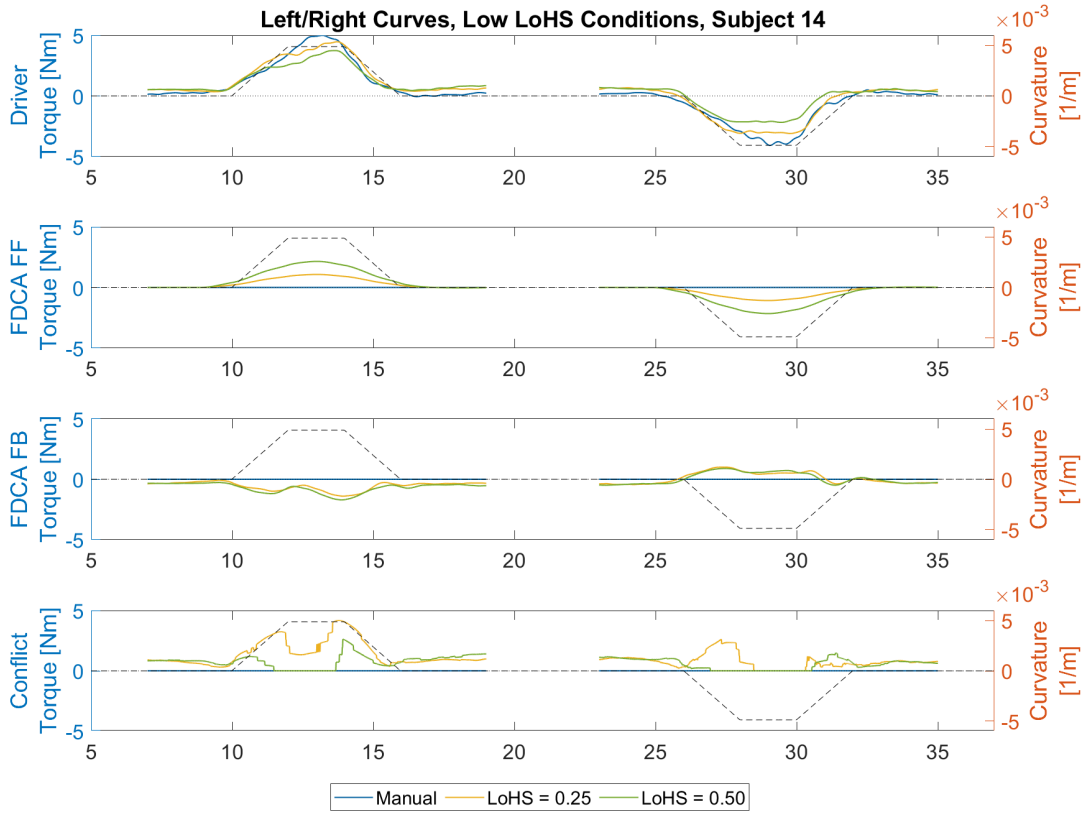

Figure A.27: Torque data averaged for left and right curves for subject 14 for the three lower LoHS conditions

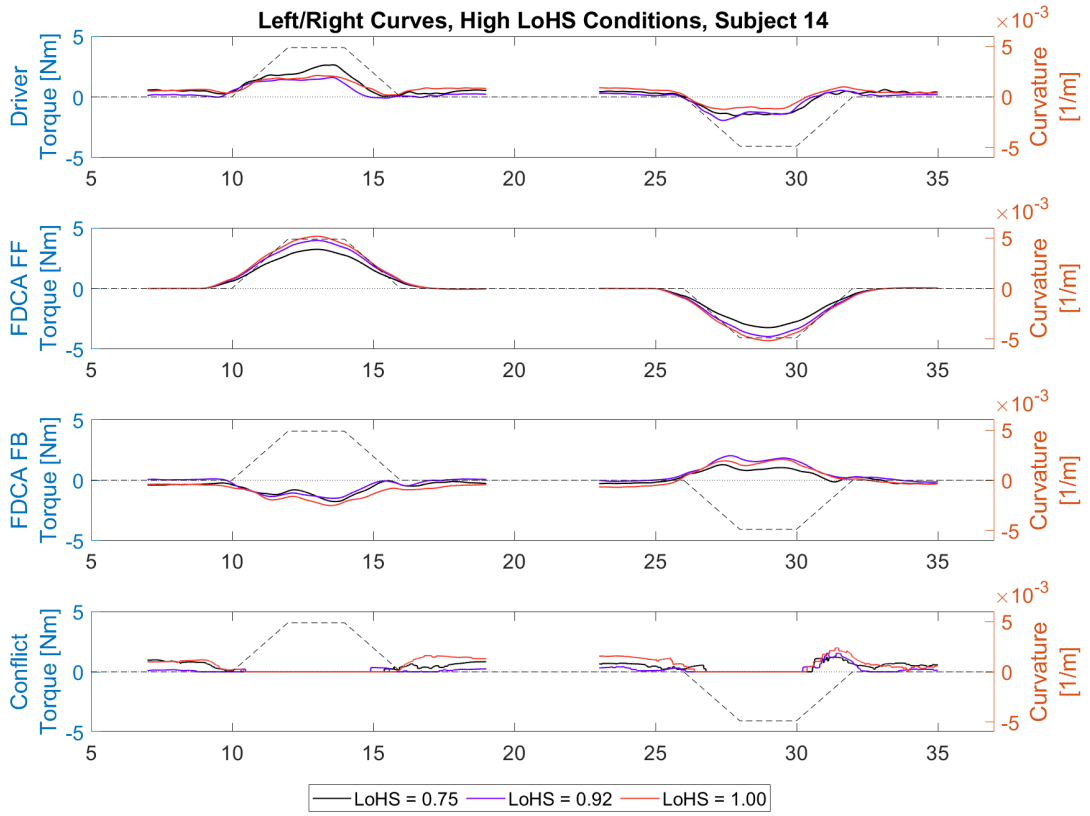

Figure A.28: Torque data averaged for left and right curves for subject 14 for the three higher LoHS conditions

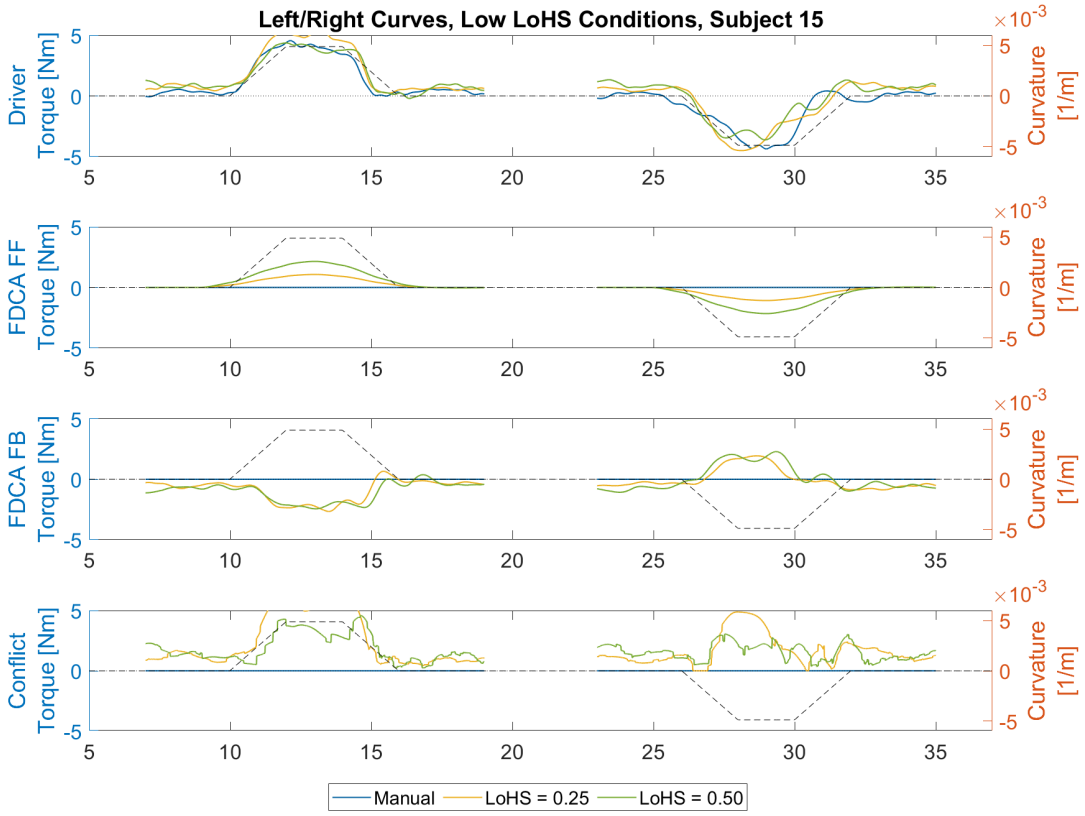

Figure A.29: Torque data averaged for left and right curves for subject 15 for the three lower LoHS conditions

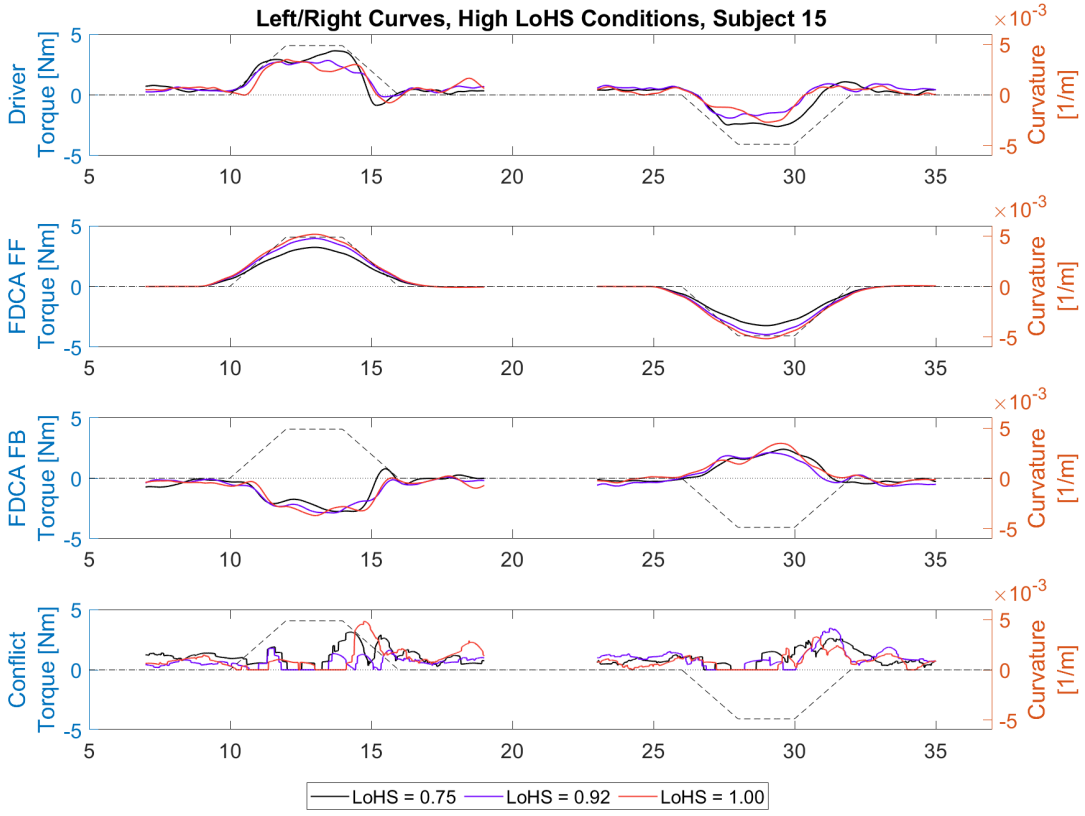

Figure A.30: Torque data averaged for left and right curves for subject 15 for the three higher LoHS conditions

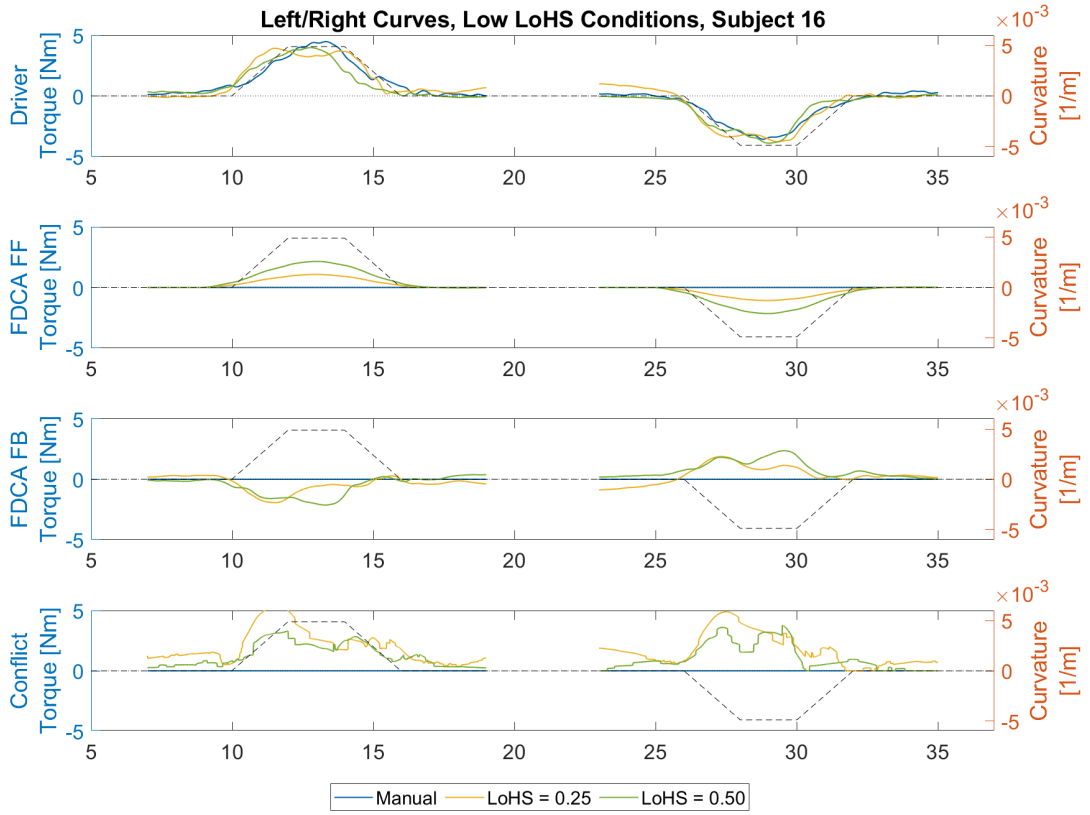

Figure A.31: Torque data averaged for left and right curves for subject 16 for the three lower LoHS conditions

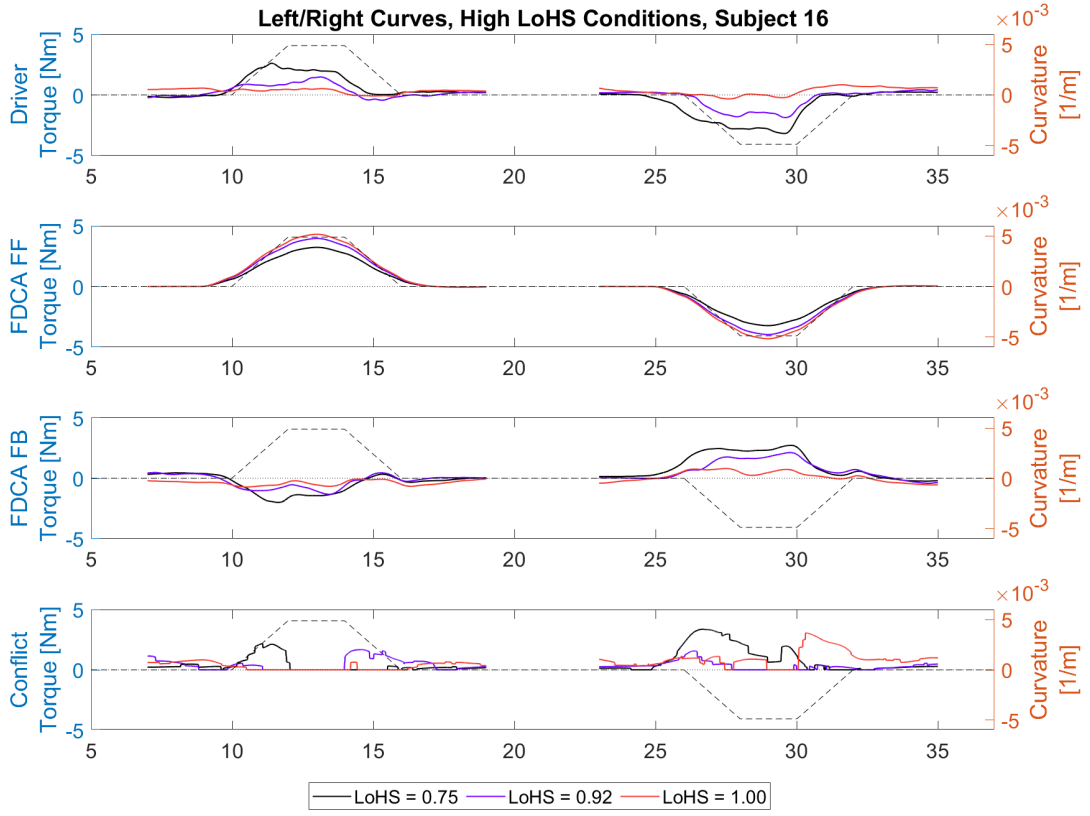

Figure A.32: Torque data averaged for left and right curves for subject 16 for the three higher LoHS conditions

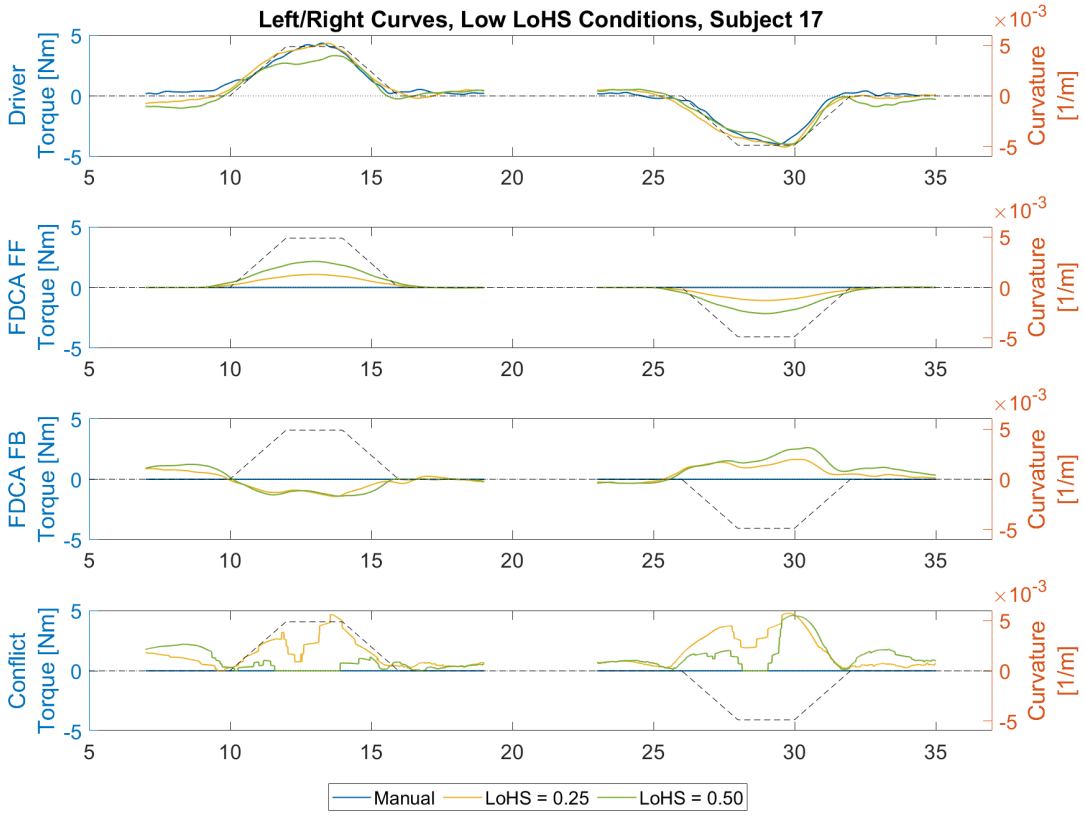

Figure A.33: Torque data averaged for left and right curves for subject 17 for the three lower LoHS conditions

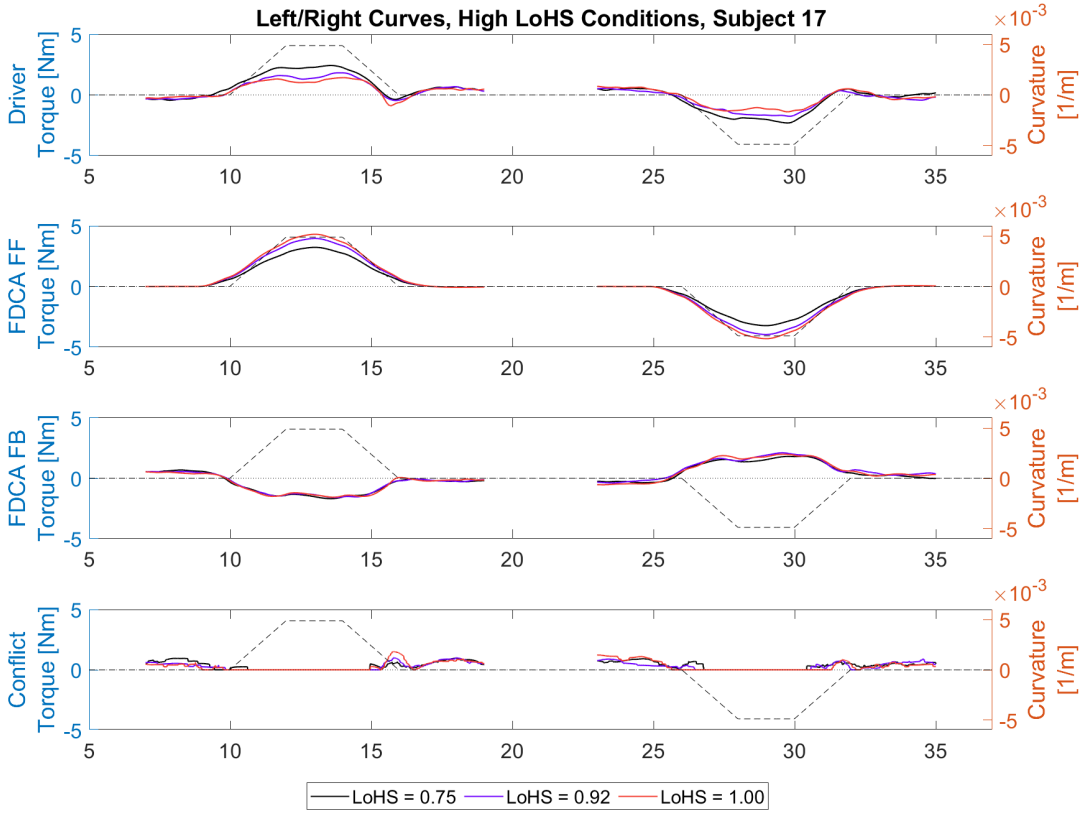

Figure A.34: Torque data averaged for left and right curves for subject 17 for the three higher LoHS conditions

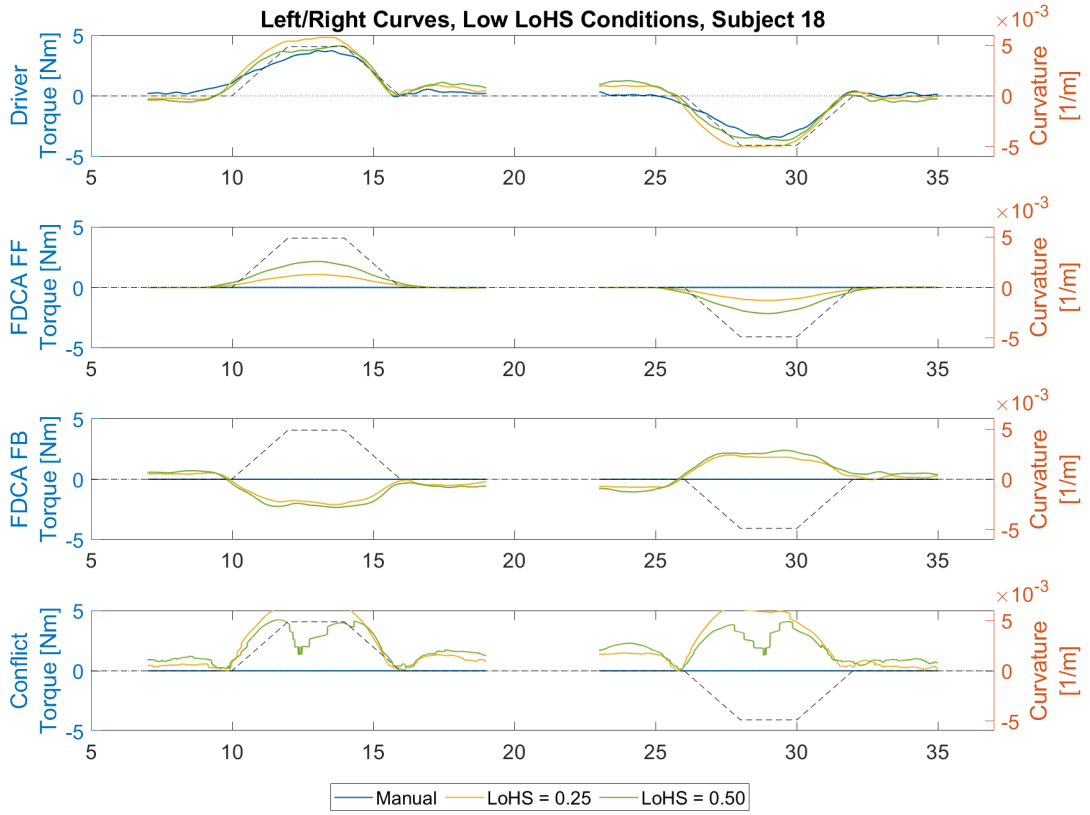

Figure A.35: Torque data averaged for left and right curves for subject 18 for the three lower LoHS conditions

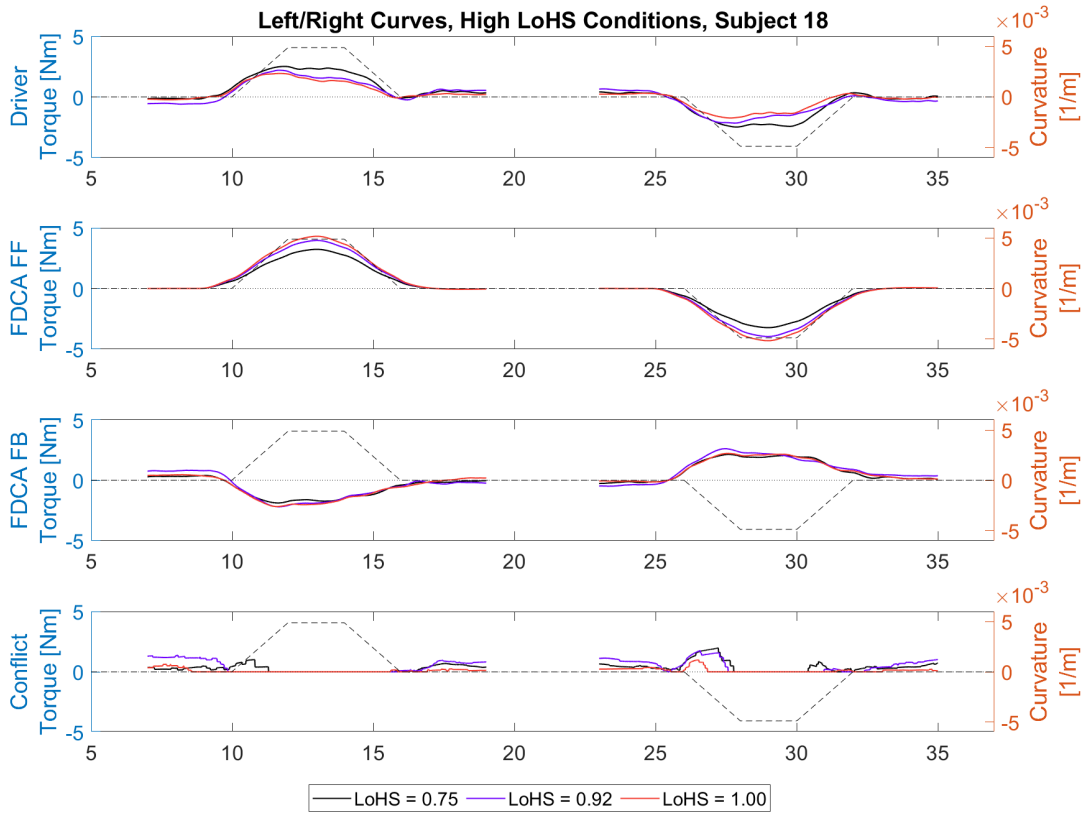

Figure A.36: Torque data averaged for left and right curves for subject 18 for the three higher LoHS conditions

B

Individual Driver Results - Conflict Time Trace Plots

The time trace plots are provided here which indicate the driver and FDCA torques as well as the conflict between the human and the haptic support in red. Time traces for the manual driving condition are also included for comparison. Since there is only a human torque input in this case there is no conflict.

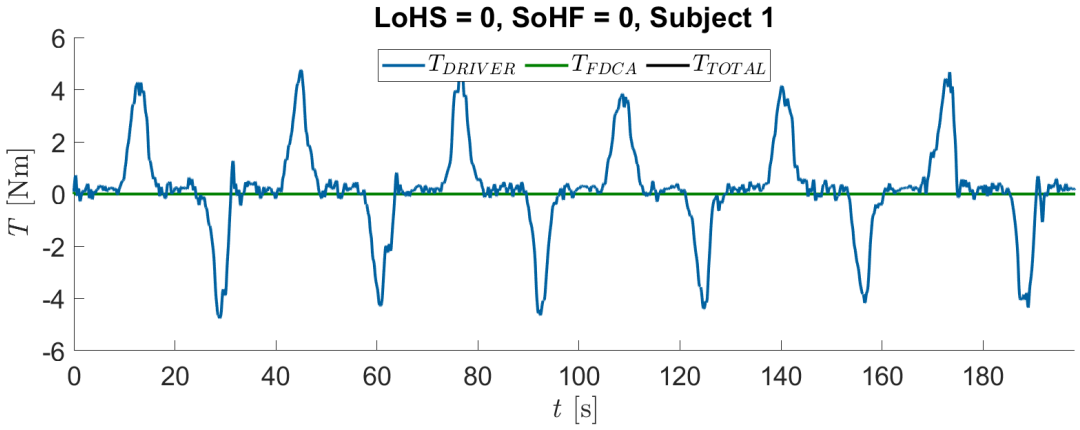

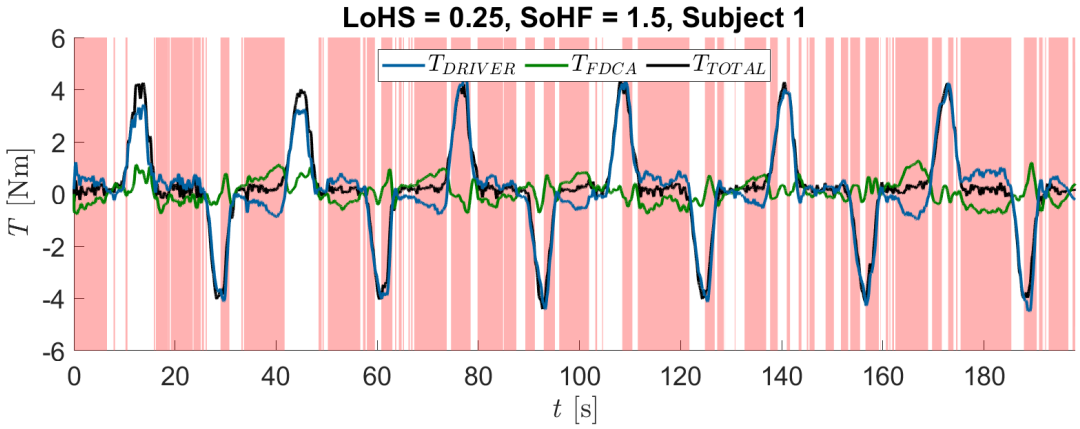

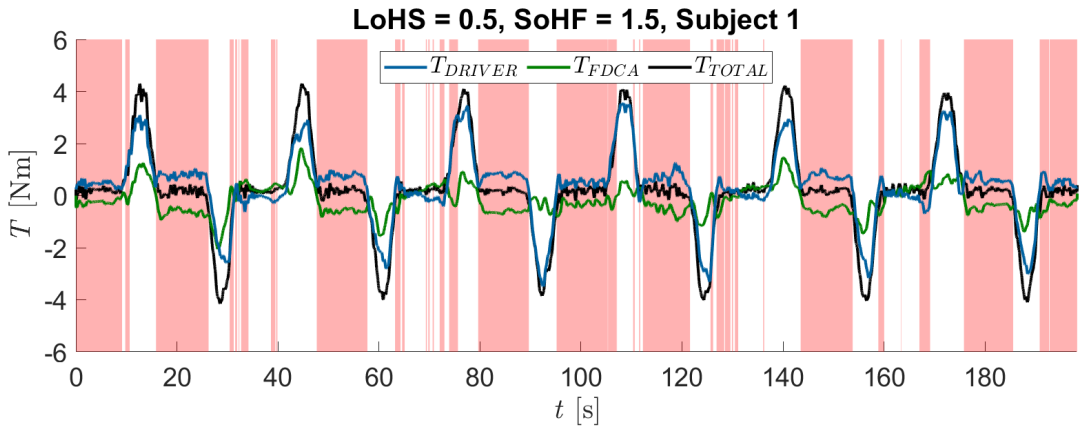
LoHS = 0.5, SoHF = 1.5, Subject 1
T_{DRIVER} T_{FDCA} T_{TOTAL}
T [Nm]
t [s]

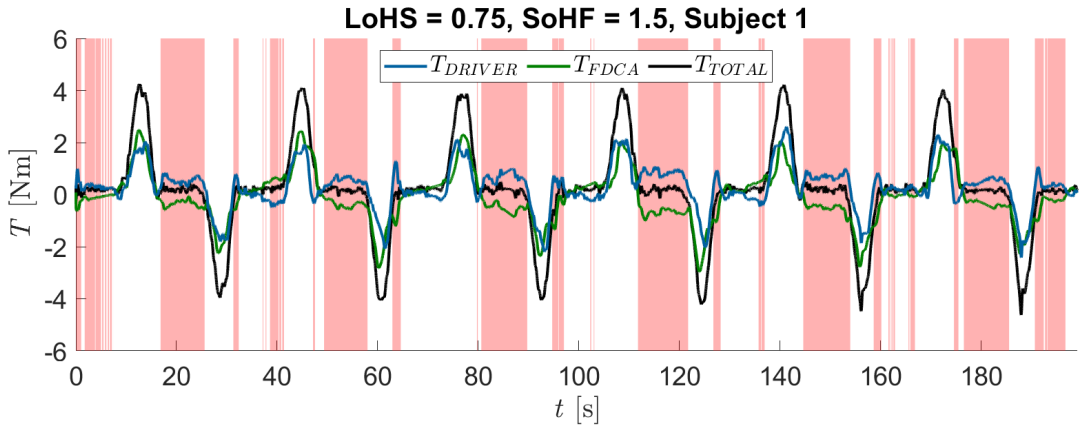
LoHS = 0.75, SoHF = 1.5, Subject 1
T_{DRIVER} T_{FDCA} T_{TOTAL}
T [Nm]
t [s]

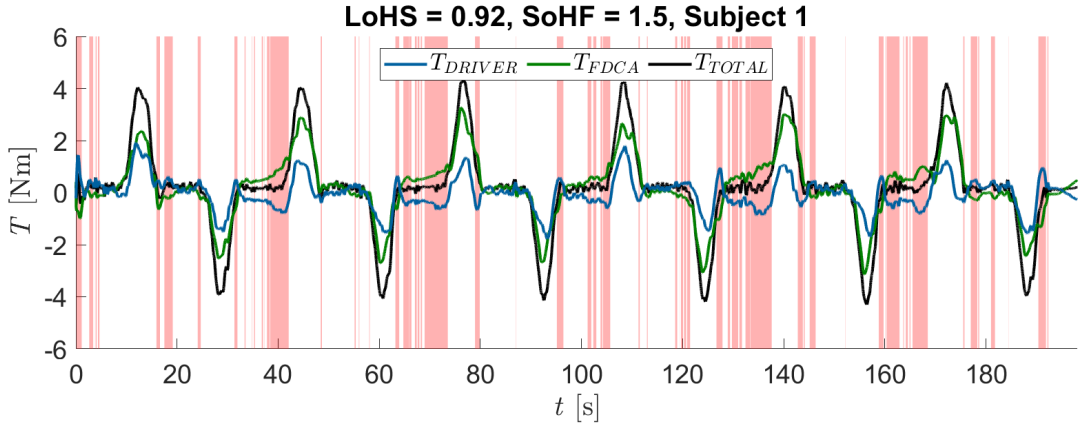
LoHS = 0.92, SoHF = 1.5, Subject 1
T_{DRIVER} T_{FDCA} T_{TOTAL}
T [Nm]
t [s]

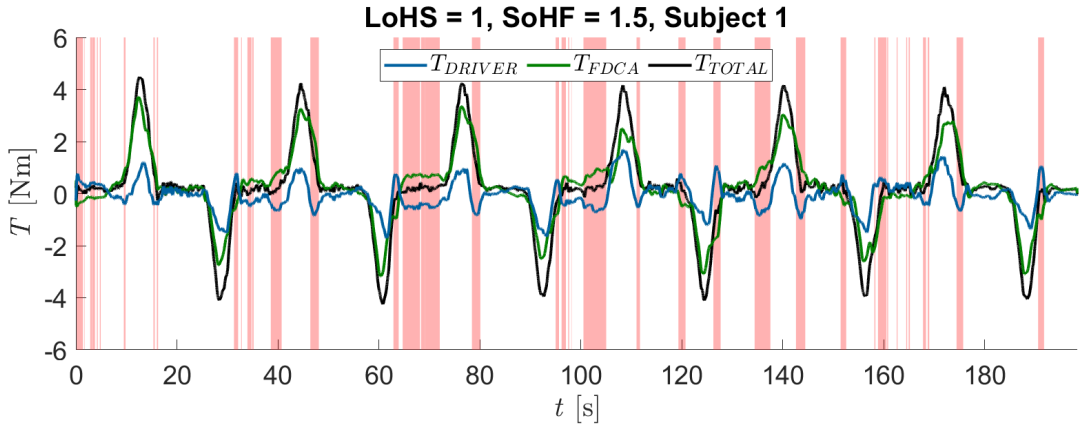
LoHS = 1, SoHF = 1.5, Subject 1
T_{DRIVER} T_{FDCA} T_{TOTAL}
T [Nm]
t [s]

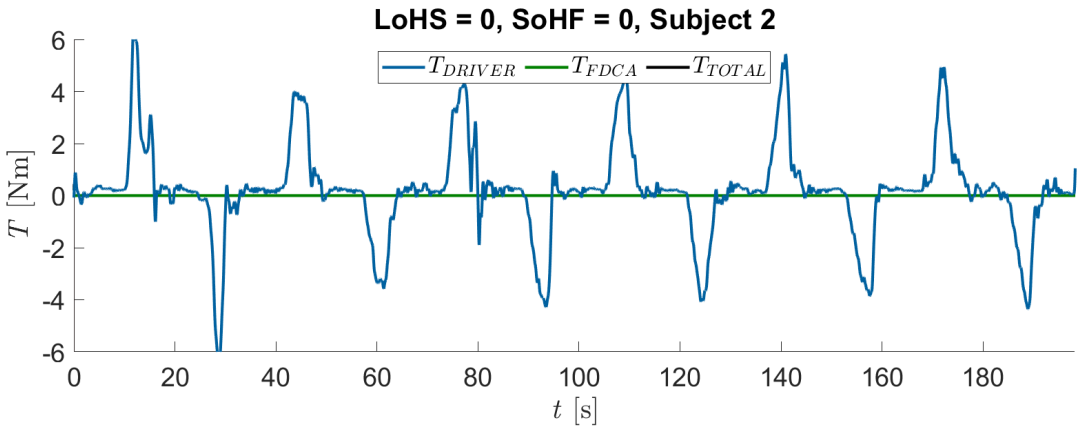
LoHS = 0, SoHF = 0, Subject 2
T_{DRIVER} T_{FDCA} T_{TOTAL}
T [Nm]
t [s]

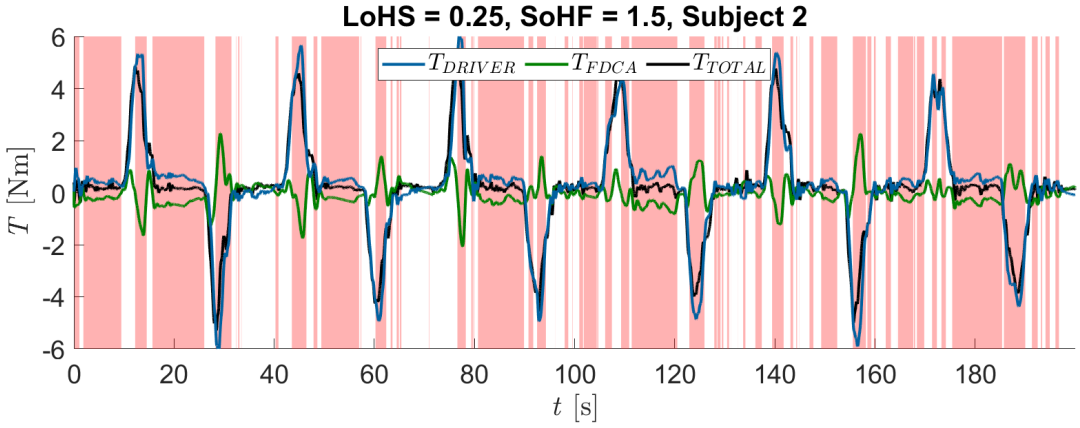
LoHS = 0.25, SoHF = 1.5, Subject 2
T_{DRIVER} T_{FDCA} T_{TOTAL}
T [Nm]
t [s]

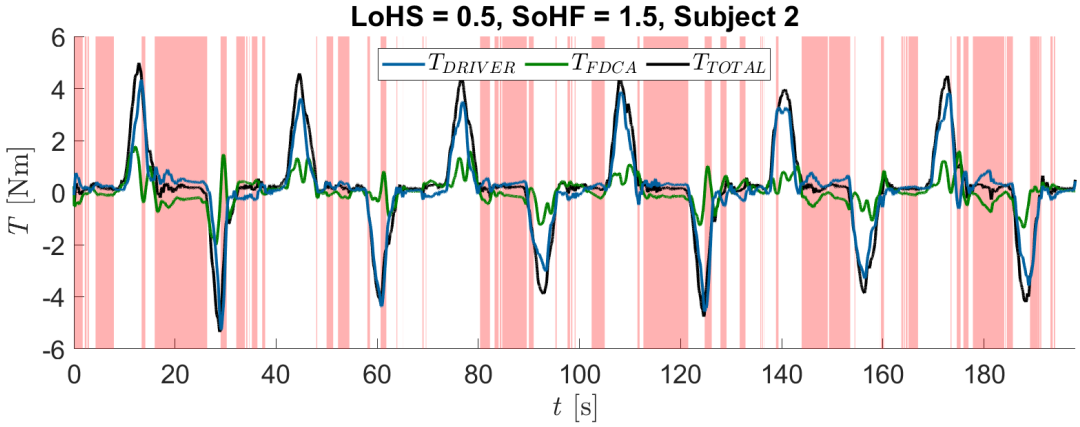
LoHS = 0.5, SoHF = 1.5, Subject 2
T_{DRIVER} T_{FDCA} T_{TOTAL}
T [Nm]
t [s]

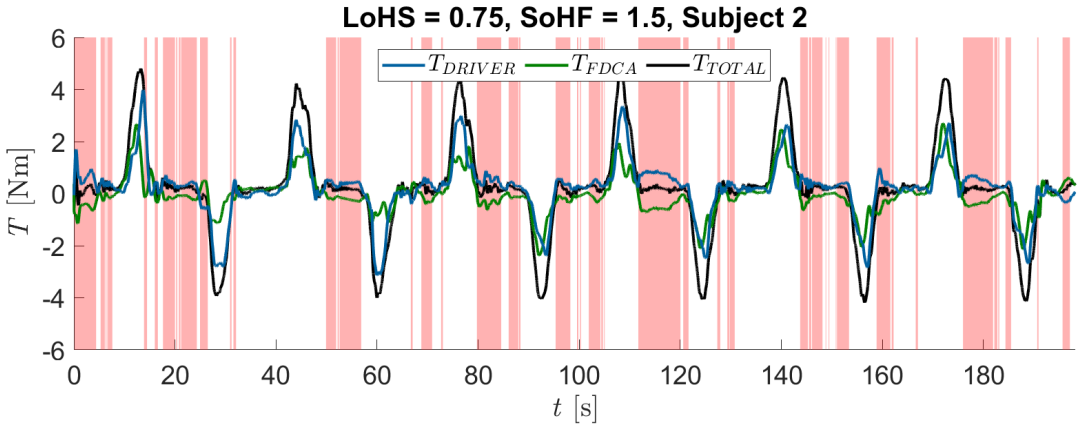
LoHS = 0.75, SoHF = 1.5, Subject 2
T_{DRIVER} T_{FDCA} T_{TOTAL}
T [Nm]
t [s]

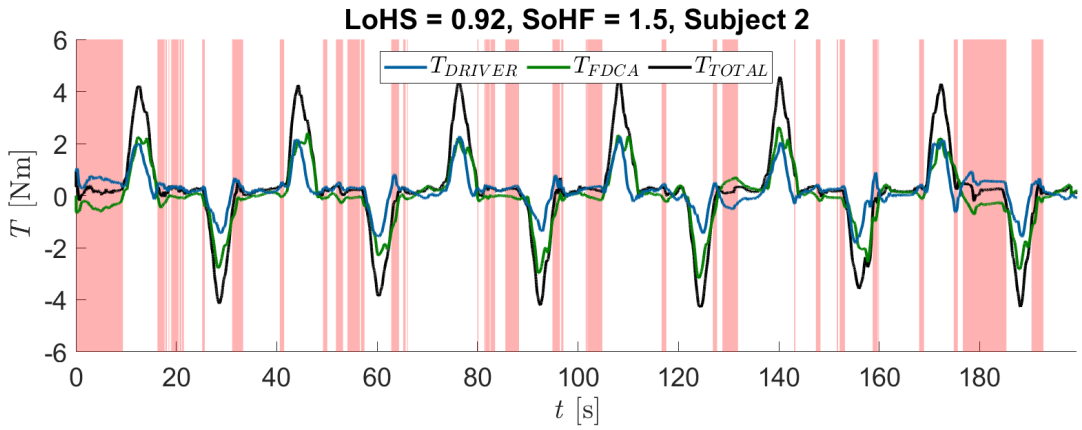
LoHS = 0.92, SoHF = 1.5, Subject 2
T_{DRIVER} T_{FDCA} T_{TOTAL}
T [Nm]
t [s]

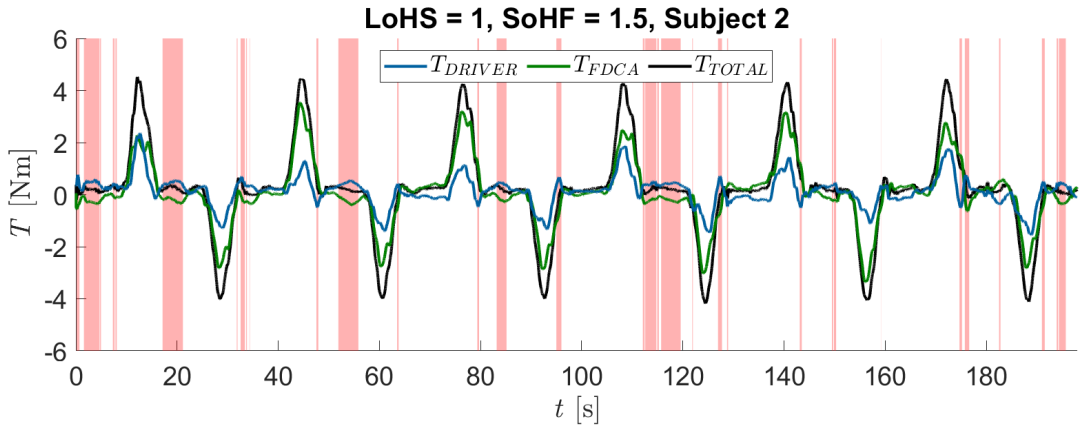
LoHS = 1, SoHF = 1.5, Subject 2
T_{DRIVER} T_{FDCA} T_{TOTAL}
T [Nm]
t [s]

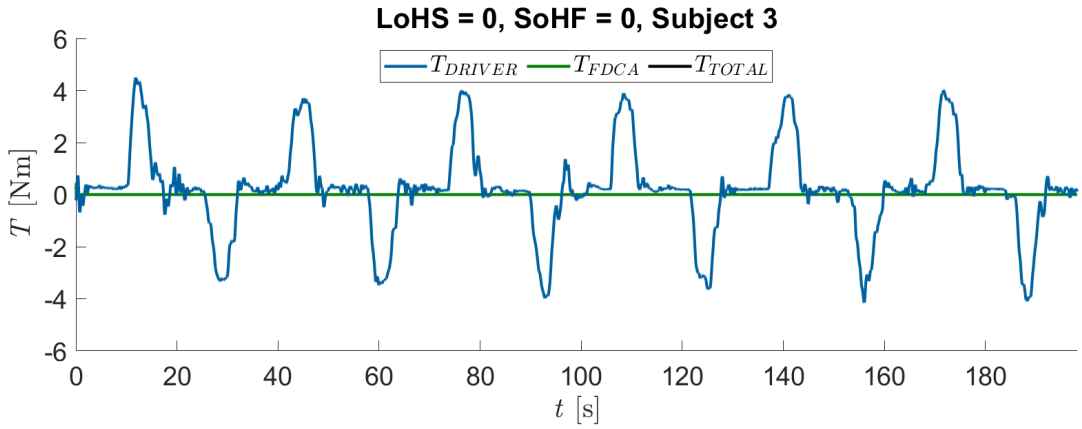
LoHS = 0, SoHF = 0, Subject 3
T_{DRIVER} T_{FDCA} T_{TOTAL}
T [Nm]
t [s]

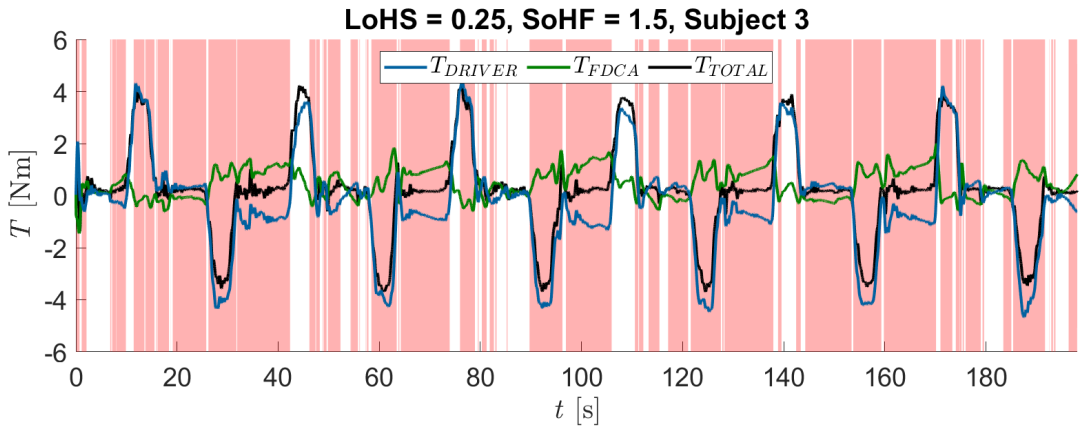
LoHS = 0.25, SoHF = 1.5, Subject 3
T_{DRIVER} T_{FDCA} T_{TOTAL}
T [Nm]
t [s]

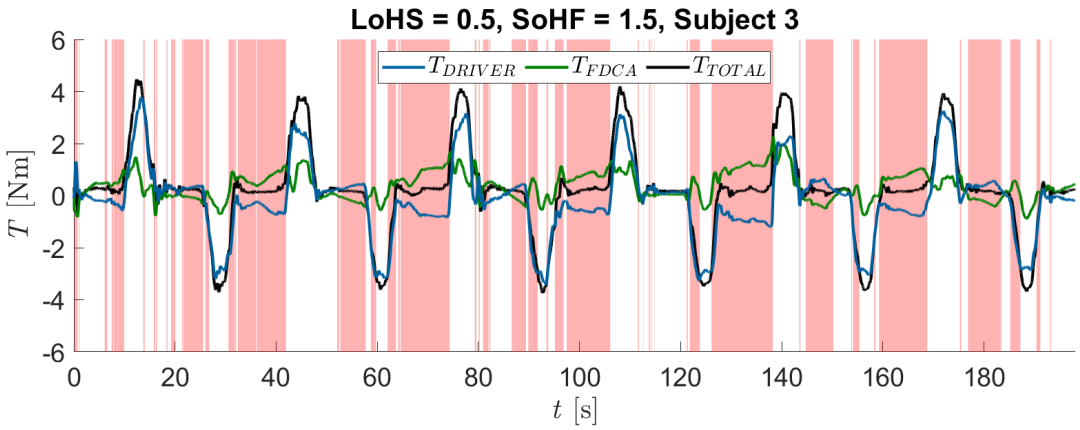
LoHS = 0.5, SoHF = 1.5, Subject 3
T_{DRIVER} T_{FDCA} T_{TOTAL}
T [Nm]
t [s]

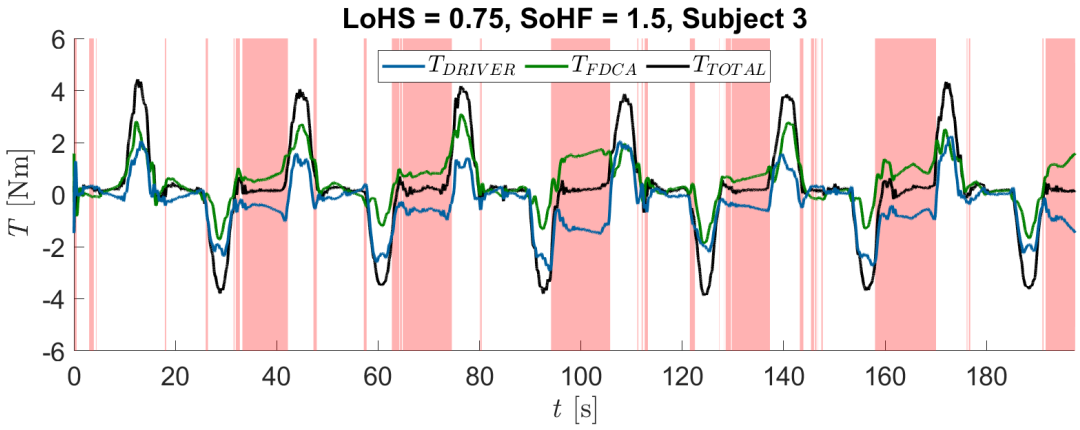
LoHS = 0.75, SoHF = 1.5, Subject 3
T_{DRIVER} T_{FDCA} T_{TOTAL}
T [Nm]
t [s]

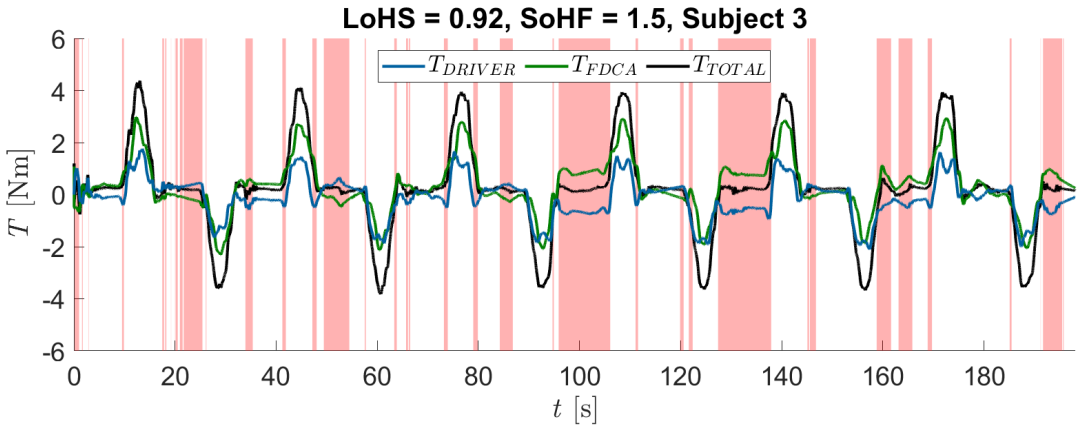
LoHS = 0.92, SoHF = 1.5, Subject 3
T_{DRIVER} T_{FDCA} T_{TOTAL}
T [Nm]
t [s]

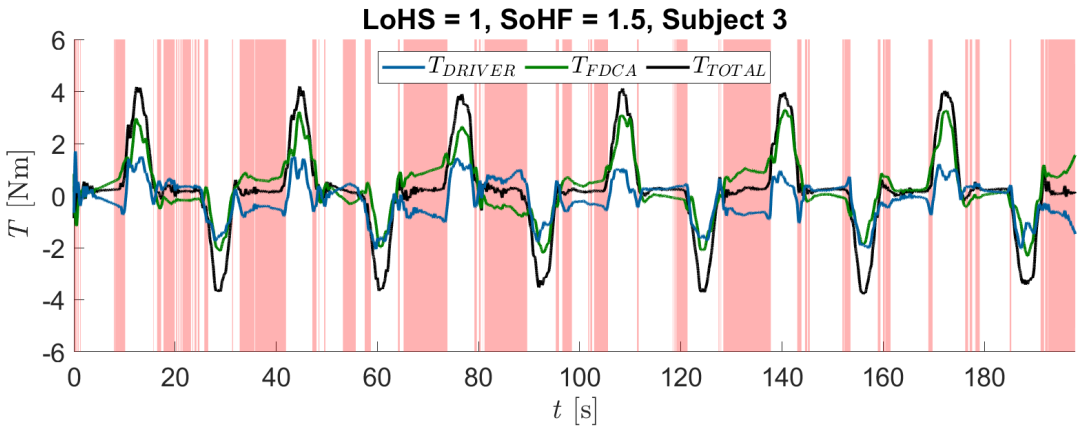
LoHS = 1, SoHF = 1.5, Subject 3
T_{DRIVER} T_{FDCA} T_{TOTAL}
T [Nm]
t [s]

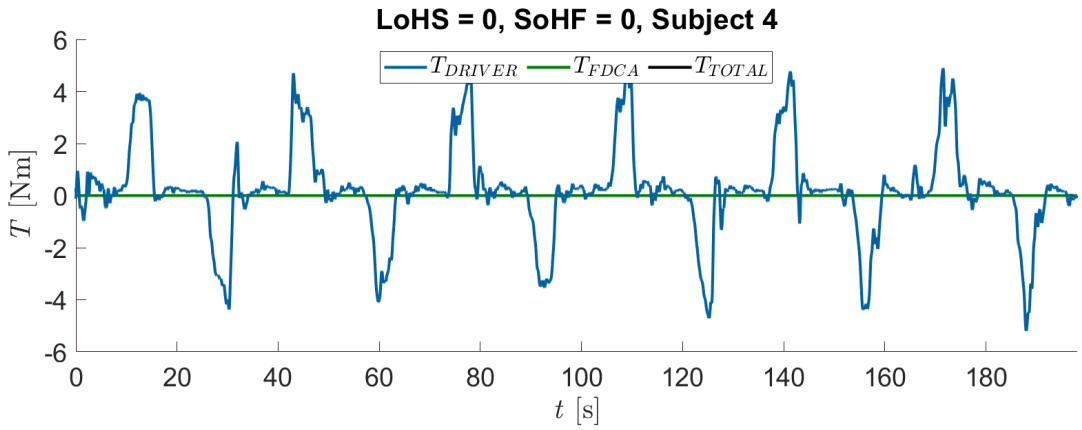
LoHS = 0, SoHF = 0, Subject 4
T_{DRIVER} T_{FDCA} T_{TOTAL}
T [Nm]
t [s]

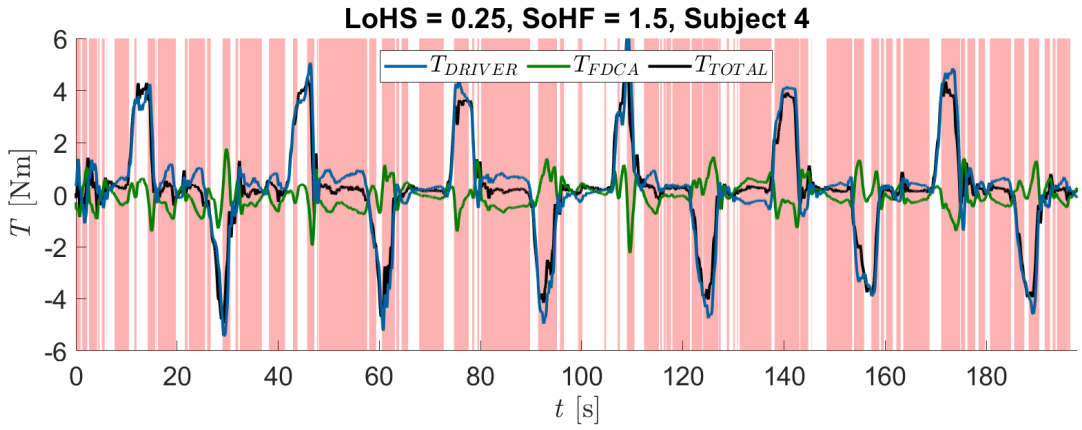
LoHS = 0.25, SoHF = 1.5, Subject 4
T_{DRIVER} T_{FDCA} T_{TOTAL}
T [Nm]
t [s]

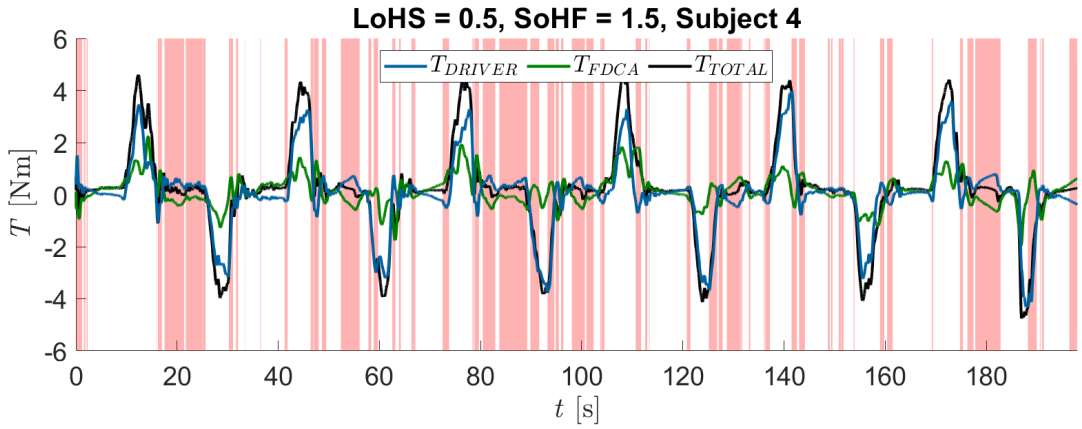
LoHS = 0.5, SoHF = 1.5, Subject 4
T_{DRIVER} T_{FDCA} T_{TOTAL}
T [Nm]
t [s]

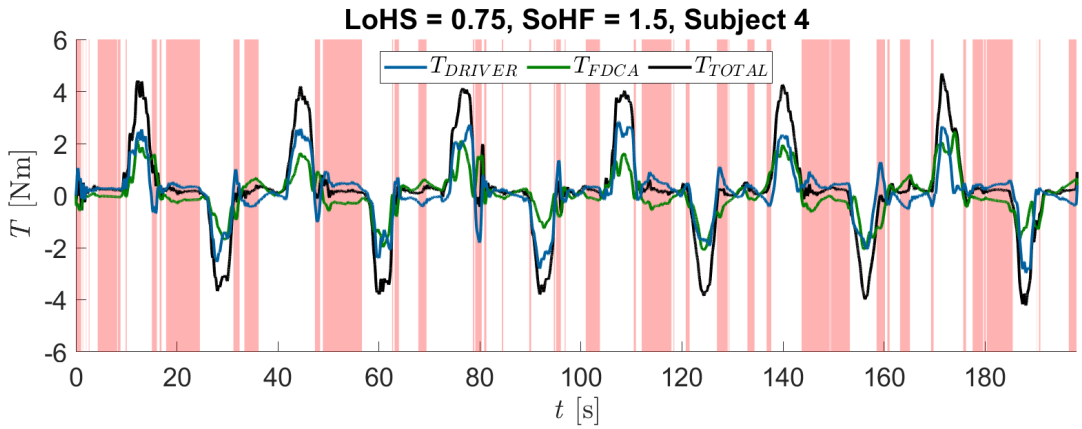
LoHS = 0.75, SoHF = 1.5, Subject 4
T_{DRIVER} T_{FDCA} T_{TOTAL}
T [Nm]
t [s]

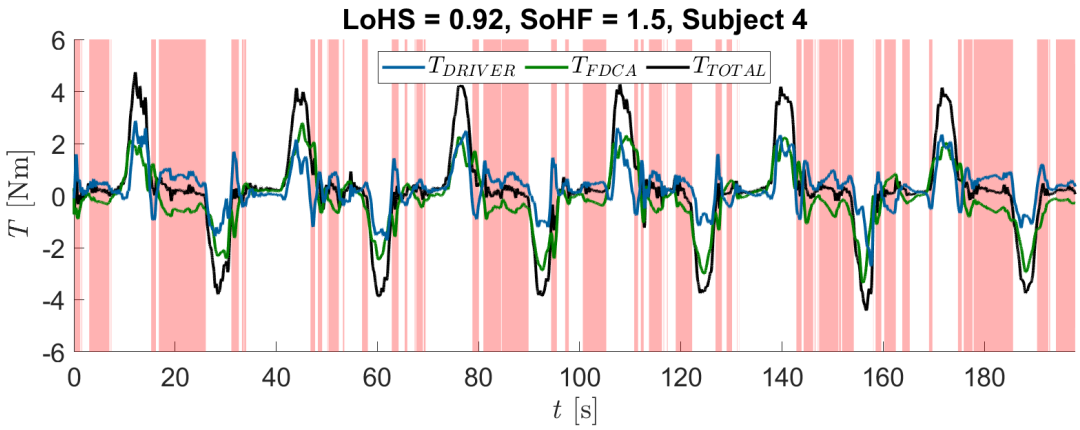
LoHS = 0.92, SoHF = 1.5, Subject 4
T_{DRIVER} T_{FDCA} T_{TOTAL}
T [Nm]
t [s]

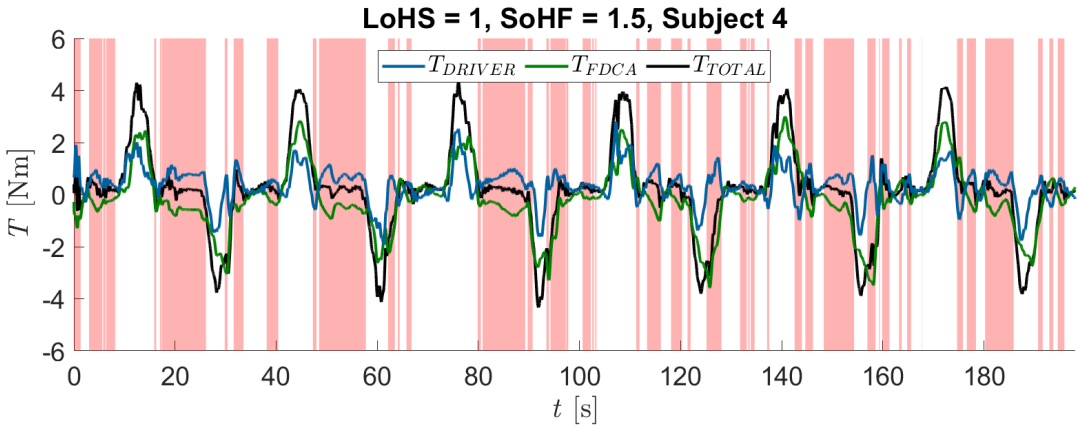
LoHS = 1, SoHF = 1.5, Subject 4
T_{DRIVER} T_{FDCA} T_{TOTAL}
T [Nm]
t [s]

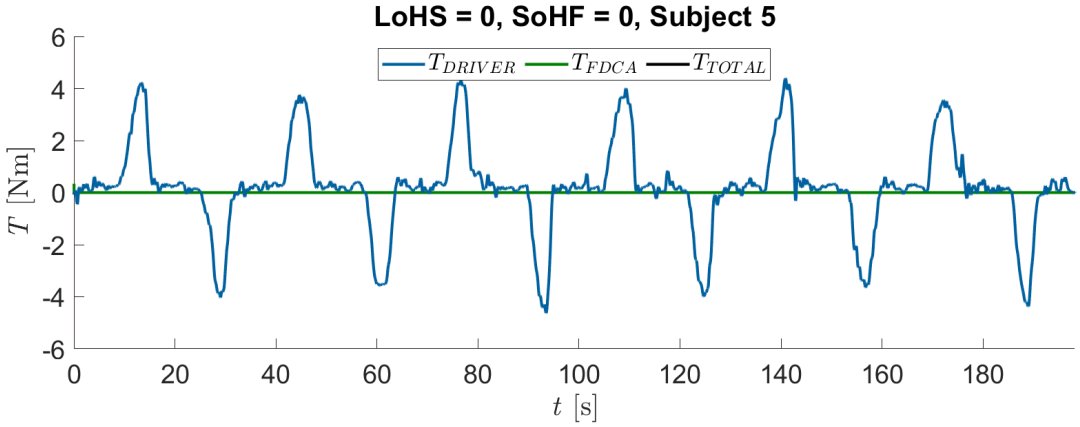
LoHS = 0, SoHF = 0, Subject 5
T_{DRIVER} T_{FDCA} T_{TOTAL}
T [Nm]
t [s]

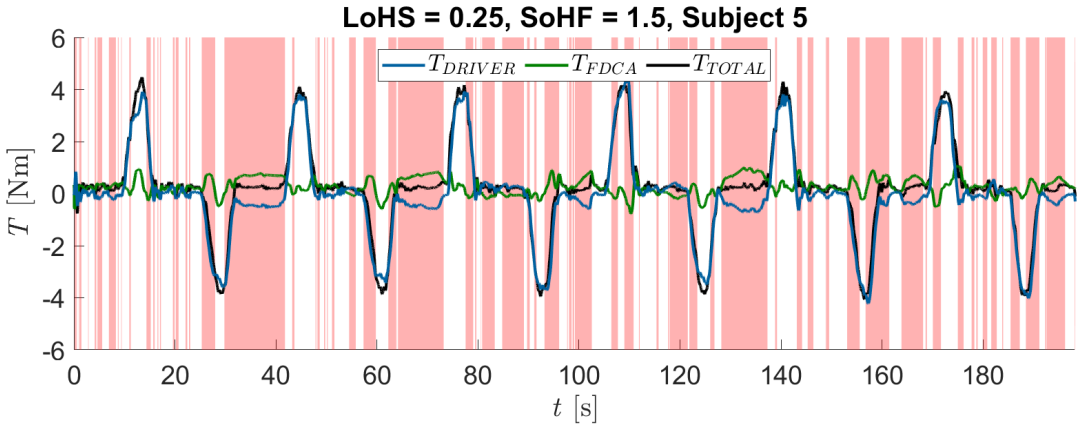
LoHS = 0.25, SoHF = 1.5, Subject 5
T_{DRIVER} T_{FDCA} T_{TOTAL}
T [Nm]
t [s]

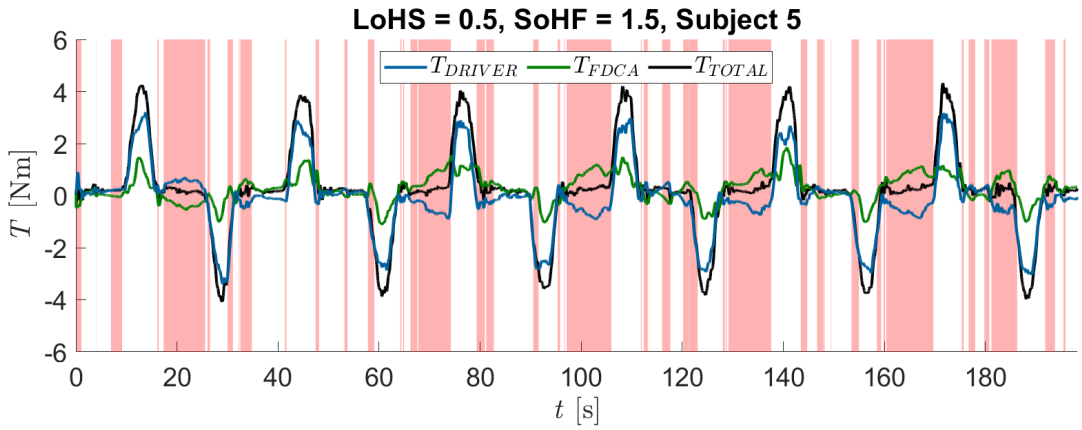
LoHS = 0.5, SoHF = 1.5, Subject 5
T_{DRIVER} T_{FDCA} T_{TOTAL}
T [Nm]
t [s]

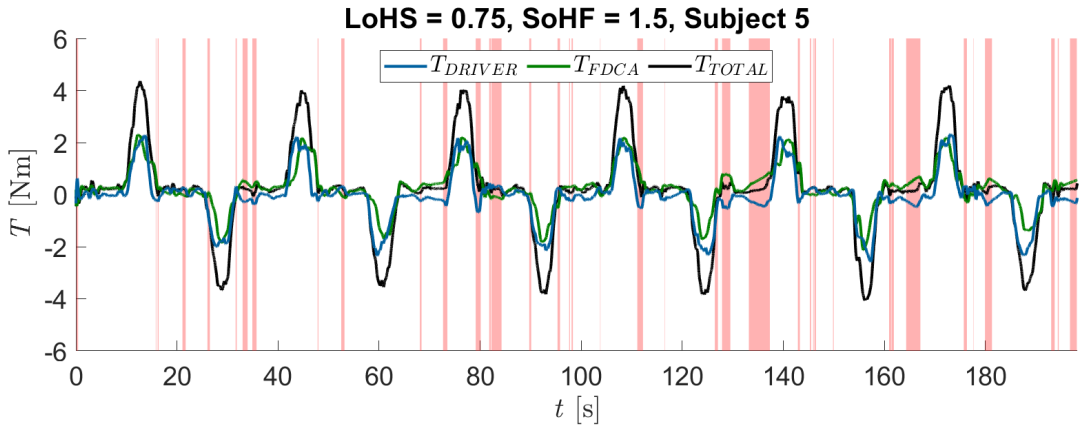
LoHS = 0.75, SoHF = 1.5, Subject 5
T_{DRIVER} T_{FDCA} T_{TOTAL}
T [Nm]
t [s]

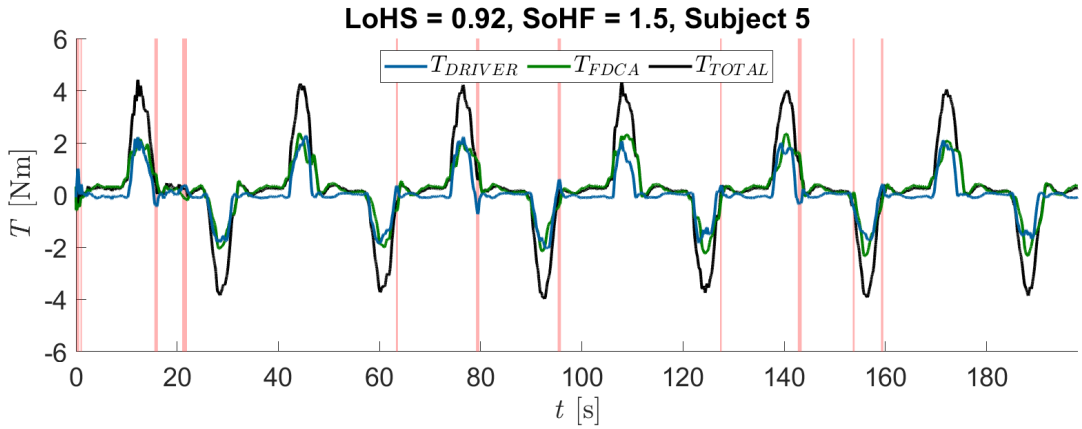
LoHS = 0.92, SoHF = 1.5, Subject 5
T_{DRIVER} T_{FDCA} T_{TOTAL}
T [Nm]
t [s]

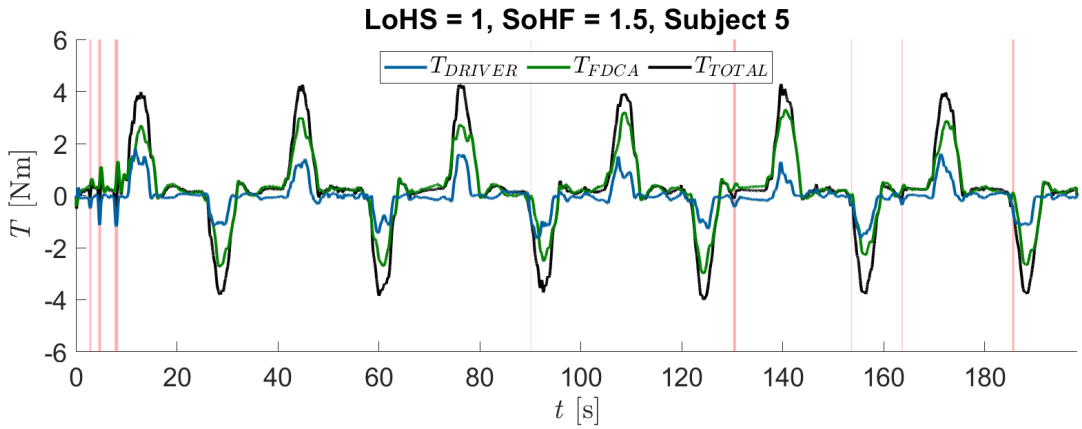
LoHS = 1, SoHF = 1.5, Subject 5
T_{DRIVER} T_{FDCA} T_{TOTAL}
T [Nm]
t [s]

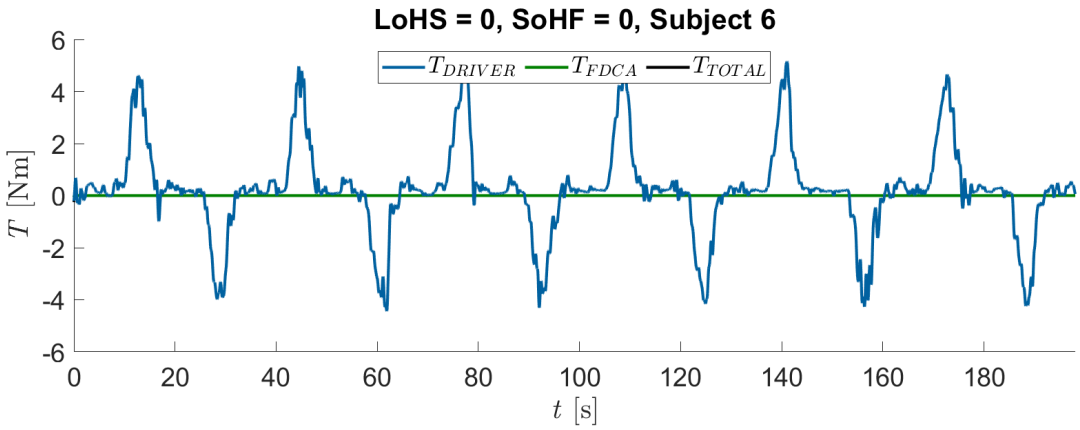
LoHS = 0, SoHF = 0, Subject 6
T_{DRIVER} T_{FDCA} T_{TOTAL}
T [Nm]
t [s]

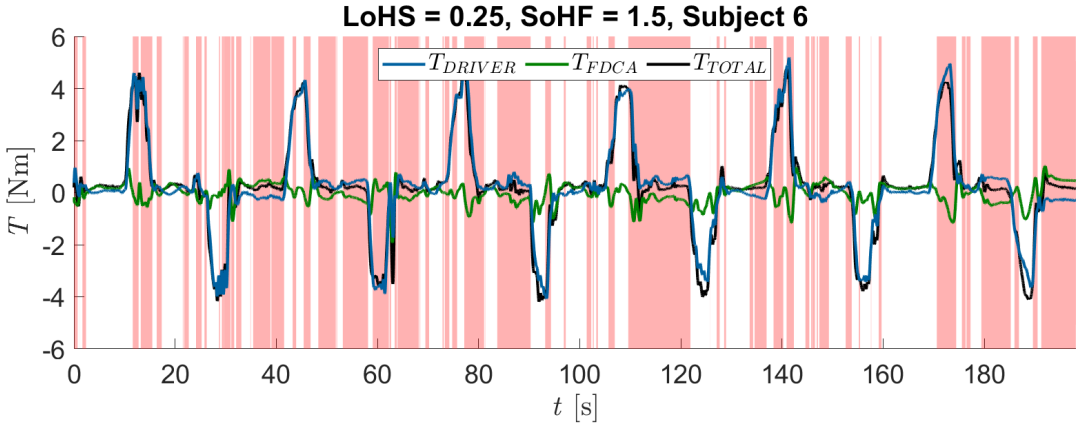
LoHS = 0.25, SoHF = 1.5, Subject 6
T_{DRIVER} T_{FDCA} T_{TOTAL}
T [Nm]
t [s]

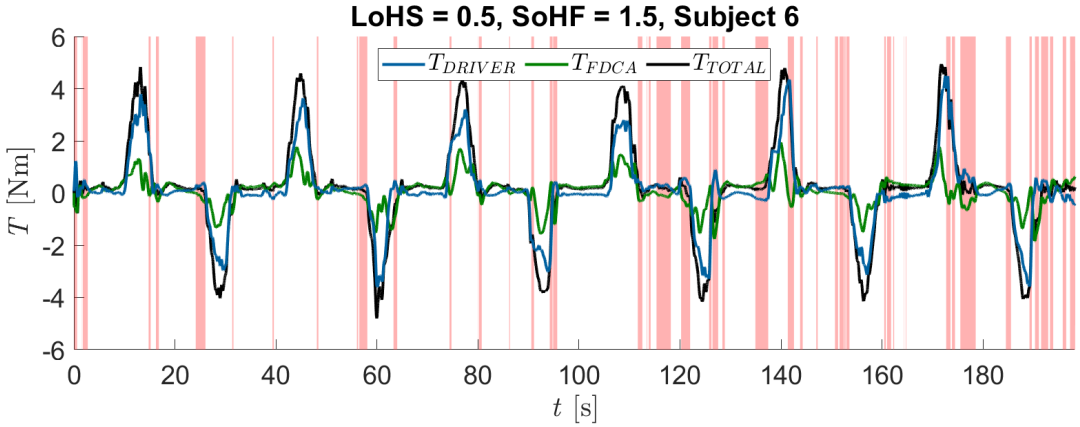
LoHS = 0.5, SoHF = 1.5, Subject 6
T_{DRIVER} T_{FDCA} T_{TOTAL}
T [Nm]
t [s]

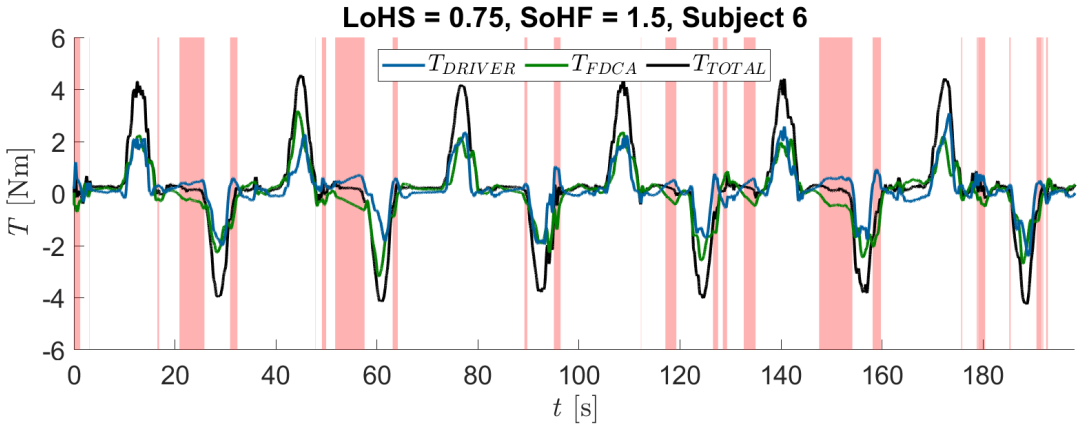
LoHS = 0.75, SoHF = 1.5, Subject 6
T_{DRIVER} T_{FDCA} T_{TOTAL}
T [Nm]
t [s]

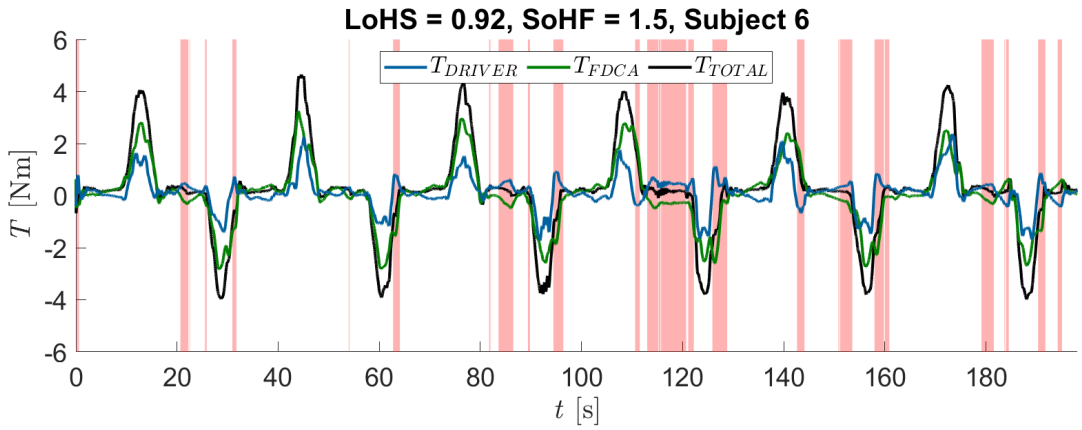
LoHS = 0.92, SoHF = 1.5, Subject 6
T_{DRIVER} T_{FDCA} T_{TOTAL}
T [Nm]
t [s]

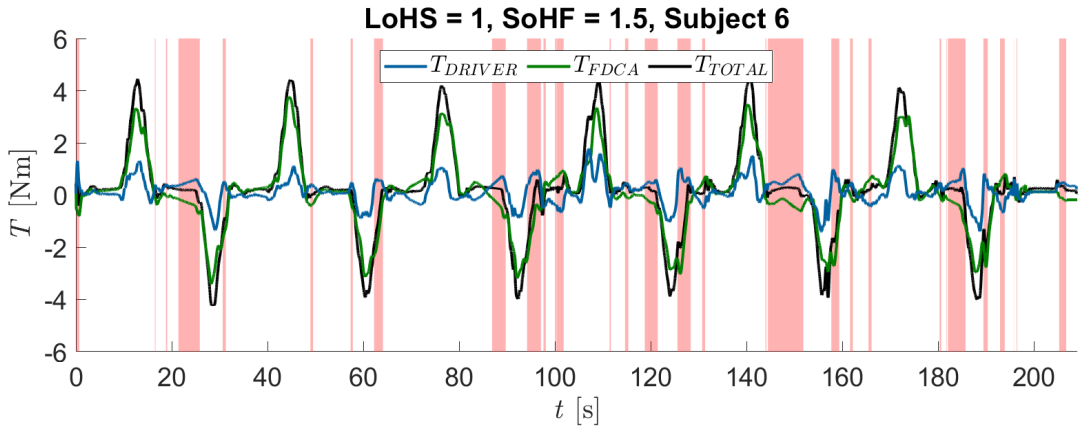
LoHS = 1, SoHF = 1.5, Subject 6
T_{DRIVER} T_{FDCA} T_{TOTAL}
T [Nm]
t [s]

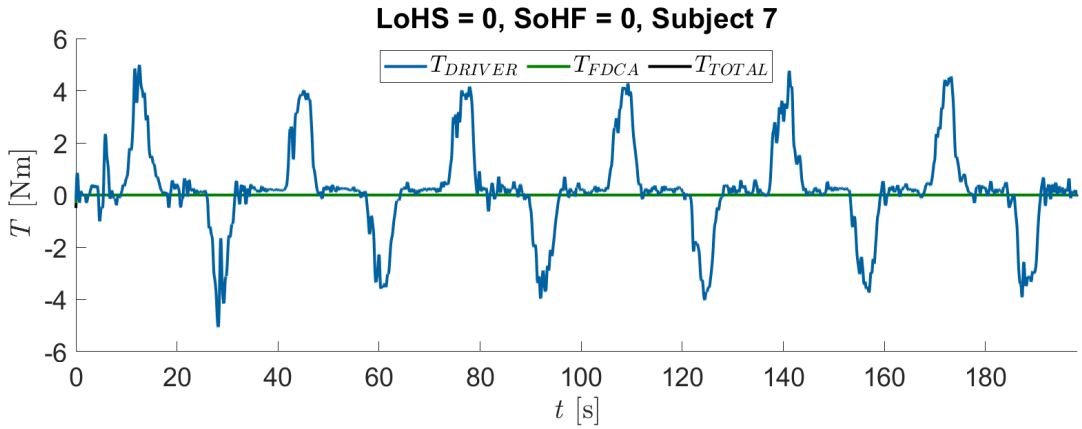
LoHS = 0, SoHF = 0, Subject 7
T_{DRIVER} T_{FDCA} T_{TOTAL}
T [Nm]
t [s]

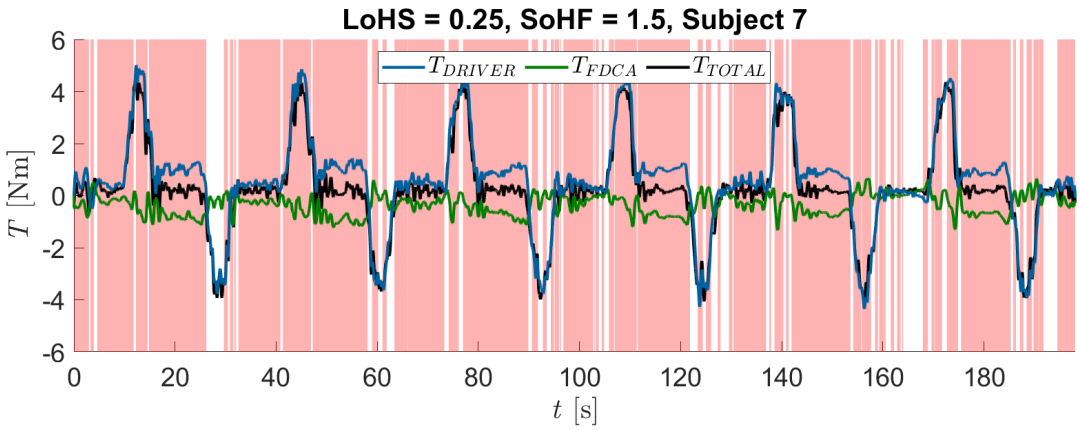
LoHS = 0.25, SoHF = 1.5, Subject 7
T_{DRIVER} T_{FDCA} T_{TOTAL}
T [Nm]
t [s]

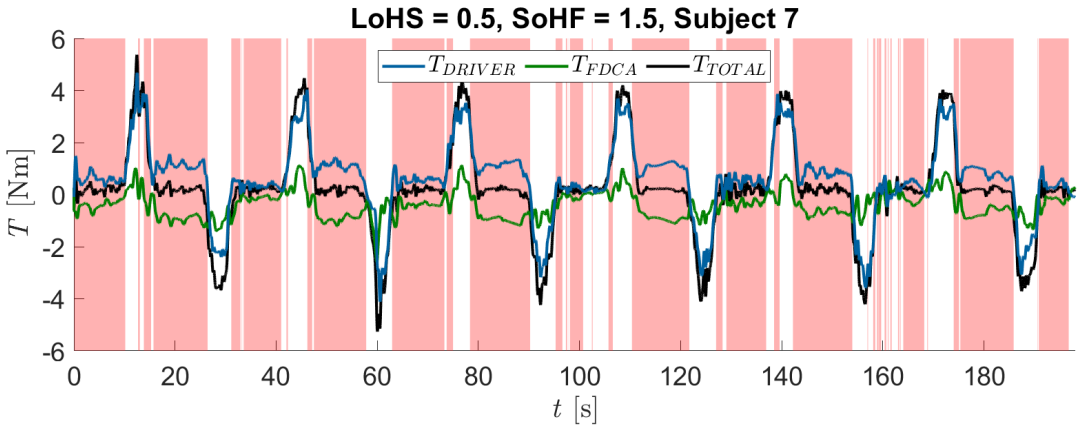
LoHS = 0.5, SoHF = 1.5, Subject 7
T_{DRIVER} T_{FDCA} T_{TOTAL}
T [Nm]
t [s]

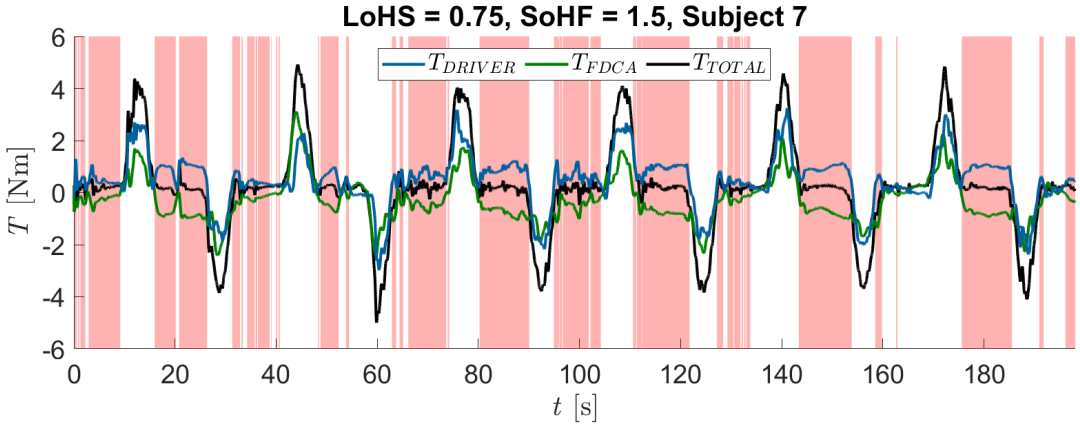
LoHS = 0.75, SoHF = 1.5, Subject 7
T_{DRIVER} T_{FDCA} T_{TOTAL}
T [Nm]
t [s]

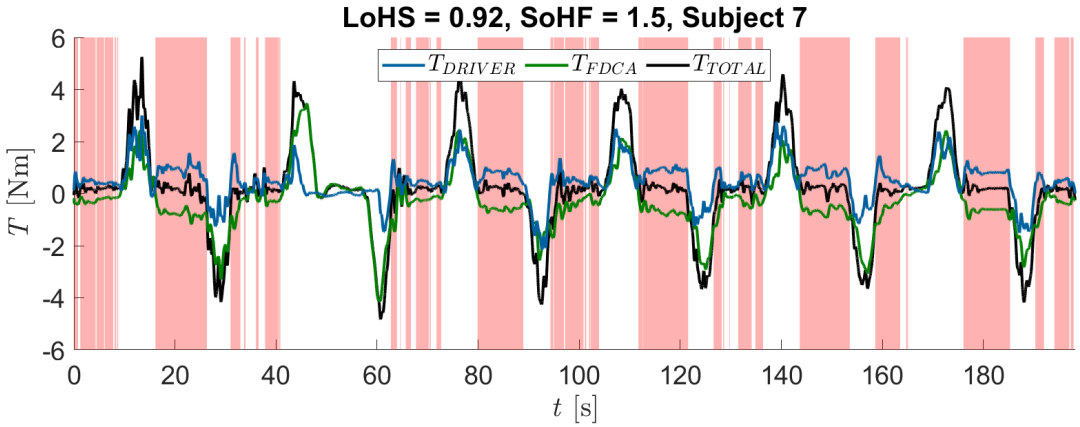
LoHS = 0.92, SoHF = 1.5, Subject 7
T_{DRIVER} T_{FDCA} T_{TOTAL}
T [Nm]
t [s]

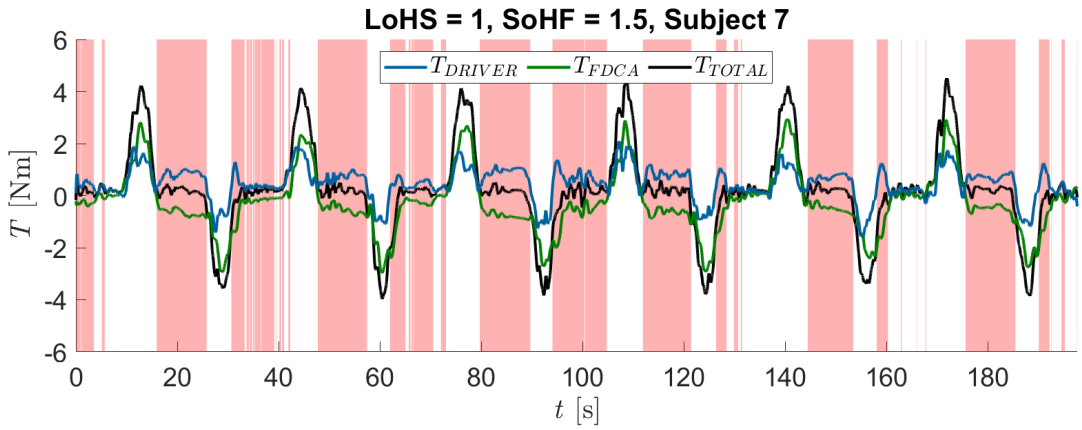
LoHS = 1, SoHF = 1.5, Subject 7
T_{DRIVER} T_{FDCA} T_{TOTAL}
T [Nm]
t [s]

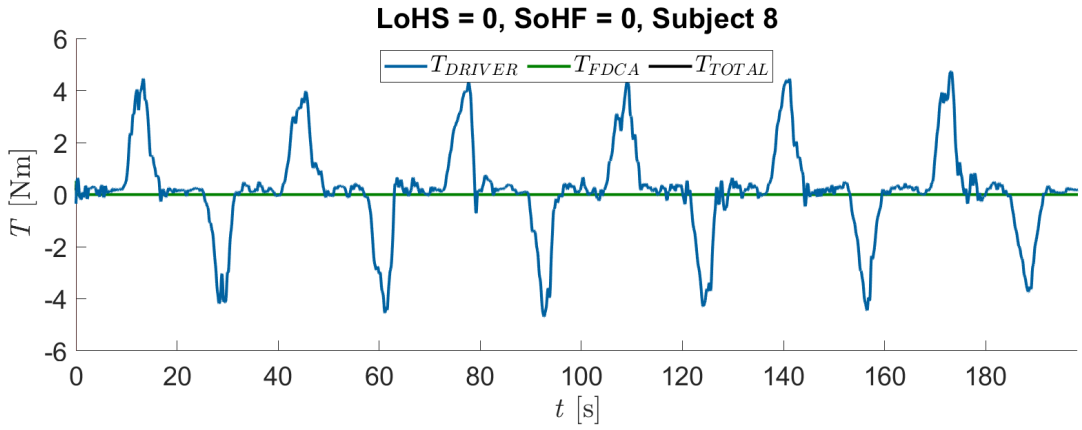
LoHS = 0, SoHF = 0, Subject 8
T_{DRIVER} T_{FDCA} T_{TOTAL}
T [Nm]
t [s]

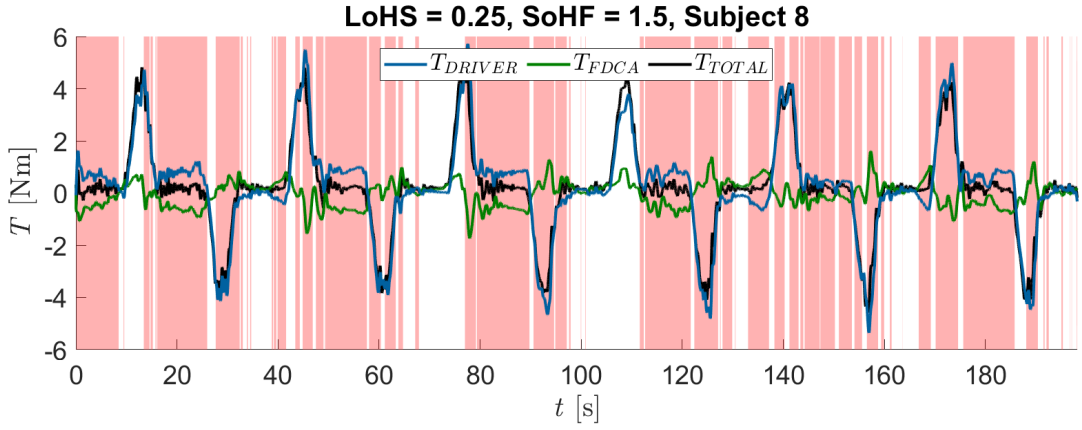
LoHS = 0.25, SoHF = 1.5, Subject 8
T_{DRIVER} T_{FDCA} T_{TOTAL}
T [Nm]
t [s]

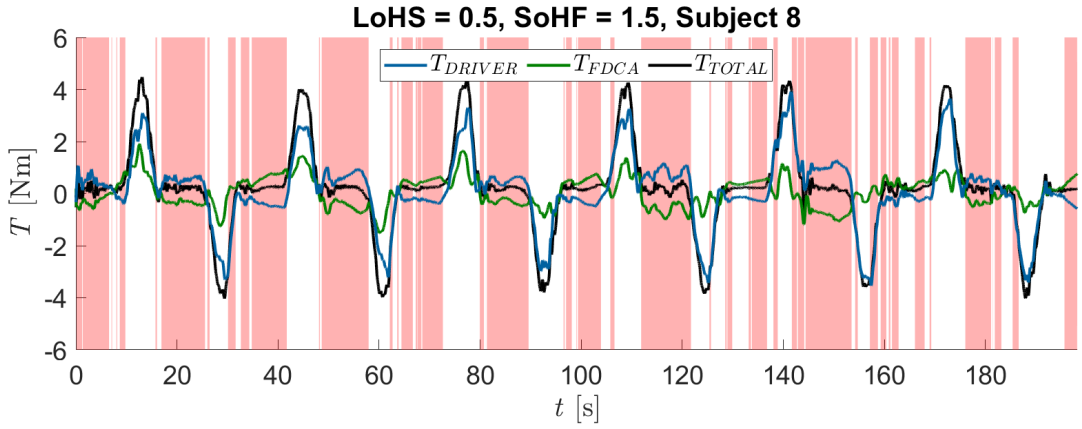
LoHS = 0.5, SoHF = 1.5, Subject 8
T_{DRIVER} T_{FDCA} T_{TOTAL}
T [Nm]
t [s]

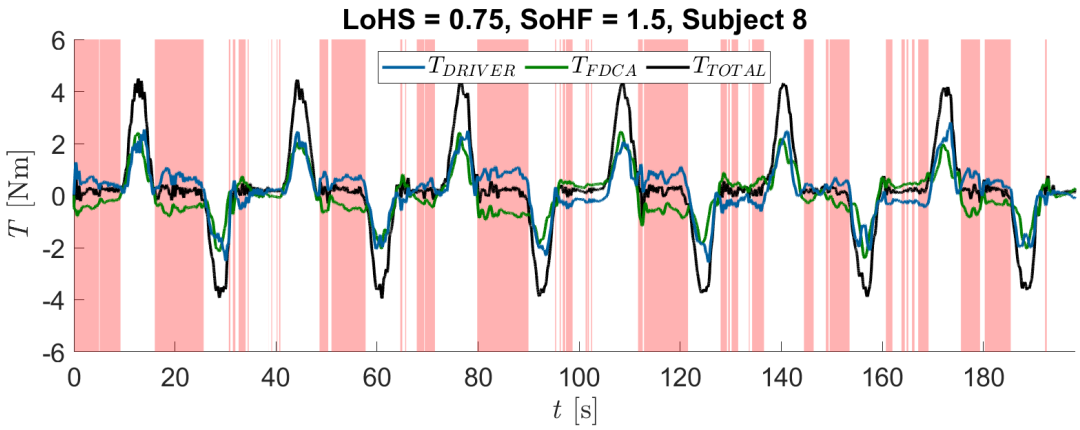
LoHS = 0.75, SoHF = 1.5, Subject 8
T_{DRIVER} T_{FDCA} T_{TOTAL}
T [Nm]
t [s]

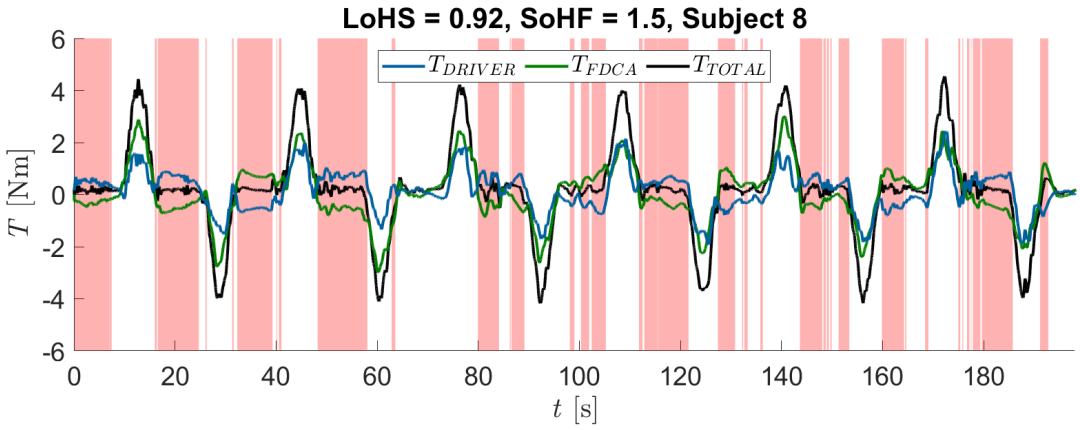
LoHS = 0.92, SoHF = 1.5, Subject 8
T_{DRIVER} T_{FDCA} T_{TOTAL}
T [Nm]
t [s]

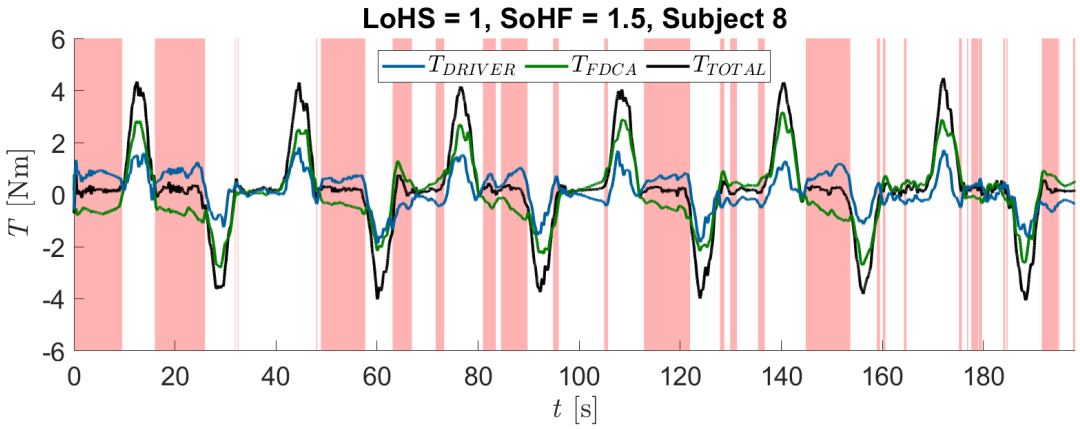
LoHS = 1, SoHF = 1.5, Subject 8
T_{DRIVER} T_{FDCA} T_{TOTAL}
T [Nm]
t [s]

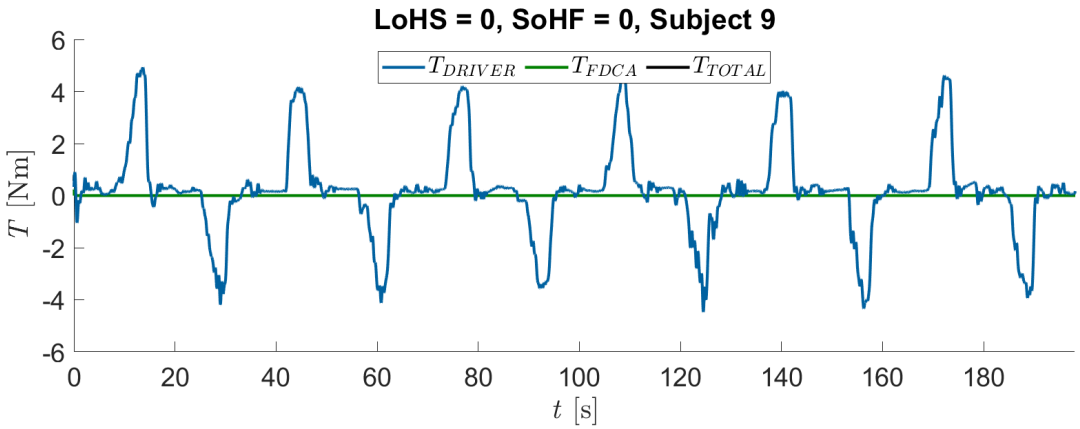
LoHS = 0, SoHF = 0, Subject 9
T_{DRIVER} T_{FDCA} T_{TOTAL}
T [Nm]
t [s]

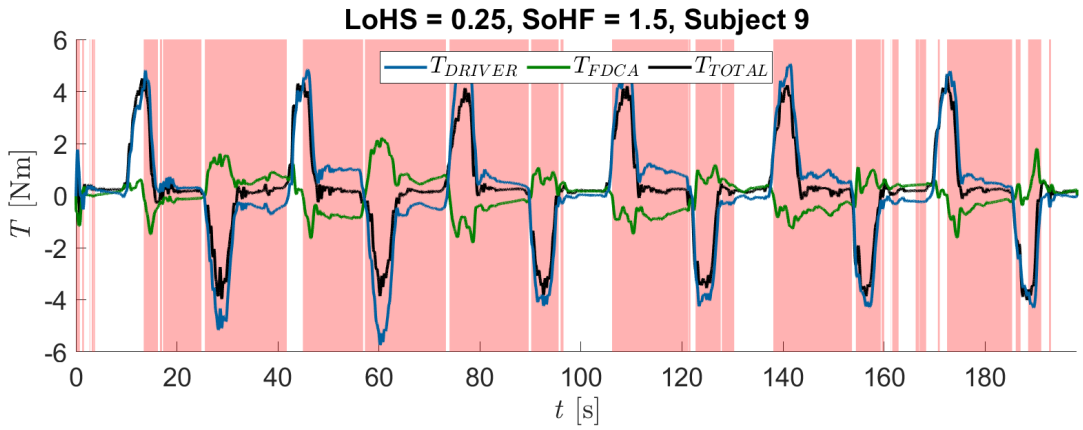
LoHS = 0.25, SoHF = 1.5, Subject 9
T_{DRIVER} T_{FDCA} T_{TOTAL}
T [Nm]
t [s]

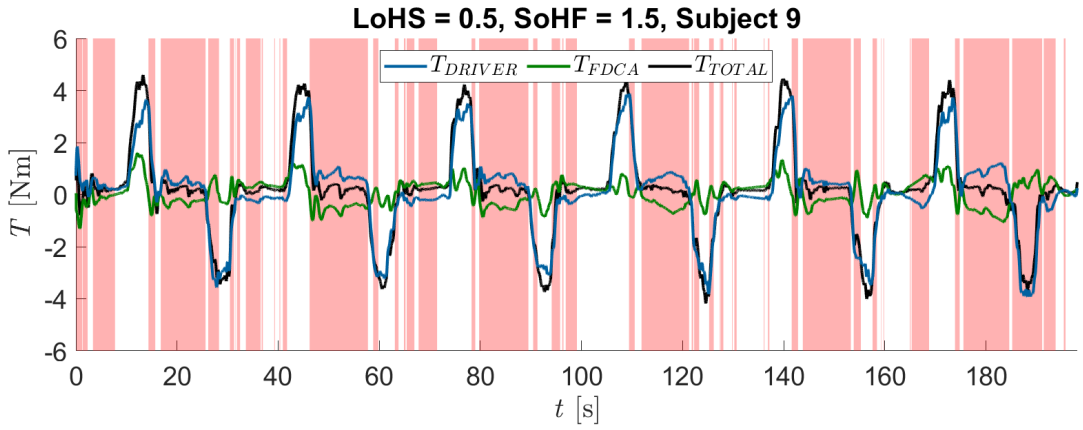
LoHS = 0.5, SoHF = 1.5, Subject 9
T_{DRIVER} T_{FDCA} T_{TOTAL}
T [Nm]
t [s]

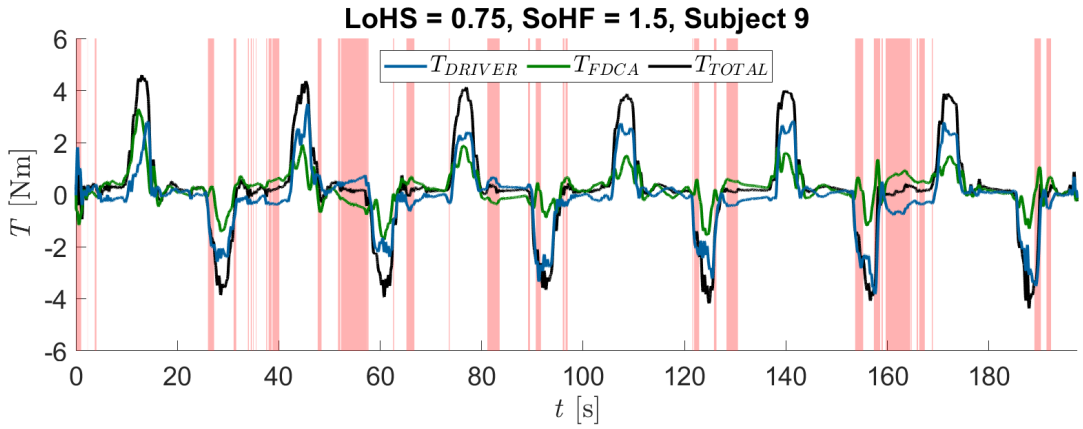
LoHS = 0.75, SoHF = 1.5, Subject 9
T_{DRIVER} T_{FDCA} T_{TOTAL}
T [Nm]
t [s]

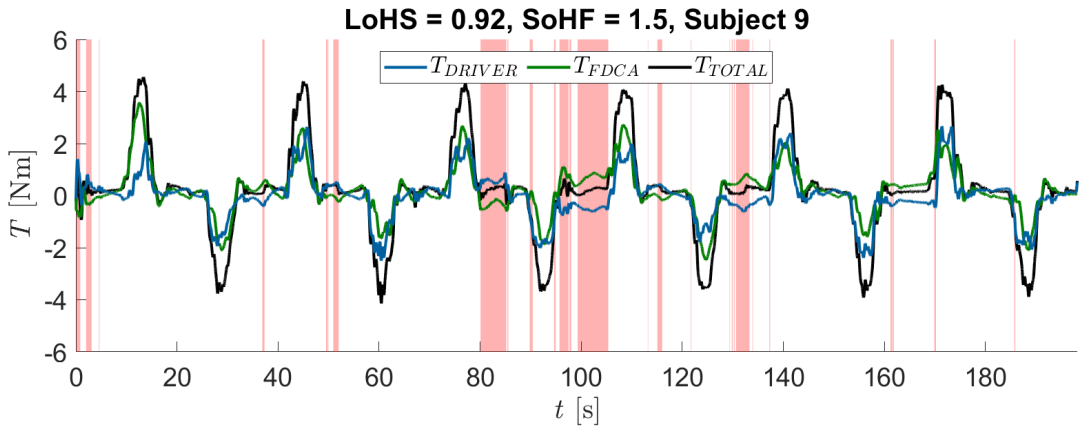
LoHS = 0.92, SoHF = 1.5, Subject 9
T_{DRIVER} T_{FDCA} T_{TOTAL}
T [Nm]
t [s]

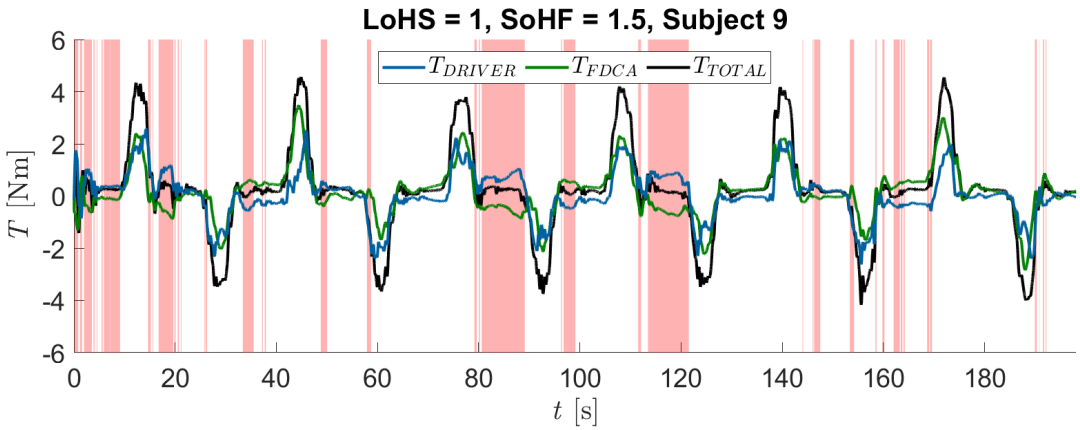
LoHS = 1, SoHF = 1.5, Subject 9
T_{DRIVER} T_{FDCA} T_{TOTAL}
T [Nm]
t [s]

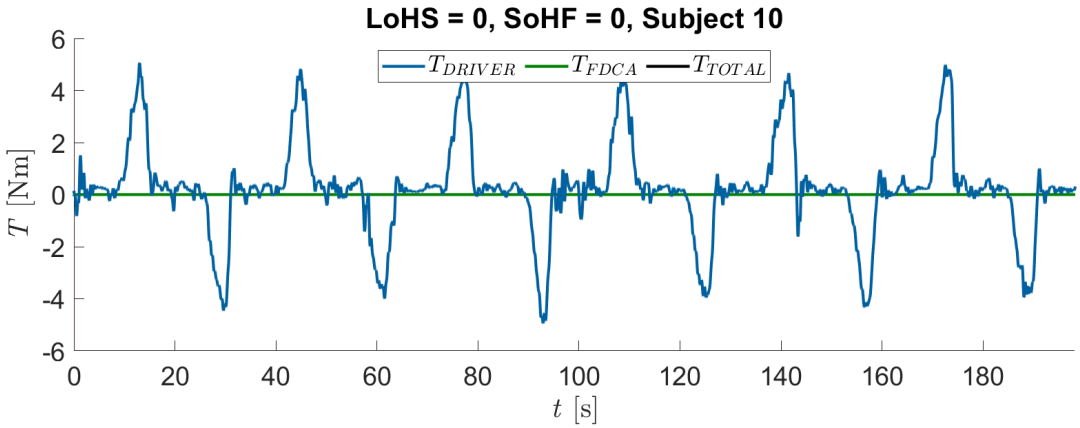
LoHS = 0, SoHF = 0, Subject 10
T_{DRIVER} T_{FDCA} T_{TOTAL}
T [Nm]
t [s]

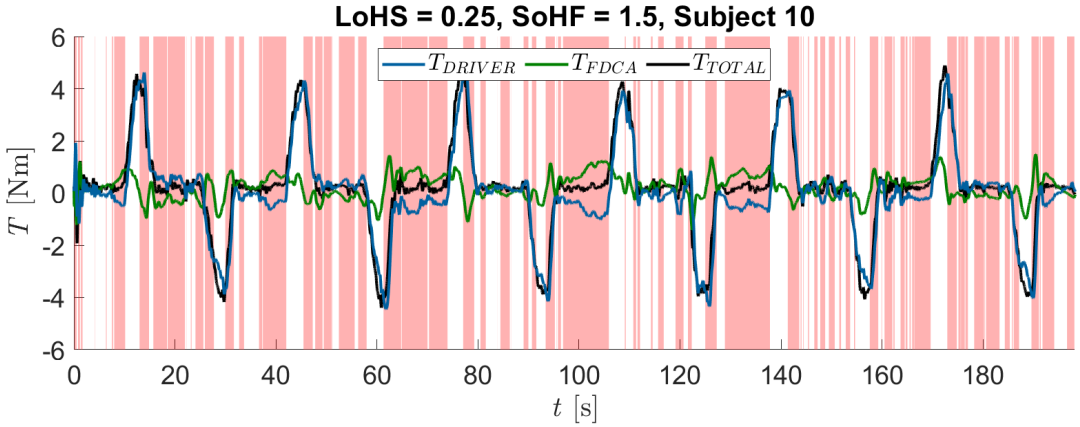
LoHS = 0.25, SoHF = 1.5, Subject 10
T_{DRIVER} T_{FDCA} T_{TOTAL}
T [Nm]
t [s]

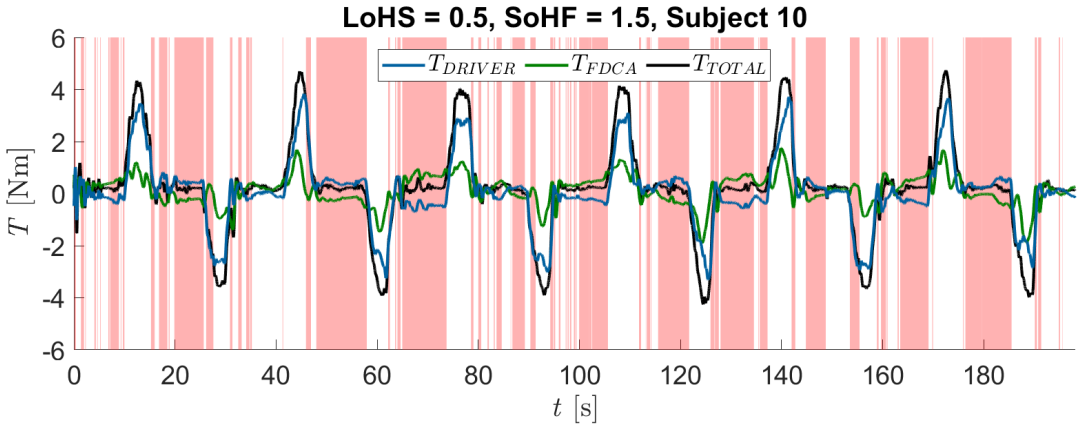
LoHS = 0.5, SoHF = 1.5, Subject 10
T_{DRIVER} T_{FDCA} T_{TOTAL}
T [Nm]
t [s]

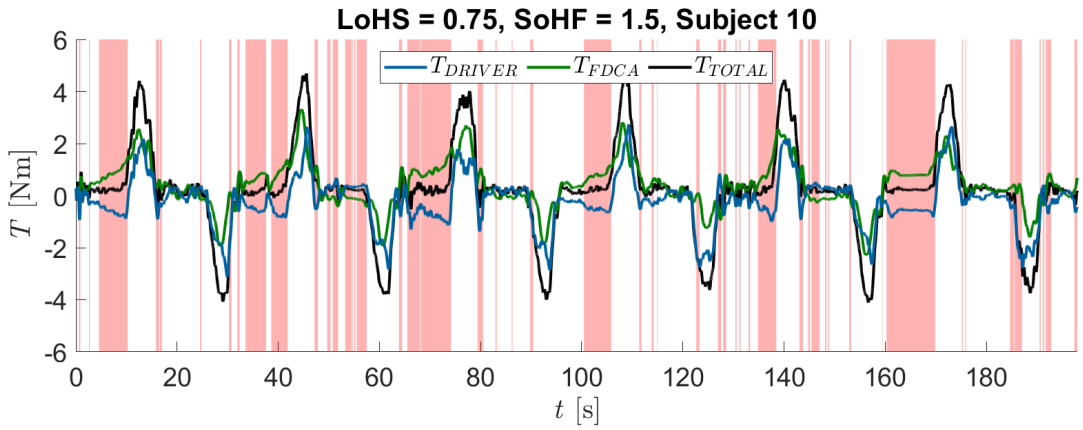
LoHS = 0.75, SoHF = 1.5, Subject 10
T_{DRIVER} T_{FDCA} T_{TOTAL}
T [Nm]
t [s]

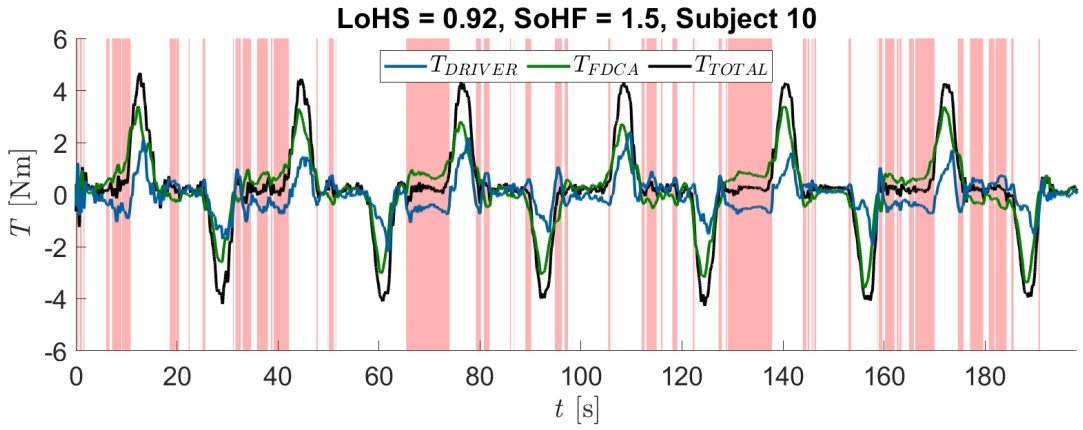
LoHS = 0.92, SoHF = 1.5, Subject 10
T_{DRIVER} T_{FDCA} T_{TOTAL}
T [Nm]
t [s]

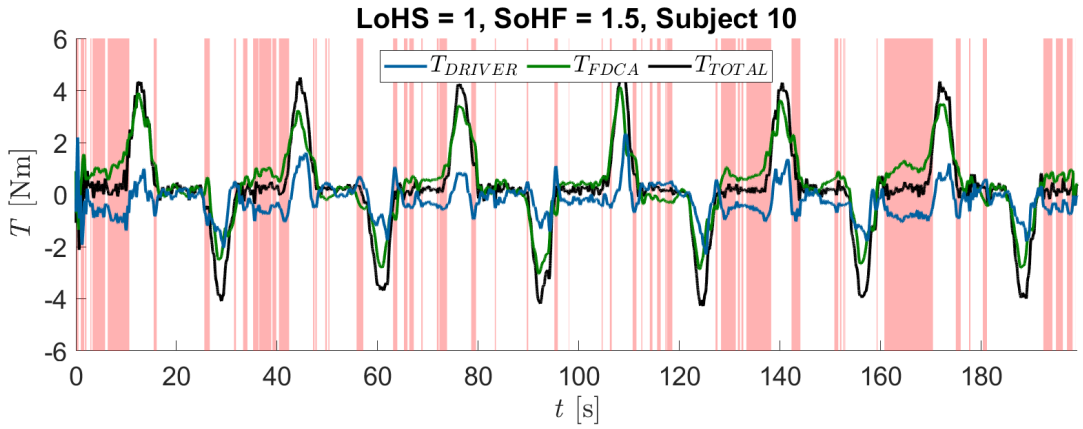
LoHS = 1, SoHF = 1.5, Subject 10
T_{DRIVER} T_{FDCA} T_{TOTAL}
T [Nm]
t [s]

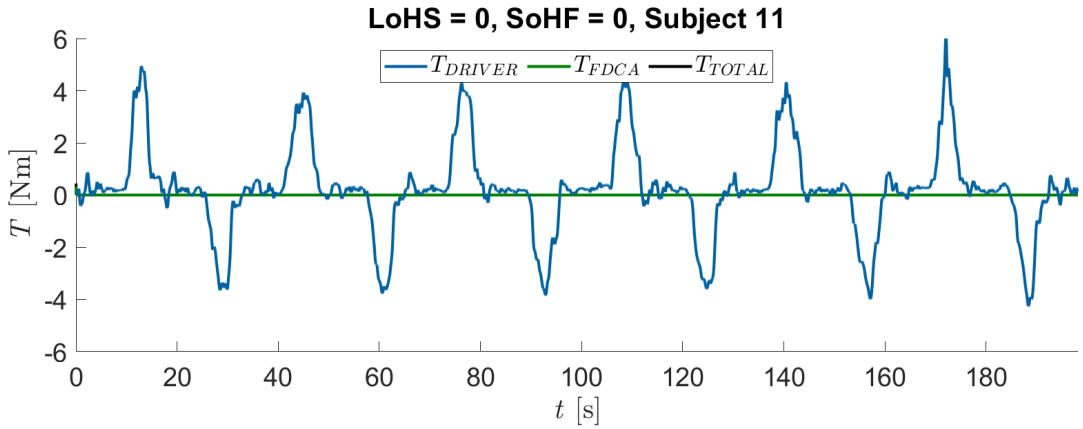
LoHS = 0, SoHF = 0, Subject 11
T_{DRIVER} T_{FDCA} T_{TOTAL}
T [Nm]
t [s]

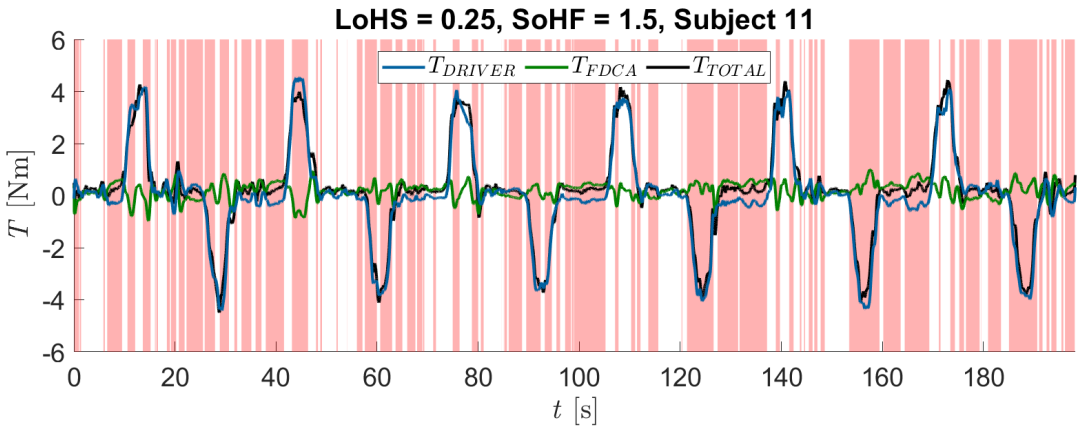
LoHS = 0.25, SoHF = 1.5, Subject 11
T_{DRIVER} T_{FDCA} T_{TOTAL}
T [Nm]
t [s]

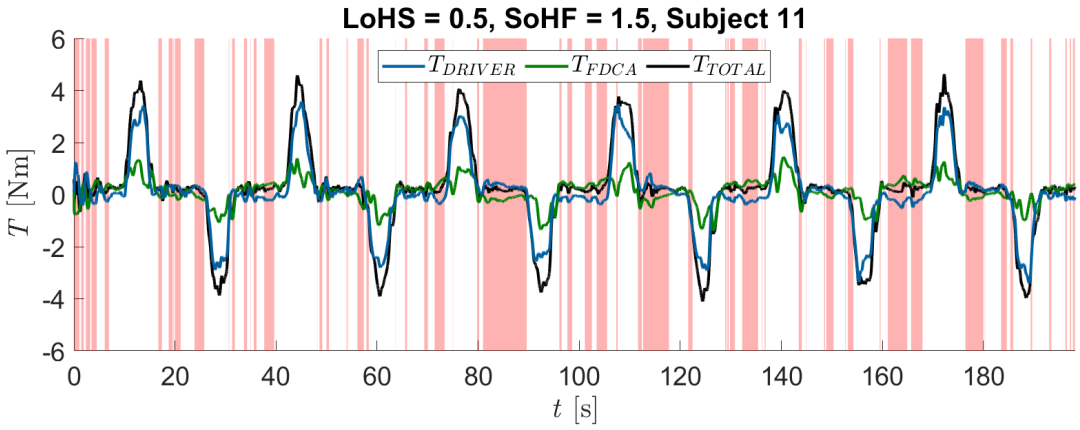
LoHS = 0.5, SoHF = 1.5, Subject 11
T_{DRIVER} T_{FDCA} T_{TOTAL}
T [Nm]
t [s]

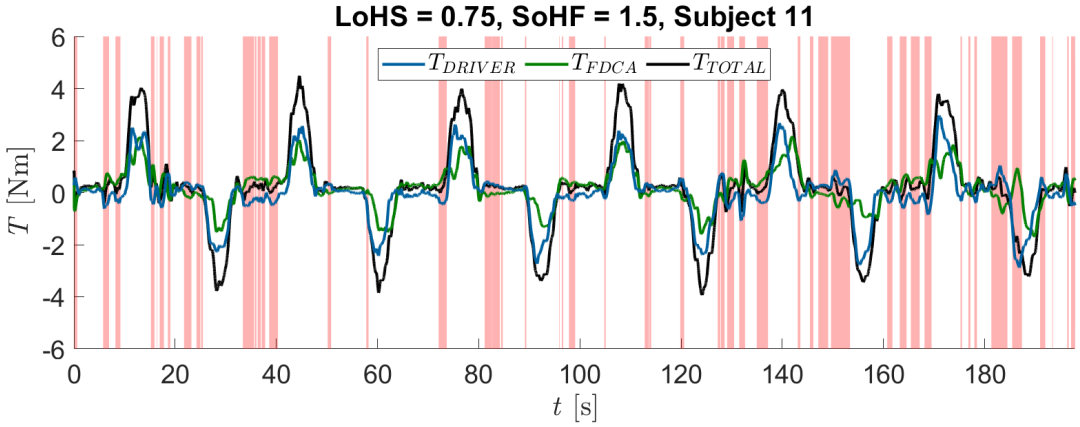
LoHS = 0.75, SoHF = 1.5, Subject 11
T_{DRIVER} T_{FDCA} T_{TOTAL}
T [Nm]
t [s]

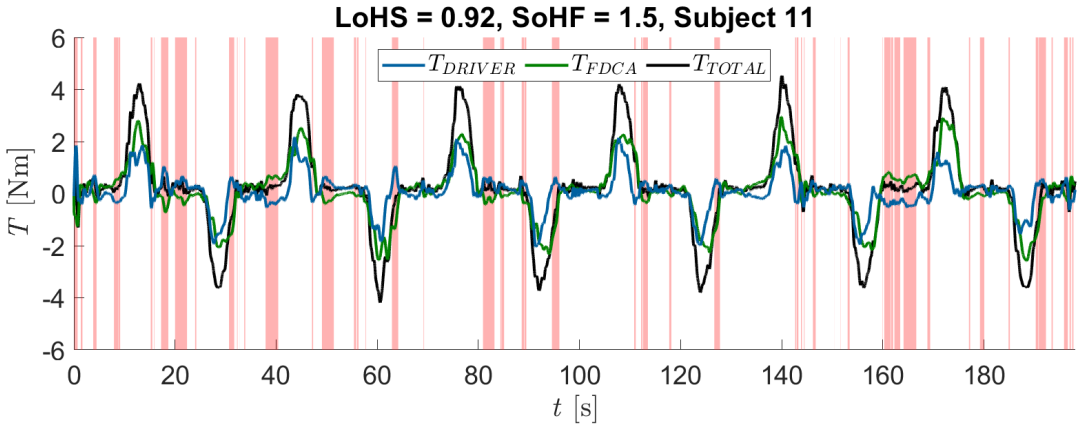
LoHS = 0.92, SoHF = 1.5, Subject 11
T_{DRIVER} T_{FDCA} T_{TOTAL}
T [Nm]
t [s]

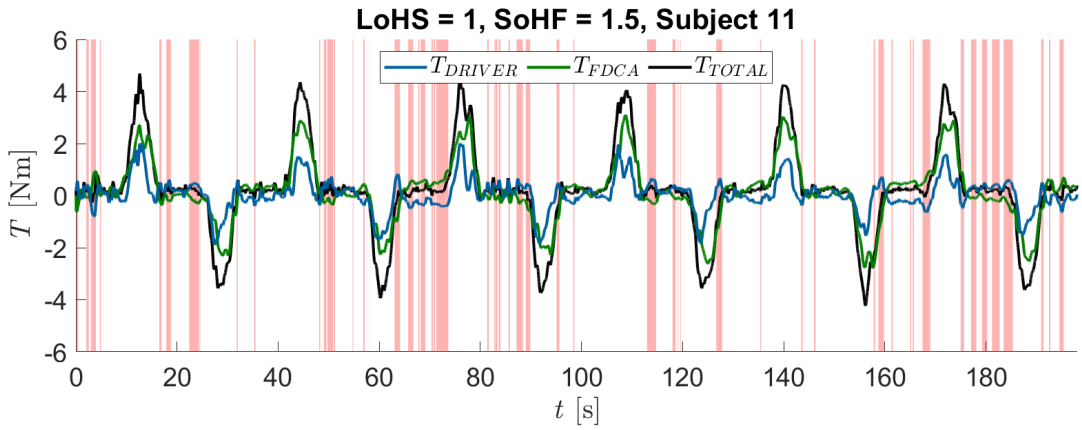
LoHS = 1, SoHF = 1.5, Subject 11
T_{DRIVER} T_{FDCA} T_{TOTAL}
T [Nm]
t [s]

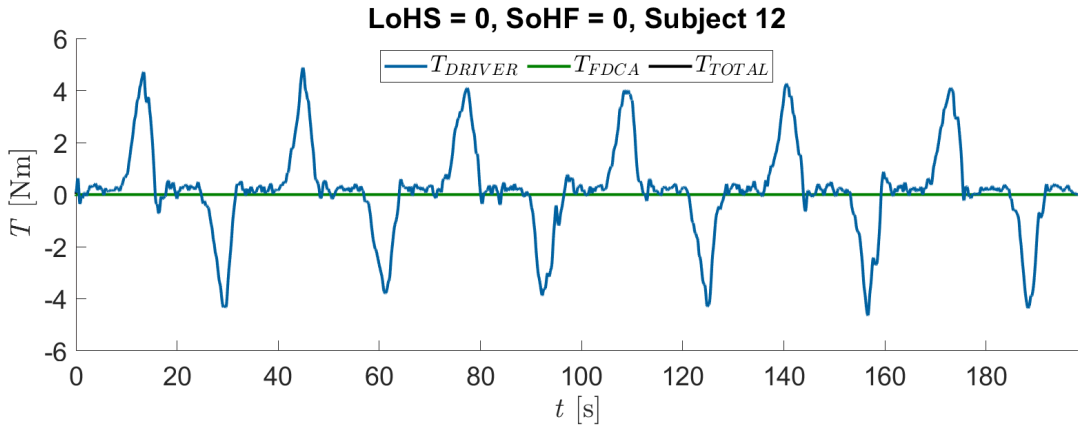
LoHS = 0, SoHF = 0, Subject 12
T_{DRIVER} T_{FDCA} T_{TOTAL}
T [Nm]
t [s]

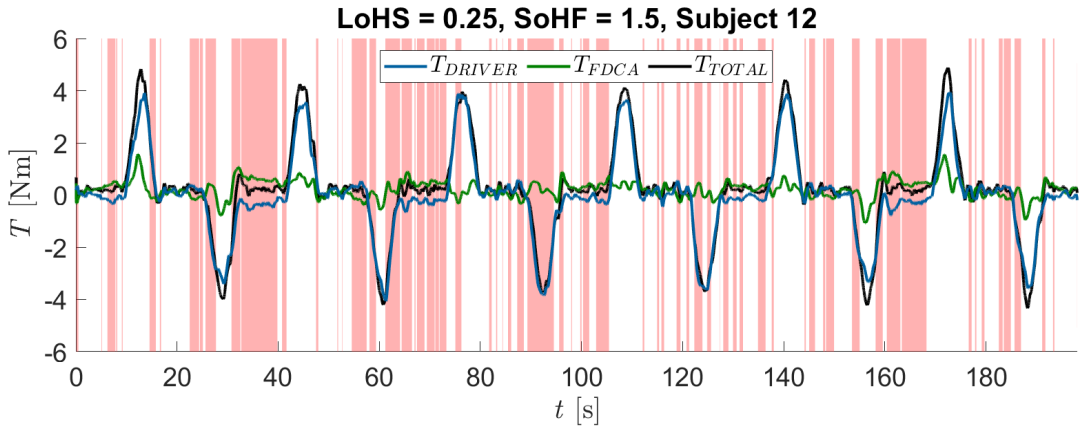
LoHS = 0.25, SoHF = 1.5, Subject 12
T_{DRIVER} T_{FDCA} T_{TOTAL}
T [Nm]
t [s]

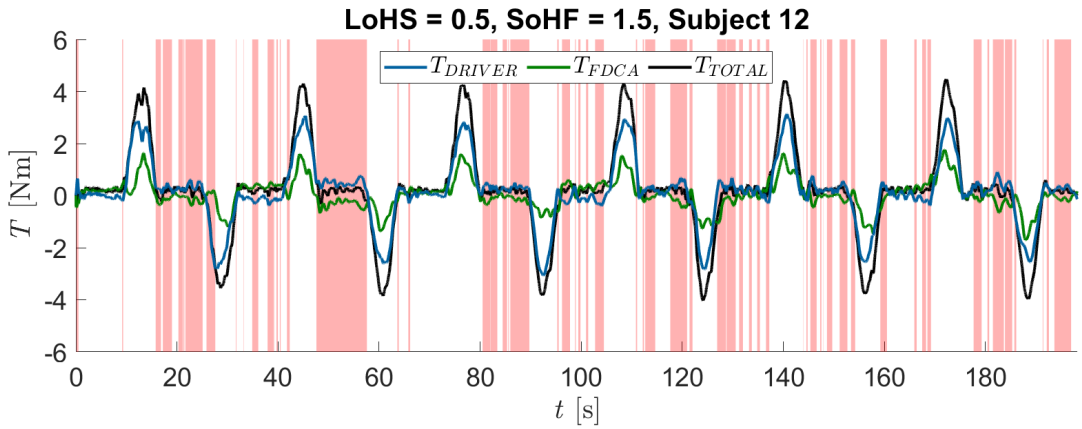
LoHS = 0.5, SoHF = 1.5, Subject 12
T_{DRIVER} T_{FDCA} T_{TOTAL}
T [Nm]
t [s]

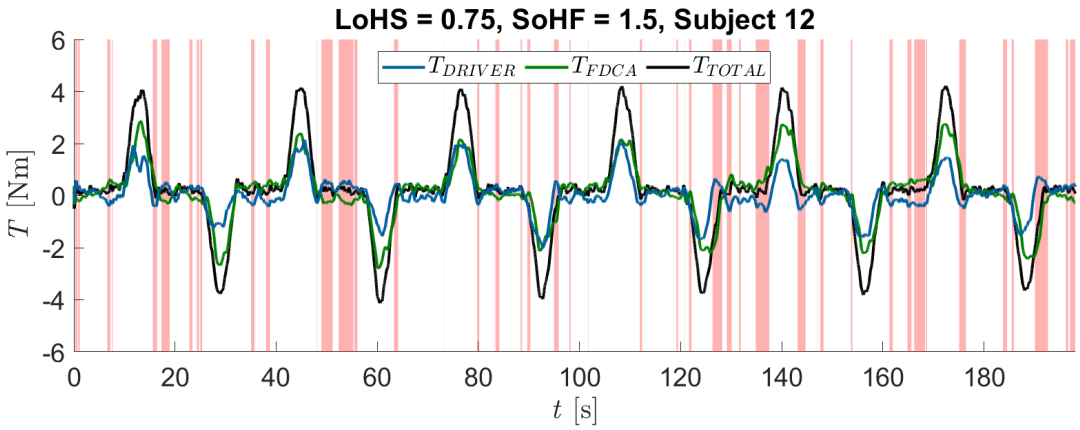
LoHS = 0.75, SoHF = 1.5, Subject 12
T_{DRIVER} T_{FDCA} T_{TOTAL}
T [Nm]
t [s]

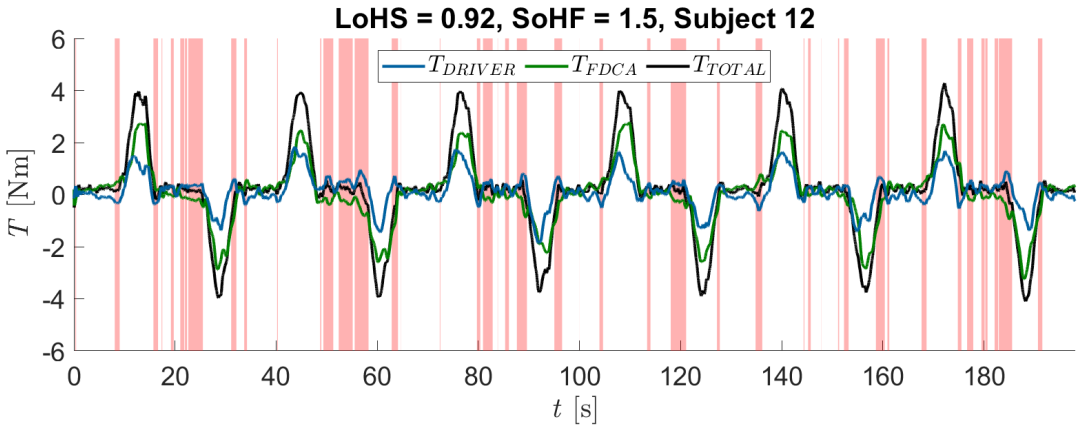
LoHS = 0.92, SoHF = 1.5, Subject 12
T_{DRIVER} T_{FDCA} T_{TOTAL}
T [Nm]
t [s]

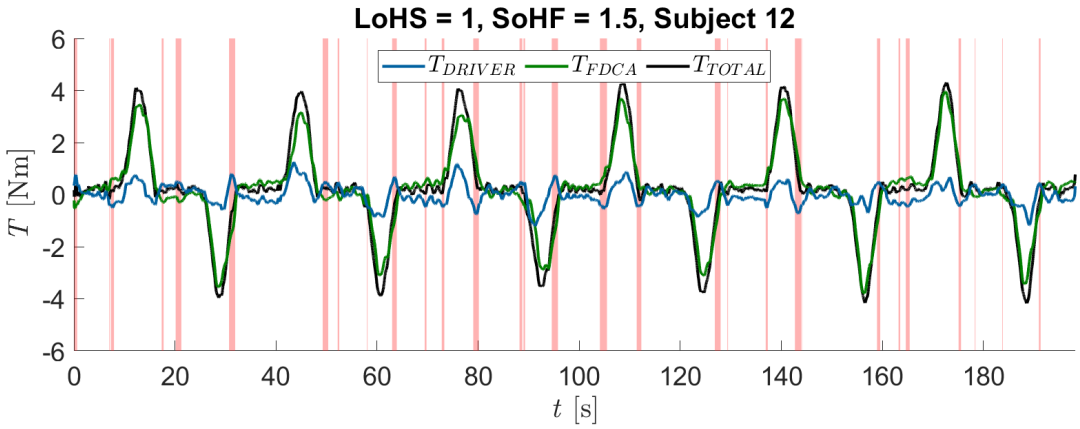
LoHS = 1, SoHF = 1.5, Subject 12
T_{DRIVER} T_{FDCA} T_{TOTAL}
T [Nm]
t [s]

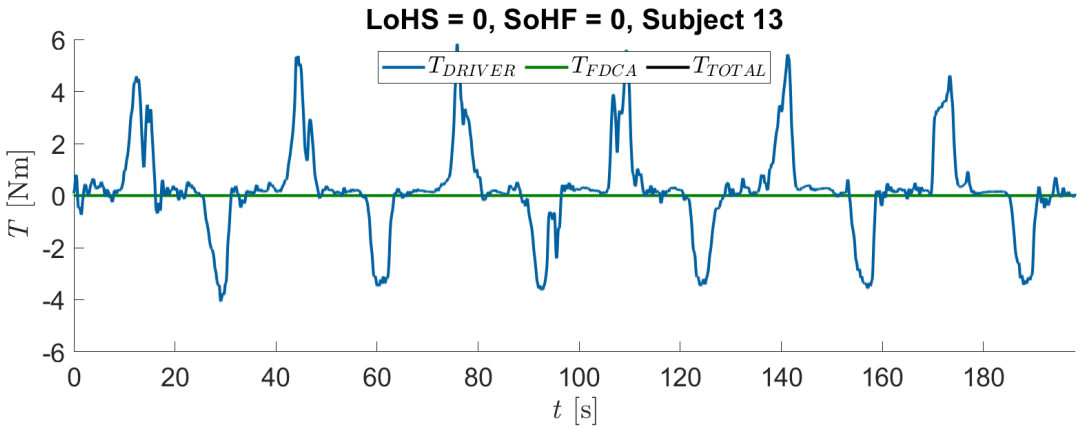
LoHS = 0, SoHF = 0, Subject 13
T_{DRIVER} T_{FDCA} T_{TOTAL}
T [Nm]
t [s]

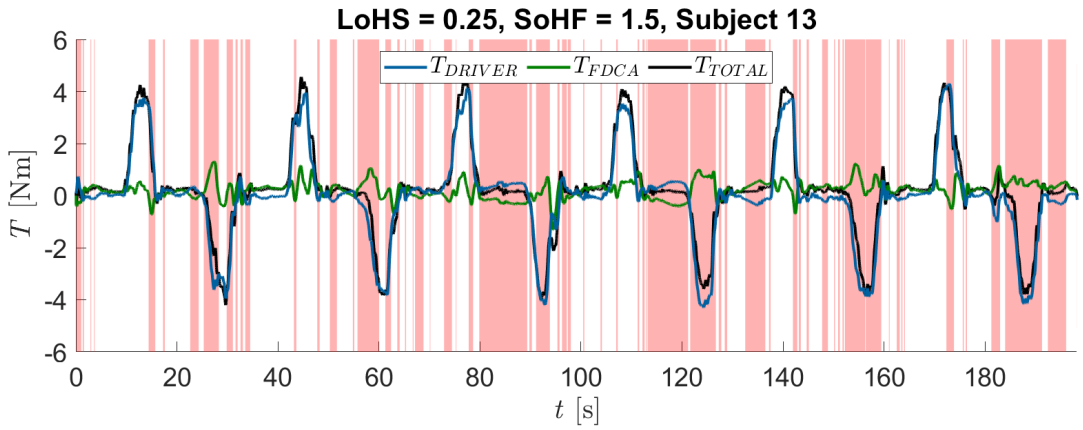
LoHS = 0.25, SoHF = 1.5, Subject 13
T_{DRIVER} T_{FDCA} T_{TOTAL}
T [Nm]
t [s]

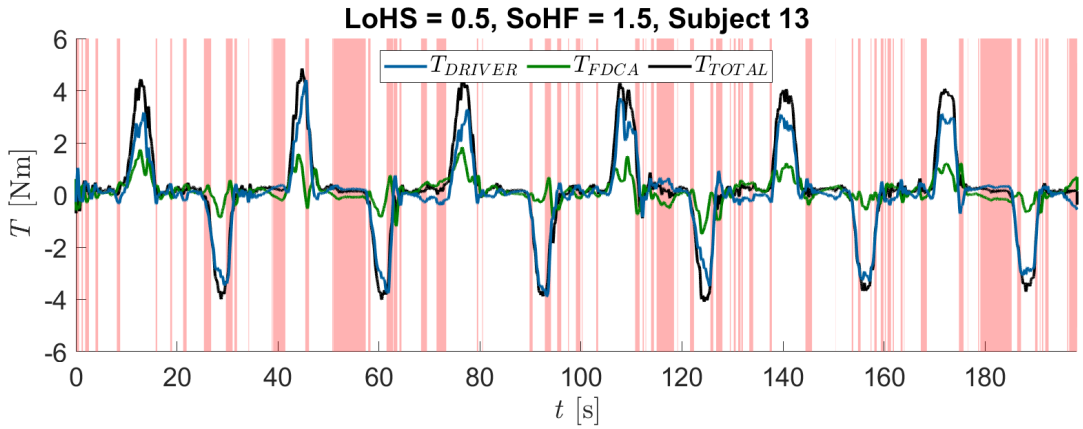
LoHS = 0.5, SoHF = 1.5, Subject 13
T_{DRIVER} T_{FDCA} T_{TOTAL}
T [Nm]
t [s]

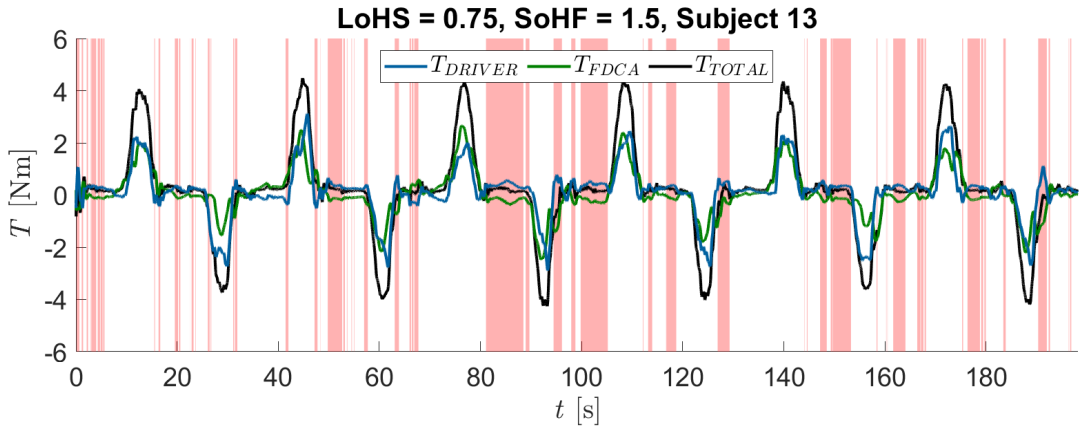
LoHS = 0.75, SoHF = 1.5, Subject 13
T_{DRIVER} T_{FDCA} T_{TOTAL}
T [Nm]
t [s]

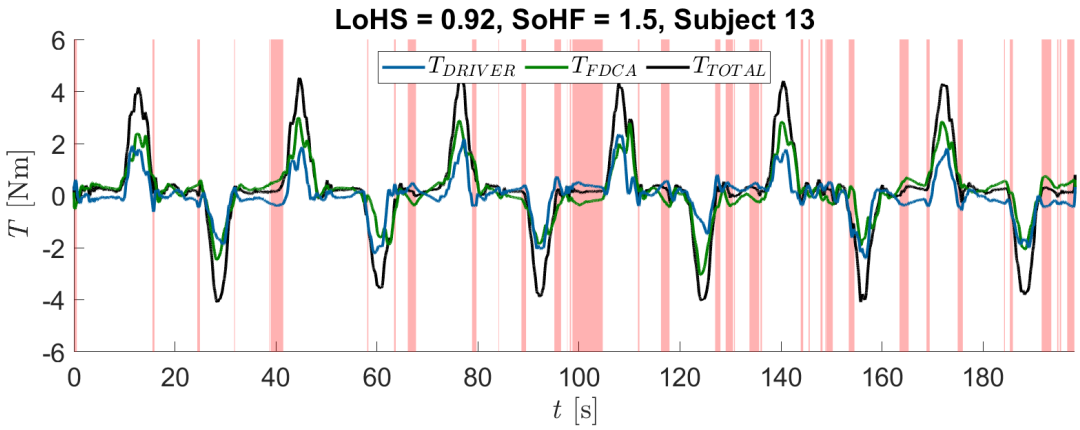
LoHS = 0.92, SoHF = 1.5, Subject 13
T_{DRIVER} T_{FDCA} T_{TOTAL}
T [Nm]
t [s]

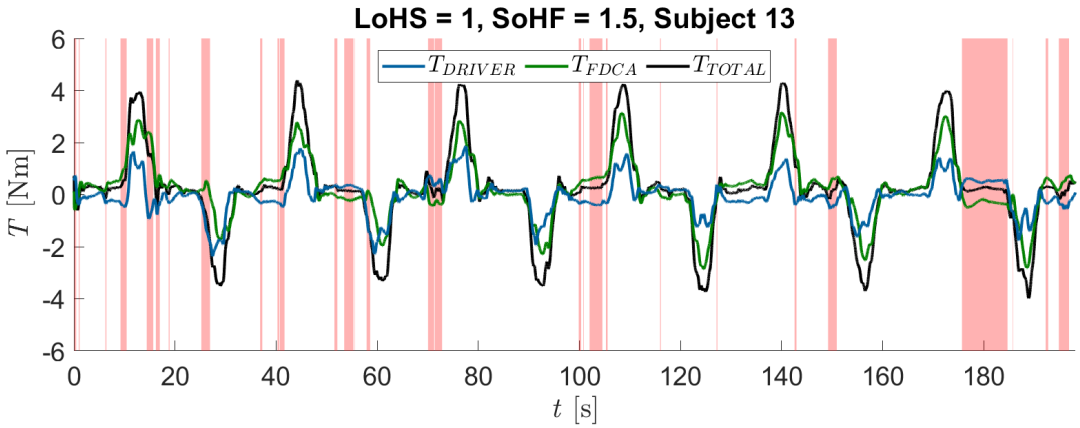
LoHS = 1, SoHF = 1.5, Subject 13
T_{DRIVER} T_{FDCA} T_{TOTAL}
T [Nm]
t [s]

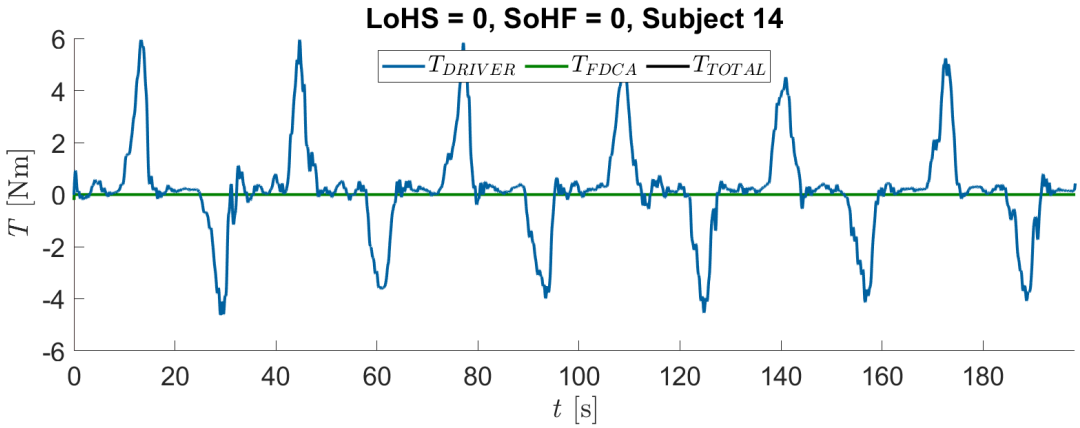
LoHS = 0, SoHF = 0, Subject 14
T_{DRIVER} T_{FDCA} T_{TOTAL}
T [Nm]
t [s]

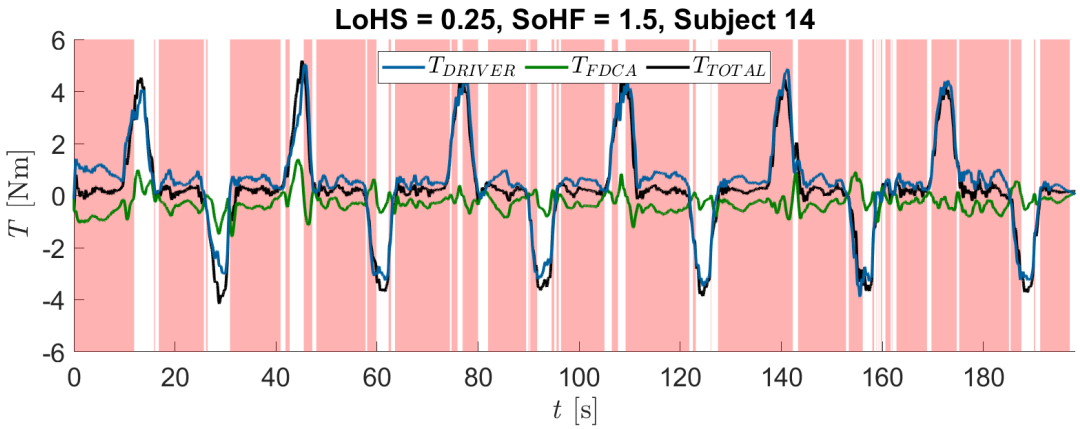
LoHS = 0.25, SoHF = 1.5, Subject 14
T_{DRIVER} T_{FDCA} T_{TOTAL}
T [Nm]
t [s]

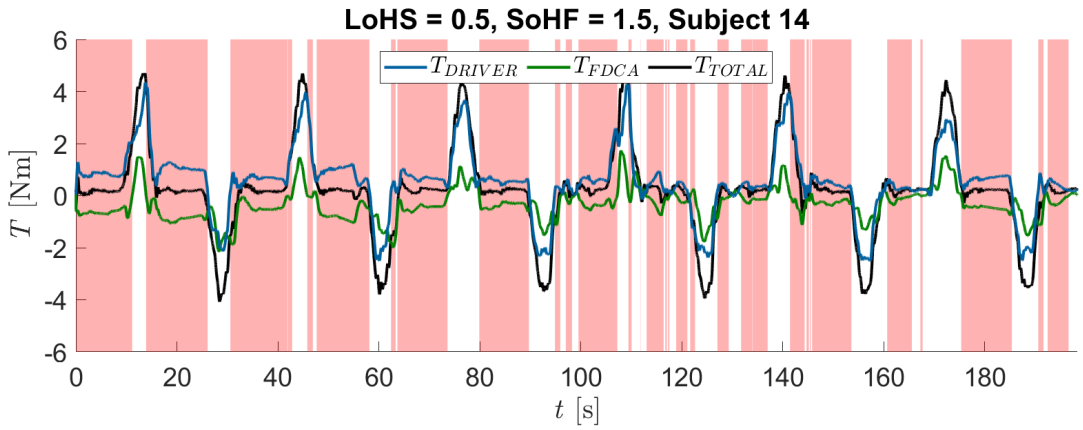
LoHS = 0.5, SoHF = 1.5, Subject 14
T_{DRIVER} T_{FDCA} T_{TOTAL}
T [Nm]
t [s]

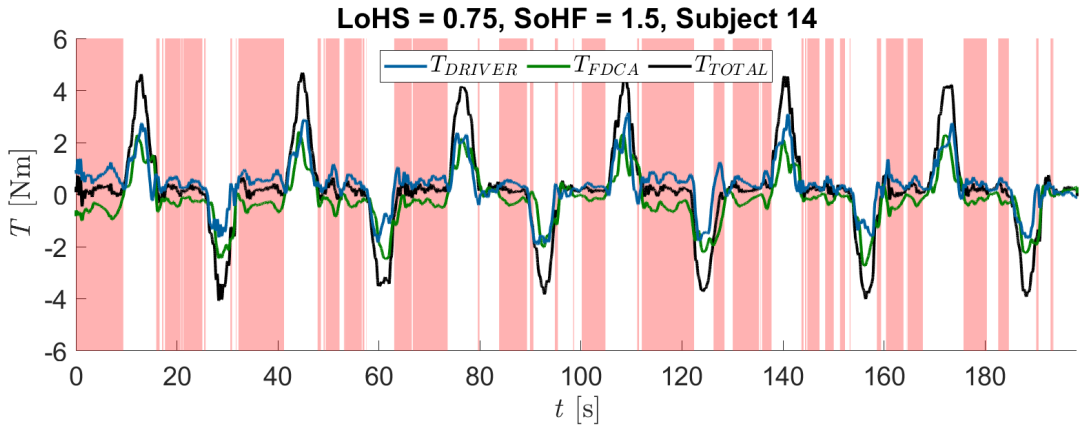
LoHS = 0.75, SoHF = 1.5, Subject 14
T_{DRIVER} T_{FDCA} T_{TOTAL}
T [Nm]
t [s]

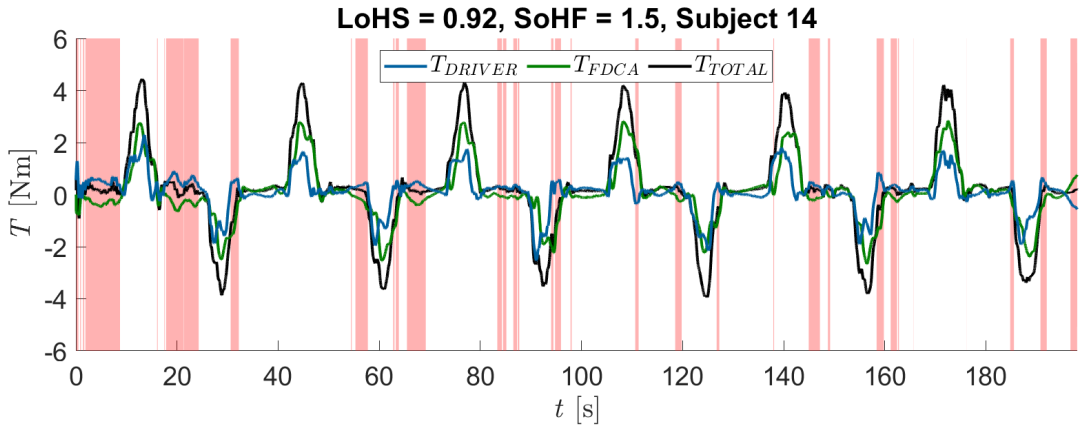
LoHS = 0.92, SoHF = 1.5, Subject 14
T_{DRIVER} T_{FDCA} T_{TOTAL}
T [Nm]
t [s]

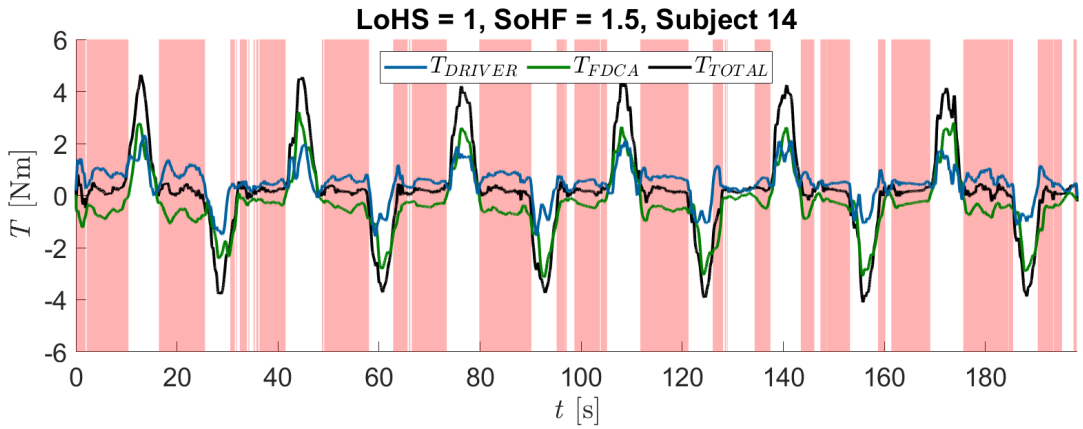
LoHS = 1, SoHF = 1.5, Subject 14
T_{DRIVER} T_{FDCA} T_{TOTAL}
T [Nm]
t [s]

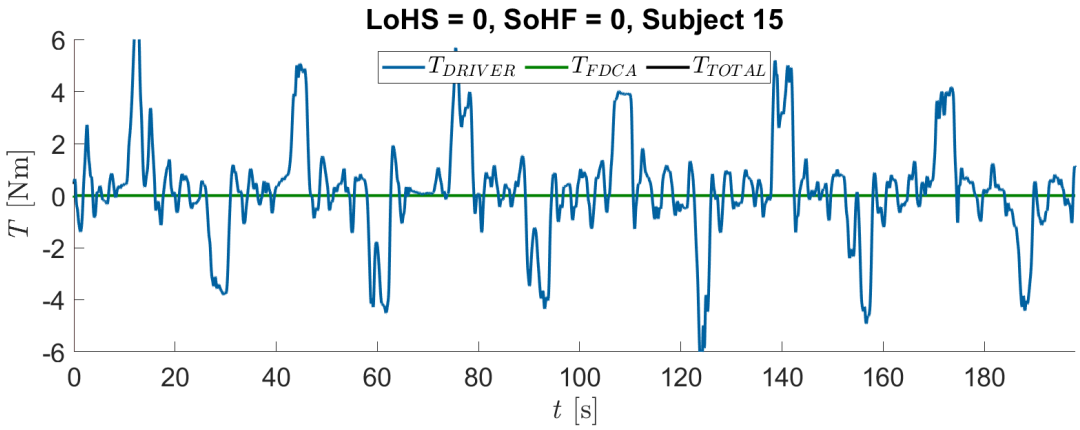
LoHS = 0, SoHF = 0, Subject 15
T_{DRIVER} T_{FDCA} T_{TOTAL}
T [Nm]
t [s]

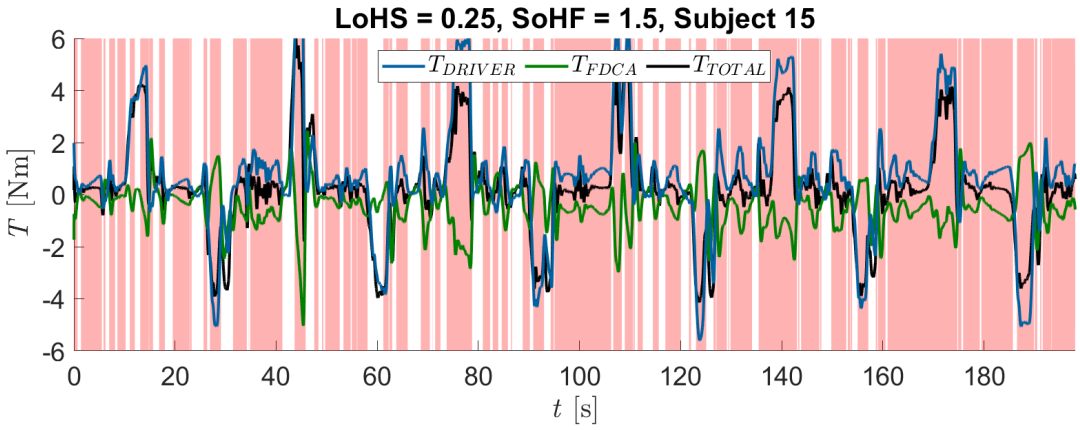
LoHS = 0.25, SoHF = 1.5, Subject 15
T_{DRIVER} T_{FDCA} T_{TOTAL}
T [Nm]
t [s]

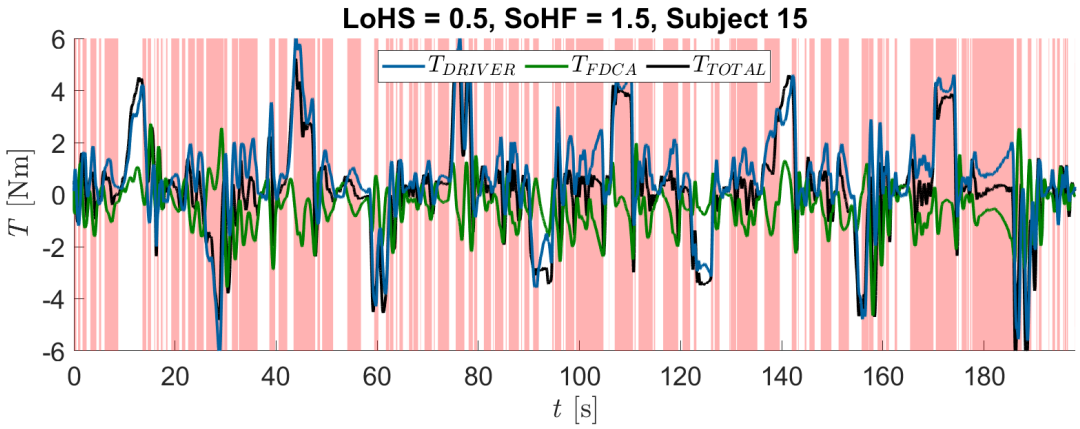
LoHS = 0.5, SoHF = 1.5, Subject 15
T_{DRIVER} T_{FDCA} T_{TOTAL}
T [Nm]
t [s]

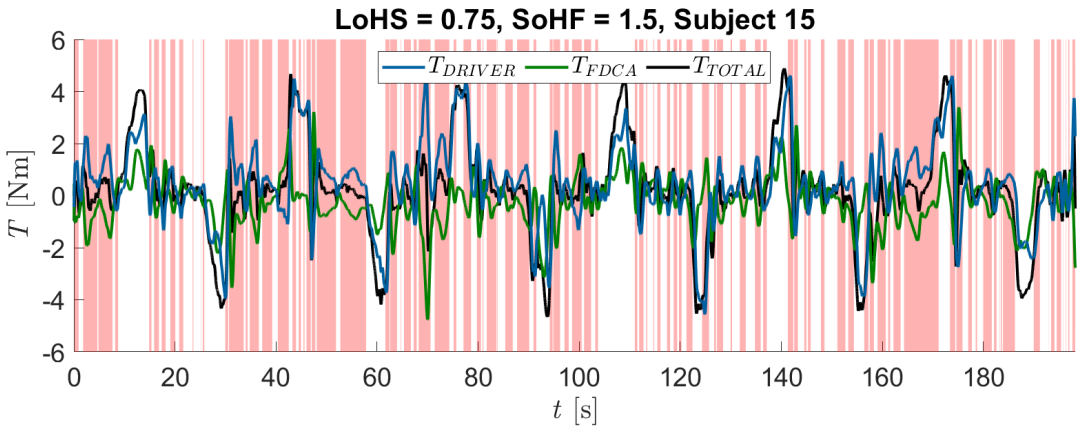
LoHS = 0.75, SoHF = 1.5, Subject 15
T_{DRIVER} T_{FDCA} T_{TOTAL}
T [Nm]
t [s]

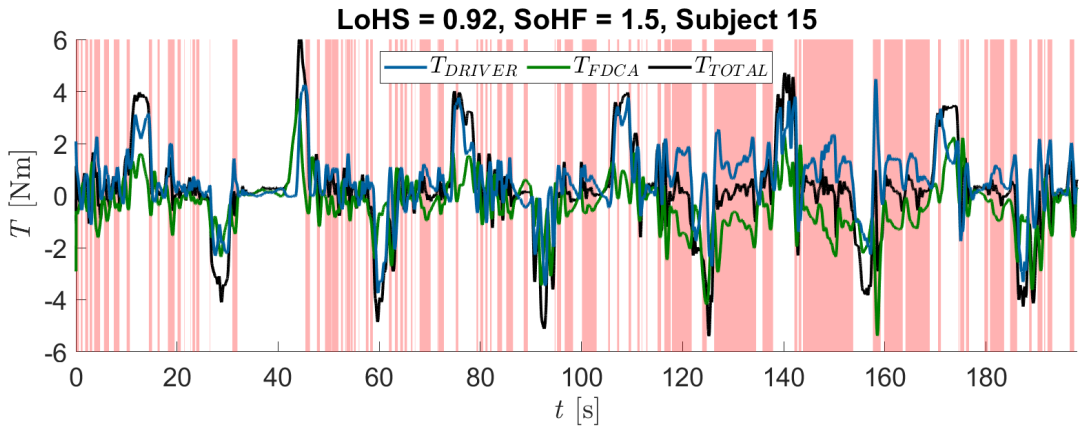
LoHS = 0.92, SoHF = 1.5, Subject 15
T_{DRIVER} T_{FDCA} T_{TOTAL}
T [Nm]
t [s]

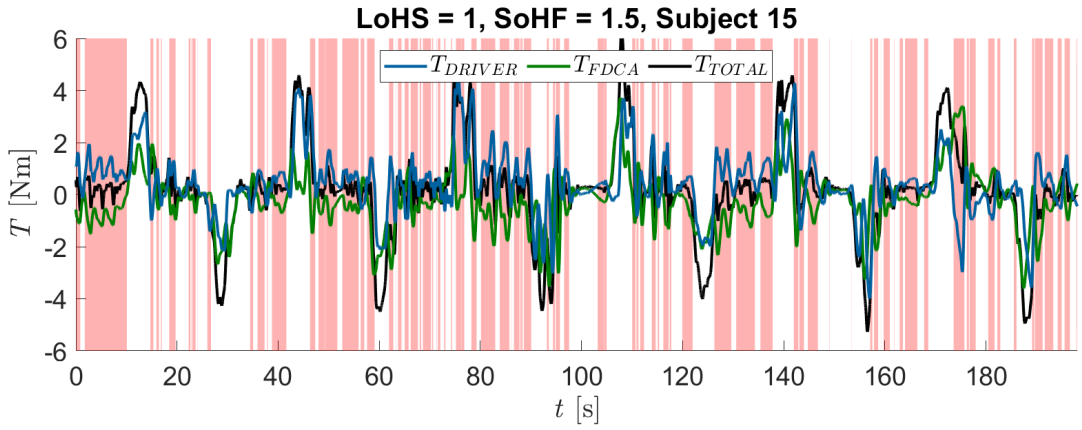
LoHS = 1, SoHF = 1.5, Subject 15
T_{DRIVER} T_{FDCA} T_{TOTAL}
T [Nm]
t [s]

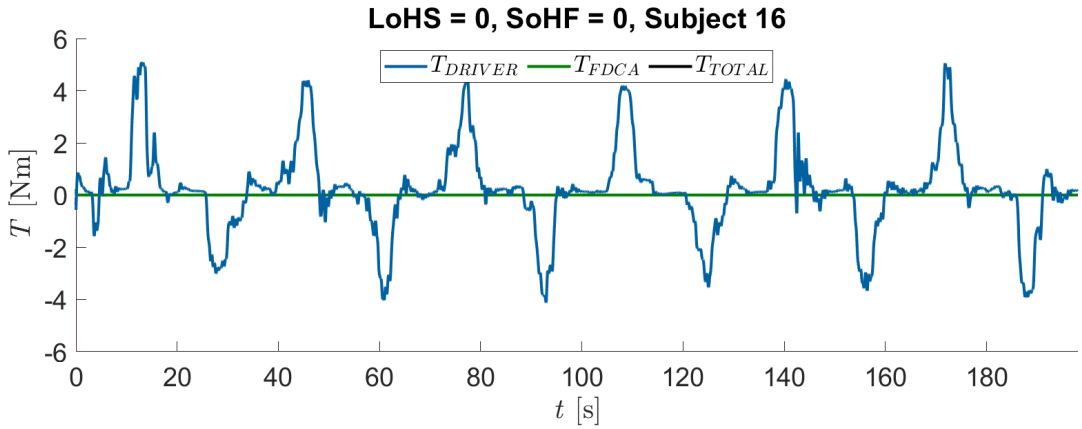
LoHS = 0, SoHF = 0, Subject 16
T_{DRIVER} T_{FDCA} T_{TOTAL}
T [Nm]
t [s]

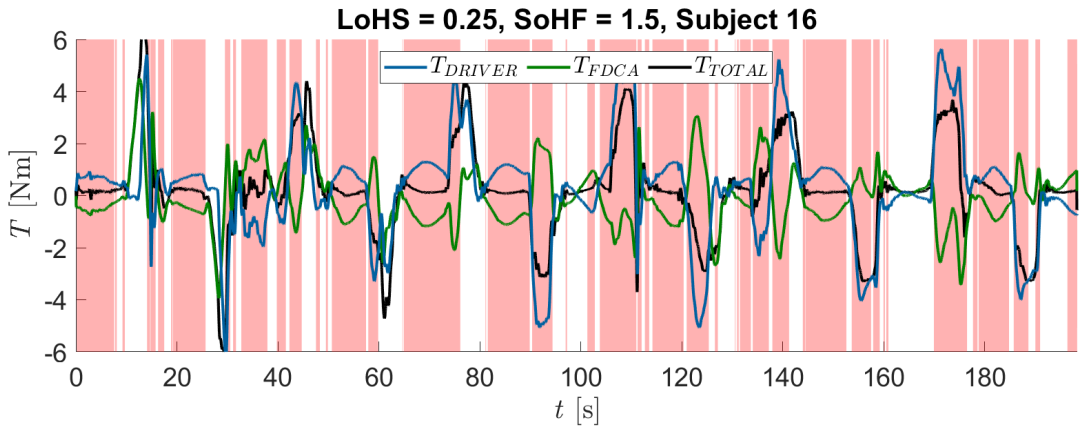
LoHS = 0.25, SoHF = 1.5, Subject 16
T_{DRIVER} T_{FDCA} T_{TOTAL}
T [Nm]
t [s]

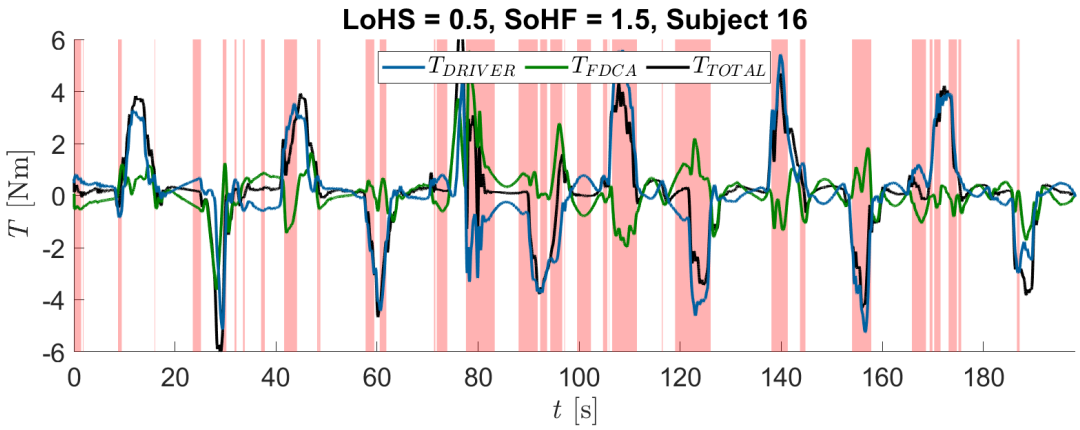
LoHS = 0.5, SoHF = 1.5, Subject 16
T_{DRIVER} T_{FDCA} T_{TOTAL}
T [Nm]
t [s]

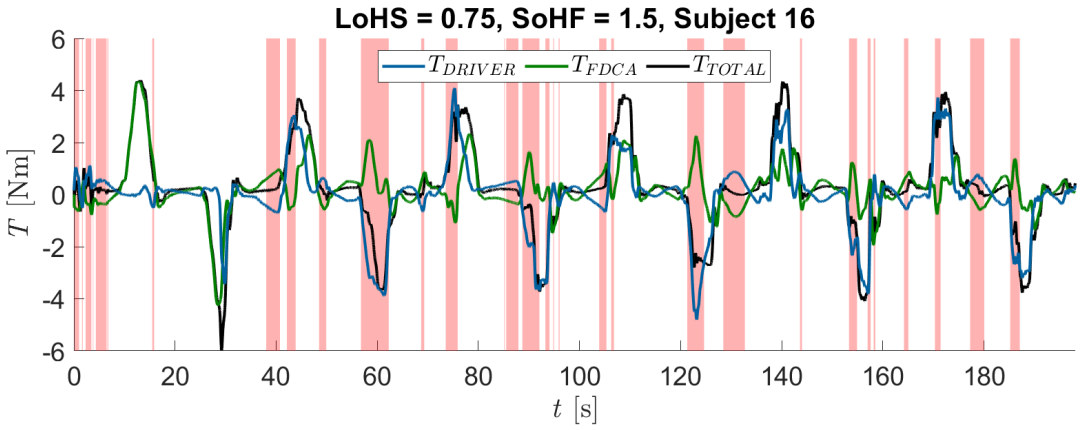
LoHS = 0.75, SoHF = 1.5, Subject 16
T_{DRIVER} T_{FDCA} T_{TOTAL}
T [Nm]
t [s]

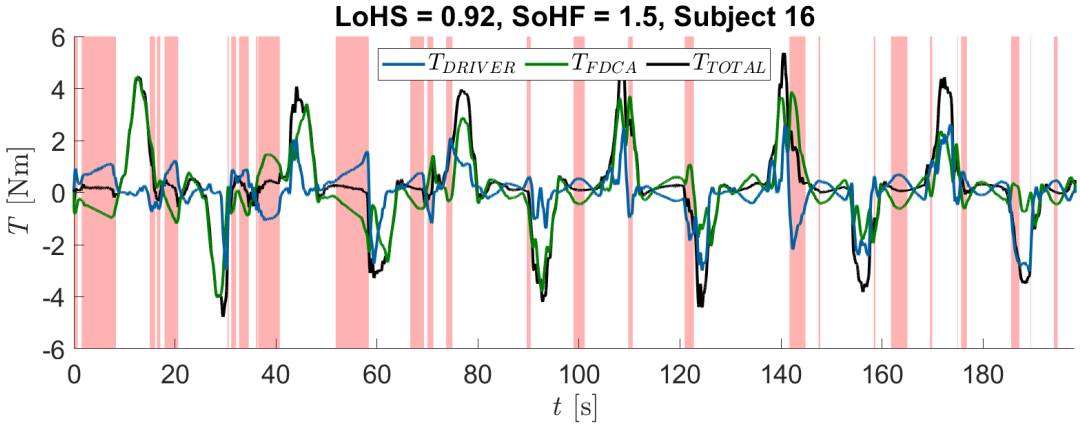
LoHS = 0.92, SoHF = 1.5, Subject 16
T_{DRIVER} T_{FDCA} T_{TOTAL}
T [Nm]
t [s]

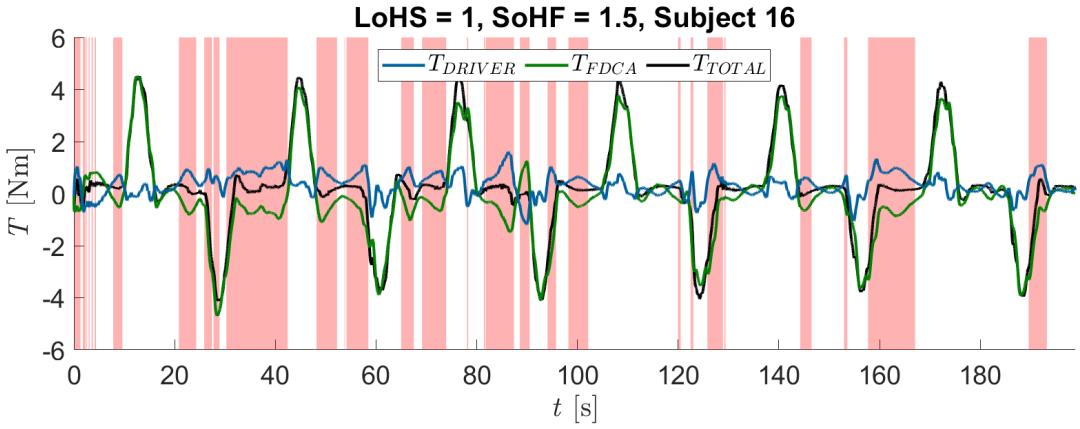
LoHS = 1, SoHF = 1.5, Subject 16
T_{DRIVER} T_{FDCA} T_{TOTAL}
T [Nm]
t [s]

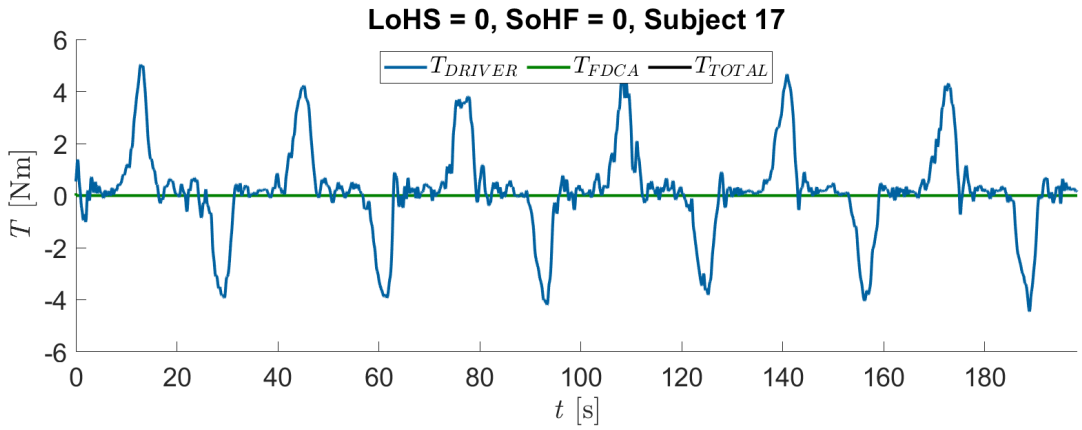
LoHS = 0, SoHF = 0, Subject 17
T_{DRIVER} T_{FDCA} T_{TOTAL}
T [Nm]
t [s]

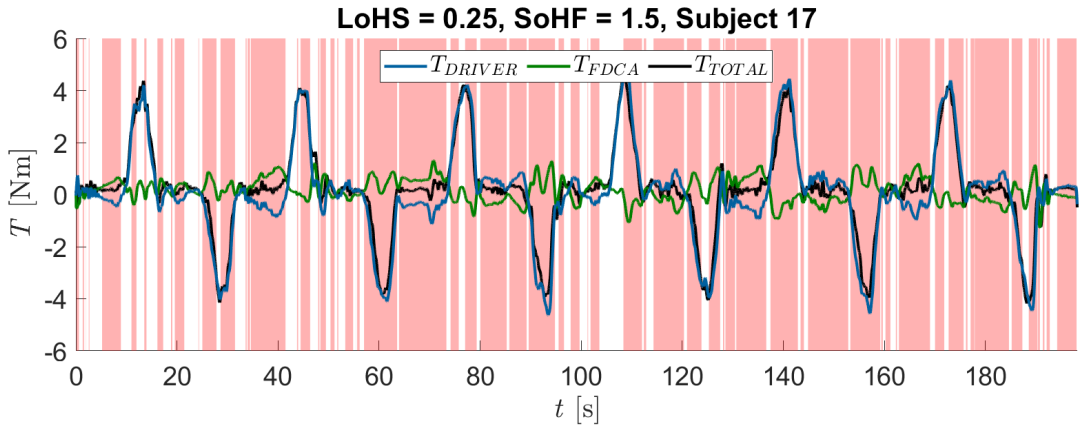
LoHS = 0.25, SoHF = 1.5, Subject 17
T_{DRIVER} T_{FDCA} T_{TOTAL}
T [Nm]
t [s]

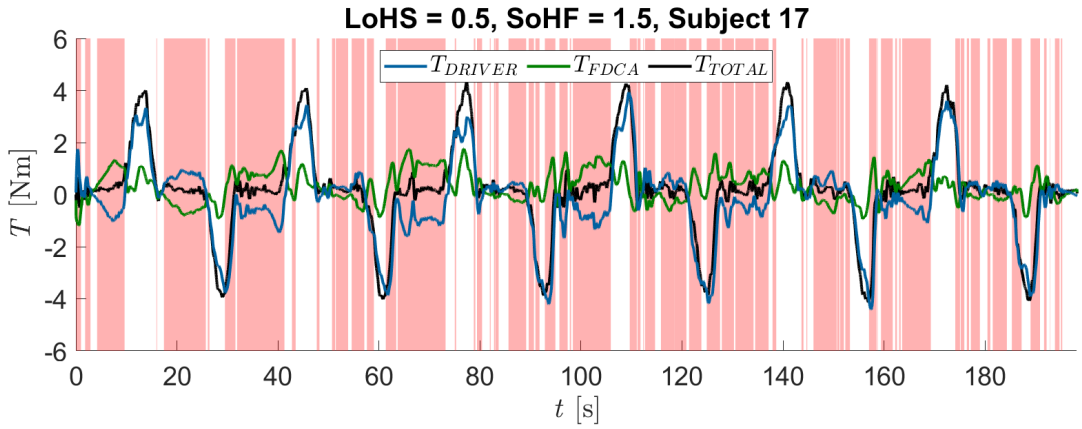
LoHS = 0.5, SoHF = 1.5, Subject 17
T_{DRIVER} T_{FDCA} T_{TOTAL}
T [Nm]
t [s]

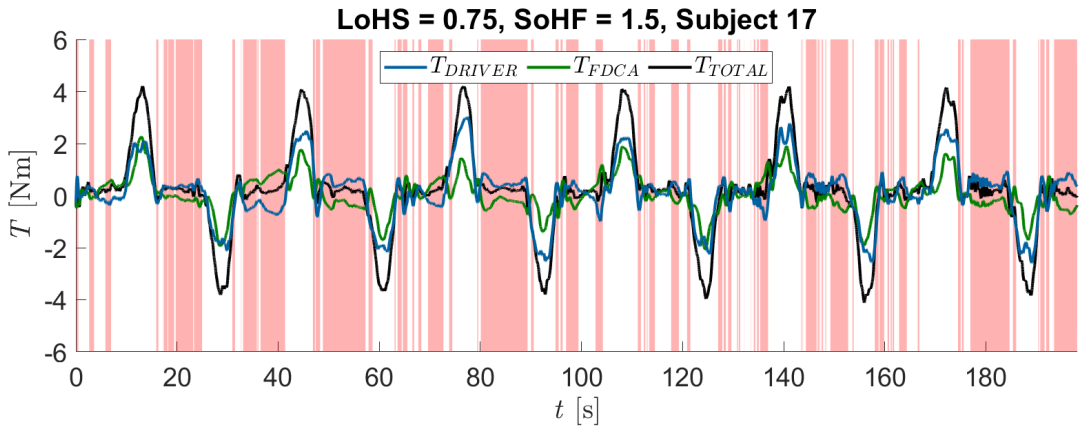
LoHS = 0.75, SoHF = 1.5, Subject 17
T_{DRIVER} T_{FDCA} T_{TOTAL}
T [Nm]
t [s]

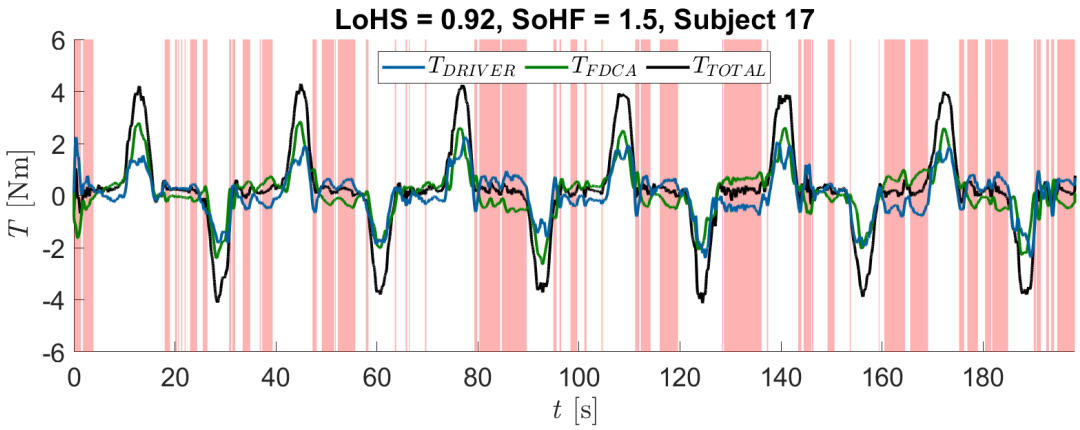
LoHS = 0.92, SoHF = 1.5, Subject 17
T_{DRIVER} T_{FDCA} T_{TOTAL}
T [Nm]
t [s]

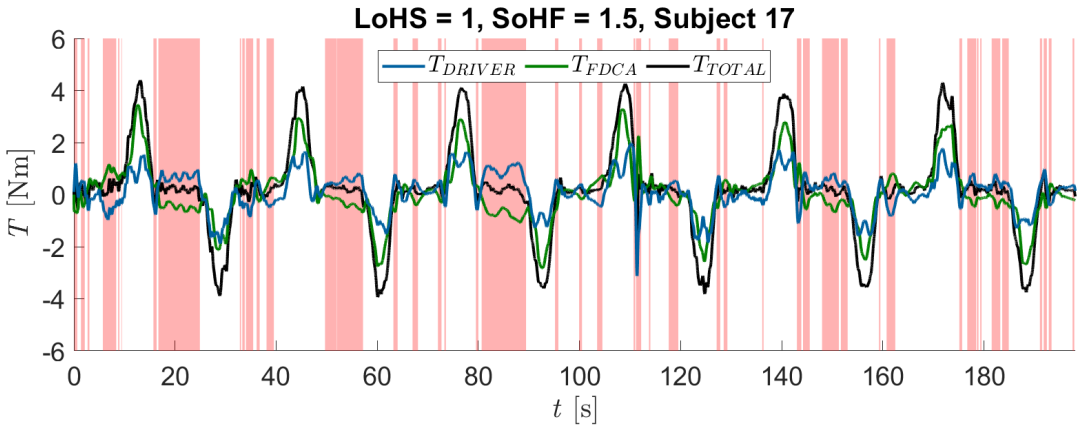
LoHS = 1, SoHF = 1.5, Subject 17
T_{DRIVER} T_{FDCA} T_{TOTAL}
T [Nm]
t [s]

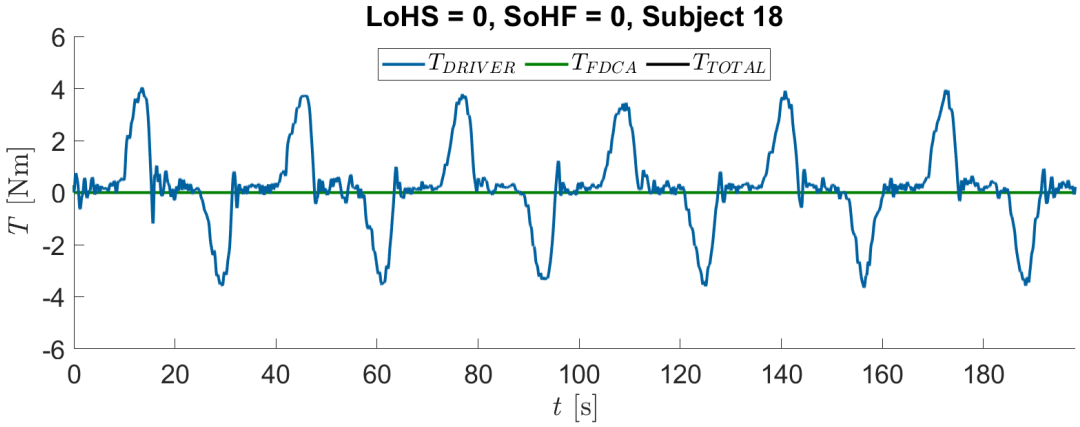
LoHS = 0, SoHF = 0, Subject 18
T_{DRIVER} T_{FDCA} T_{TOTAL}
T [Nm]
t [s]

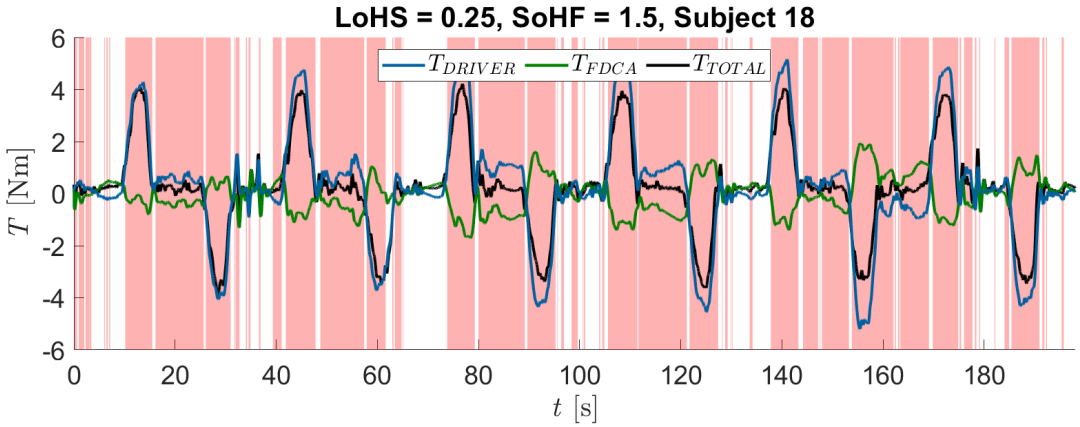
LoHS = 0.25, SoHF = 1.5, Subject 18
T_{DRIVER} T_{FDCA} T_{TOTAL}
T [Nm]
t [s]

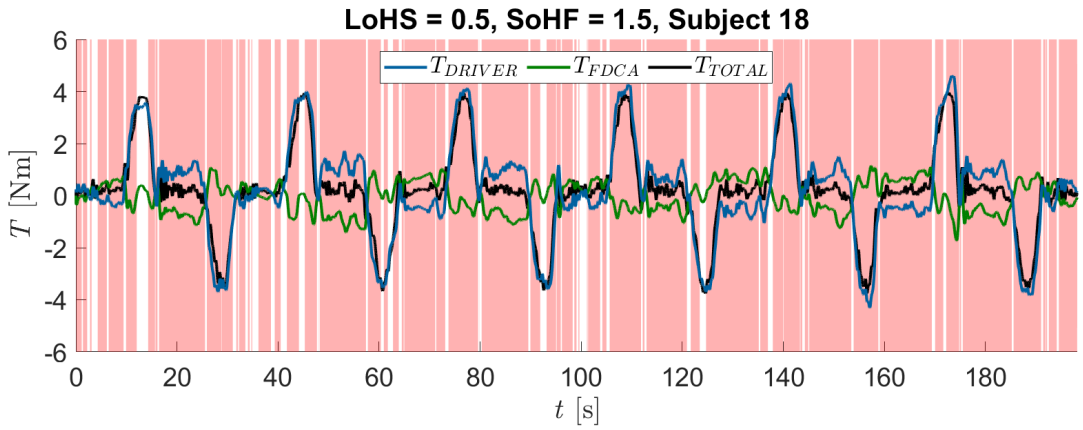
LoHS = 0.5, SoHF = 1.5, Subject 18
T_{DRIVER} T_{FDCA} T_{TOTAL}
T [Nm]
t [s]

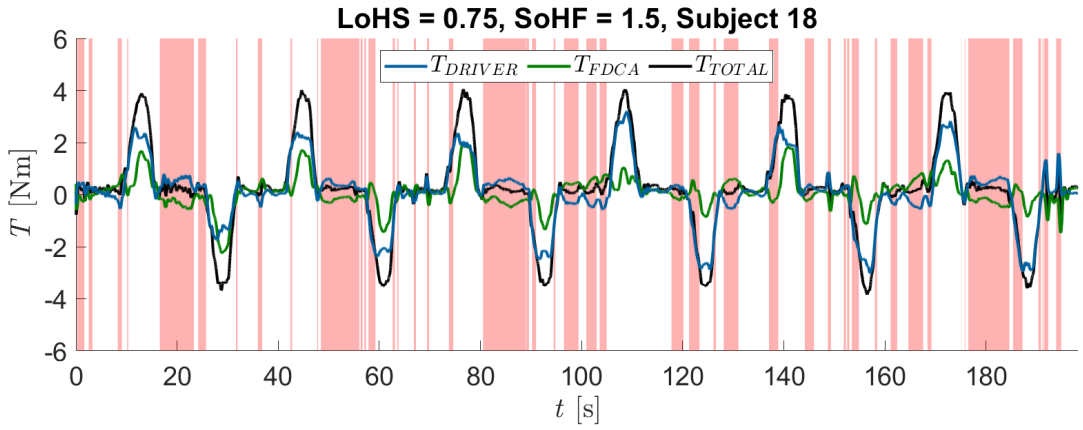
LoHS = 0.75, SoHF = 1.5, Subject 18
T_{DRIVER} T_{FDCA} T_{TOTAL}
T [Nm]
t [s]

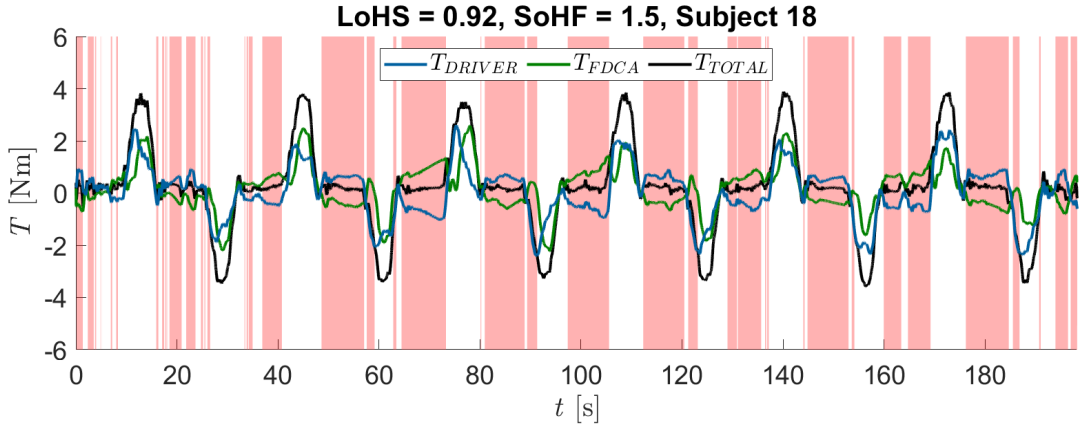
LoHS = 0.92, SoHF = 1.5, Subject 18
T_{DRIVER} T_{FDCA} T_{TOTAL}
T [Nm]
t [s]

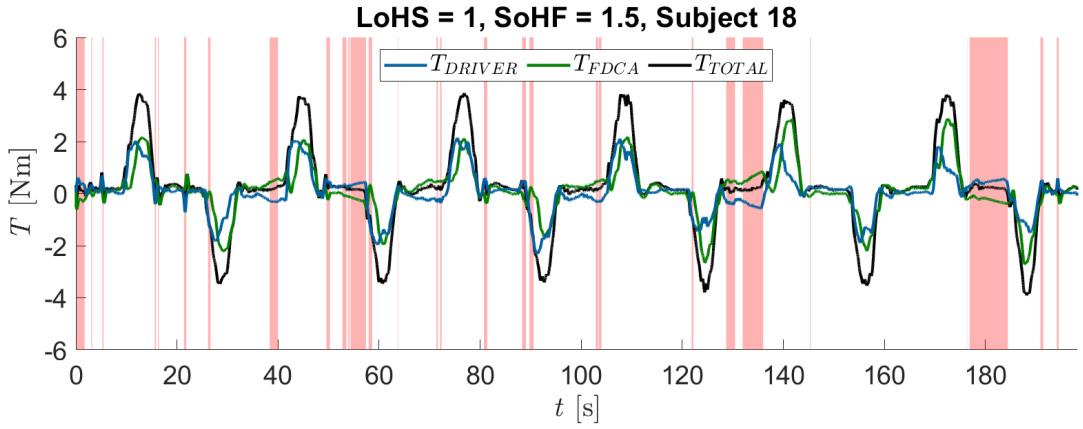
LoHS = 1, SoHF = 1.5, Subject 18
T_{DRIVER} T_{FDCA} T_{TOTAL}
T [Nm]
t [s]

C

Individual Driver Results - Lateral Position and Steering Data

This appendix contains the lateral position and steering results for all eighteen participants in the experiment for the three lowest and highest LoHS conditions. Firstly, the lateral position, steering wheel and filtered steering wheel rate data are given for the full road. Additionally, these variables are averaged over the left and right curves and the results are provided again for every subject.

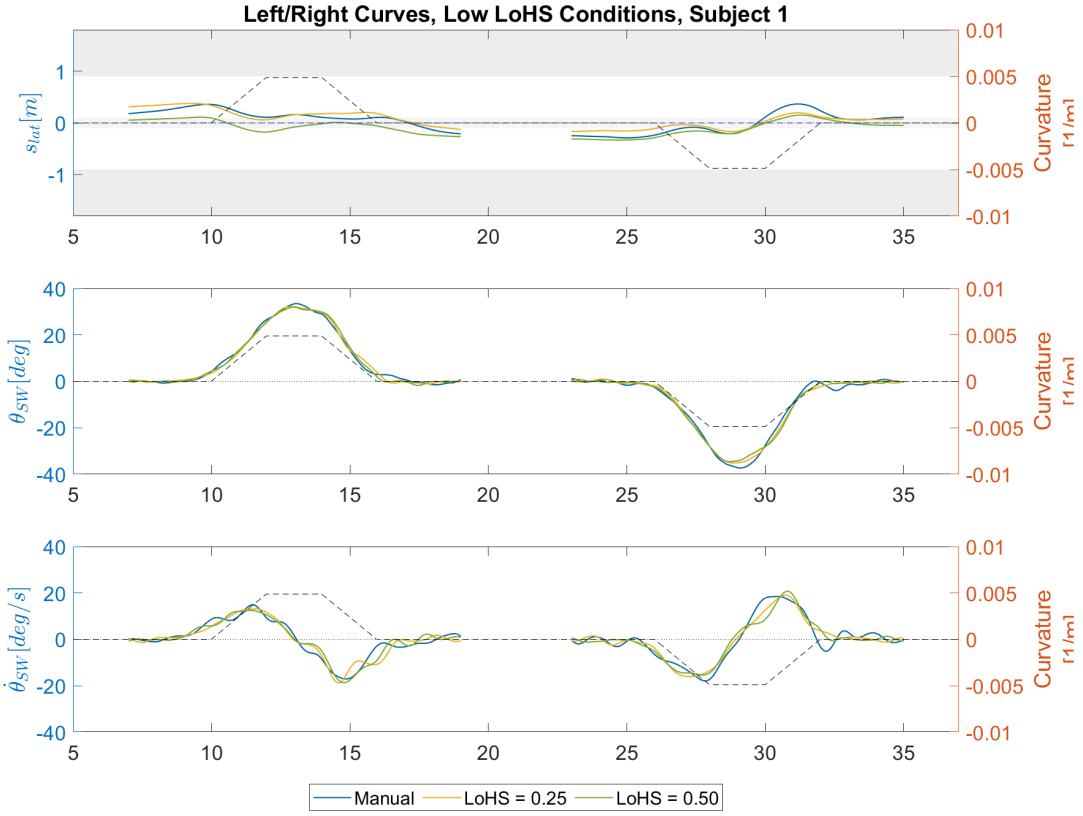

Figure C.1: Average road lateral position, steering wheel and steering rate data for subject 1 for the three lower LoHS conditions for left and right curves

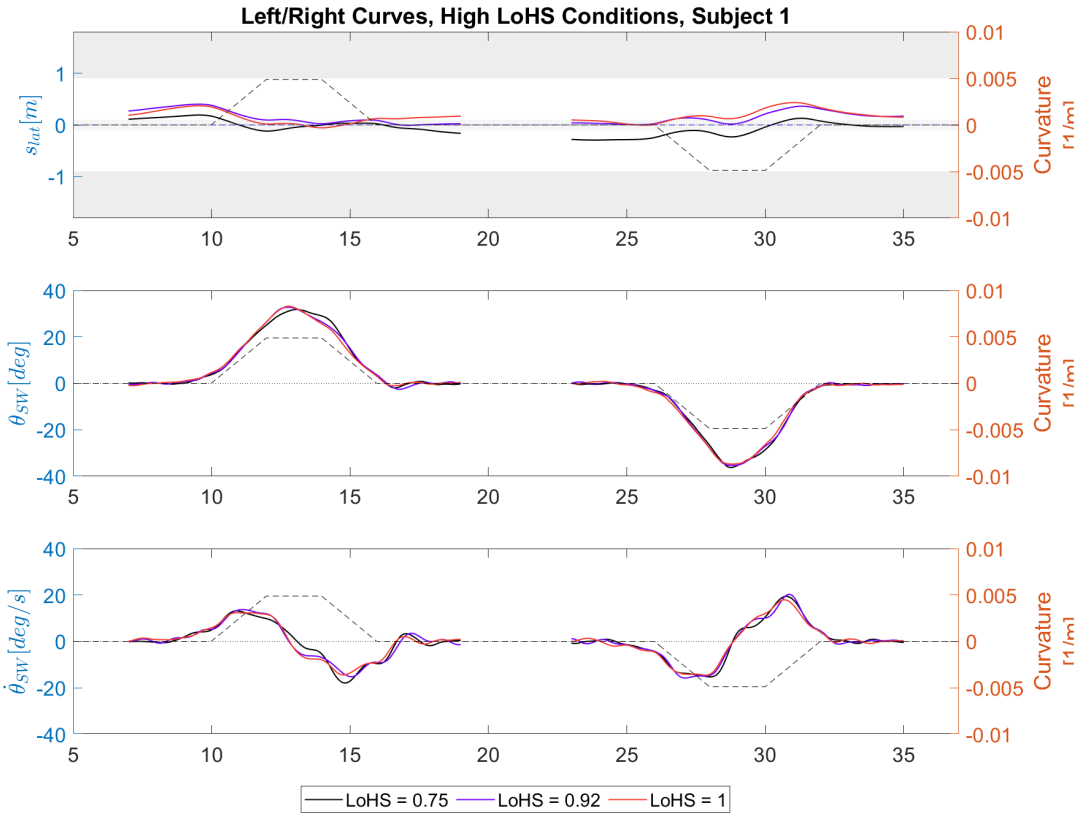

Figure C.2: Average road lateral position, steering wheel and steering rate data for subject 1 for the three higher LoHS conditions for left and right curves

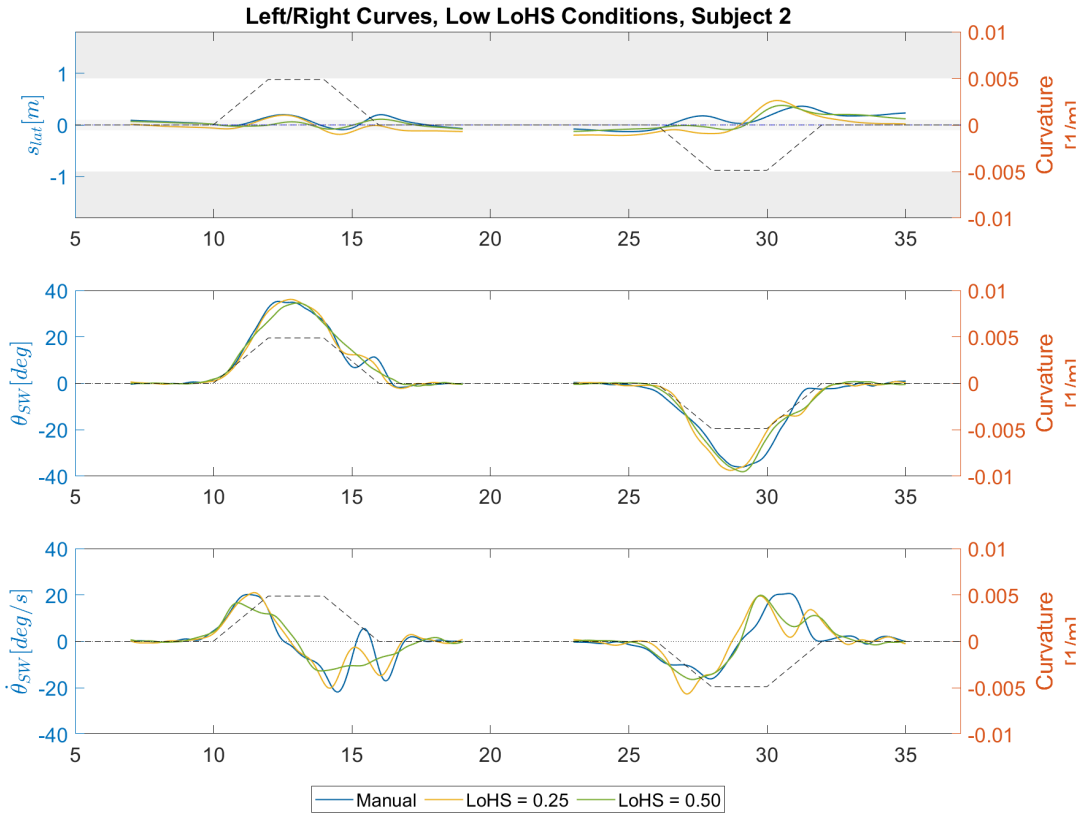

Figure C.3: Average road lateral position, steering wheel and steering rate data for subject 2 for the three lower LoHS conditions for left and right curves

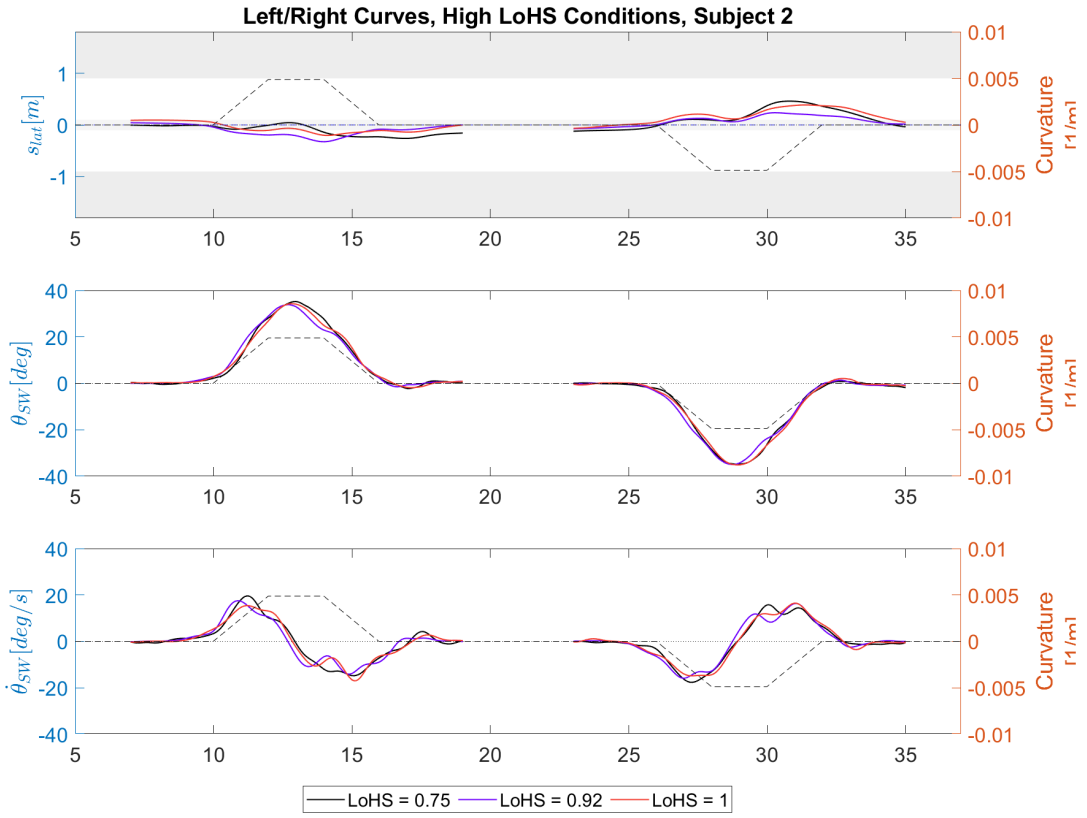

Figure C.4: Average road lateral position, steering wheel and steering rate data for subject 2 for the three higher LoHS conditions for left and right curves

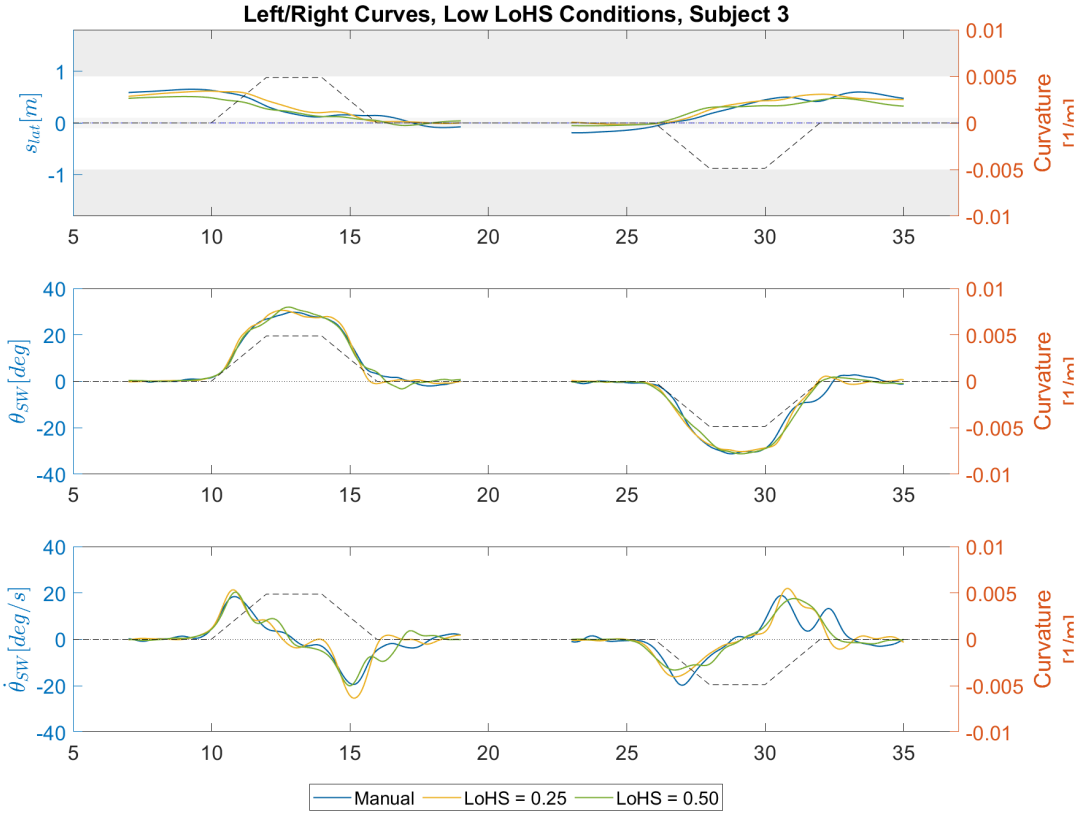

Figure C.5: Average road lateral position, steering wheel and steering rate data for subject 3 for the three lower LoHS conditions for left and right curves

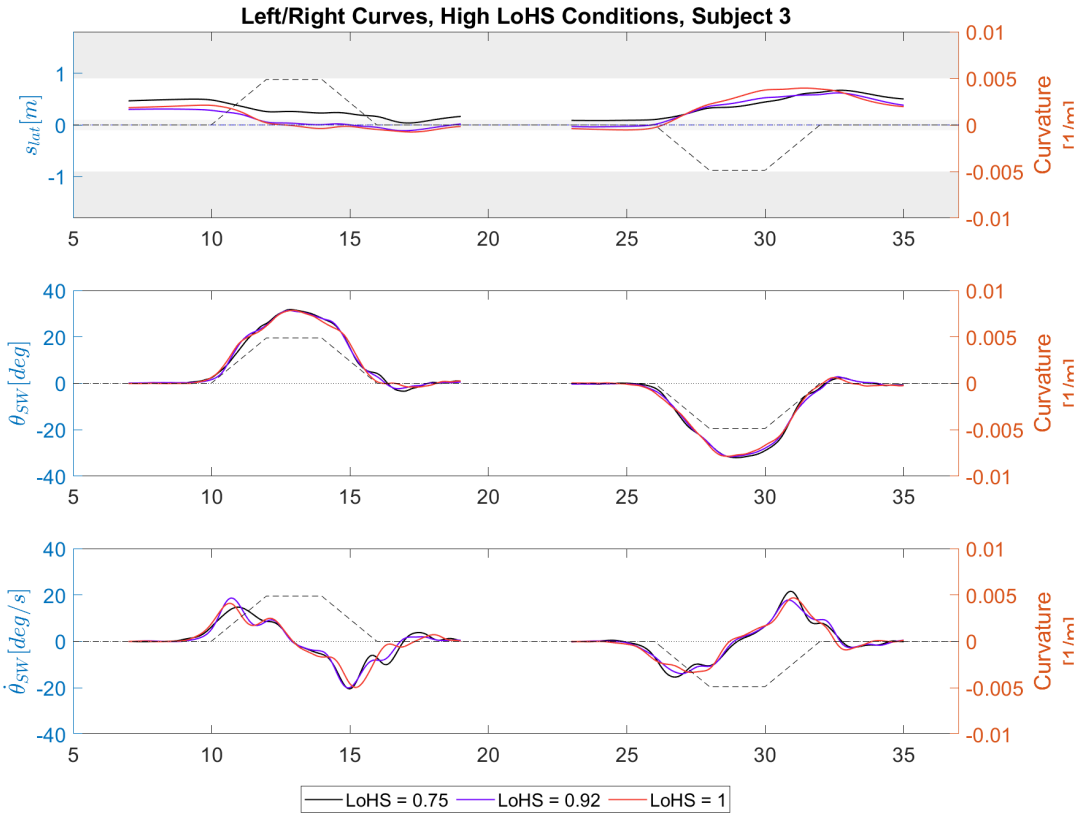

Figure C.6: Average road lateral position, steering wheel and steering rate data for subject 3 for the three higher LoHS conditions for left and right curves

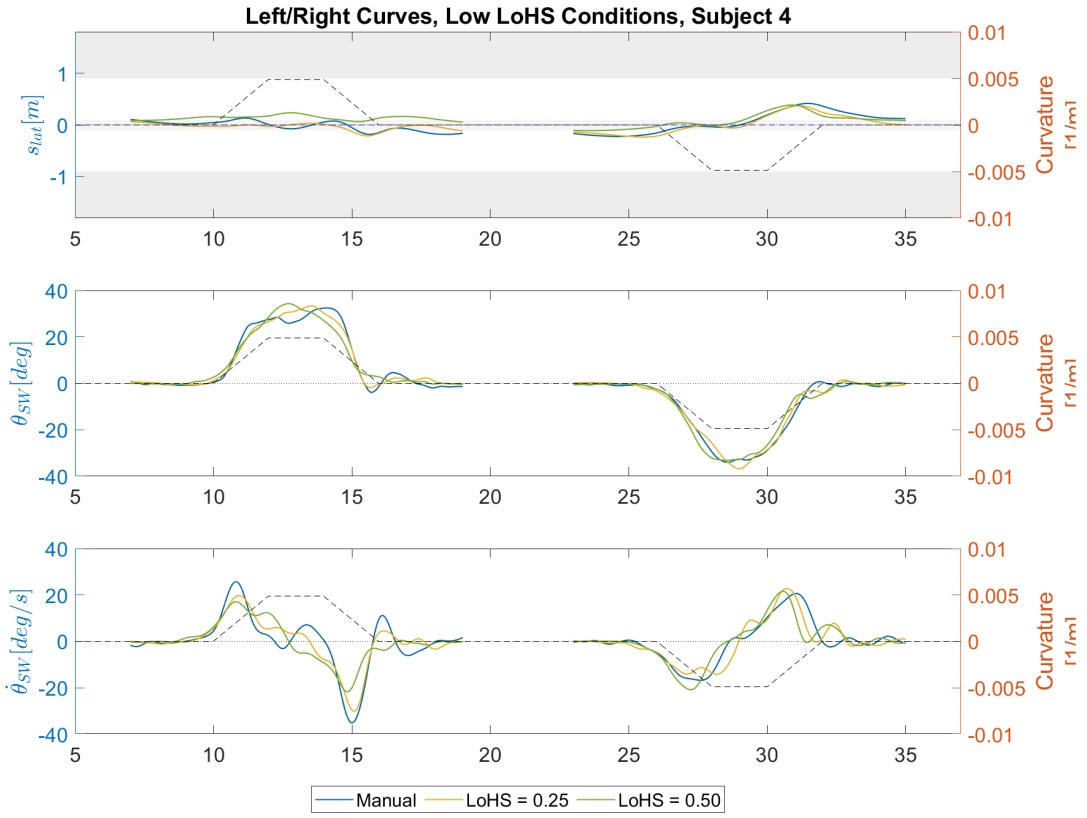

Figure C.7: Average road lateral position, steering wheel and steering rate data for subject 4 for the three lower LoHS conditions for left and right curves

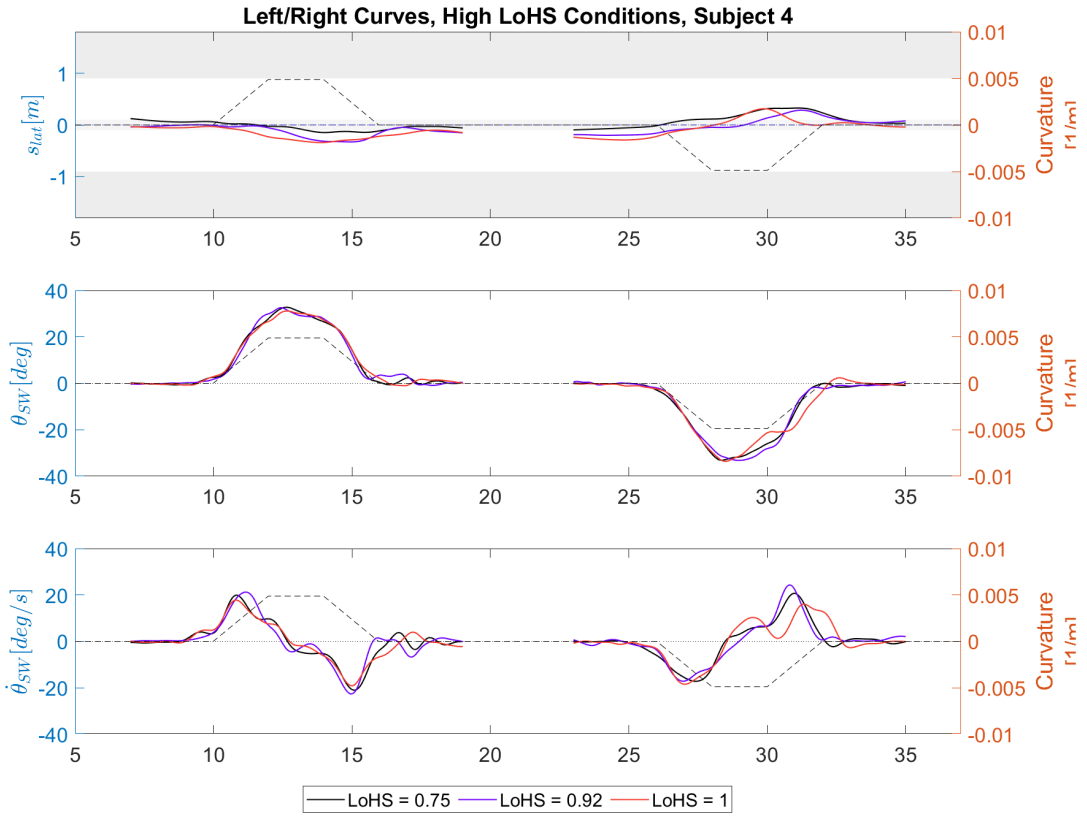

Figure C.8: Average road lateral position, steering wheel and steering rate data for subject 4 for the three higher LoHS conditions for left and right curves

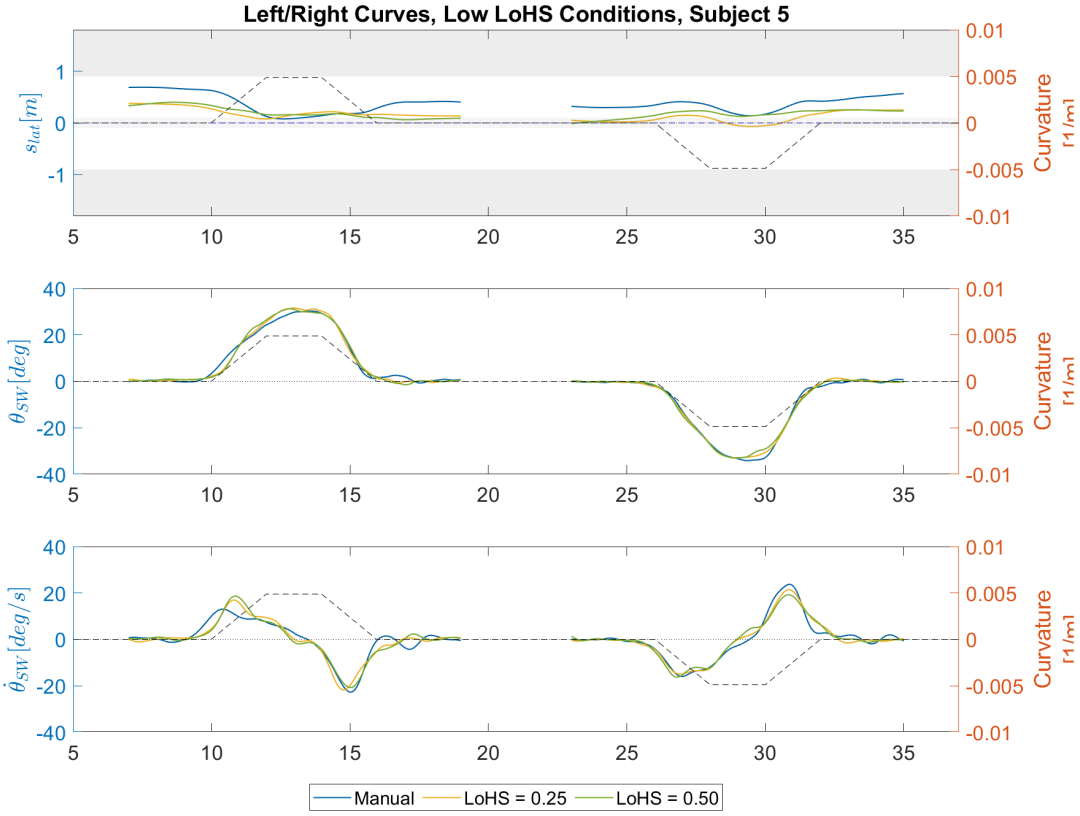

Figure C.9: Average road lateral position, steering wheel and steering rate data for subject 5 for the three lower LoHS conditions for left and right curves

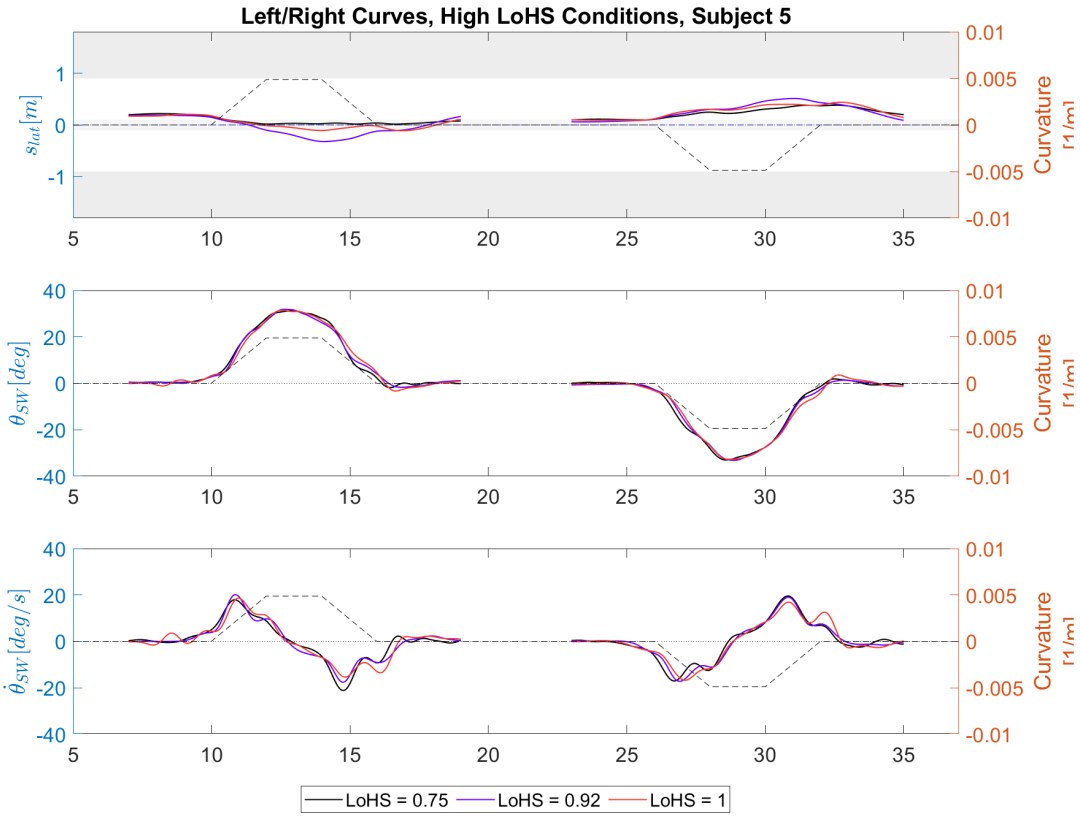

Figure C.10: Average road lateral position, steering wheel and steering rate data for subject 5 for the three higher LoHS conditions for left and right curves

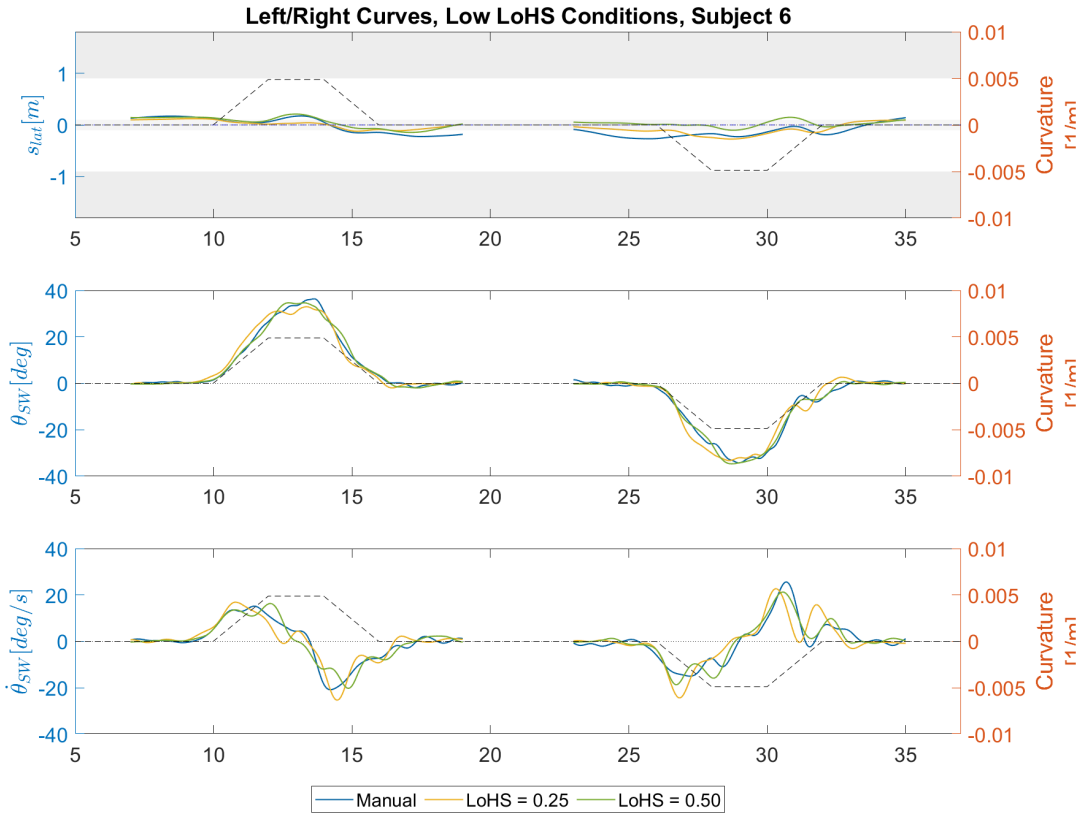

Figure C.11: Average road lateral position, steering wheel and steering rate data for subject 6 for the three lower LoHS conditions for left and right curves

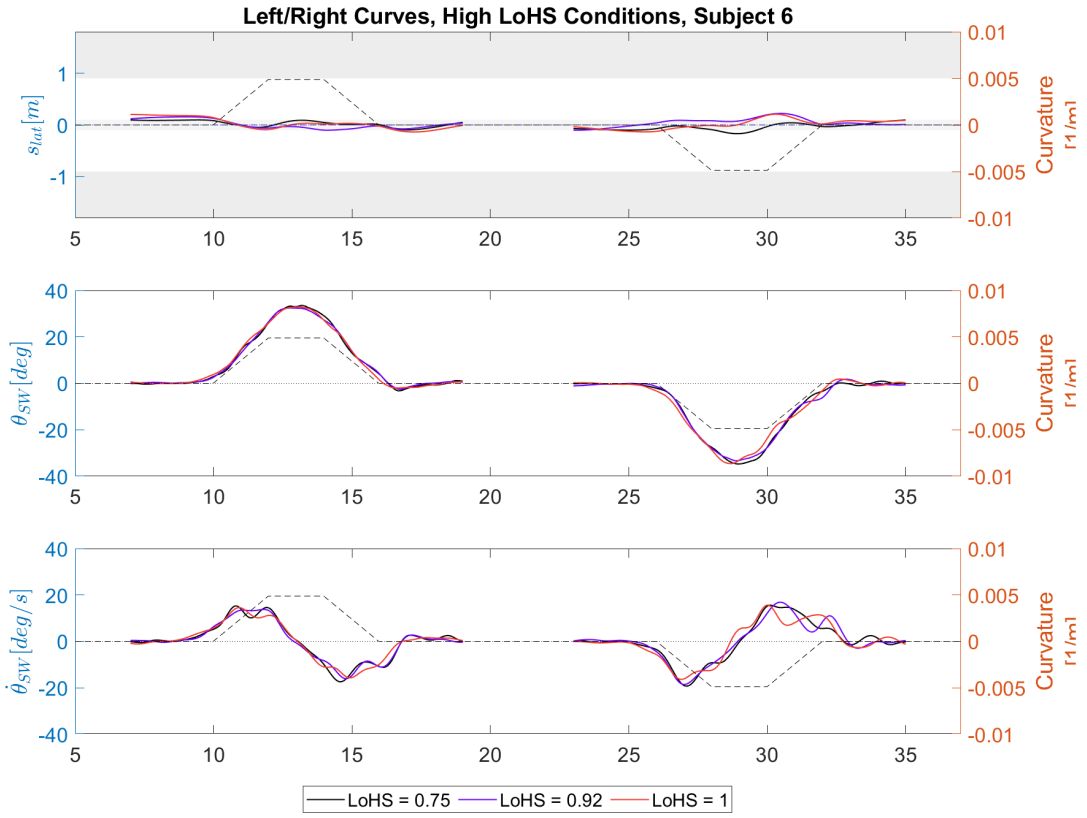

Figure C.12: Average road lateral position, steering wheel and steering rate data for subject 6 for the three higher LoHS conditions for left and right curves

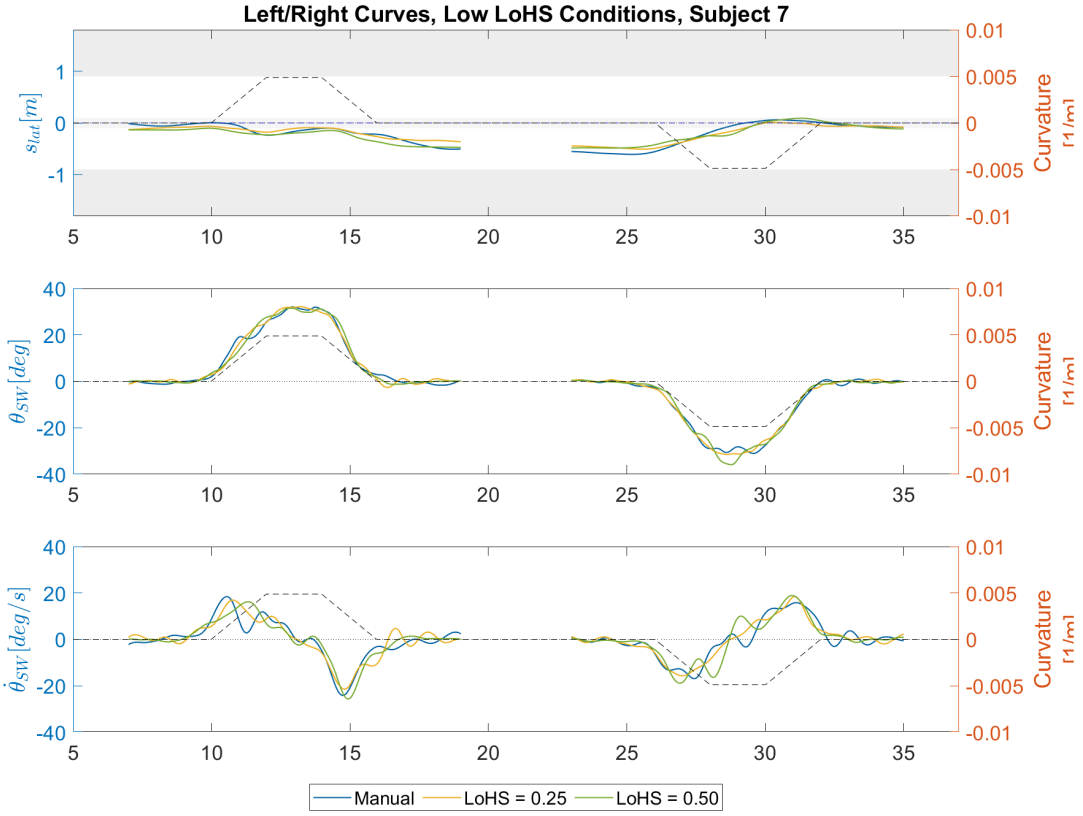

Figure C.13: Average road lateral position, steering wheel and steering rate data for subject 7 for the three lower LoHS conditions for left and right curves

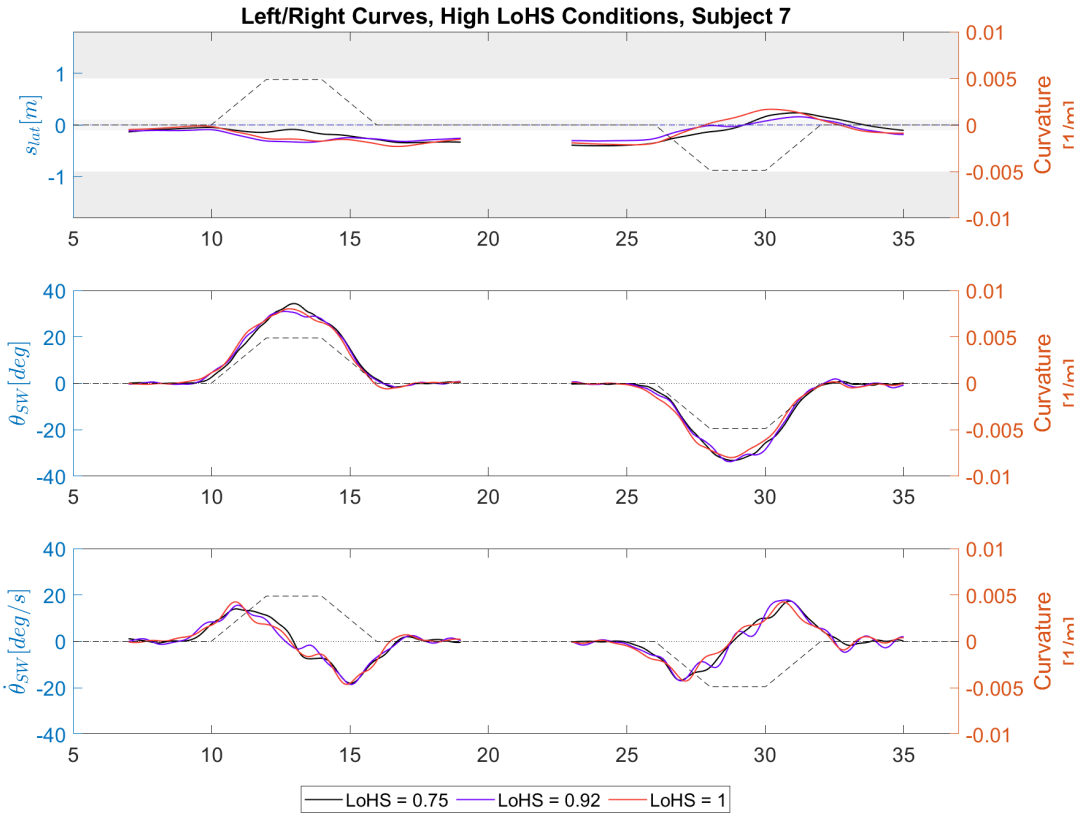

Figure C.14: Average road lateral position, steering wheel and steering rate data for subject 7 for the three higher LoHS conditions for left and right curves

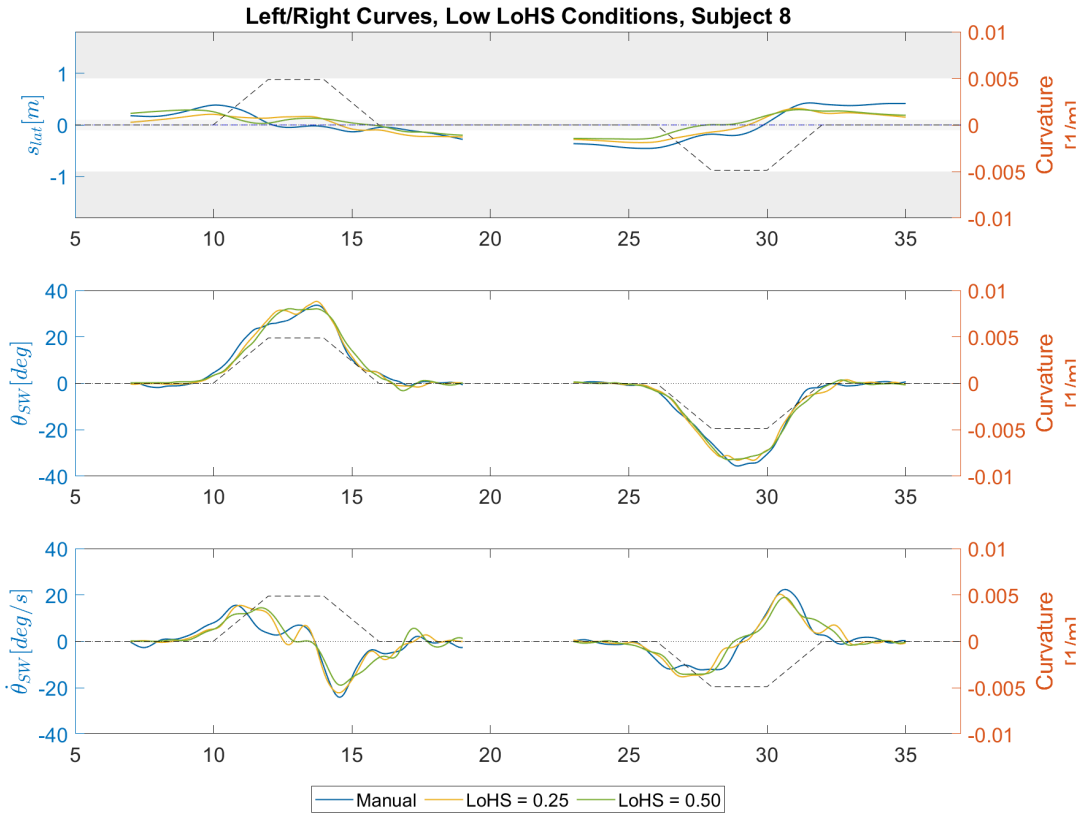

Figure C.15: Average road lateral position, steering wheel and steering rate data for subject 8 for the three lower LoHS conditions for left and right curves

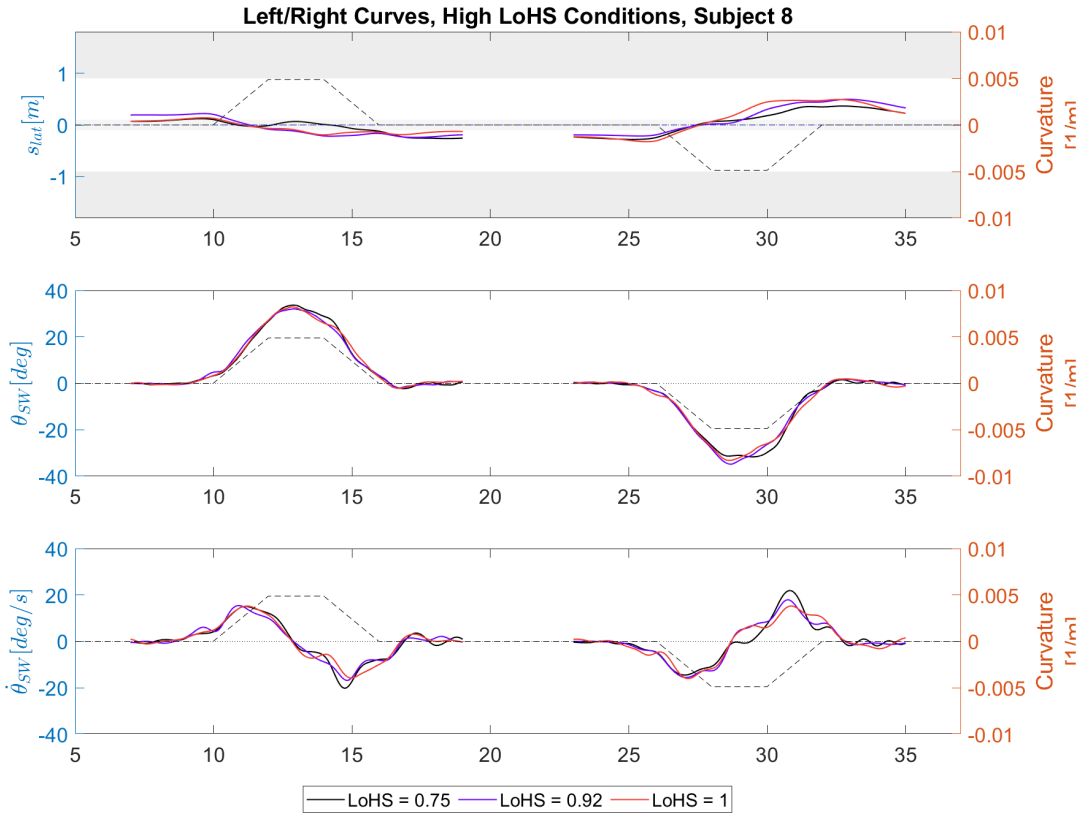

Figure C.16: Average road lateral position, steering wheel and steering rate data for subject 8 for the three higher LoHS conditions for left and right curves

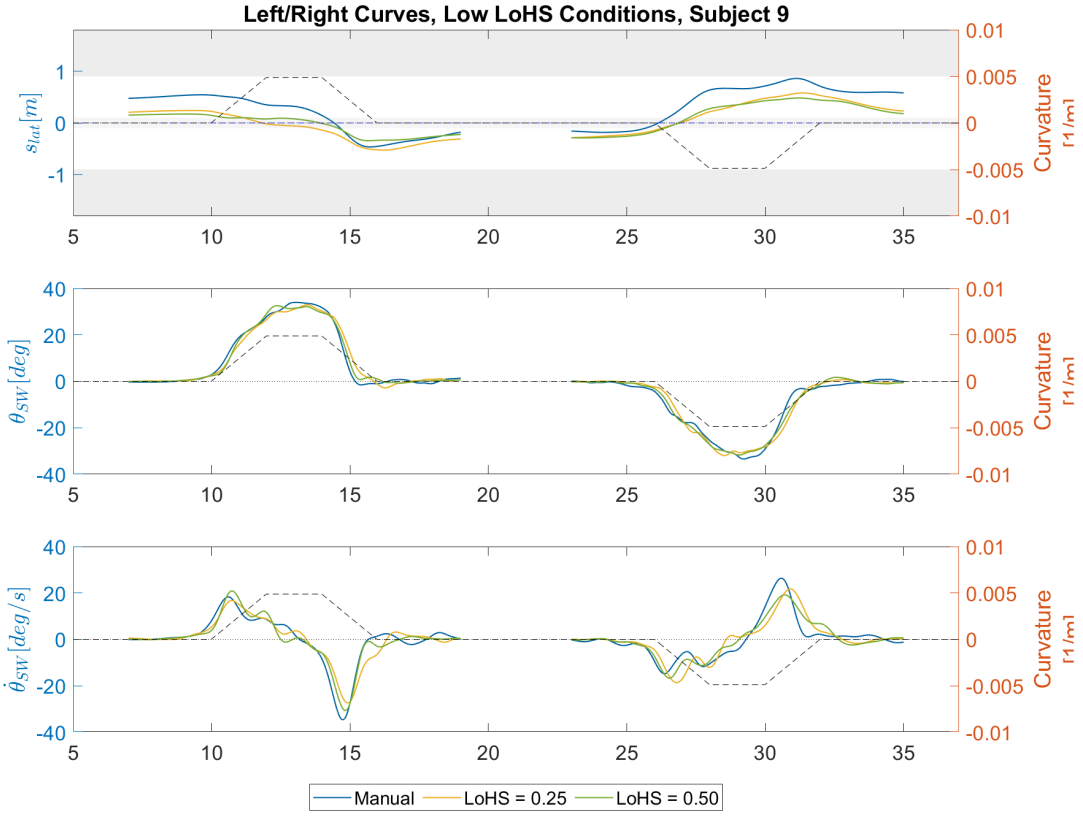

Figure C.17: Average road lateral position, steering wheel and steering rate data for subject 9 for the three lower LoHS conditions for left and right curves

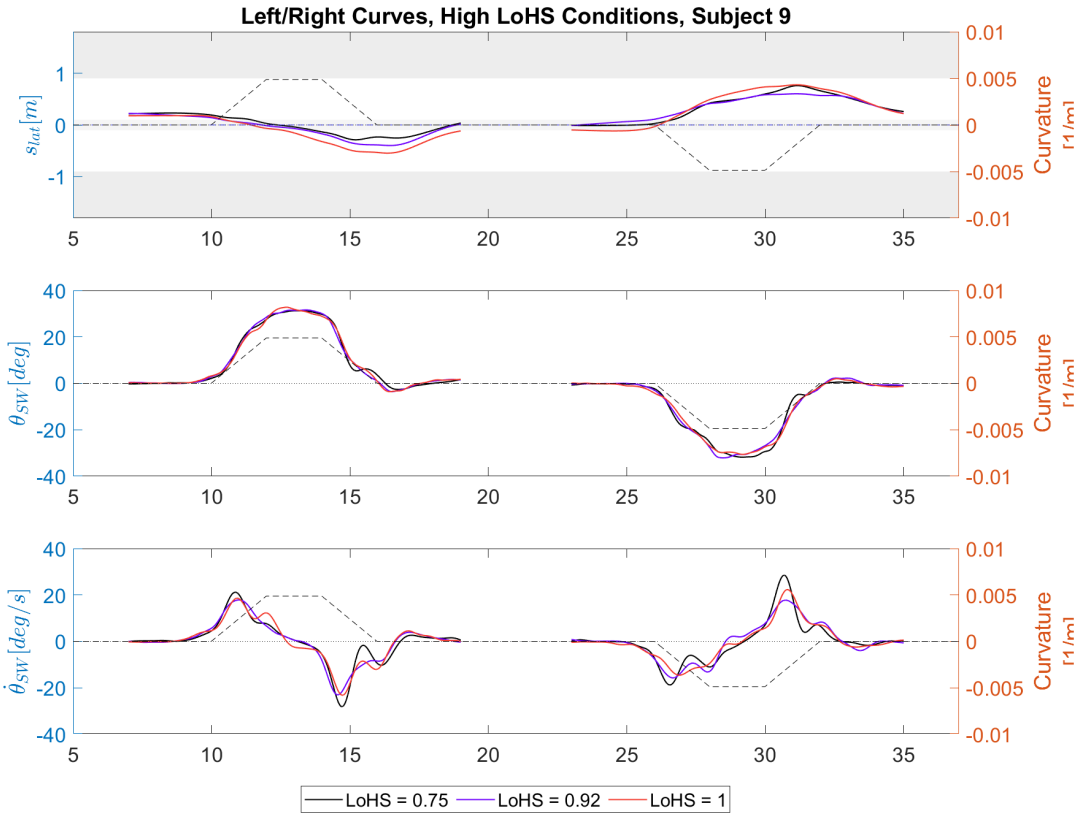

Figure C.18: Average road lateral position, steering wheel and steering rate data for subject 9 for the three higher LoHS conditions for left and right curves

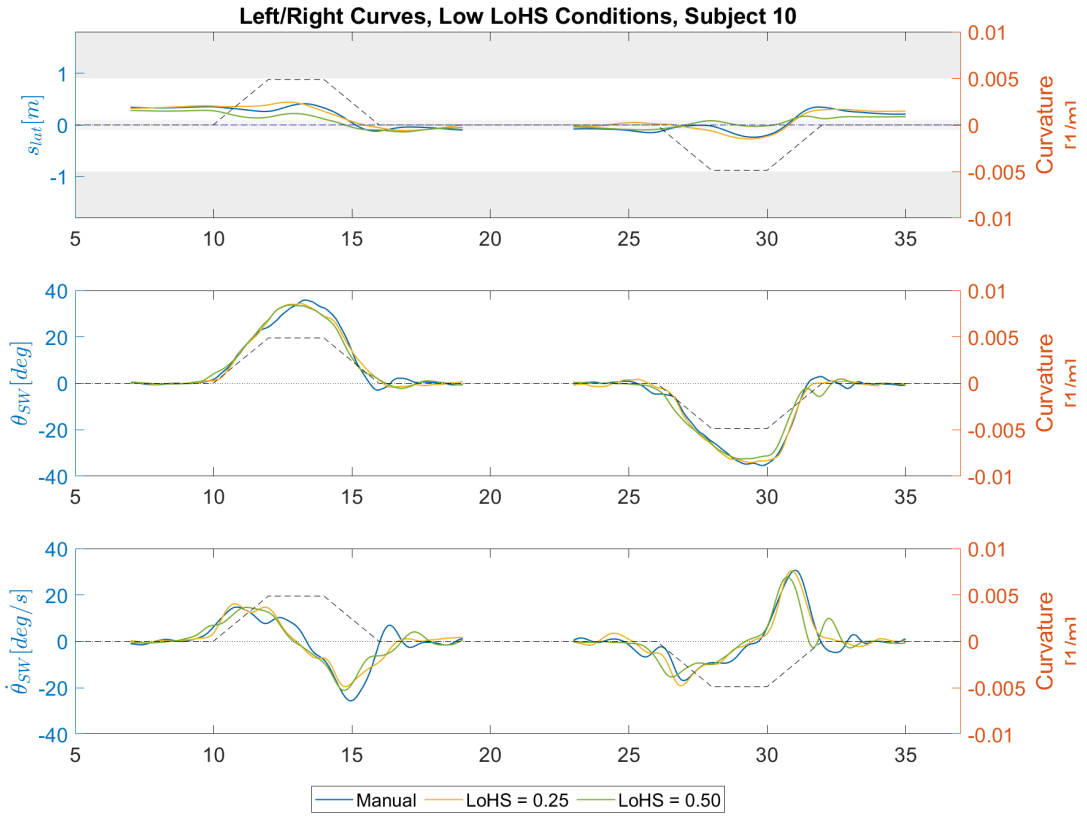

Figure C.19: Average road lateral position, steering wheel and steering rate data for subject 10 for the three lower LoHS conditions for left and right curves

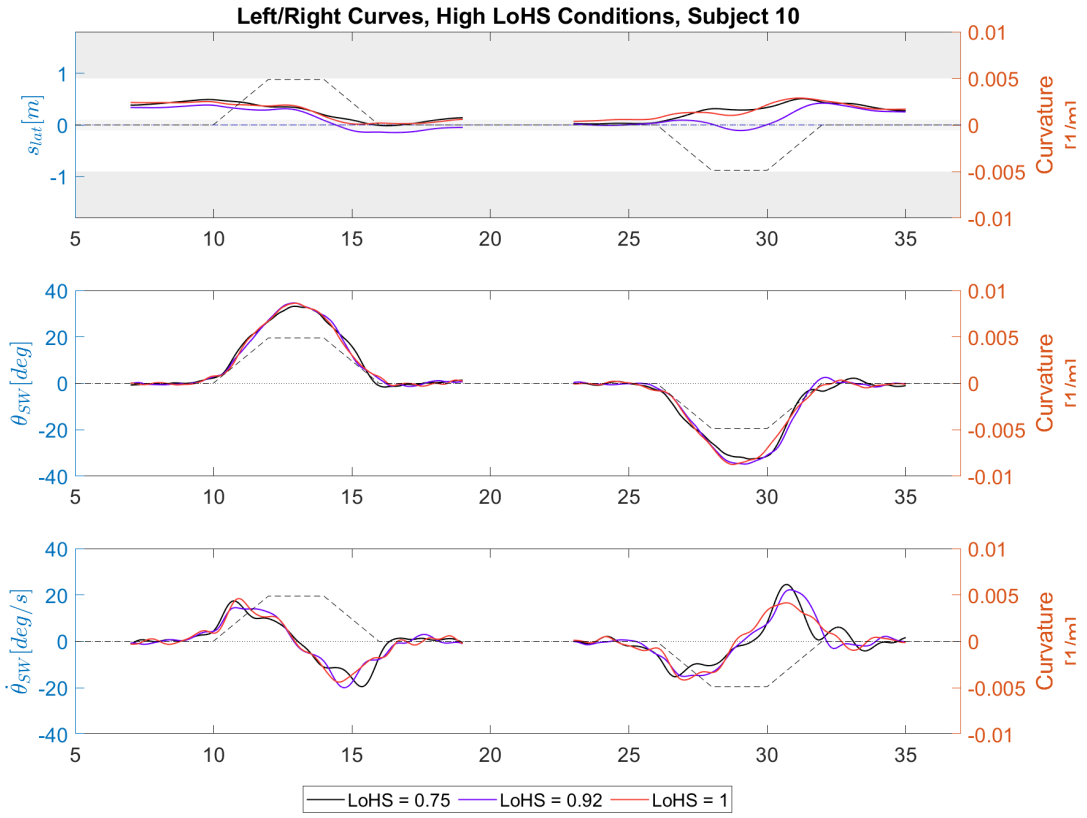

Figure C.20: Average road lateral position, steering wheel and steering rate data for subject 10 for the three higher LoHS conditions for left and right curves

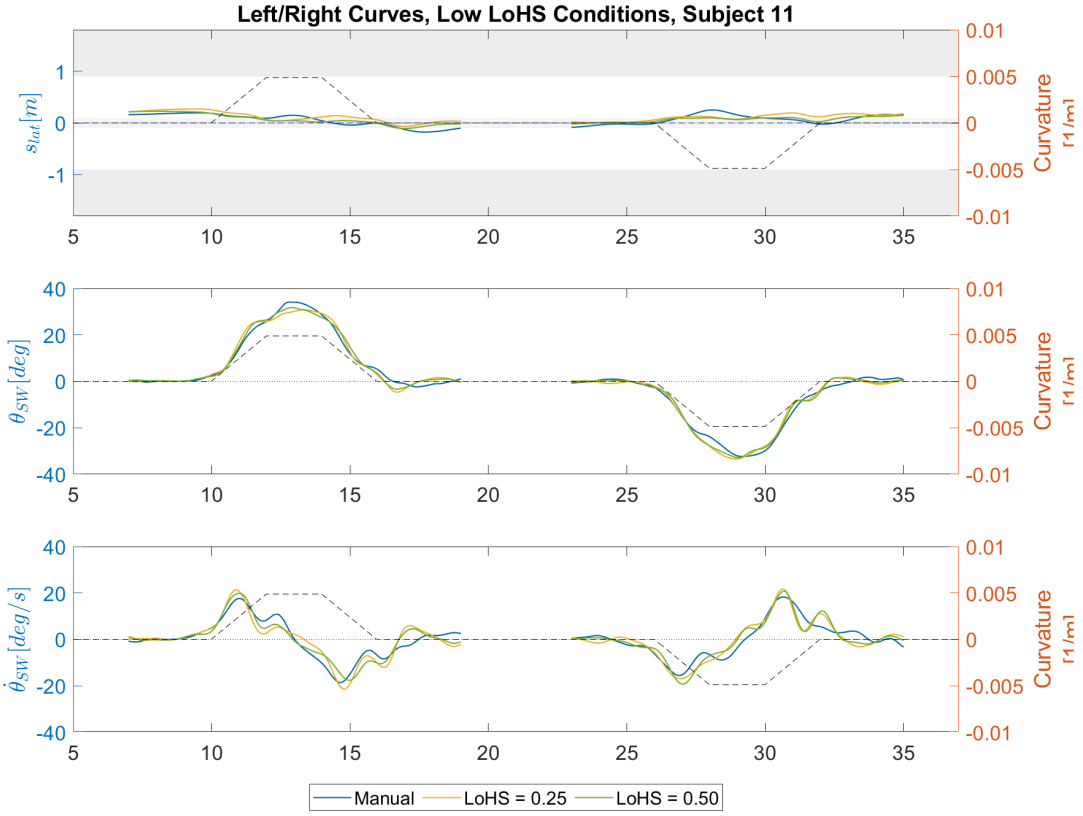

Figure C.21: Average road lateral position, steering wheel and steering rate data for subject 11 for the three lower LoHS conditions for left and right curves

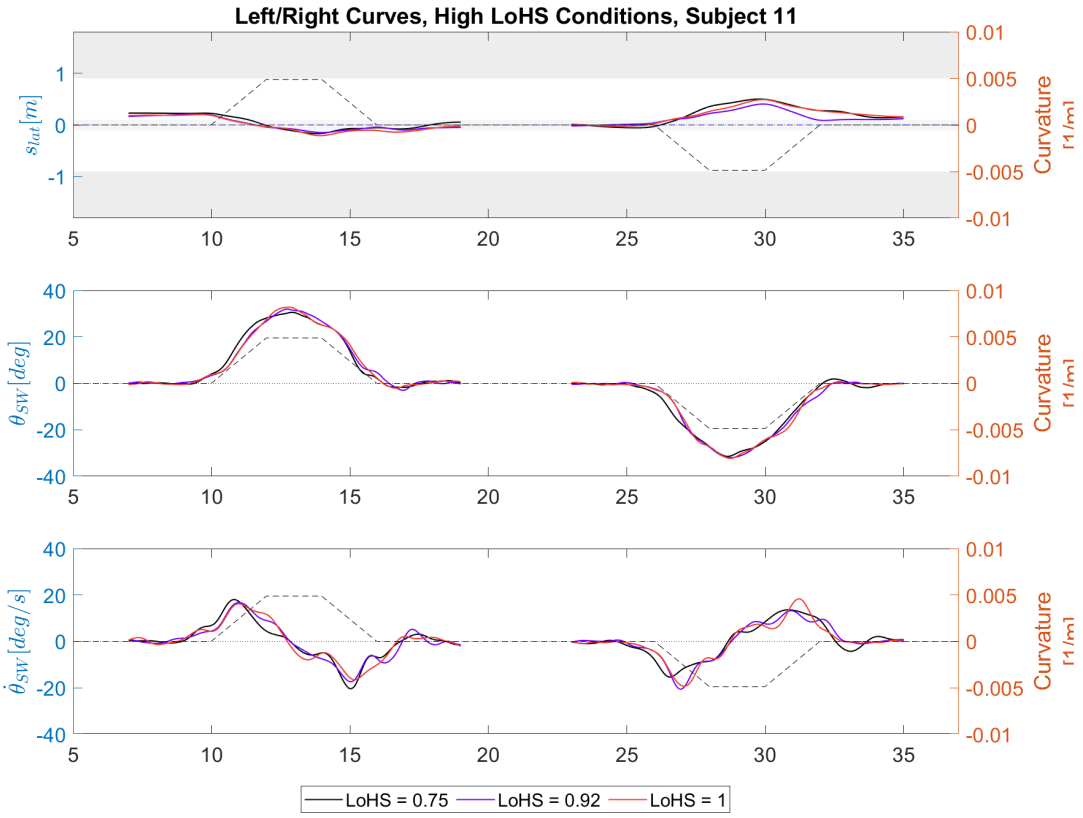

Figure C.22: Average road lateral position, steering wheel and steering rate data for subject 11 for the three higher LoHS conditions for left and right curves

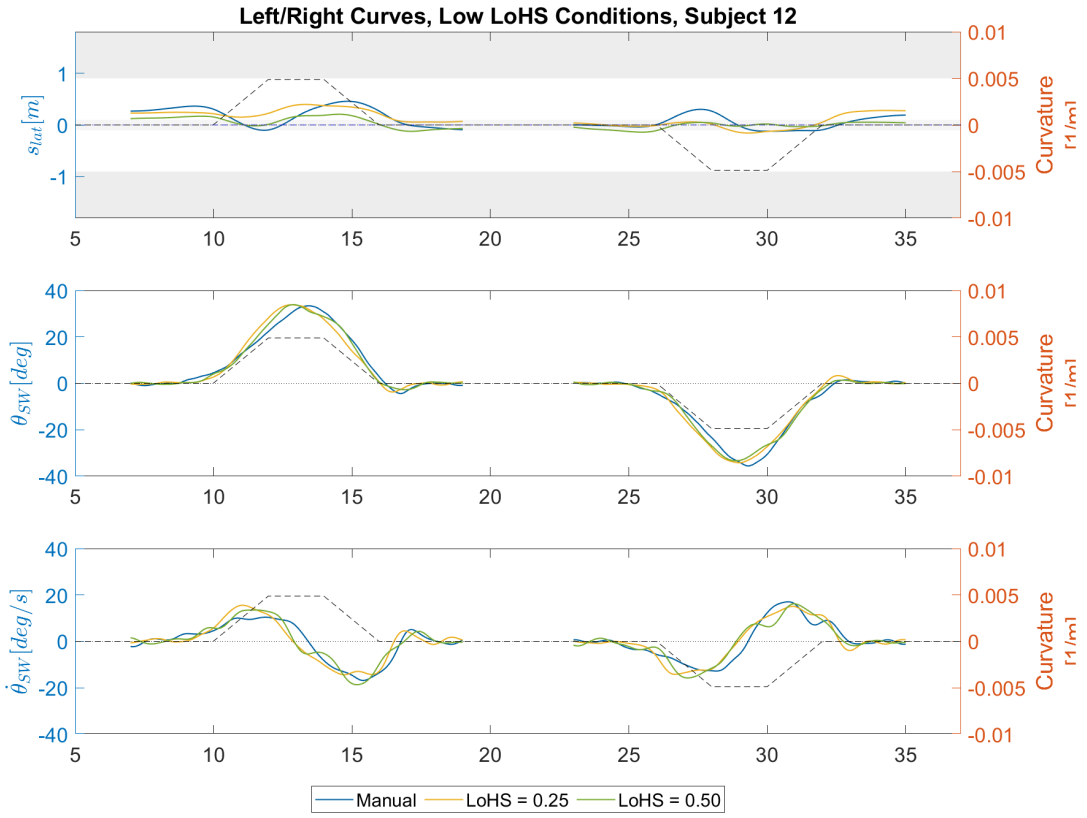

Figure C.23: Average road lateral position, steering wheel and steering rate data for subject 12 for the three lower LoHS conditions for left and right curves

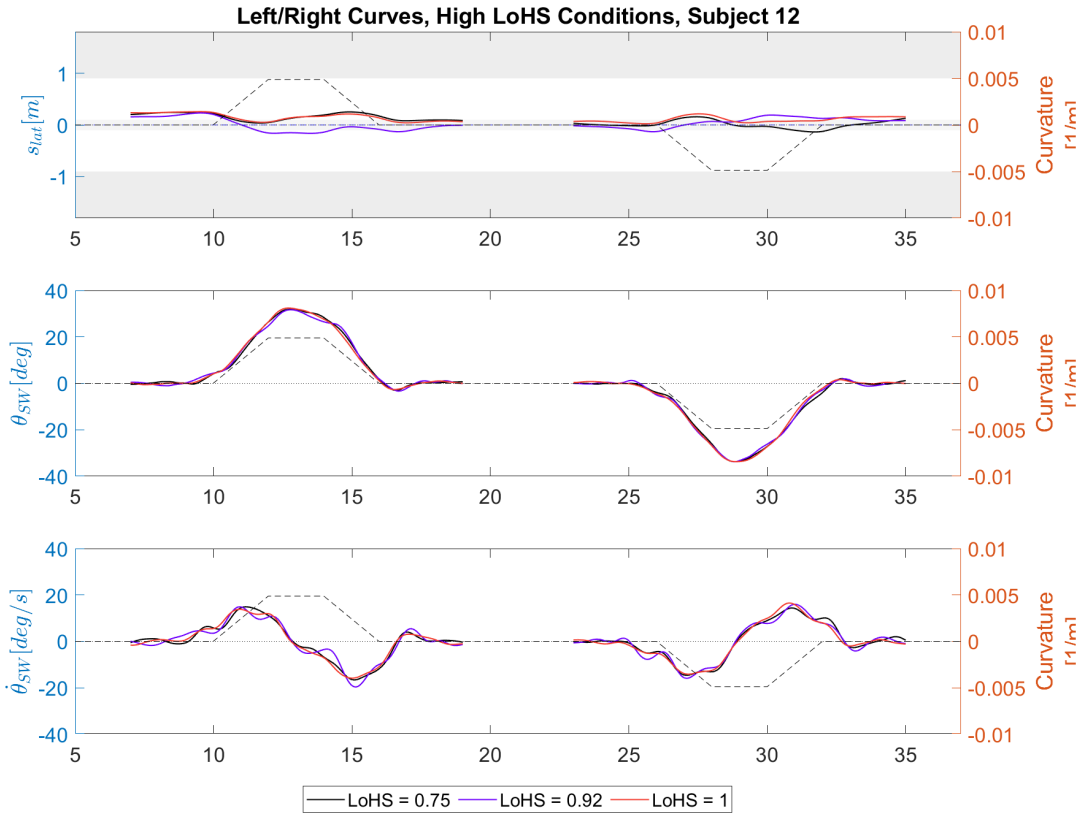

Figure C.24: Average road lateral position, steering wheel and steering rate data for subject 12 for the three higher LoHS conditions for left and right curves

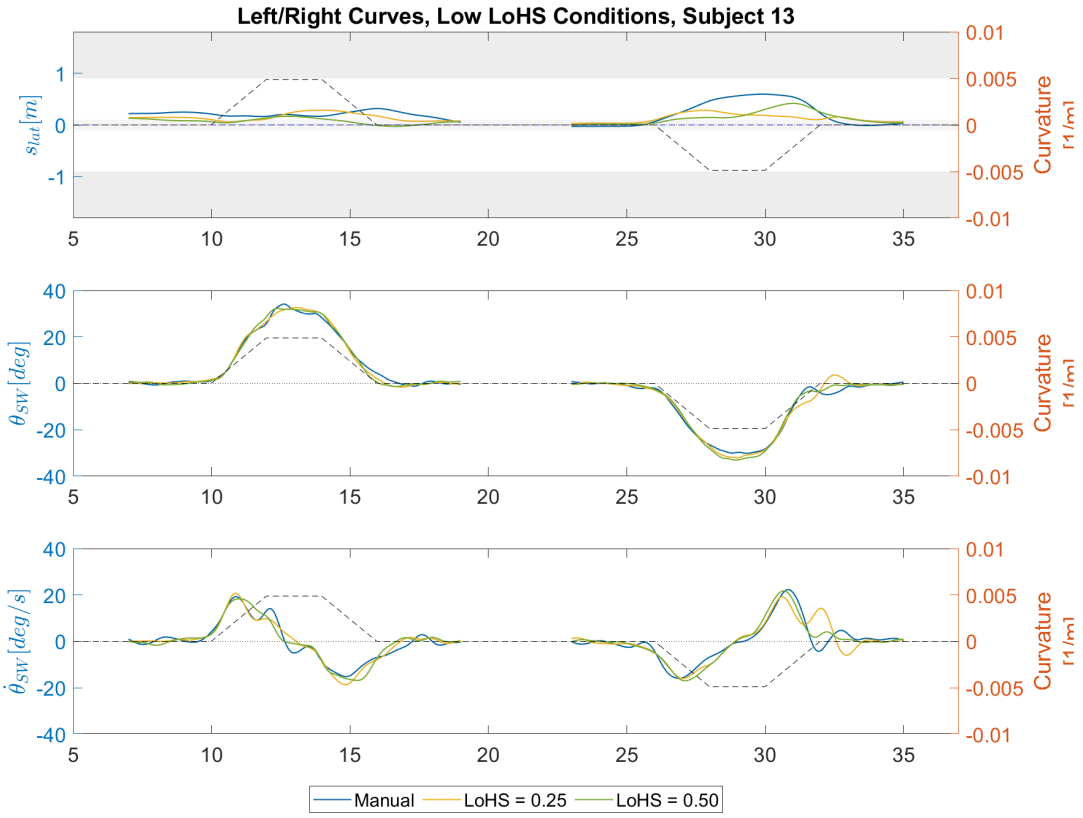

Figure C.25: Average road lateral position, steering wheel and steering rate data for subject 13 for the three lower LoHS conditions for left and right curves

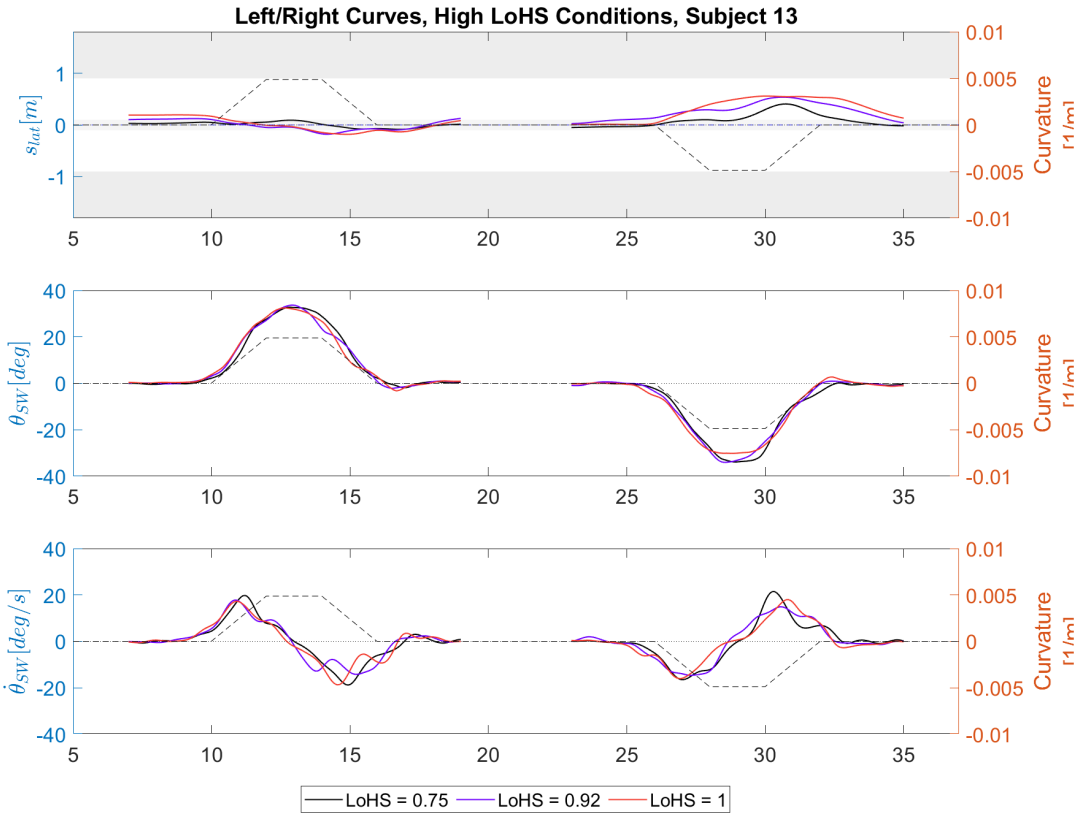

Figure C.26: Average road lateral position, steering wheel and steering rate data for subject 13 for the three higher LoHS conditions for left and right curves

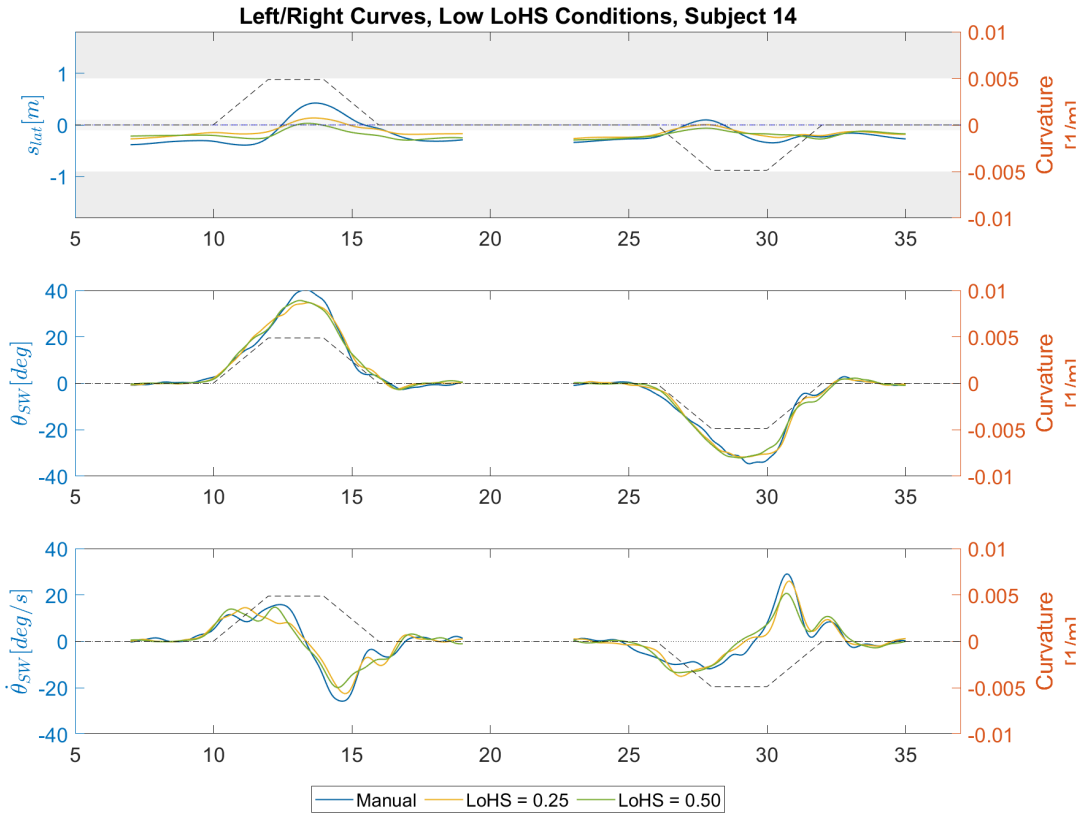

Figure C.27: Average road lateral position, steering wheel and steering rate data for subject 14 for the three lower LoHS conditions for left and right curves

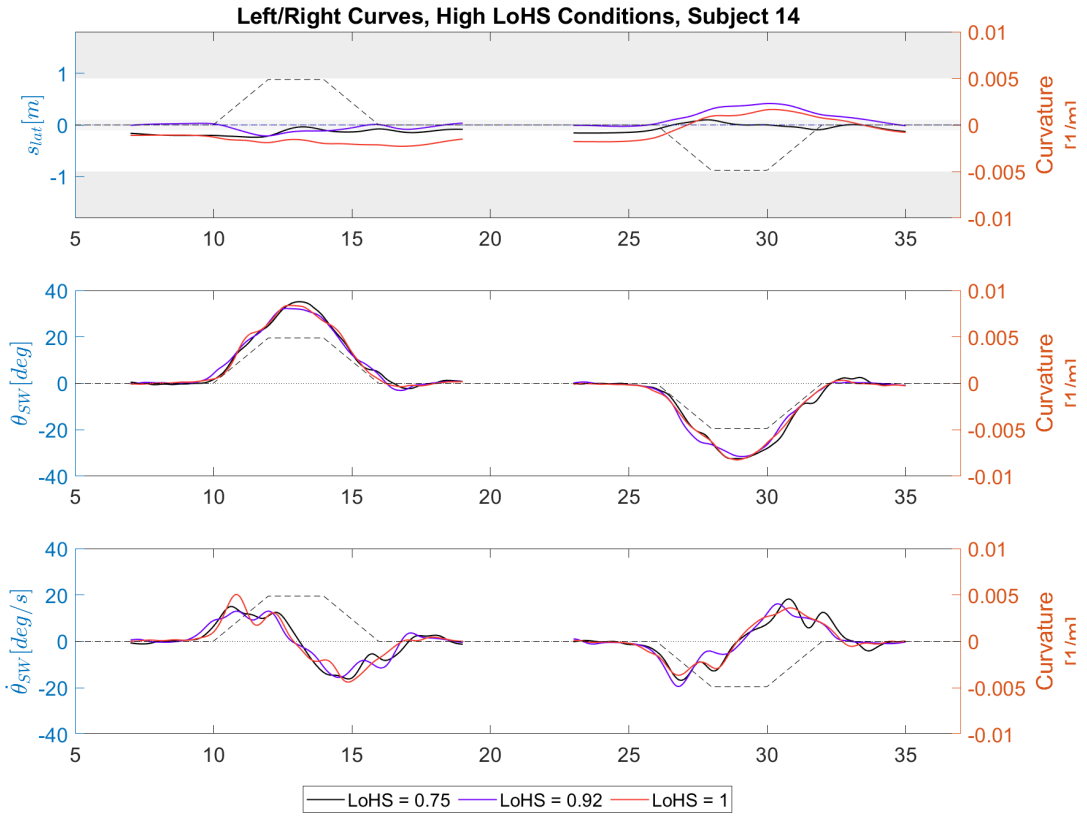

Figure C.28: Average road lateral position, steering wheel and steering rate data for subject 14 for the three higher LoHS conditions for left and right curves

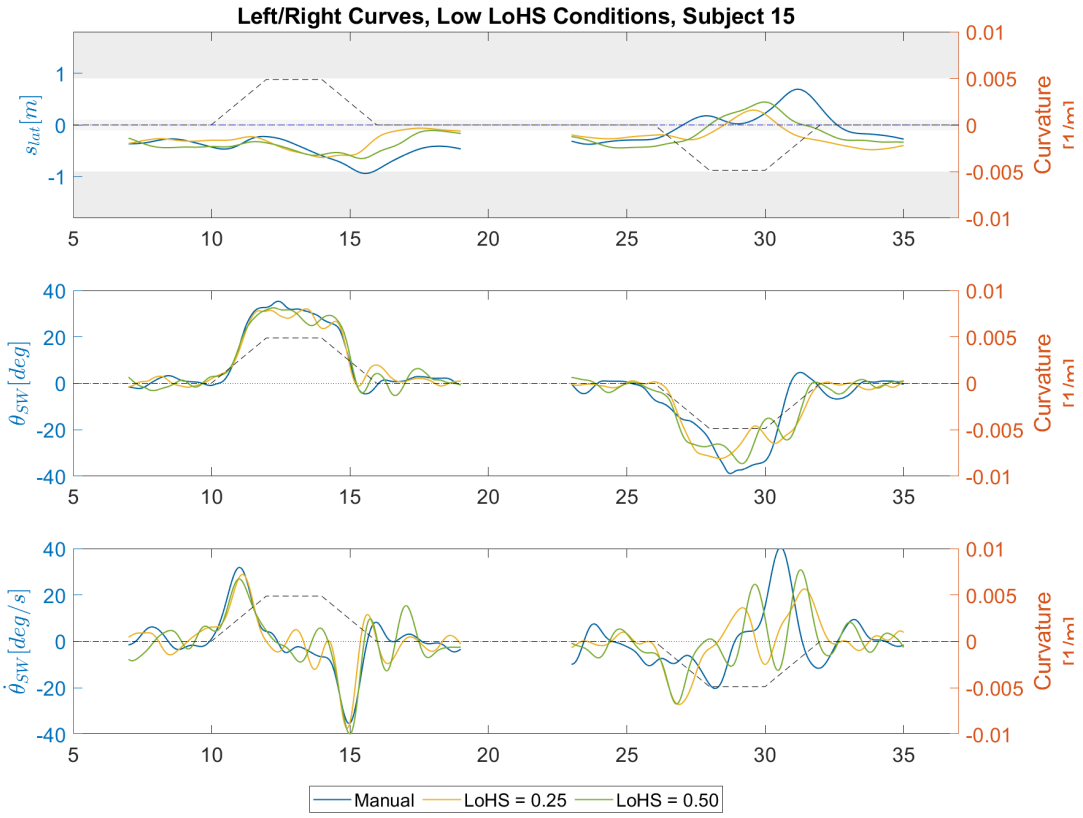

Figure C.29: Average road lateral position, steering wheel and steering rate data for subject 15 for the three lower LoHS conditions for left and right curves

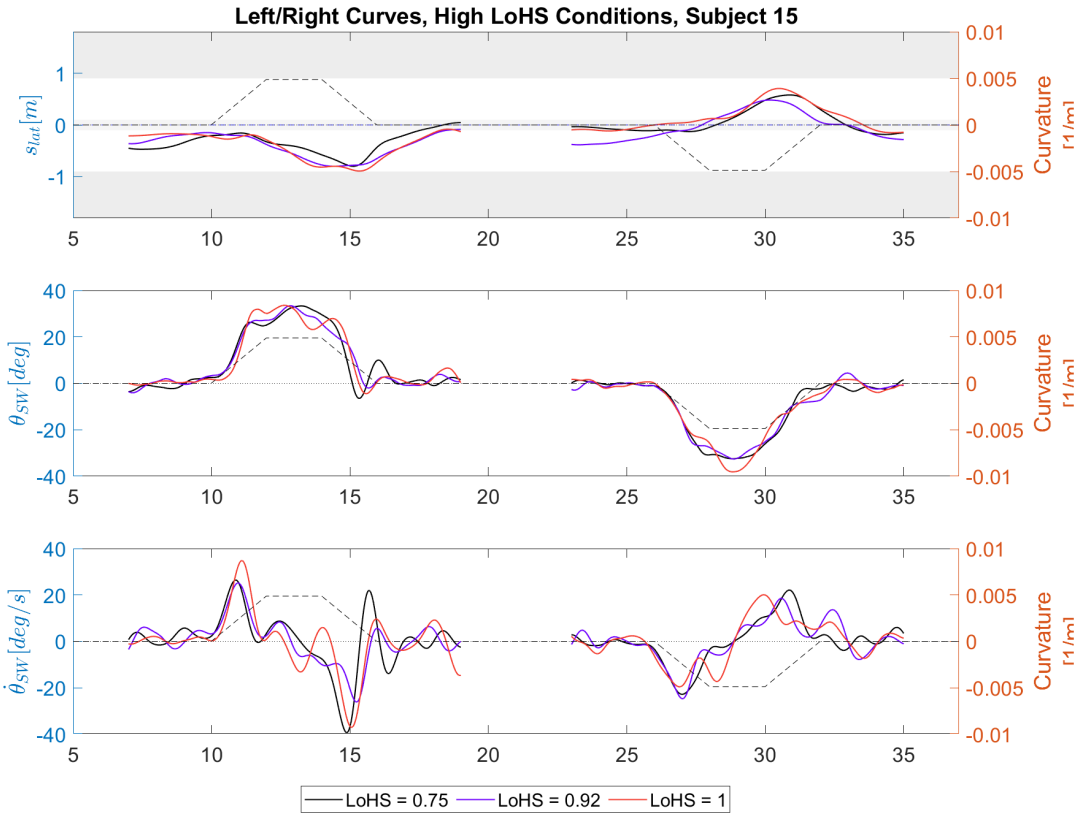

Figure C.30: Average road lateral position, steering wheel and steering rate data for subject 15 for the three higher LoHS conditions for left and right curves

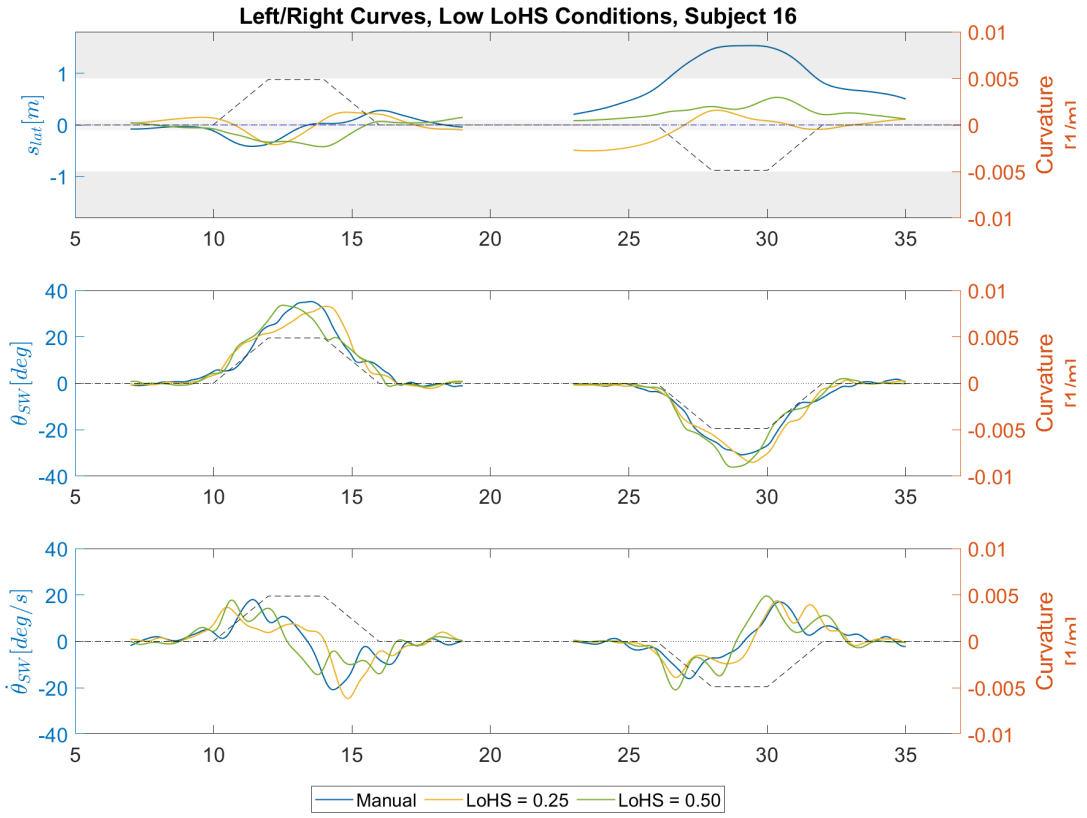

Figure C.31: Average road lateral position, steering wheel and steering rate data for subject 16 for the three lower LoHS conditions for left and right curves

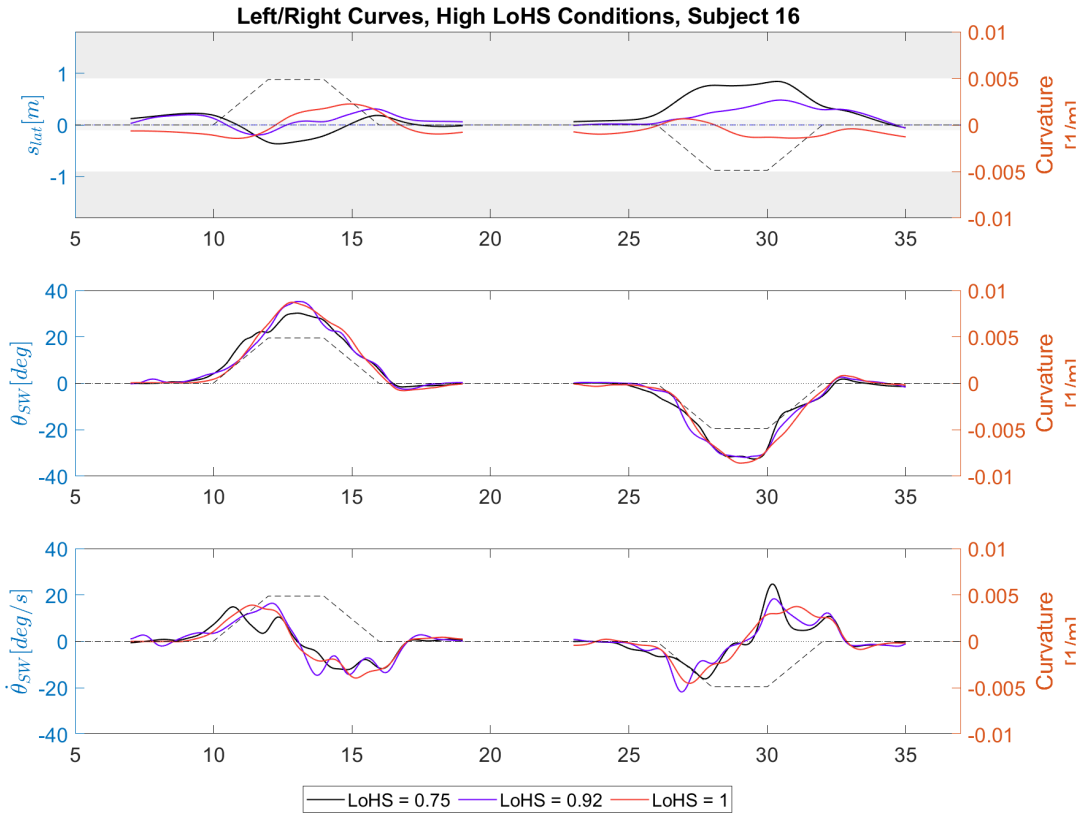

Figure C.32: Average road lateral position, steering wheel and steering rate data for subject 16 for the three higher LoHS conditions for left and right curves

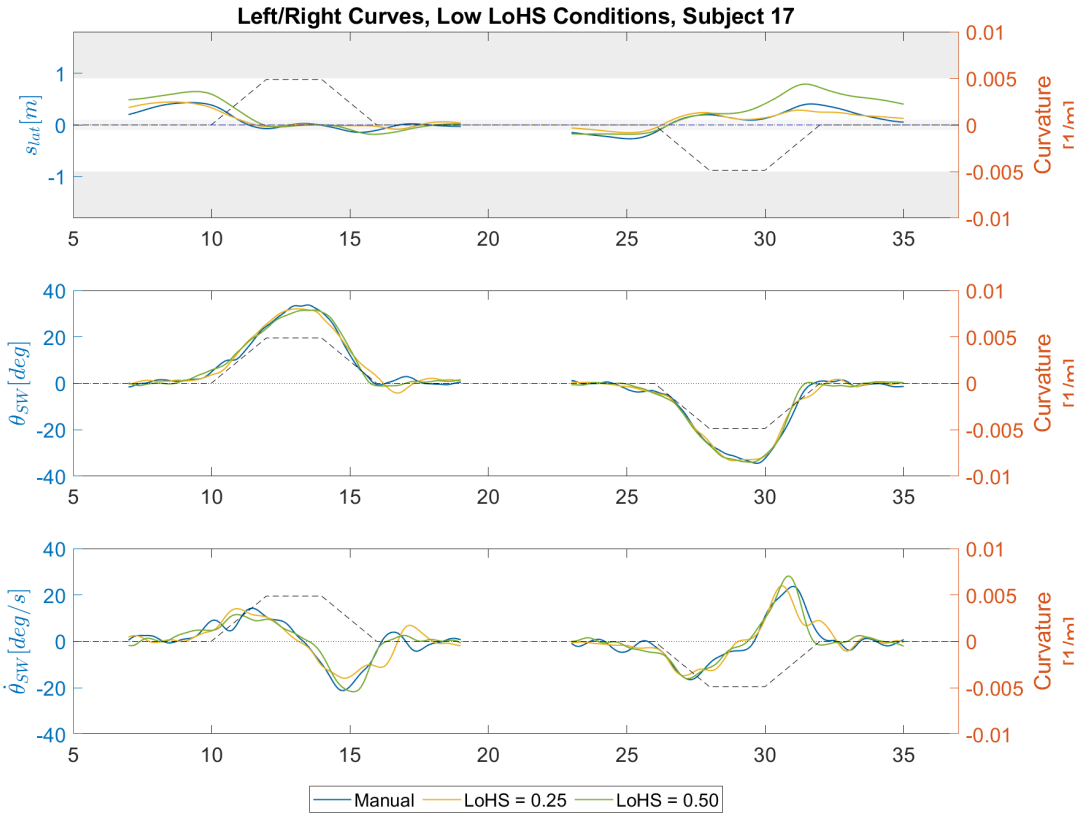

Figure C.33: Average road lateral position, steering wheel and steering rate data for subject 17 for the three lower LoHS conditions for left and right curves

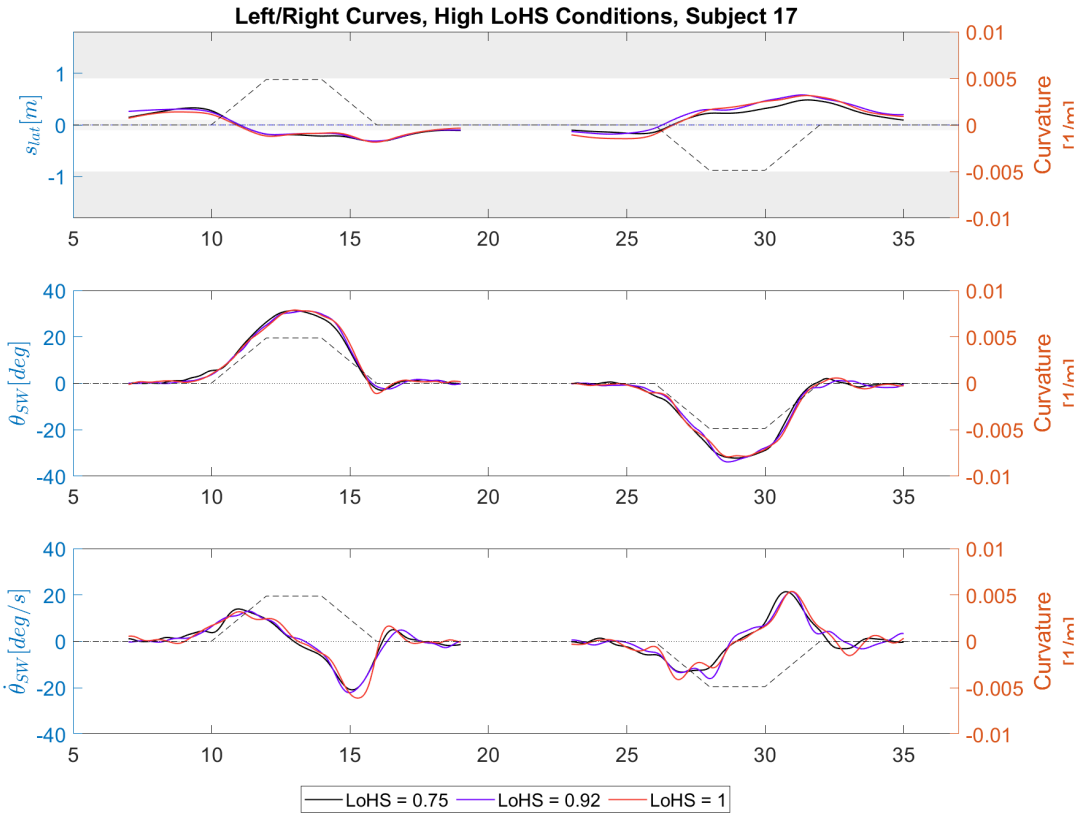

Figure C.34: Average road lateral position, steering wheel and steering rate data for subject 17 for the three higher LoHS conditions for left and right curves

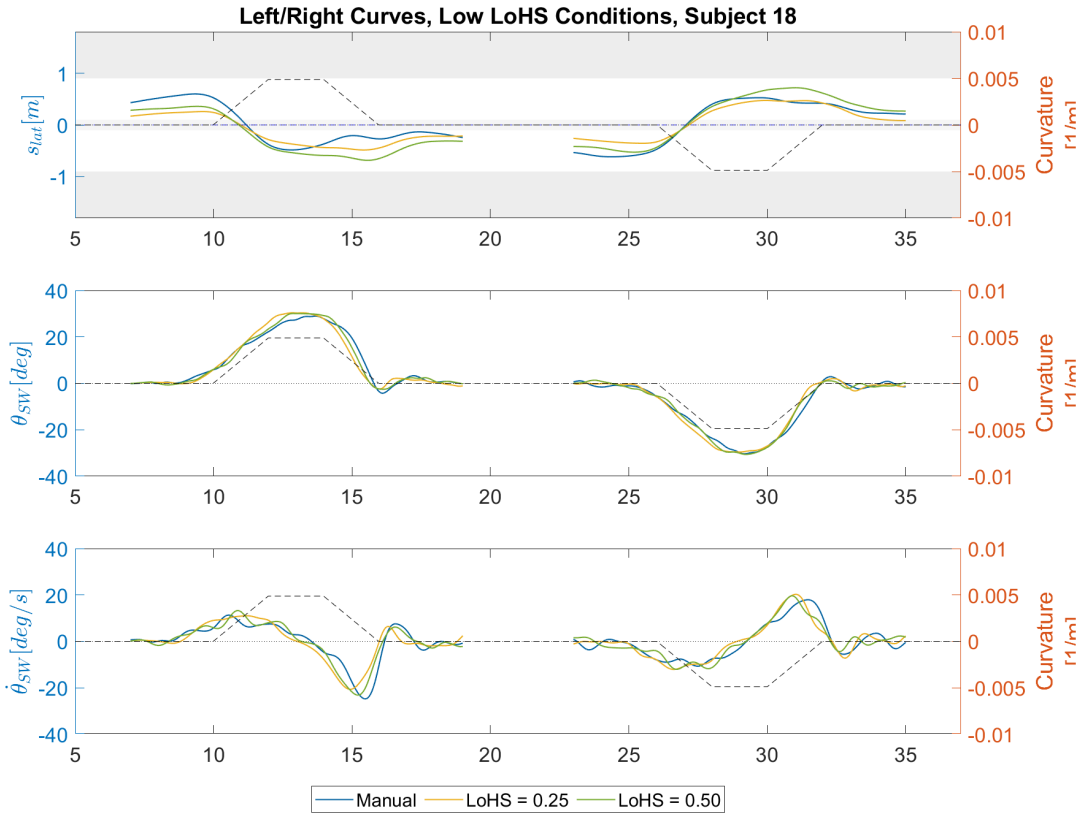

Figure C.35: Average road lateral position, steering wheel and steering rate data for subject 18 for the three lower LoHS conditions for left and right curves

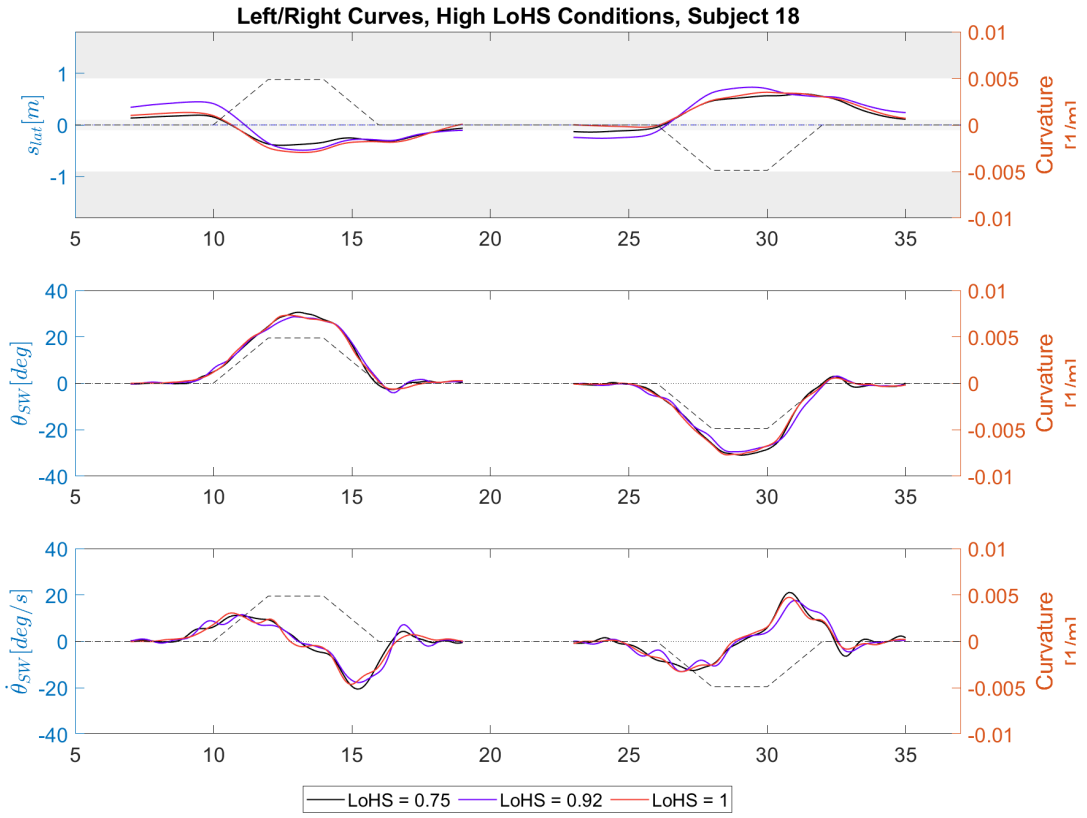

Figure C.36: Average road lateral position, steering wheel and steering rate data for subject 18 for the three higher LoHS conditions for left and right curves

D

Questionnaire Data

This appendix includes the full data for the Van der Laan and Controller Acceptance Rating Scale questionnaires as collected during the experiment. The color for each of the top rows corresponds to the used colors for every experimental condition in the individual results of the previous appendices.

LoHS = 0.25											
Subject	CARS	Confidence	Q1	Q2	Q3	Q4	Q5	Q6	Q7	Q8	Q9
1	7	B	0	0	0	-1	0	0	0	-1	1
2	6	C	0	-1	0	-2	0	-1	1	-2	1
3	8	B	0	-1	1	-1	0	-1	1	-1	-1
4	5	A	-1	0	0	0	-1	0	-1	0	0
5	8	B	-1	1	1	1	-1	1	0	0	0
6	6	B	-1	-1	-1	0	-1	0	-1	-1	2
7	5	A	0	-1	-1	-1	0	-1	1	-1	-1
8	4	B	-2	-1	-1	-1	-1	-1	-2	-2	1
9	10	A	0	0	0	0	-2	0	-1	0	0
10	6	A	0	0	0	-1	1	0	0	-1	0
11	5	B	0	0	1	1	-1	0	-1	0	1
12	7	B	0	0	0	0	1	0	1	1	1
13	9	B	1	1	1	1	1	1	1	1	2
14	7	C	1	0	0	0	0	0	1	-1	0
15	8	A	1	0	2	2	2	1	1	1	2
16	5	A	0	0	0	-1	0	0	0	-1	1
17	8	A	1	1	1	1	1	0	1	1	-1
18	6	A	1	1	1	0	1	-1	0	1	1

LoHS = 0.50											
Subject	CARS	Confidence	Q1	Q2	Q3	Q4	Q5	Q6	Q7	Q8	Q9
1	9	B	1	1	1	1	0	0	0	0	1
2	7	B	0	0	0	-1	1	-1	0	-1	1
3	6	B	-1	0	0	0	-1	0	0	-1	0
4	3	A	1	0	0	0	1	-1	0	-1	-1
5	7	A	0	0	0	-1	1	-1	0	0	1
6	8	A	1	1	1	0	1	1	2	1	2
7	7	B	1	0	0	0	0	-1	1	0	0
8	8	B	1	1	2	1	1	1	1	1	1
9	10	A	0	2	0	1	1	1	0	0	0
10	6	A	0	0	0	-1	0	-1	1	-1	0
11	9	B	1	2	1	1	1	1	1	2	1
12	8	B	1	1	1	1	1	0	1	0	0
13	6	B	-1	0	-1	-2	0	-1	0	0	2
14	8	C	1	1	0	1	0	1	1	0	1
15	7	A	1	0	1	0	1	0	1	0	1
16	6	B	1	1	1	0	0	0	1	0	1
17	7	A	1	1	1	1	1	1	1	1	1
18	4	A	-2	-2	-1	-1	-1	-1	-1	-1	-1

LoHS = 0.75											
Subject	CARS	Confidence	Q1	Q2	Q3	Q4	Q5	Q6	Q7	Q8	Q9
1	9	B	1	1	0	1	1	0	1	0	0
2	8	A	1	2	2	2	1	1	2	0	-1
3	10	B	2	2	1	2	1	2	1	1	0
4	8	A	2	1	1	1	1	1	2	0	1
5	6	A	1	0	-1	-1	1	0	0	-1	1
6	9	A	2	1	2	1	2	1	2	2	1
7	6	B	1	-1	0	0	1	0	1	0	0
8	7	B	0	-1	-1	-1	0	-1	0	0	0
9	10	A	0	1	0	0	0	0	1	0	0
10	9	A	2	2	1	2	2	1	2	1	0
11	9	B	1	1	1	1	1	2	1	1	0
12	7	B	0	0	1	-1	0	0	1	0	0
13	7	A	0	1	0	0	1	0	1	1	2
14	8	B	2	1	1	1	1	1	2	0	-1
15	7	A	1	0	1	0	1	1	1	1	1
16	9	B	2	2	2	2	2	1	2	2	-1
17	8	A	1	1	1	1	1	1	1	1	-1
18	8	A	1	1	1	1	1	0	1	1	-1

LoHS = 0.92											
Subject	CARS	Confidence	Q1	Q2	Q3	Q4	Q5	Q6	Q7	Q8	Q9
1	10	A	2	1	1	1	1	1	1	0	-1
2	8	A	2	1	2	1	2	0	1	1	1
3	8	C	1	0	1	1	1	1	0	0	-2
4	7	A	1	0	1	0	1	0	1	0	0
5	9	B	1	2	1	2	1	2	0	1	0
6	10	A	2	2	2	2	2	2	2	2	-1
7	7	B	1	0	1	-1	1	-1	2	1	1
8	7	B	1	0	1	0	1	0	1	0	1
9	10	A	0	1	0	0	1	0	1	0	0
10	8	A	2	1	2	1	2	2	2	2	1
11	8	B	1	1	1	2	0	1	2	0	0
12	8	B	0	0	0	0	-1	0	1	0	-1
13	8	B	1	0	0	-1	1	0	1	1	2
14	8	B	2	1	1	1	1	1	2	0	-1
15	7	A	1	0	1	1	1	0	1	0	1
16	7	B	1	0	0	0	1	0	1	1	0
17	8	A	2	2	2	2	2	2	2	1	0
18	8	A	1	1	1	1	1	1	1	1	1

LoHS = 1											
Subject	CARS	Confidence	Q1	Q2	Q3	Q4	Q5	Q6	Q7	Q8	Q9
1	9	A	1	1	0	1	1	1	1	0	0
2	9	A	2	2	2	2	2	2	2	2	-2
3	9	A	2	1	1	1	2	0	2	1	-1
4	5	B	1	0	1	0	1	0	1	1	-1
5	9	B	2	1	1	0	1	0	1	2	-1
6	10	A	2	2	2	2	2	2	2	2	-2
7	9	A	2	2	2	2	2	2	2	2	0
8	9	A	2	2	2	2	2	1	2	1	0
9	10	A	0	1	1	0	1	1	0	0	0
10	8	A	1	2	1	1	1	1	2	0	-1
11	9	A	2	2	1	2	1	2	1	1	-1
12	9	A	1	1	1	1	-1	1	1	1	-1
13	9	B	1	1	1	1	1	1	2	1	2
14	9	B	2	1	1	1	1	1	2	0	0
15	7	B	1	1	1	1	1	1	1	1	2
16	10	A	2	2	2	2	2	1	2	1	0
17	9	A	2	2	2	2	2	2	2	2	1
18	9	A	2	2	2	2	2	2	2	2	-2

E

Experiment Briefing and Consent Form

This appendix contains the experiment briefing that was used to inform the participants about the experiment as well as the consent form that they were asked to sign.

Experiment Briefing

Effects and acceptance of haptic shared control design choices for car steering

Thank you for participating in this experiment! The experiment, conducted in the Human-Machine Interaction Laboratory (HMILab), analyses human steering behaviour. The experiment consists of a steering task supported by haptic force feedback on the steering wheel. This briefing will introduce you to the experiment and what is expected of you as a participant.

Experiment Goal

In *haptic shared control*, a human operator performs a control task (such as road driving) in cooperation with an automated controller. Interaction between the human and automation is realised through force feedback on the steering wheel. The goal of this experiment is to investigate the acceptance of different haptic force feedback designs. To do this, a simulated road is driven with some assistance of the automatic controller. The simulation mimics real-life car steering on a winding road at medium to high speed. The results of the experiment should clarify what haptic settings are seen as more desirable by drivers.

Experiment Task

In this task, you will perform a driving task along a winding road with curves. It is your task to drive along the road and complete the curves similar to how you would choose to take these corners in real life. The car drives at a fixed speed so only the steering wheel can be used to drive along the road. During the task, haptic force feedback will be applied to the steering wheel, in order to assist you in the steering task.

Figure 1: Illustration of HMILab. The experiment will use the left side of the simulator, using the steering wheel.

Experiment Procedures

Throughout the experiment, several different haptic guidance settings will be presented to you in a random order. You are asked to perform the steering task several times. The researcher will keep track of your performance and will announce when the experiment has been completed. You will start the experiment by doing a practice run *without* haptic support, to familiarise yourself with the task.

Each driving run lasts about 3 to 4 minutes. After each run, you will be asked to fill out a Van der Laan questionnaire as well as a Controller Acceptance Rating Scale (CARS) questionnaire, rating the haptic guidance that you received during the run. Furthermore, after each completed run the researcher will ask for a rating on the Misery Scale (MISC), see Fig. 2 to keep track of your comfort level. Short breaks can be taken between runs to alleviate any discomfort that might occur due to controlling the steering wheel or after sitting in a fixed position for a prolonged period of time. Longer breaks will be taken after every 5 or 6 runs, where you will be taken out of the simulator for 5-10 minutes. The experiment will last approximately 60 minutes.

Symptom	Severity	Score
No problems		0
Uneasiness (no typical symptoms)		1
Dizziness, warmth, headache, stomach awareness, sweating, and other symptoms	Vague Slight Fairly Severe	2 3 4 5
Nausea	Slight Fairly Severe	6 7 8
Retching		9
Vomiting		10

Figure 2: Misery Rating Scale

For each driving trial, the subsequent procedure will be followed:

1. The researcher applies the settings for the next run.
2. The researcher checks whether the participant is ready to proceed (i.e., MISC level) and initiates the run after a countdown from 3 (3-2-1-go).
3. The participant performs the steering task.

COVID-19 protocol

Due to the ongoing COVID-19 (’coronavirus’) pandemic, several measures are taken to reduce the risk of spreading it. First and foremost, researcher and participant will follow the guidelines as indicated on the Dutch government website[1] on the day of the experiment. Related to this experiment, the following four measures are taken:

- Both researcher and participants confirm they do not have symptoms related to COVID-19.
- 1.5 meter distance will be kept between researcher and participant at all times.
- All touched objects in the simulator will be disinfected by the researcher before and after the experiment.
- Before and after the experiment both researcher and participant will wash or disinfect their hands.

This experiment will be performed following the most recent "COVID-19 Protocols for Human Subject Experiments" of the Control and Simulation department.

- ***Experiment briefing continues on next page*** -

[1] https://www.rijksoverheid.nl/coronavirus

Your rights

Participation in the experiment is voluntary. This means that you can terminate your cooperation at any time. By participating in the experiment you agree that the collected data may be published. Your data will remain confidential and anonymous, so only the experimenter can link the results to a particular participant. To make sure that you understand and comply with the conditions of the experiment, you will be asked to sign an informed consent form.

Thank you for participating!

Experiment Consent Form

Effects and acceptance of haptic shared control design choices for car steering

I hereby confirm, by ticking each box, that:

1. I volunteer to participate in the experiment conducted by **Kelsey Huijsing** under supervision of **Dr.ir. Daan Pool** from the Faculty of Aerospace Engineering of TU Delft. I understand that my participation in this experiment is voluntary and that I may withdraw and discontinue participation at any time, for any reason. ☐

2. I confirm that the researcher has provided me with detailed safety instructions to ensure my experiment session can be performed in line with current RIVM COVID-19 regulations at all times and that these instructions are fully clear to me. ☐

3. I confirm that (*tick the appropriate box*):
   - I am a student or staff member at TU Delft and am aware of the requirements for self-testing for COVID-19 for on-campus activities ☐

   or
   - I am not a student or employee at TU Delft and have presented the researcher with a valid 'CoronaCheck' QR code upon my arrival for the experiment ☐

4. I have read the experiment briefing and confirm that I understand the instructions and have had all my remaining questions answered to my satisfaction. ☐

5. I understand that my participation involves performing a steering task in a fixed-based simulator, with different settings of haptic feedback on the steering wheel. ☐

6. I confirm that the researcher has provided me with detailed safety and operational instructions for the hardware (simulator setup, control-loaded steering wheel, fire escape) used in the experiment. ☐

7. I understand that (though very unlikely) it is possible that I may develop some feelings of discomfort caused by the fixed-base driving simulator setup. If this is the case, I will inform the experimenter. I also understand that the experiment may be discontinued for this reason. ☐

8. I understand that the researcher will not identify me by name in any reports or publications that will result from this experiment, and that my confidentiality as a participant in this study will remain secure. Only my personal signature and name on this form will be stored safely on a secure TU Delft Project Drive on the TU Delft network. ☐

9. I understand that this research study has been reviewed and approved by the TU Delft Human Research Ethics Committee (HREC). To report any problems regarding my participation in the experiment, I know I can contact the researchers using the contact information below. ☐

My Signature	Date
My Printed Name	Signature of researcher